

November, 1961

published monthly by The Institute of Radio Engineers, Inc.

Proceedings of the IRE®

contents

Poles and Zeros.....	1613
M. W. Bullock, Director, 1961-1962	1614
Scanning the Issue.....	1615
PAPERS	
The Cryosistor—A Field-Effect Controlled Impact Ionization Switch, <i>I. Melngailis and A. G. Milnes</i>	1616
A New Semiconductor Tetrode—The Surface-Potential Controlled Transistor, <i>C. T. Sah</i>	1623
Correction to "Statistical Analysis of Certain Binary Division Algorithms," <i>C. V. Freiman</i>	1634
The Pulsed Ruby Maser as a Light Amplifier, <i>P. P. Kisliuk and W. S. Boyle</i>	1635
Correction to "The Elimination of Intersymbol Interference by Input Signal Shaping," <i>I. Gerst</i>	1639
Inductance in Thin-Film Superconducting Structures, <i>Norman H. Meyers</i>	1640
Reduction of the Frequency-Temperature Shift of Piezoelectric Resonators by Mechanical Stress, <i>E. A. Gerber and M. H. Miles</i>	1650
Fundamental Limitations to Optical Doppler Measurements for Space Navigation, <i>R. H. Norton and R. L. Wildey</i>	1655
Timing Potentials of Loran-C, <i>R. H. Doherty, G. Heffley, and R. F. Linfield</i>	1659
A Provisional Ground Conductivity Map for Canada, <i>G. Clement Ireland</i>	1674

CORRESPONDENCE

Tunnel-Diode Series Resistance, <i>E. L. Bonin and J. R. Biard</i>	1679
Some Measurements on an Iris Beam Waveguide, <i>J. R. Christian and G. Goubau</i>	1679
Ionospheric Contributions to the Doppler Shift at VHF from Near-Earth Satellites, <i>William H. Guier</i>	1680
WWV and WWVH Standard Frequency and Time Transmissions, <i>National Bureau of Standards</i>	1681
Persistent-Current Memory Circuit, <i>W. C. Stewart, H. A. Owen, M. S. P. Lucas, and C. R. Vail</i>	1681
A C-Band Parametric Amplifier with Large Bandwidth, <i>B. T. Vincent, Jr.</i>	1682
Multiple Reflections of Microwaves Propagating Through a Semiconductor Medium, <i>H. Jacobs, F. A. Brand, J. D. Meindl, and R. Benjamin</i>	1683
Correlation Optical Radar, <i>M. Katzman and E. Frost</i>	1684
Unidirectional Lower Sideband Parametric Amplifier Without Circulator, <i>G. H. B. Thompson</i>	1684
One-Tunnel-Diode Flip-Flop HF Behavior, <i>Henry Guckel</i>	1685
Additional Information on "An Interaction Circuit for Traveling-Wave Tubes," <i>R. M. White, C. K. Birdsall, D. E. Chaffee, P. J. Crepeau, and I. Itzkan</i>	1686
Comments on "Design Theory of Optimum Negative-Resistance Amplifiers," <i>H. J. Carlin, L. I. Smilen, D. C. Youla, E. S. Kuh, and J. D. Patterson</i>	1687
Noise in Tunnel-Diode Mixers, <i>Shih-Fang Lo</i>	1688
Comments on "Tunnel-Diode Microwave Oscillators," <i>G. Fuller, G. W. H. Wooding, D. Sterzer, and D. E. Nelson</i>	1689
Gravitational Fields, <i>Jovan Djurić</i>	1689
The <i>gh</i> -Field Theory, <i>Jovan Djurić</i>	1690
X-Band Electronically-Variable Attenuator, <i>P. L. Fleming</i>	1690
A Method of Displaying Ultra-Fast Limit Cycles or Three-Parameter Trajectories, <i>William T. Rhoades</i>	1691
An Extension of Newtonian Relativity to Include Electromagnetic Phenomena, <i>Pascal M. Rapier</i>	1691
Maser Terminology, <i>William R. Mallory</i>	1692
Technique for Amplitude Modulating a Van Atta Radar Reflector, <i>William F. Bahret</i>	1692
Some Ladder Networks Representing Certain Transcendental Numbers—Classroom Note, <i>F. Reza</i>	1693
Performance Degradation of Linear FM-Pulse-Compression Systems Due to the Doppler Effect, <i>H. O. Ramp and E. R. Wingrove, Jr.</i>	1693
Doppler-Shift Effects in Space Propagation, <i>R. P. Haviland</i>	1694
Comment on Shot-Noise Smoothing Mechanism Proposed by LaRosa and Wilhelmsen, <i>C. A. Lee and A. Yariv</i>	1695
Vacuum-Tube Networks, <i>George D. O'Neill</i>	1695
Flow Graphs and Tapered Transmission Lines, <i>Frank M. Brown</i>	1696
Large Signal Interaction Between a Spiraling Electron Beam and the TE ₁₀ Rectangular Waveguide Mode, <i>W. L. Dickson, C. C. Johnson, and R. W. Grow</i>	1696

COVER

Shown on the cover is a three-dimensional diagram of the equipotential contours of the new surface-potential controlled transistor described on page 1623.

Proceedings of the IRE[®]

continued

On Backward-Wave Oscillator Stabilization, <i>R. B. Clark and W. D. Comstock</i>	1697
Education and Creativity, <i>B. F. Miessner</i>	1697
A Simple Method for the Supervision of the Orbital Period of Artificial Satellites, <i>P. R. Arendt and L. H. Manamon</i>	1698
Comment on "A Theoretical Comparison of Average- and Spot-Noise Figure in Transistor Amplifiers," <i>Paul J. Bénétiau</i>	1699
The Directional Coupler Core of an Arbitrary, Lossless, Reciprocal 4-Port, <i>W. K. Kahn and R. L. Kyhl</i>	1699
Spectral Response of a Nonlinear Device, <i>William B. Ribbens</i>	1700
On a Mathematical Description of Noisy Measurement System Performance, <i>J. L. Hammond, Jr.</i>	1701
The Delta Function and the Fourier Integral, <i>A. W. McMurtry</i>	1702
An Electronically Tunable Up-Converter, <i>George L. Matthaei</i>	1703
The Linearized Transfer Function of a Phase-Locked Loop Containing an IF Amplifier, <i>R. Lawhorn and C. S. Weaver</i>	1704
Infrared Fluorescence and Stimulated Emission of Nd ³⁺ in CaWO ₄ , <i>L. F. Johnson and K. Nassau</i>	1704
Maser Oscillation Observed from HCN Maser at 88.6 kMc, <i>Dietrich Marcuse</i>	1706
High-Speed Silicon Computer Diodes as RF Switches, <i>R. E. Aitchison</i>	1707
Use of a Coherent Memory Filter in Spectral Measurements of Atmospheric Whistlers, <i>J. Capon and M. R. Weiss</i>	1707
Injection Efficiency in Double Diffused Transistors, <i>Melvin Klein</i>	1708
Antenna Size for a Space Vehicle, <i>C. S. Lorens</i>	1708
Input-Output Relationships for Multisampled Loop Systems, <i>George G. Lendaris</i>	1709

REVIEWS

Books:	
"Adaptive Control Processes: A Guided Tour," by Richard Bellman, <i>Reviewed by L. A. Zadeh</i>	1712
"The Physical Theory of Transistors," by Leopoldo B. Valdes, <i>Reviewed by M. A. Clark</i>	1712
"An Introduction to the Principles of Communication Theory," by John C. Hancock, <i>Reviewed by Warren D. White</i>	1713
"Proceedings of URSI Thirteenth General Assembly," John P. Hagen, Ed., <i>Reviewed by E. C. Jordan</i>	1713
"The Antenna," by H. Thourel, <i>Reviewed by Seymour B. Cohn</i>	1713
"Antenna Engineering Handbook," Henry Jasik, Ed., <i>Reviewed by George Sinclair</i>	1714
"Electronic Circuits, Signals and Systems," by S. J. Mason and H. J. Zimmerman, <i>Reviewed by W. H. Huggins</i>	1714
Recent Books.....	1715
Scanning the TRANSACTIONS.....	1715

ABSTRACTS

Abstracts of IRE TRANSACTIONS.....	1716
Abstracts and References.....	1726

IRE NEWS AND NOTES

Current IRE Statistics.....	14A
Calendar of Coming Events and Authors' Deadlines.....	14A
Obituaries.....	15A
Program:	
Seventh Conference on Magnetism and Magnetic Materials.....	16A
Professional Groups, Sections and Subsections.....	22A

DEPARTMENTS

Contributors.....	1710
IRE People.....	44A
Industrial Engineering Notes.....	35A
Meetings with Exhibits.....	8A
Membership.....	92A
News—New Products.....	96A
Positions Open.....	99A
Positions Wanted by Armed Forces Veterans.....	106A
Professional Group Meetings.....	32A
Section Meetings.....	36A
Advertising Index.....	161A

BOARD OF DIRECTORS, 1961

*L. V. Berkner, *President*
 *J. F. Byrne, *Vice President*
 Franz Ollendorff, *Vice President*
 *S. L. Bailey, *Treasurer*
 *Haraden Pratt, *Secretary*
 *F. Hamburger, Jr., *Editor*
 *Ernst Weber
Senior Past President
 *R. L. McFarlan
Junior Past President

1961
 C. W. Carnahan (R7)
 B. J. Dasher (R3)
 A. N. Goldsmith
 *P. E. Haggerty
 C. F. Horne
 R. E. Moe (R5)

D. E. Noble
 B. M. Oliver
 J. B. Russell, Jr. (R1)

1961-1962
 A. B. Bereskin (R4)
 M. W. Bullock (R6)
 A. B. Giordano (R2)
 W. G. Shepherd
 G. Sinclair
 B. R. Tupper (R8)

1961-1963
 E. F. Carter
 L. C. Van Atta

*Executive Committee Members

EXECUTIVE SECRETARY

George W. Bailey
 John B. Buckley, *Chief Accountant*
 Laurence G. Cumming, *Professional Groups Secretary*
 Joan Kearney, *Assistant to the Executive Secretary*
 Emily Sirjane, *Office Manager*

ADVERTISING DEPARTMENT
 William C. Copp, *Advertising Manager*
 Lillian Petranek, *Assistant Advertising Manager*

EDITORIAL DEPARTMENT

Alfred N. Goldsmith, *Editor Emeritus*
 F. Hamburger, Jr., *Editor*
 E. K. Gannett, *Managing Editor*
 Helene Frischauer, *Associate Editor*

EDITORIAL BOARD

F. Hamburger, Jr., *Chairman*
 T. A. Hunter, *Vice Chairman*
 E. K. Gannett
 T. F. Jones, Jr.
 J. D. Ryder
 G. K. Teal
 Kiyoo Tomiyasu
 A. H. Waynick



PROCEEDINGS OF THE IRE, published monthly by The Institute of Radio Engineers, Inc., at 1 East 79 Street, New York 21, N. Y. Manuscripts should be submitted in triplicate to the Editorial Department. Correspondence column items should not exceed four double-spaced pages (illustrations count as one-half page each). Responsibility for contents of papers published rests upon the authors, and not the IRE or its members. All republication rights, including translations, are reserved by the IRE and granted only on request. Abstracting is permitted with mention of source.

Thirty days advance notice is required for change of address. Price per copy: members of the Institute of Radio Engineers, one additional copy \$1.25; non-members \$2.25. Yearly subscription price: to members \$9.00, one additional subscription \$13.50; to non-members in United States, Canada, and U. S. possessions \$18.00; to non-members in foreign countries \$19.00. Second-class postage paid at Menasha, Wisconsin, under the act of March 3, 1879. Acceptance for mailing at a special rate of postage is provided for in the act of February 28, 1925, embodied in Paragraph 4, Section 412, P. L. and R., authorized October 26, 1927. Printed in U.S.A. Copyright © 1961 by The Institute of Radio Engineers, Inc.

Proceedings of the IRE



Poles and Zeros



Ex-Editor Month. IRE celebrates its fiftieth anniversary in 1962. During its half century of existence it has had remark-

ably few Editors, six by actual count. This amazing record is entirely due to the energy, wisdom, and stamina of Alfred N. Goldsmith, Editor Emeritus, IRE Founder, and Charter Member. Dr. Goldsmith served IRE as Editor continuously from 1912 through 1953, with the single exception of the year 1929. The 1929 Editor was W. G. Cady.

Since the year 1953, IRE has been served by a less hardy group. For two-year periods the Editors have been J. R. Pierce, D. G. Fink, J. D. Ryder, and the incumbent. Just to prove that old Editors never stop writing, this month's Poles and Zeros' page comprises items directly attributable to past Editors. The first item to follow was prepared in its entirety by J. D. Ryder, the second results from a communication from J. R. Pierce, and the third from the activity of the Editor Emeritus.

Travel Still Broadens. Under a similar heading we reported in 1958 on a visit to the electronic industry of Japan, and to other oriental points. We return to report once more on travel—this time primarily to India to visit educational institutions.

Our first impression was of people, people everywhere—hands that must be kept busy, and mouths which must be fed. In talking with Indian engineers, and long-time British and American residents, we were told that India is indeed making progress on its population and economic problems. Our second impression was of the excellence of people in government and in the colleges—sure of their direction and that of India. In engineering education there was realization of the need for change, but some doubt as to the methods to be employed in bringing it about.

This doubt was not so apparent at a bright spot in the educational field—the Indian Institute of Science at Bangalore. We were taken in hand by Dr. S. V. C. Aiya, head of Electronics and Communications, and also immediate past president of the Institute of Telecommunications Engineers of India. A fast tour revealed excellent research facilities and plans for more. Areas of activity included atmospheric noise, artificial dielectrics, surface-wave transmission, information content of languages (for which India provides ample material), and some very pure acoustic-research on the Indian drum. We say pure, since the results are not likely to be applied to drum design, especially when the research shows the design produced by 2000 years of empirical effort to be correct!

Being a professor—part time—we willingly accepted Dr. Aiya's invitation to address a meeting of students, faculty, and Bangalore communications engineers, and we can at least report that the event was enjoyed by the speaker.

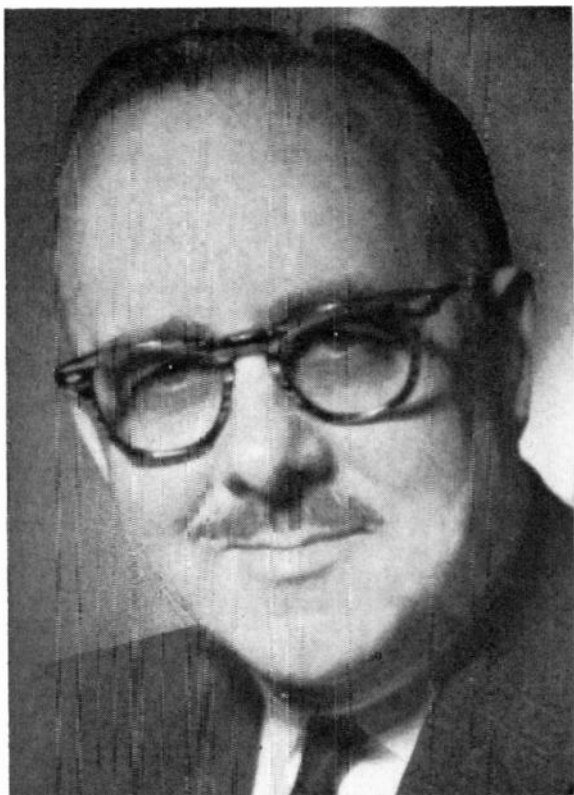
Bombay, Madras, Calcutta, Delhi all were points of educational interest and the Taj Mahal surpassed all words or pictures. We returned ready to go again.—J.D.R.

Editorial Faux Pas. Ex-Editor J. R. Pierce wrote, in a letter to President Berkner: "People who write papers want to see them in print as soon as possible. People who read papers find them most valuable when they are freshest. Editors, editorial staff, and reviewers of the IRE know this, and they mean to act promptly and sensibly. Usually they succeed. But, the price of promptness is eternal vigilance. I think it is salutary to consider what can (and did) happen to one good paper."

The letter then contains ten indictments of the editorial procedure and the crucial statement: "In short, it took 21 months for a good paper to get from submission to acceptance for publication." The Editor, the Managing Editor, and the IRE publication staff express sincere regret to the rightfully offended author. Ex-Editor Pierce concluded his letter: "Please, reviewers, editors, and staff, this shouldn't happen to even a dog of a paper." Speaking for the editors and the staff—we heartily agree. Speaking to the reviewers—we urge careful consideration and promptness in handling papers submitted for review.

There is no point in reiterating the details of the indictments. Those aspects that can be corrected in the editorial department routine have been corrected; at least we sincerely hope they have. The point that must be emphasized, however, is that all those who handle manuscripts for review should give them priority in handling—treat them as if they represented your own submission!

Anniversary Issue. Editor Emeritus Goldsmith, having accepted the appointment as Editor of the Anniversary Issue, has attacked the task with his usual vim and vigor. This issue, to appear in May, 1962, will be truly an outstanding one. It will comprise, exclusively, invited papers prepared by the most distinguished members of IRE. The issue will present papers giving the evolution, present status, and future trends as well as certain original contributions in the fields of each of the twenty-eight Professional Groups. There will also be a brief presentation of IRE, its past, present, and future together with a symposium of predictions "Communications and Electronics—2012 A.D." This one thousand page volume will be a fitting climax to IRE's first half century.—F. H., Jr.



M. W. Bullock

Director, 1961–1962

Mark W. Bullock (S'33-A'37-M'45-SM'54) was born in West Winfield, N. Y. on August 20, 1911. He received the B.A. degree in 1933 and the B.S.E.E. degree in 1934, both from the University of Nebraska in Lincoln.

From 1934 to 1937, he was Transmitter Supervisor for KOIL, Omaha, Nebr.; from 1938 to 1944, he was Technical Director of KFAB, Omaha, and KFOR, Lincoln. He was Chief Engineer of KFNF, Shenandoah, Iowa, from 1948 to 1951. During World War II, he designed shortwave transmission facilities for the Bureau of Communications Facilities, Office of War Information, Washington, D.C.

He joined Continental Electronics Manufacturing Company, Dallas, Tex., in 1951 and was in charge of the design of broadcast transmitters. He became Engineering Manager in 1953. The manufacture of BMEWS radar transmitters required the establishment of a separate Production Division, and he was Manager of this operation from 1958 to 1960. He is now Vice President for Engineering, and in this position he is Engineering Manager, directing the design and development of super-power radio and radar transmitting equipment. This includes the BMEWS surveillance and tracker radars and the Nike Zeus acquisition radar.

His IRE activities include having been the first Chairman of the Omaha-Lincoln Section, 1948–1959. In the Dallas-Fort Worth Section he has served as Secretary-Treasurer, 1953–1954; Vice Chairman, 1954–1955, and Chairman, 1955–1956. The Southwest IRE Conference elected him Chairman of the Board of Advisors for 1956–1957. In the Dallas Section, he has served as Professional Group Advisor, 1956–1957; Nominating Committee, 1957–1958 and 1958–1959; SWIRECO Section Co-ordinator, 1959; SWIRECO Board of Advisors, 1959–1961.

He holds patents covering a cabinet design for transmitting equipment and the screen modulation-regulation circuit used in Continental Electronics transmitters.

Mr. Bullock is a member of AIEE, Texas Society for Professional Engineers, National Society of Professional Engineers, and he is a Registered Professional Engineer in the States of Nebraska and Texas.

Scanning the Issue

The Cryosistor: A Field-Effect Controlled Impact Ionization Switch (Melngailis and Milnes, p. 1616)—When a semiconductor is subjected to very low temperatures (about 4° K), a small applied voltage will cause a rapid ionization of impurities, resulting in an avalanche breakdown. This phenomenon, known as impact ionization, has been employed lately in the development of several novel cryogenic devices. Notable among these is the cryosar, a two-terminal computer switch and memory element described here two years ago. Since then it has been found that the breakdown in compensated germanium is filamentary in nature, that is, before breakdown the current is distributed throughout the bulk of the material but after breakdown it is confined to an ionized filament of very small cross section. This discovery has now led to the development of a new three-element switch, called the cryosistor, in which the ionization process, because it is restricted to a small region, can be field-effect controlled by the third element. The many interesting properties of the new device suggest a variety of applications, including memory, logic and counter elements for computers as well as pulse amplifiers and thyratron-type trigger circuits.

A New Semiconductor Tetrode—The Surface-Potential Controlled Transistor (Sah, p. 1623)—In the preceding paper a field-effect electrode was added to a device to control internal phenomena; in this paper a field-effect electrode has been added to control surface phenomena. The device in question is a common planar transistor to which a fourth electrode has been affixed to the oxide which covers the surface of the emitter-base junction. The result is a tetrode device in which the additional terminal serves as a grid to control the surface potential, surface recombination rate and the size of the surface channel, and thereby the current gain of the transistor. Thus, we have a new family of semiconductor devices which, thanks to the additional control element, can provide heretofore unobtainable electrical performance.

The Pulsed Ruby Maser as a Light Amplifier (Kisliuk and Boyle, p. 1635)—The successful operation of optical maser oscillators has left no doubt that the gain of a maser is sufficient to make up for losses at the end mirrors. However, past experiments have given no independent measurement of the gain or loss separately. The difficulty in observing amplification directly is that of distinguishing coherent maser light from the natural fluorescent light of the maser. The authors have solved this difficulty by generating a coherent light which was so bright that the amount of fluorescence was small by comparison. They accomplished this by setting up two ruby masers in tandem. The output of one maser, operating as an oscillator, was beamed into the other, operating as an amplifier. Amplification of light by a factor of two was observed. This is the first published description of an optical maser experiment designed to observe and measure such large amplification directly.

Inductance in Thin-Film Superconducting Structures (Meyers, p. 1640)—There is widespread interest today in thin-film superconducting components and circuits for digital computers. Much of the attention to date has been focused on new devices or circuit arrangements and on fabrication techniques. This paper deals with another important aspect of the subject, namely, methods of evaluating the electrical characteristics and behavior of such components and circuits. Most components and their associated interconnections take the form of coupled strip-transmission lines, with resistance, inductance and capacitance all entering into the behavior of such structures. The author's chief interest here is the inductance because it is the most difficult parameter to calculate and plays a dominant role in determining the gain and bandwidth of the circuitry. Among other things he

points out the considerations that are necessary and sufficient for calculating inductances up to about 1 kMc and the pitfalls of using the familiar flux-per-unit-current definition of inductance. Device designers will be particularly interested in the relatively simple formula which the author develops for calculating the inductance of a strip line.

Reduction of the Frequency-Temperature Shift of Piezoelectric Resonators by Mechanical Stress (Gerber and Miles, p. 1650)—It has been known for several years that the frequency of a quartz resonator can be changed by applying external pressure to the crystal. The authors have succeeded in utilizing this effect to counteract, and thus drastically reduce, frequency shifts which result from changes in temperature. The applied pressure must, of course, be made a function of temperature. This is accomplished by attaching bimetallic strips at selected spots on the circumference of the crystal disk. This technique represents an outstanding advance in practical frequency control methods. It will make it possible to achieve a high degree of frequency stability without using crystal ovens, an advantage of considerable practical importance in military and satellite applications where space and power are at a premium.

Fundamental Limitations to Optical Doppler Measurements for Space Navigation (Norton and Wildey, p. 1655)—Last year in the Space Electronics Issue of the PROCEEDINGS it was suggested that a spacecraft might obtain midcourse navigational guidance by performing optical Doppler measurements of astronomical objects to determine the spacecraft's velocity. This paper examines the accuracy with which such measurements might be made. The author first considers the maximum Doppler variations that might be caused by various physical mechanisms at work in the stellar atmosphere and then examines the accuracy of present-day measuring equipment. His results shed considerable light on the principal causes of inaccuracy, revealing that the stellar variations rather than the measuring instruments pose the major problem, and, indirectly, underscoring the importance of developing integration techniques to modify the effects of such variations.

Timing Potentials of Loran-C (Doherty, *et al.*, p. 1659)—This paper describes a highly accurate pulse navigation system operating on a basic frequency of 100 kc. The system consists of a master station and two or more slave stations, with the slave station clocks synchronized to the master station clock. An outstanding feature of the system is the accuracy with which the several clocks in the system are synchronized with one another—an accuracy of better than one microsecond. This makes it possible for the system to provide both position and time with great precision over wide areas. Loran-C will find many important applications in the future. Among the many possibilities are providing precise time for large areas of the world, determining the position of aircraft, missiles, satellites, thunderstorms and nuclear detonations, surveying remote areas, and measurement of various radio propagation phenomena.

A Provisional Ground Conductivity Map for Canada (Ireland, p. 1674)—On January 1 of this year the Department of Transport in Ottawa issued a new ground conductivity map for Canada. The map, together with a discussion of how it was derived, is presented in this paper. The word "provisional" in the title indicates that this map, when used in conjunction with the U. S. ground conductivity map (published in the September, 1954 PROCEEDINGS), produces a few anomalies along the U. S.-Canadian boundary which will be mutually resolved at a later date. The numerical data provided by the map will be of value to those concerned with the propagation of radio waves in Canada.

The Cryosistor—A Field-Effect Controlled Impact Ionization Switch*

I. MELNGAILIS†, MEMBER, IRE, AND A. G. MILNES‡

Summary—The cryosistor is a new three-terminal device in which the low-temperature (4.2°K) impact ionization of impurities in germanium is controlled by means of the depletion field effect of a reverse-biased p - n junction. Compensated germanium has an inherent bistable voltage-current characteristic at liquid helium temperature. With such a material, bistable switching by means of pulses applied to the gate-junction located between two ohmic contacts is shown to be possible. The critical gate voltages may be calculated from elementary consideration and a wide range of values of the switching voltages, as well as power dissipation, is shown to be possible with suitable choice of material and physical dimensions. The switching speed is basically limited by the ionization and recombination times of the bulk material and may be as fast as a few nsec, depending upon the amplitude of the switching pulse.

Possible applications of the device at 4.2°K include computer components such as binary counters, logic functions, and memory arrays, in addition to pulse amplifiers and trigger circuits of the thyatron type. The localized nature of the ionization should permit the construction of a large number of independent cryosistors on a single germanium wafer.

INTRODUCTION

THE cryosar, a previously described two-terminal computer switch or memory element,¹ depends for its action on the bulk voltage-current characteristics resulting from impact ionization in germanium at 4.2°K. In this device partially compensated germanium provides the possibility of bistable operation, since the ionization breakdown is followed by a drop of voltage with increasing current (negative resistance). Recent experiments have indicated the filamentary nature of the breakdown in compensated germanium.² The current before breakdown is distributed throughout the bulk, but after breakdown, conduction occurs in an ionized filament of a very small cross section. The size of the ionized region has been studied in cylindrical field-effect structures in which the diameter of the conduction channel can be reduced by reverse biasing a ring-shaped p - n junction alloyed around a small cylindrical bar.³

* Received by the IRE, July 7, 1961; revised manuscript received, September 1, 1961. This work represents partial fulfillment by Melngailis of requirements for the Ph.D. degree at Carnegie Institute of Technology, Pittsburgh, Pa. Financial support was received in part from the Office of Naval Research, Contract Nonr 760(09).

† Now at Lincoln Laboratory, Lexington, Mass.

‡ Carnegie Institute of Technology, Pittsburgh, Pa.

¹ A. L. McWhorter and R. H. Rediker, "The Cryosar—A new low-temperature computer component," *Proc. IRE*, vol. 47, pp. 1207–1213; July, 1959.

² A. L. McWhorter, "Impact Ionization of Impurities in Compensated Germanium," M.I.T. Lincoln Lab., Cambridge, Mass., Rept. 85 C-006; August, 1960.

³ "Filamentary Impact Ionization in Compensated Germanium at 4.2°K" (paper in preparation).

An interesting consequence of this filament study has been the discovery that cylindrical or planar field-effect devices made of compensated germanium offer new and worthwhile three-terminal properties at 4.2°K. The name "cryosistor" has been given to this class of device structure.

STATIC CHARACTERISTICS

In unipolar (field effect) transistors,^{4,5} a reverse bias applied to a junction depletes carriers from a region under the junction forming a space-charge layer. The depletion region is found to be very nearly the same at liquid helium temperature as at room temperature since fields near the junction are sufficiently large to deplete bound carriers from the impurity level at low temperatures. Thus, in a unipolar transistor configuration, the biased junction provides an insulating layer which can prevent the formation of an ionized filament between the "drain" and "source" ohmic contacts.

For ease of fabrication, most of the structures investigated here are in the form of rectangular wafers of n -type compensated germanium ($\rho = 6.5$ ohm-cm, $N_D = 2.25 \times 10^{15}$ cm⁻³, and $n_A = 2.0 \times 10^{16}$ cm⁻³), with two ohmic contacts and a long indium-alloyed junction on one face [Fig. 1(a)]. The wafer under the junction is etched thin electrolytically, so that this region can be depleted of carriers at a desired reverse bias of the junction.

Fig. 1(b) shows the dc circuit of a cryosistor with the gate voltage V_g and current I_g , the drain voltage V_d and current I_d and the source current I_s . The operation of a cryosistor can be understood in terms of the schematic representation of its characteristics in Fig. 1(c) which shows the variation of drain current I_d with drain voltage V_d at different values of gate bias V_g . With $V_g = 0$, the drain has the bistable characteristic of the bulk material with a breakdown voltage V_B , breakdown current I_B , sustaining voltage V_H , and sustaining current I_H . For $V_g > 0$, the drain current saturates as the channel is pinched off, before or after ionization in the channel, depending on the value of V_g . The total reverse bias of the junction near the drain is the sum of the externally applied voltage V_g and the voltage drop across parts d_j and d_s . The length d_s is chosen so that this voltage drop is an

⁴ W. Shockley, "A unipolar 'field-effect' transistor," *Proc. IRE*, vol. 40, pp. 1365–1376; November, 1952.

⁵ G. C. Dacey and I. M. Ross, "Unipolar 'field-effect' transistor," *Proc. IRE*, vol. 48, p. 970–979; August, 1953.

appreciable fraction of the junction voltage at which the channel is pinched off. Because of the bistable voltage-current characteristic of the channel material, the voltage across d_s is greater just before breakdown than after breakdown. This implies that within a certain range of values of the applied voltage V_g , the drain circuit may have a different characteristic curve for the same V_g , depending on the order in which V_g and V are applied.

For example, if V_g is set at V_{g0} and V is then increased to $V_0 > V_B$ (where V_B is the breakdown voltage of the undepleted channel), no breakdown occurs since the drain current saturates at a value which is less than the current necessary for ionization [Fig. 1(c), point 1]. If V_g is now reduced to $V_{g2} < V_{g0}$, thereby increasing the saturation current to I_B , the channel ionizes and the drain current shifts along the load line to point 3. The total junction voltage now is reduced because the voltage across d_s has dropped. In order to cause the channel to de-ionize and return to the high-impedance region, V_g has to be increased to a value $V_{g1} > V_{g0}$ (point 4), to reduce the saturation current below the value necessary to sustain an ionized filament. The de-ionization is accompanied by an increase in the total junction voltage, and the drain current decreases to the value at point 5.

This indicates the possibility of bistable switching by means of pulses applied to the gate. With $V_g = V_{g0}$, a positive voltage pulse will cause ionization and a jump from point 1 to 6. To return the drain current to 1, a negative pulse is required.

The critical values of the gate voltage V_{g1} and V_{g2} , which determine bistable operation can be calculated with an accuracy somewhat better than 10% by simply considering the voltages which make up the total junction voltage at points 2 and 4. If at 2 the junction voltage near the edge of the junction close to the drain is W_2 (the value which causes the drain current to saturate just at the breakdown current I_B), then W_2 is the sum of V_{g2} and the appropriate fraction of the drain voltage, determined by the location of the gate along the bar:

$$W_2 = V_{g2} + \frac{d_s + d_j}{d_t} V_B \tag{1}$$

Similarly, at point 4 there is a value W_1 with a saturation current just equal to the minimum required to sustain ionization:

$$W_1 = V_{g1} + \frac{d_s + d_j}{d_t} V_H \tag{2}$$

Experiments with a number of cryosistors have shown W_1 and W_2 to be nearly equal, when estimated from (1) and (2), as shown in Table I. This may be expected, considering that a certain minimum cross section (10^{-6} cm²) of undepleted material is necessary for an ionized filament to form and to be sustained. Consistent with this consideration, the values of W_1 and W_2 in most cases are somewhat lower than the pinchoff voltages W_0 measured in liquid nitrogen.

Setting $W_1 = W_2 = W_k$, the two critical values of V_g are

$$\begin{aligned} V_{g1} &= W_k - (d_s + d_j) E_H \\ V_{g2} &= W_k - (d_s + d_j) E_B \end{aligned} \tag{3}$$

and

$$V_{g1} - V_{g2} = \Delta V_g = (d_s + d_j)(E_B - E_H),$$

where E_B and E_H are the breakdown and sustaining fields, respectively, and are characteristic of the channel material.

For most purposes it is sufficient to assume $W_k = W_0$ and to evaluate the latter at room temperature using results derived previously for an abrupt depletion layer:⁴

$$W_0 = \frac{1}{2} \frac{a^2}{\rho \mu \epsilon} \tag{4}$$

where a is the thickness of the wafer under the junction in cm [Fig. 1(a)], ρ is the room temperature resistivity in ohm-cm, μ is the majority carrier mobility in cm² volts⁻¹ sec⁻¹ and ϵ is the dielectric constant in farads cm⁻¹.

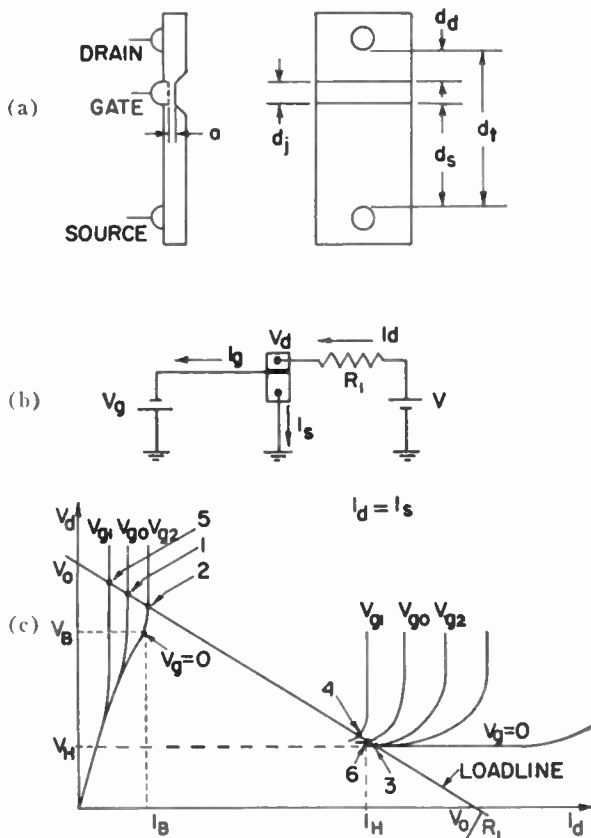


Fig. 1—(a) Top and side views of an experimental cryosistor showing the gate-junction and the drain and source ohmic contacts. (b) The dc circuit used with a cryosistor indicating the proper polarities of applied voltages. (c) Schematic representation of the drain characteristics before and after breakdown. A typical loadline with reference to the circuit of (b) is shown.

TABLE I
PROPERTIES OF CRYOSISTORS*

No.	Dimensions [Fig. 1(a)]				Break-down Voltage V_B	Sustaining Voltage V_H	Critical Gate Voltages		Junction Voltages calculated from V_{g1} and V_{g2}		Pinchoff Voltage at 77°K W_0
	a (cm)	d_d (cm)	d_j (cm)	d_s (cm)			V_{g1}	V_{g2}	W_1	W_2	
C1	1.6×10^{-3}	9.1×10^{-2}	4.1×10^{-2}	20.6×10^{-2}	34	19	21	12	36	37	37.4
C2	1.5×10^{-3}	8.2×10^{-2}	4.6×10^{-2}	21×10^{-2}	32	17	17	7.8	30	31	33.3
C3	1.8×10^{-3}	8.2×10^{-2}	4.6×10^{-2}	21×10^{-2}	33	17	38	29	52	54	55
C4	8.0×10^{-2}	8.0×10^{-2}	6.0×10^{-2}	21.8×10^{-2}	32	18	0.7	-10	15	15.5	17.2
T2		4.3×10^{-2}	1.8×10^{-2}	5.8×10^{-2}	15	9	1.4	-1.8	7.3	8.1	8.13

* C1 to C4 are planar structures with $\rho(300^\circ) = 6.5$ ohm-cm, $N_D = 2.25 \times 10^{15}$ cm $^{-3}$, $N_A = 2 \times 10^{16}$ cm $^{-3}$. T2 is cylindrical in shape with a channel diameter of 3.3×10^{-3} cm, $\rho(300^\circ) = 15$ ohm-cm, $N_D = 1.0 \times 10^{15}$ cm $^{-3}$, and $N_A = 0.9 \times 10^{16}$ cm $^{-3}$.

Fig. 2 shows a plot of drain voltage before and after breakdown in the channel as a function of drain current for cryosistor C1 with the gate voltage as a parameter. The resistance of the channel before breakdown is seen to be quite nonlinear. At currents near breakdown the nonlinearity is a bulk effect resulting from partial ionization, since it has been observed in wafers as well as bars.¹ For lower currents surface leakage may be an important factor because the surface to volume ratio is large.

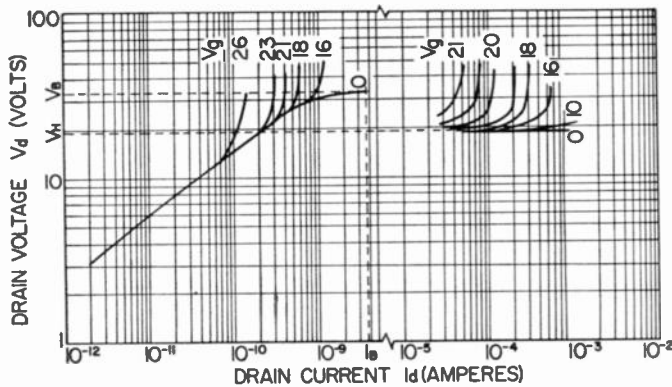


Fig. 2—Drain voltage as a function of drain current in cryosistor C1 with the gate voltage as a parameter before and after ionization in the channel.

The characteristics after breakdown have a slope of zero for values of gate bias not too close to the pinch-off voltage since the drain voltage begins to increase only when the ionized filament has spread over the available channel. Accurate calculation of the characteristics is difficult to make in planar structures, because the ionized filament is restricted by the depletion layer only in one dimension, permitting a further spreading parallel to the gate junction. The gate characteristics indicate a very low reverse leakage current ($< 10^{-10}$ amp) for the junction at low voltages (< 30 volts).

DESIGN CONSIDERATIONS

From (3) and (4) the critical voltages V_{g1} and V_{g2} are determined by device dimensions and the breakdown and sustaining fields of the material. This allows for

considerable flexibility in design, particularly because the breakdown fields are found to vary between 10 and 200 volts/cm.

In an example of a low-power design consider a compensated material with $E_B = 140$ v/cm and $E_H = 35$ v/cm. Then (3) and (4) give $V_{g1} = 0.54$ volt and $V_{g2} = -0.54$ volt for the dimensions $a = 3 \times 10^{-4}$ cm, $d_t = 1.5 \times 10^{-2}$ cm, $d_j = 0.4 \times 10^{-2}$ cm and $d_s = 0.6 \times 10^{-2}$ cm. The estimated minimum power consumption in the "on" state is about 1.6 microwatts, which could be tolerated in large arrays. The 3-micron active layer could be vapor-grown on a thicker wafer of germanium with a higher breakdown field to act as an effective insulator. [Such an arrangement is suggested in Fig. 10(a) in connection with a proposed memory array.] The voltages V_{g1} and V_{g2} can be chosen equal and of opposite sign to avoid the necessity of an external gate bias for bistable operation.

DYNAMIC CHARACTERISTICS

Measuring System

The response speed of bistably operated cryosistors was studied in the circuit of Fig. 3. Coaxial 50-ohm cables, terminated with 50-ohm resistors in all pulsed parts of the circuit, were used as transmission lines to the device in the helium Dewar flask. The drain and the gate were biased with $V_d > V_B$ and V_{g0} such that $V_{g2} < V_{g0} < V_{g1}$. The 0.1- μ f capacitors serve to isolate the dc bias. Resistors R_1 and R_2 (10 to 100 K Ω) were used to establish the drain loadline and to isolate the drain from the biasing cable and the voltage probe. A single pulse from a mercury relay pulse generator (rise time < 0.5 nsec) was reflected from a shorted cable (C) to provide a turn-on pulse followed by a turn-off pulse after a time equal to twice the transit time of the cable length (about 100 nsec for the traces of Fig. 4, for example). For an off-on switching sequence the polarity of the input pulse was simply reversed. The resulting current pulse i_s was observed by means of a type-555 Tektronix dual-beam oscilloscope. The entire pulse was displayed by one of the beams using a type-L high-sensitivity preamplifier, and the rise and fall times were measured by means of a type-N sampling unit used with the other beam.

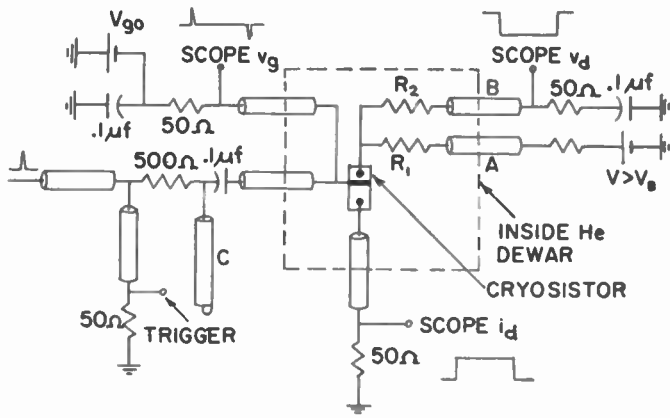


Fig. 3—Circuit for measuring cryosistor switching speed.

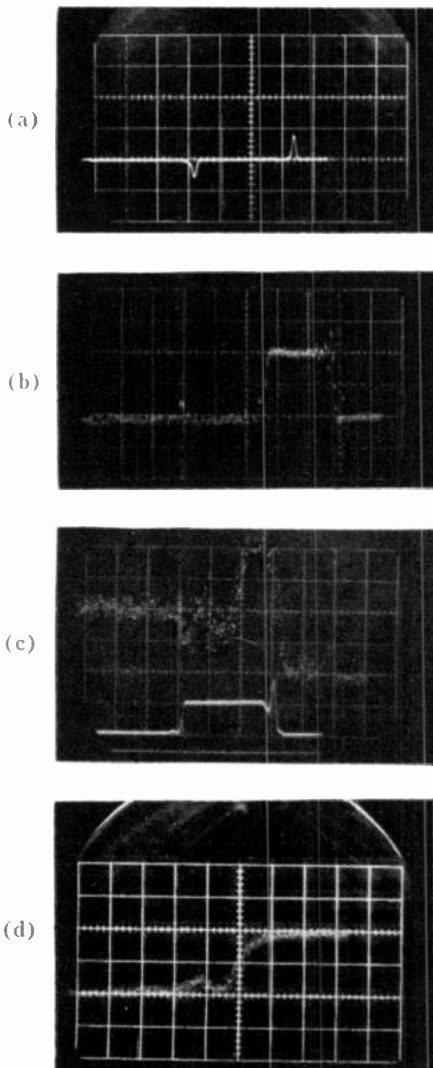


Fig. 4—Switching response of cryosistor C1. (a) 10-nsec switching pulses applied to gate (time increases to left). Vertical scale, 0.5 volt per large division. Horizontal scale, 100 nsec per division. (b) Positive switching pulse displayed by sampling unit indicates rise-time limitation of preamplifier to be about 10 nsec. Vertical scale, 2 v per division. Horizontal scale, 5 nsec per division. (c) Lower trace is the resulting pulse of cryosistor source current. Vertical scale, 0.4 ma per division. Horizontal scale, 100 nsec per division. Upper trace shows detail of current rise. Vertical scale, 0.2 ma per division. Horizontal scale, 10 nsec per division. (d) Detail of current fall. Vertical scale, 0.2 ma per division. Horizontal scale, 1 nsec per division.

Rise Time

The voltage pulses applied to the gate and the resulting source current as functions of time in sample C1 with biasing values $V_{g0}=17$ volts and $V=45$ volts are shown in the oscilloscope traces of Fig. 4. The captions under each photograph explain the parameters for each trace.

The switching operation can be understood in terms of the equivalent circuit of Fig. 5. The depletion capacitance of the junction C_j is of the order of $10 \mu\mu\text{f}$ from room temperature measurements. This should be the same in liquid helium, since the depletion layer is unchanged, judging from the similarity of helium and room temperature pinch-off voltages. R_d and R_s represent portions of the channel on the drain and source side of the junction respectively. L_d , L_g and L_s are small lead inductances. Because of the large value of the resistance R_s before breakdown (5×10^9 ohms) the incoming switching pulse bypasses the junction impedance and appears across R_s for a time sufficient to trigger the breakdown of R_s . Thus the switching speed is limited by the impact ionization process rather than by circuit parameters.

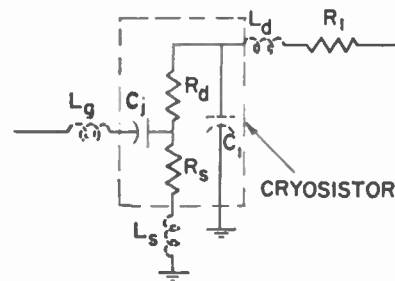


Fig. 5—Equivalent circuit of the cryosistor, showing capacitance of junction C (typically about $10 \mu\mu\text{f}$), bulk resistances R_d and R_s on the drain and source side of the junction, respectively; stray lead inductances L_g , L_d , and L_s ; contact and lead capacitance C_1 , and external resistance R_1 (10 to 100 K ohms).

A small induced pulse marks the beginning of the switching pulse in Fig. 4(c) [upper trace]. This is followed by an apparent delay of about 15 nsec, after which the current rises with an overshoot above the steady-state value. As in other impact ionization devices,¹ the current rise time is inversely related to the amplitude of the switching pulse. However, if pulses which are too large (>10 volts) are supplied to the gate, spurious switching results from oscillations associated with the small lead inductances and device capacitances. Some improvement can be expected if the lead length (about 2.5 cm in the present case) is reduced or eliminated by a different method of mounting, such as incorporating the device in a stripline. Decreased junction area, and hence lower junction capacitance, should also help to prevent oscillations. To assist in estimating ultimate limitations to cryosistor switching speed, current rise times were measured in a small two-terminal bar (length 0.56 mm, square cross-sectional area $1.3 \times 10^{-3} \text{ mm}^2$) and in cryosistor C1 with the gate contact disconnected and the

voltage pulse applied between the drain and source contacts. The rise time (up to 90 per cent of the final value) is plotted in Fig. 6 as a function of the overdrive ratio $(V - V_B)/V_B$. Curves 1 and 2 are for cryosistor C1 and the bar, respectively, and the slopes are -0.96 and -0.84 , *i.e.*, sufficiently close to -1 to suggest inverse proportionality between rise time and overdrive:

$$\frac{1}{\tau} \sim \frac{V - V_B}{V_B}$$

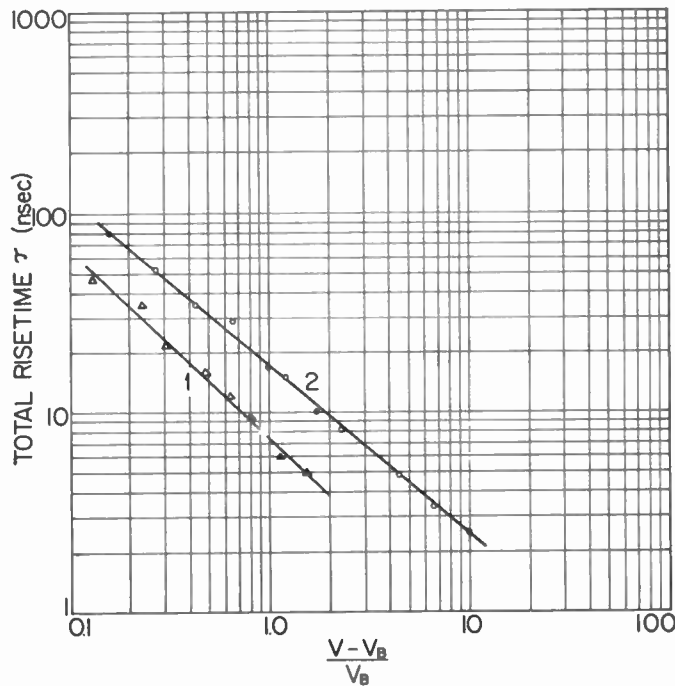


Fig. 6—Total current rise time (measured to 90 per cent of the final value) as a function of the pulse voltage in excess of the breakdown voltage. Curves 1 and 2 are for the channel of cryosistor C1 and for a two-terminal bar respectively.

Such a relation has been found previously in two terminal wafers.⁶ The difference in magnitudes of curves 1 and 2 may be a result of differences in material. Fig. 6 indicates that, with high overdrive rise times as short as a few nsec are possible. To predict the approximate rise time in the three-terminal circuit from this graph, the voltage appearing across R_s (Fig. 5) for the duration of the gate pulse must be considered. Since the dc voltage in R_s before switching is nearly equal to the breakdown voltage, the overdrive voltage is just the switching pulse amplitude. On this basis, a rise time of 24 nsec may be predicted from Fig. 6 for test conditions that actually result [Fig. 4(c)] in a rise time of about 20 nsec. A faster rise could be expected in the three-terminal operation because, here, the ionization is aided by the large value of drain bias, once the gate pulse initiates an avalanche.

⁶ R. C. Johnston, "Considerations in the Design of a Random-Access Cryosar Memory," MIT Lincoln Lab., Cambridge, Mass., Rept. 536-0039; July, 1960.

Fall Time

In the turn-off operation a negative gate pulse reduces the current in R_s below the sustaining current and R_s switches to the high impedance state. This results in an increasing of junction bias sufficient to pinch off the channel. The fall time of the current, observed in Fig. 4, is not more than 1 nsec long. As this is comparable with the response time of the external circuit and the sampling system without the specimen present, it appears that the cryosistor recovery time is faster than can be observed with these measuring techniques.

Measurements of recombination transients in two-terminal bars of the same material showed maximum time constants of about 5 nsec as compared to 80 nsec published for uncompensated germanium.⁷ It is to be expected that recombination should be faster in compensated crystals because of a larger density of recombination centers resulting from compensation.

The fact that the recovery time in the cryosistors made from this material appears to be even faster than 5 nsec is attributed to the lower current level and the large amplitude switching pulse in this device.

APPLICATIONS

The bistable operation of the cryosistor suggests its use as a fast three-terminal memory element. In addition, the combination of gating control and the naturally bistable drain characteristic allows a variety of other circuit functions. In addition to bistable switching, monostable operation is also possible with a sufficiently large gate bias. This implies the possibility of simple pulse amplification where this is required at cryogenic temperatures.

Some proposals for circuit applications are presented in the remainder of the paper.

"Thyratron" Operation

If the load line of the drain circuit intersects the negative resistance region of the voltage-current characteristic [line 1 in Fig. 7(a)], the channel will not stay ionized in the steady state, but relaxation oscillations associated with stray capacitance (C_d) will normally result. Attempts to stabilize the circuit have failed. If, however, the gate is biased between the two critical values $V_{\phi 1}$ and $V_{\phi 2}$ [see (3)], and a small positive pulse is applied to the gate to cause breakdown, then the ionization will be sustained only during one discharge of the drain capacitance. As soon as the drain current falls below the sustaining value I_H the channel switches back to its high impedance state and stays there because the increased junction voltage pinches off the channel. The path of this cycle is indicated in Fig. 7(a). The length of the discharge can be increased by adding an external capacitance, for example in Fig. 7(b), in the form of a transmission line.

⁷ S. H. Koenig, "Recombination of thermal electrons in *n*-type germanium below 10°K," *Phys. Rev.*, vol. 110, pp. 988-990; May 15, 1958.

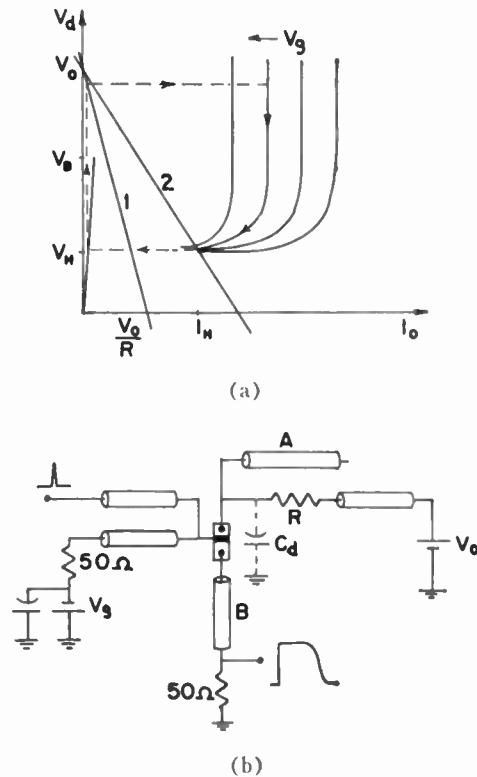


Fig. 7—"Thyratron" switching of a cryosistor. (a) Drain characteristics with steady-state loadline: 1) for "thyratron" operation, and 2) for pulse amplification. (b) "Thyratron" circuit with discharge line A.

Tests with this circuit have borne out the predicted operation. While the rise time of the output pulse is limited by impact ionization, the fall time is determined by the RC time constant of the drain circuit (including line A), since the device resistance $R_d + R_s$ is larger than the characteristic impedance of the discharge line.

Pulse Amplification

To amplify pulse voltages, the gate is biased for monostable ($V_g > V_{g1}$) switching with the loadline of the drain intersecting the drain characteristic at a stable point [line 2 in Fig. 7(a)]. Then a positive ionizing pulse at the gate causes a drop in the drain voltage of magnitude $V_0 - V_H$ for the duration of the pulse and so results in a large negative output pulse. Since V_H is a constant parameter of the device, the amplitude of the output depends on V_0 , which is limited only by the reverse breakdown of the gate junction (typically larger than 100 volts for good junctions). The minimum required amplitude for the switching pulses depends largely on the breakdown field of the material and on the device dimensions. This could be reduced to a fraction of one volt with suitable design.

Logic Functions

In monostable operation the cryosistor can also perform the function of a simple gate, whereby strongly localized conduction after ionization provides the possibility of fabricating arrays of cryosistors on the same

wafer without harmful interactions. Fig. 8(a) shows a proposed OR gate where the junction strips are made long compared to the channel length to prevent undesired breakdown. A positive pulse to any of the four gate junctions causes an output signal to appear. A possible configuration for an AND gate is indicated in Fig. 8(b). The number of inputs here may be limited by the voltage drop in the channel.

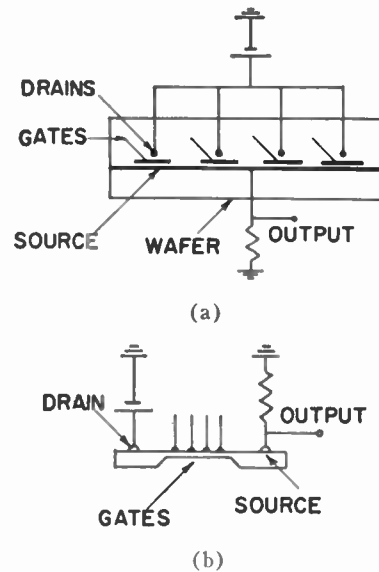


Fig. 8—Examples of cryosistor logic structures. (a) OR gate. (b) AND gate.

Counter Circuits

Two bistable cryosistors can be combined in the circuit of Fig. 9(a) to produce a flip-flop for a conventional binary counter. A positive pulse at the gate of each cryosistor can cause breakdown in the channel and a downward shift along the loadline from V_0 to V_H in Fig. 9(b), whereas a negative pulse is followed by an upward shift.

To understand the flip-flop operation, assume that unit A is in the ON state while B is on the OFF state. Then the voltages at points 1 and 2 are V_H and V_0 respectively. If a negative pulse is now applied to the input I, the pulse will appear at point 2 (since B presents a high impedance) and cause de-ionization in A. This, in turn, results in an increase of the voltage at 1 from V_H to V_0 and a positive ionizing pulse appears at the gate of B. By contrast, a positive pulse of the same magnitude in the input does not cause switching because only a fraction of it appears at the gate of the deionized unit since the pulse is attenuated by the other unit, which is ionized.

Connecting a number of such flip-flops in series results in a binary counter. The wave shapes of Fig. 9(c) result because each stage is switched only by the negative output pulses of the preceding one. The resistors R_0 may be needed to provide a discharge path for the coupling capacitors.

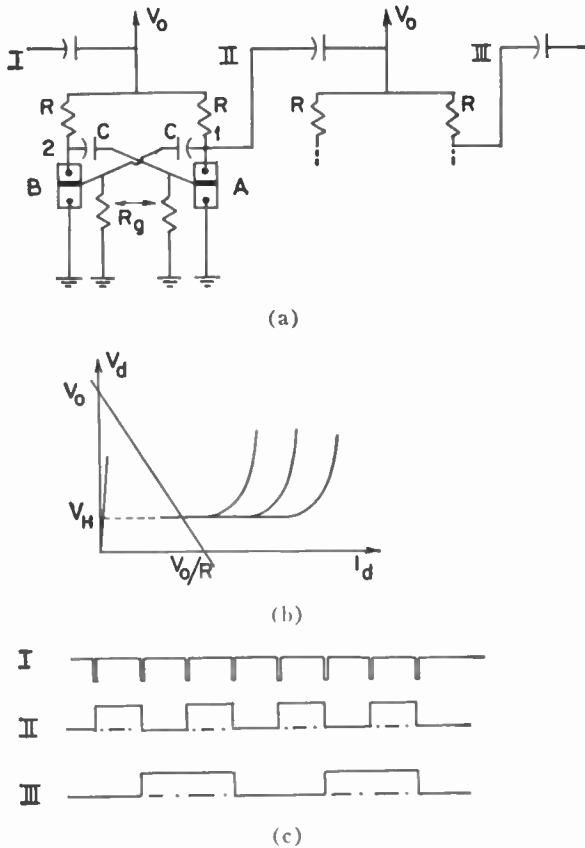


Fig. 9—Circuit and waveshapes of a binary counter resulting from a series connection of cryosistor flip-flops.

If the two gates *A* and *B* are biased sufficiently to prevent ionization in the steady state, the basic circuit should operate as a free running multivibrator with a square-wave output and a period determined by the R_0C time constant.

Cryosistor Memory

The bistable characteristic of compensated germanium has already been used in designing the two-terminal random-access cryosar memory.^{1,6} A three-terminal cryosistor memory may have some advantage in improved stability at the expense of a somewhat more complex array such as in Fig. 10(a). Coincident switching can be achieved by a positive pulse to all the gates of a column (word line) and a negative pulse to the common source of a row (digit line) in Fig. 10(b). The total gate voltage at the coincident element is the sum of the two pulses and switching occurs along the solid loadline of Fig. 10(c). A nondestructive readout is obtained by a positive pulse to the drain contacts of a

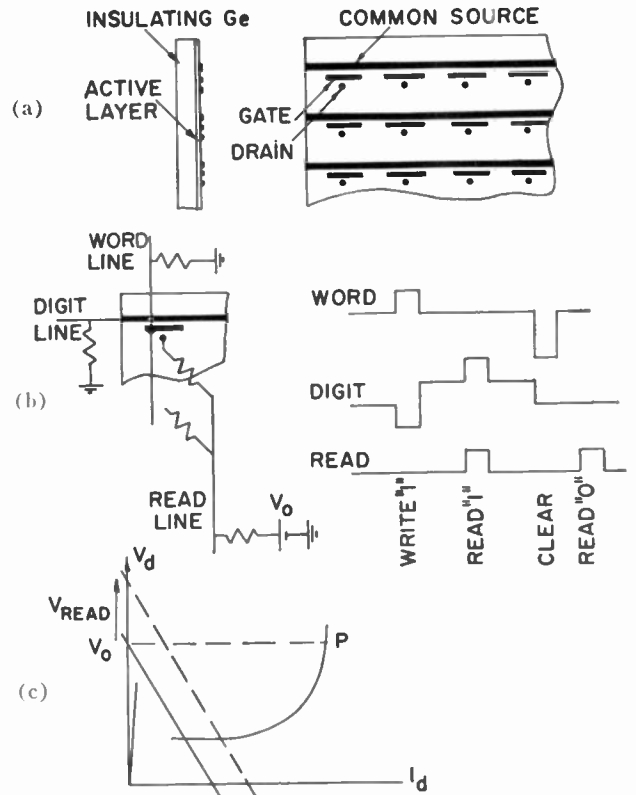


Fig. 10—(a) Proposed cryosistor memory array with a thin active layer on the surface of an insulating germanium wafer. (b) and (c) Operation of a voltage-coincident random-access memory with a nondestructive readout.

column. The READ signal shifts the loadline of each drain circuit upward, as shown in Fig. 10(b). A current pulse is detected on the digit line if the element is in the ON state. To clear all elements in a column the word line is pulsed with a sufficiently large negative pulse.

The READ operation requires a resistor for each drain, which could be made in the form of another germanium wafer alloyed to the contact. To avoid the necessity for a resistor the elements could be switched to point *P* and READ by means of a negative pulse which would decrease the source current but would not be sufficient to cause deionization.

ACKNOWLEDGMENT

The authors wish to thank Dr. J. B. Woodford for advice during the early stages of this work and Dr. R. H. Rediker and Dr. A. L. McWhorter for helpful discussions. The compensated crystals used here were supplied by the Massachusetts Institute of Technology Lincoln Laboratory.

A New Semiconductor Tetrode—The Surface-Potential Controlled Transistor*

C. T. SAH†, MEMBER, IRE

Summary—The theory and operating characteristics of a new semiconductor tetrode is discussed in this paper. This semiconductor junction device has the usual geometry of the planar transistor, but with an additional metal electrode placed on the oxide which covers the surface of the emitter-base junction. This electrode serves as a grid. The grid-base voltage controls the surface potential, surface recombination rate and the size of the surface channel, and thereby the current gain of the transistor. In the common emitter connection the grid serves as a second input in addition to the base input. Input impedance of the grid is typically in the range of 1 to 100 pf and 10^{16} ohms. Transconductances dI_C/dV_{GE} of several thousand micromhos have been achieved in the common emitter connection. The cutoff frequency of the transconductance is approximately the same as that of the h_{f_r} .

I. INTRODUCTION

IT is well known that surface plays a very important part in controlling the electrical characteristics of transistors and diodes. It has been demonstrated recently that surface protection by thermal oxidation of silicon transistor (the planar transistor) greatly improves the low-current characteristics such as the leakage current and the current-gain factor h_{FE} .¹ In addition oxide surface protection has provided orders of magnitude improvement in the stability and reliability in the over-all performance of transistors and diodes.

The development of the silicon-oxide surface-protection techniques has facilitated the study of surface effects on the electrical characteristics of $p-n$ junctions through controlled and designed experiments.² In addition it has considerably simplified the fabrication problems of silicon semiconductor components which have rather complicated geometries, such as the various microcircuit elements (*i.e.*, flip-flops, gates, half-shift registers, etc.), which consist of transistors, diodes, resistors and capacitors all built on the same block of silicon by solid-state diffusion techniques. In this paper one of a new family of semiconductor devices will be described which may be considered as an integrated cir-

cuit consisting of a surface-potential controlled junction and a transistor triode.

This family of semiconductor junction devices consists of modified versions of the usual diodes, triodes and $p-n-p-n$ or multijunction switches. In addition to the usual electrodes, these devices have one or more metal electrodes placed on top of the oxides which cover the surface of the junction transition regions. A cross-sectional view of the tetrode is shown in Fig. 1.

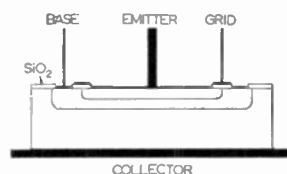


Fig. 1—A cross-sectional view of the surface-potential controlled tetrode.

Both the emitter-base and the collector-base junctions are oxide protected. A grid electrode is placed on the oxide of the emitter-base junction surface. The voltage applied to the metal electrode, or the grid, controls the surface potential, the recombination rate, and the size of the surface channel. The modulation of the reverse current-voltage characteristics of the junction by the grid voltage is somewhat similar to the effect of the gate voltage on the source to drain current-voltage characteristics of the field-effect transistor.³ However, there is a major difference: in the surface-potential controlled devices, minority carrier recombination and generation in the channel provides a considerable amount of junction current, while in the field effect transistors the modulation of the source to drain characteristics by the gate voltage is obtained through the control of the channel conductance of the majority carriers. In this paper the electrical performance and the physical theory of the tetrode will be discussed.

II. ELECTRICAL CHARACTERISTICS

Experimental measurements on a number of $n-p-n$ - and $p-n-p$ -type surface-potential controlled tetrodes are made. Families of electrical characteristics will be presented.

* W. Shockley, "A unipolar field effect transistor," Proc. IRE, vol. 40, pp. 1365-1376; November, 1952.

* Received by the IRE, July 5, 1961; revised manuscript received, September 1, 1961. This paper was presented at the WESCON Convention, San Francisco, Calif.; August 25, 1961.

† Fairchild Semiconductor, Div. of Fairchild Camera and Instrument Corp., Palo Alto, Calif.

¹ J. A. Hoerni, "Planar Transistors," presented at the IRE Annual Electron Devices Conf., Washington, D. C.; October 27-29, 1960. Published as Fairchild Tech. Paper TP-14.

² C. T. Sah, "Effect of Surface Recombination and Channel on Diode and Transistor Characteristics," presented at the AIEE-IRE Solid State Device Res. Conf., Stanford University, Calif.; June 26-28, 1961.

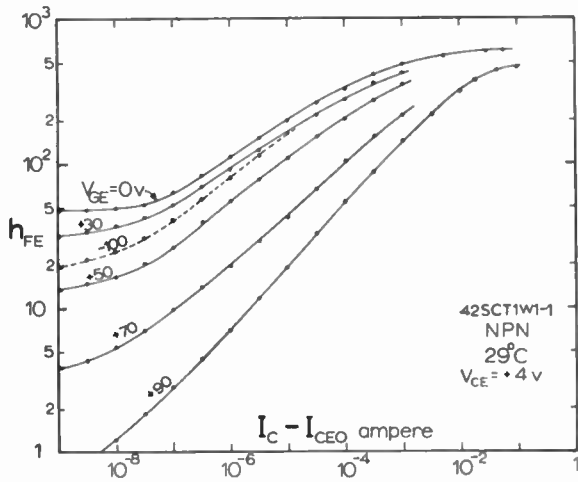


Fig. 2—The dc current gain h_{FE} for an $n-p-n$ tetrode plotted as a function of collector current for several grid voltages.

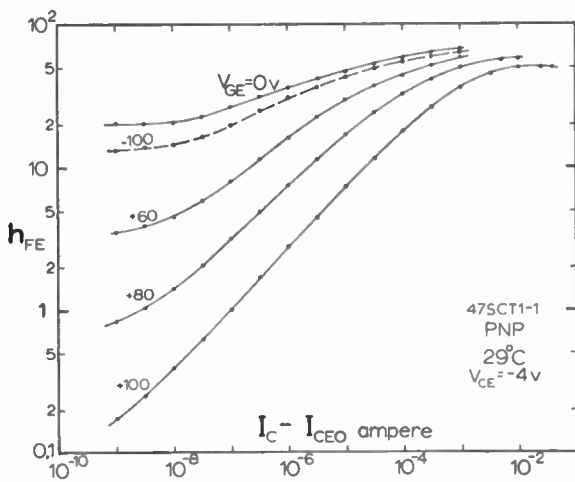


Fig. 3—The dc current gain h_{FE} for a $p-n-p$ tetrode plotted as a function of collector current for several grid voltages.

A. $h_{FE} - I_C$

The dc beta or h_{FE} is measured as a function of collector current in the common-emitter configuration with the grid voltage as a parameter.⁴ The experimental data are plotted for the high-voltage version of the $n-p-n$ and $p-n-p$ units in Figs. 2 and 3. The leakage current I_{CEO} is less than 0.5 $m\mu a$ for both units. The characteristics are very similar and show considerable reduction of current gain at low current and large grid voltage. The slope of the curves asymptotically approaches 0.5 at large grid voltage and low currents; *i.e.*, $h_{FE} = (I_C - I_{CEO}) / I_B \sim \sqrt{I_C}$, indicating that the base current varies approximately as $\sqrt{I_C}$. It has been observed² that the collector current varies as $\exp(qV_{EB}/kT)$ over almost ten decades of collector current; thus the base current varies as $\exp(qV_{EB}/2kT)$.

⁴ The definition of h_{FE} in this paper is slightly different from that of the IRE Standard, as pointed out by R. L. Pritchard to us during the WESCON. The defining equation for h_{FE} used in this paper is $h_{FE} = (I_C - I_{CEO}) / I_B$, which is more useful than the standard definition $h_{FE} = I_C / I_B$, since the latter one goes to infinite at zero base current while the former one approaches $h_{f\beta}$ at low base current and is still a meaningful quantity in equivalent circuits.

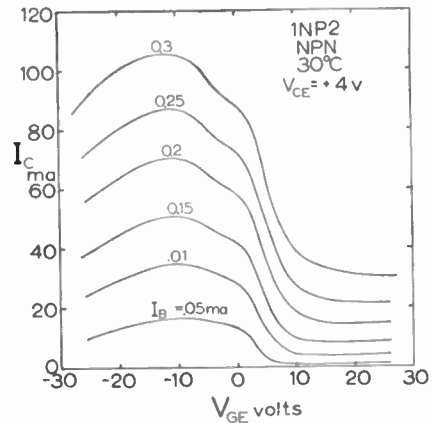


Fig. 4—The high-current transfer characteristics of an $n-p-n$ tetrode with thin oxide on the emitter-base junction in the common-emitter connection.

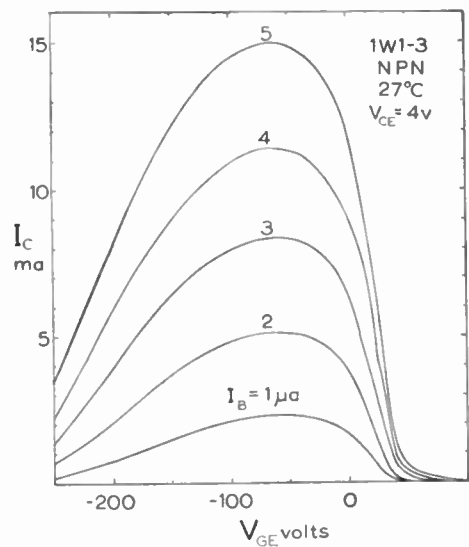


Fig. 5—The medium-current transfer characteristics of an $n-p-n$ tetrode with thick oxide on the emitter-base junction in the common-emitter connection.

B. $I_C - V_{GE}$ (Transconductance)

The transfer characteristics are also obtained in the grounded emitter configuration and are shown in Figs. 4-6. The tetrode 1NP2 of Fig. 4 is a low grid-voltage $n-p-n$ device which has thinner oxide and lower surface concentration in the base region than the $n-p-n$ tetrode 1W1-3, shown in Fig. 5.

For the low-voltage tetrode 1NP2 shown in Fig. 4, the maximum h_{FE} for a given base current is obtained at a negative grid voltage of approximately -8 volts at low current and the optimum grid voltage decreases to -12 volts at high current. The grid voltage at maximum h_{FE} varies in a similar way for the high grid-voltage device 1W1-3, shown in Fig. 5.

Maximum transconductance $g_m = dI_C/dV_{GE}$ at a given base current is reached at a positive grid voltage as indicated in Figs. 4 and 5. The transconductance also increases with base or collector current, and is nearly proportional to the base current or the square root of

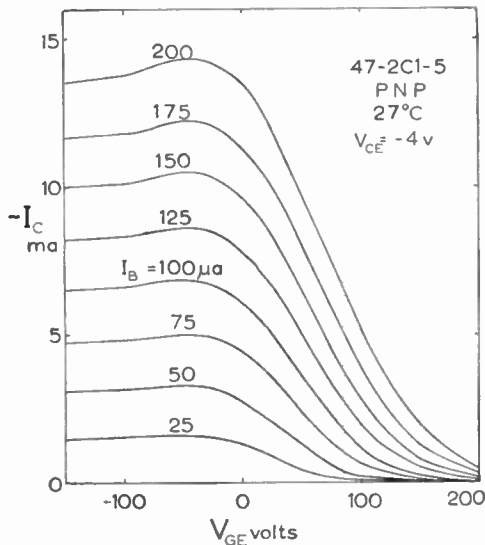


Fig. 6—The medium-current transfer characteristics of a $p-n-p$ tetrode with thick oxide on the emitter-base junction in the common-emitter connection.

the collector current at low currents. At large base current unit 1NP2 in Fig. 4 shows a g_m of 7000 $\mu mhos$ at $I_C = 50$ ma and a grid voltage of 5 volts. The sign of the transconductance is negative in the positive grid-voltage region. However, at large negative grid voltage, a positive transconductance is obtained. The magnitude of the negative grid voltage for large positive g_m approaches the destructive dielectric breakdown condition in the oxide.

An entirely similar behavior with the *same* sign for the grid voltage is observed for the transfer characteristics of $p-n-p$ tetrodes, shown in Fig. 6. Thus, a positive g_m is obtained for the $p-n-p$ devices with a positive grid voltage which is safely below the dielectric breakdown limit. It is believed that surface channel formation may account for the observed behavior of both the $n-p-n$ and the $p-n-p$ devices. In the $n-p-n$ tetrode the maximum g_m region of positive grid voltage corresponds to an increase in size of the channel formed on the surface of the p -type base under the grid-metal electrode, while for the $p-n-p$ tetrode the channel is also formed in the p -type region but in the emitter. A more detailed discussion of the physical theory will be given in a subsequent section.

C. g_m Frequency

The frequency response of the transconductance appears to be limited by the usual minority-carrier diffusion time in the base. A preliminary measurement for an $n-p-n$ tetrode is shown in Fig. 7. The 3-db point for g_m is about 600 kc, which is nearly equal to the h_{fe} cutoff frequency of this device.

D. Grid Input Impedance

The input capacitance of the grid to the combined emitter and base leads is about 4.5 pf for the high grid-voltage devices 1W1-1, 1W1-3, 47-SCT1-1 and 47-2C1-5;

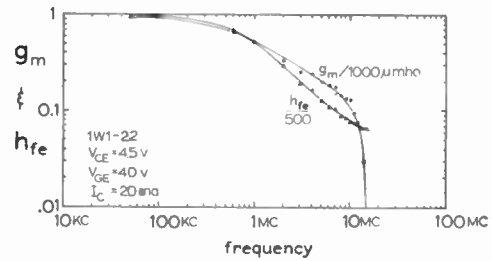


Fig. 7—The frequency dependence of the transconductance and current gain of a thick oxide $n-p-n$ tetrode.

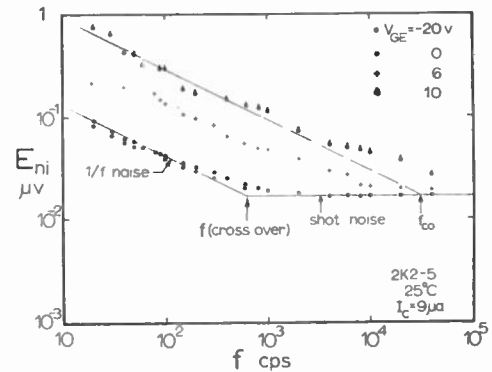


Fig. 8—The frequency dependence of base input noise voltage for several grid voltages.

and about 22.5 pf for the low grid-voltage unit 1NP2. The capacitance is independent of the grid voltage over the entire range up to the dielectric breakdown voltage corresponding to about 2 to 5×10^6 volts/cm.

The leakage or the input resistance has not been measured successfully with commercial electrometers indicating a value greater than 10^{14} ohms. An alternative approach is made by measuring the RC discharge time of the input capacitance, using the collector current as an indicator of the grid voltage, and using a constant-base current drive in the common-emitter connection. The decay time constant thus measured is from one to three hours giving a leakage resistance of greater than 10^{16} ohms for the 1W1-3 unit. The variation of the experimental results of the decay time constant appear to be associated with the humidity of the room ambient and the leakage in the lead through the glass of the transistor package.

E. Base Input Noise

The input-noise voltage referred to the base input terminal is measured as a function of frequency with the grid voltage as a parameter. In Fig. 8 the narrow-band noise voltage referred to the input is plotted as a function of frequency for a bandwidth of 6 cps and a source resistance of 500 ohms. At large positive grid voltage, the h_{fe} of the tetrode is decreased but is sufficient so that the noise from the amplifier is still unimportant. The data in Fig. 8 show that the $1/f$ noise is increased as much as 20 db at low frequencies by the grid voltage, and the crossover frequency to shot noise f_{co} is increased from 700 cps to 30 kc when the grid voltage is increased

from 0 to 10 volts. The tetrode unit shown in Fig. 8 is similar to the unit 1NP2 shown in Fig. 4. The result of the base input noise is not surprising since it is well known that in semiconductor devices the $1/f$ noise is closely associated with the formation of surface channels.⁵ The input noise referred to the grid lead at present has not been measured.

III. PHYSICAL THEORY

The design theory and the basic mechanisms which control the electrical characteristics of the surface-potential controlled transistors and diodes may be best analyzed using the physical circuit of the device shown in Fig. 9(a). An enlarged view of the region where the emitter-base junction intercepts the surface is shown and the junction transition regions are shaded in Fig. 9(a). These transition regions are defined in the sense that negligible voltage drop occurs outside these regions, *i.e.*, about kT/q or less.^{6,7} The shape of the shaded transition region near the surface corresponds to a positive voltage applied to the grid electrode relative to the base electrode, and an *n*-type surface channel on the base side is formed. This situation corresponds closely to that in the *n-p-n* tetrodes shown in Figs. 2, 4 and 5 at fairly large positive grid voltage. The potential energy diagram showing an equipotential surface for electrons is given in Fig. 10.

The equivalent circuit of the tetrode may be derived from Fig. 9(a) and is given in Fig. 9(b). The effect of the grid induced emitter-base surface channel may be conveniently included as a surface diode *SD* connected to the *external* base and emitter leads of a real silicon transistor which has no surface leakage in the emitter-base junction. Thus, the characteristics for a typical tetrode may be discussed in two parts with little interaction between the two, except through the two external lead connections.

A. The Transistor Characteristics

In addition to the usual diffusion currents, the ideal transistor shown in Fig. 9(b) includes also the recombination and generation currents in the transition regions of the junctions.⁸ Thus, the usual transistor equations in the grounded base connection are (*p-n-p*)

$$J_E = j_{ET} 2 \sinh \theta_E / 2 + j_D [(e^{\theta_E} - 1) / \gamma_N - (e^{\theta_C} - 1) \alpha_T] \quad (1)$$

$$J_C = j_{CT} 2 \sinh \theta_C / 2 + j_D [(e^{\theta_C} - 1) / \gamma_I - (e^{\theta_E} - 1) \alpha_T] \quad (2)$$

⁵ A. L. McWhorter, "1/f noise and germanium surface properties," in "Semiconductor Physics," R. H. Kingston, Ed., University of Pennsylvania Press, Philadelphia, pp. 207-228, 1957; "1/f Noise and Related Surface Effects in Germanium," Res. Lab. of Electronics, Mass. Inst. Tech., Cambridge, Tech. Rept. 295, May 20, 1955.

⁶ C. T. Sah, "Effect of electrons and holes on the transition layer characteristics of linearly graded *p-n* junctions," *PROC. IRE*, vol. 49, pp. 603-618; March, 1961.

⁷ W. Shockley, "The theory of *p-n* junctions in semiconductors and *p-n* junction transistors," *Bell Sys. Tech. J.*, vol. 28, pp. 435-489; July, 1949.

⁸ C. T. Sah, R. N. Noyce and W. Shockley, "Carrier generation and recombination in *p-n* junctions and *p-n* junction characteristics," *PROC. IRE*, vol. 45, pp. 1228-1243; September, 1957.

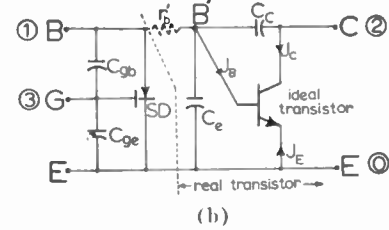
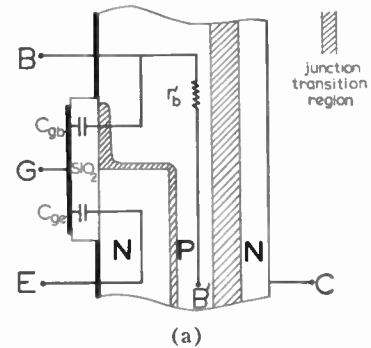


Fig. 9—(a) The physical circuit, and (b) the equivalent circuit, of the surface-potential controlled transistor tetrode.

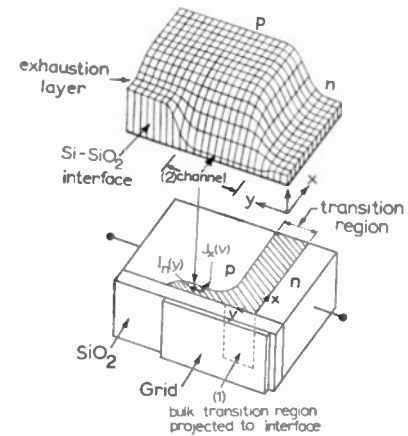


Fig. 10—The equipotential surface (top figure) and the cross-sectional view of an asymmetrical emitter-base surface diode in which the *n*-type emitter is more heavily doped than the *p*-type base.

where

$$\theta_B = qV_{EB} / kT$$

$$\theta_C = qV_{CB} / kT$$

$$\alpha_T = \text{sech} (W_B / L_B)$$

$$\gamma_N = j_D / (j_E + j_D)$$

$$\gamma_I = j_D / (j_C + j_D)$$

$$j_D = (qn_B L_B / \tau_B) \text{ctnh} (W_B / L_B)$$

$$j_C = (qn_C L_C / \tau_C) \text{ctnh} (W_C / L_C)$$

$$j_E = (qn_E L_E / \tau_E) \text{ctnh} (W_E / L_E)$$

$$j_{ET} = qn_i W_{ET} f(b_E) / \sqrt{\tau_{p0} T_{n0} \alpha_E}$$

$$j_{CT} = qn_i W_{CT} f(b_C) / \sqrt{\tau_{p0} T_{n0} \alpha_C}$$

for unit emitter and collector area.

The widths W_B , W_C , and W_E are the widths of the base, collector and emitter layers, respectively, while W_{CT} and W_{ET} are the widths of the collector and emitter transition regions. The n 's are the minority-carrier concentrations, n_i is the intrinsic carrier concentration, and

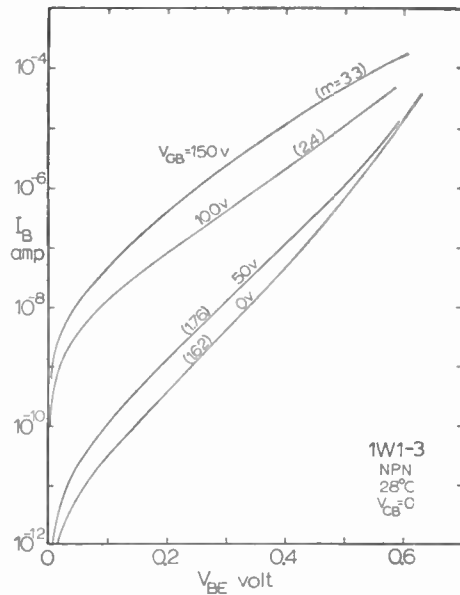


Fig. 11—The forward characteristics of an emitter-base surface diode with the grid voltage as a parameter. The quantity m is given by (3).

the τ 's are the minority-carrier lifetime in the emitter, collector and base layers. The L 's are the minority-carrier diffusion lengths given by $L = \sqrt{D\tau}$, and τ_{po} and τ_{no} are the minority-carrier lifetimes in heavily doped n - and p -type specimens, respectively. The quantity $f(b)/\alpha$ may be approximated by $2/(\sqrt{\tau_{po}/\tau_{e0}} + \sqrt{\tau_{no}/\tau_{p0}})$ for $V_{EB} > 4kT/q$ if the energy level of the recombination center is located nearly at the intrinsic Fermi level and if $\tau_{po} = \tau_{no}$.⁶ For the reverse-biased collector junction, the leakage current $J_{CNO} \cong j_{CT} 2 \sinh \theta_C/2$ is proportional to H_{CT} .⁸

The ac equations may be obtained from (1) and (2) in the usual way by expanding the currents and voltages in the form of $A = A_0 + A_1 \exp(j\omega t)$ and assuming $A_0 \gg A_1$.

B. The Emitter-Base Surface-Diode Characteristics

The theoretical analysis of the surface diode characteristics is extremely complicated since it involves the solution of three nonlinear simultaneous partial-differential equations⁷ in a two-dimensional geometry. The problem is further complicated by the discontinuity of the crystal lattice at the Si-SiO₂ interface which may result in high concentration of surface states that are continuously distributed in the energy gap. Preferential precipitation of impurities such as gold or other metals at the interface might occur due to the high electric field near the surface. These impurities may provide additional recombination sites at the interface which have surface recombination properties different from those in the bulk. The derivation of the surface-diode current-voltage relation is possible only by using rather simplified assumptions based on plausible physical considerations and experimental observations.

The observed current-voltage relation of the emitter-

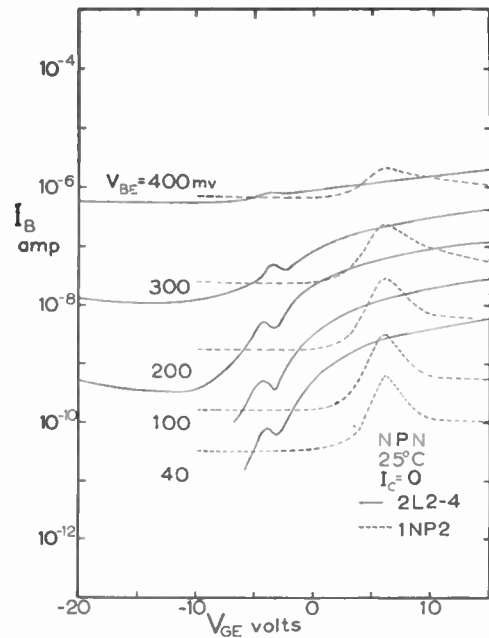


Fig. 12—The transfer characteristics of thin oxide emitter-base surface diodes with emitter-base voltage as a parameter.

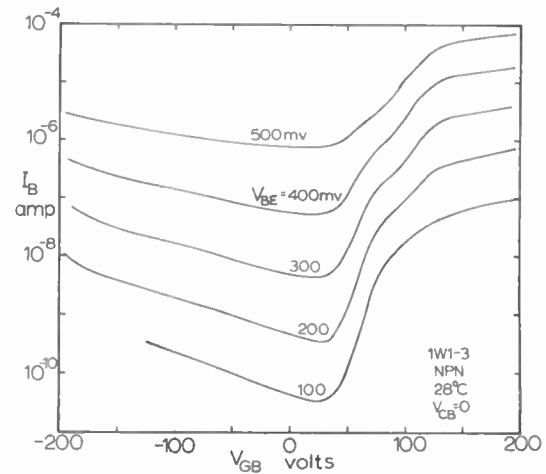


Fig. 13—The transfer characteristics of a thick oxide emitter-base surface diode with emitter-base voltage as a parameter.

base surface diode SD shown in Fig. 9(b) may be approximated by

$$J_{SD} = j_{SD} 2 \sinh (qV_{EB}/mkT), \tag{3}$$

where both j_{SD} and m are functions of the grid-base or grid-emitter voltage. The factor m may vary from 1 to as high as 10 or more, depending on the width and doping of the surface channel, and it also varies with the emitter-base voltage. The usually observed values of m for the emitter-base surface diode of the tetrodes such as that in Fig. 11 are in the range of 1.5 to 4, and the coefficient j_{SD} has a thermal activation energy of from half of the energy gap to one-fourth the energy gap in silicon.

The experimental data given in Figs. 12 and 13, where I_B is plotted against V_{GE} for two oxide thicknesses, indi-

cate that the current flowing in the surface diodes may result from two distinct mechanisms. Fig. 12 shows that 1N2P has only one type of behavior, which is characterized by the appearance of a maximum in the diode-current vs the grid-voltage characteristics. The data of the high grid-voltage tetrode 1W1-3 shown in Fig. 13 appear to have also only one type of behavior which is characterized by a monotonically increasing current with increasing or decreasing grid voltage from the minimum current point. The data for 2L2-4 given in Fig. 12 clearly show both types of behavior, indicating that both components of the surface current are present and are superimposed on each other. The fine structures near $V_{GE} = 80$ v in the characteristics of 1W1-3 in Fig. 13 suggest that a second component of surface current is probably present in this unit.

For mathematical simplicity, ease of discussion, and physical understanding, it is convenient to break up the surface into two regions: 1) the region corresponding to the projection of the emitter-base transition region onto the surface; and 2) the channel region outside of the emitter-base transition region. Both of these regions are labeled and shown in Fig. 10. In the following discussion it will be shown that the surface-current component which has a maximum vs the grid voltage may be accounted for by the recombination current in the transition region on the surface, while the surface-current component which is monotonically increasing from a minimum value with increasing or decreasing grid voltage corresponds to the recombination current flowing in the surface channels.

1) *Surface-Recombination Current in the Transition Region:* The diode current due to surface recombination in the transition region would be expected to go through a maximum when the surface potential (or the intrinsic Fermi level at the surface) is moved by the grid voltage to within $(\frac{1}{2}) \log_e (S_{po}/S_{no})$ from the average value of the quasi-Fermi levels for electrons and holes, where S_{po} and S_{no} are the surface-recombination velocities for holes and electrons on degenerate *n*- or *p*-type surfaces. The diode current from this region would decrease asymptotically to constant values when the grid voltage is either decreased or increased from the value of the maximum surface recombination. The shapes of the diode current vs grid voltage or surface-potential characteristics are very similar to those of the surface-recombination velocity observed on uniform surfaces which have no junctions. Several maxima may be expected if there are several independent surface-recombination centers.²

The derivation of this result may be developed using a simple example: the ideal symmetrical junction with linear potential variation in the junction. In Fig. 14 the energy-band diagram at the surface for a symmetrical emitter-base surface diode is shown. The surface energy-band diagram in Fig. 14(b) corresponds to the condition of zero grid voltage and forward bias of the junction. The diagram in Fig. 14(c) includes only the surface

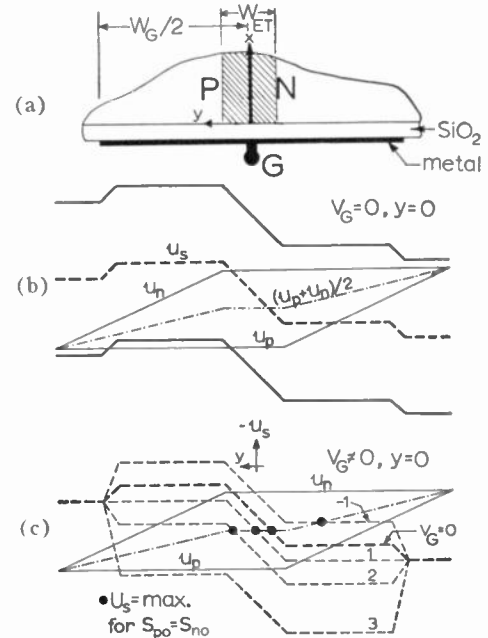


Fig. 14—(a) The cross-sectional view, (b) the energy band diagram at $V_G=0$, and (c) The surface-potential variation along the surface of a hypothetical symmetrical emitter-base surface diode.

potential curves, u_s (dashed) and the quasi-Fermi levels for electrons and holes on the surface. However, Fig. 14(c) shows the relative position of the surface potential u_s , under various grid voltages.

The steady-state recombination rate per unit surface area may be obtained from the Hall-Shockley-Read statistics.⁹ It is given by

$$U_S = n_i \sqrt{S_{po} S_{no}} \sinh(qV_{BE}/2kT) \times \left\{ \cosh \left[u_s - (u_p + u_n)/2 + (1/2) \log_e S_{no}/S_{po} \right] + \exp(-qV_{BE}/2kT) \cosh \left[u_s - u_i + (1/2) \log_e S_{no}/S_{po} \right] \right\}^{-1}, \quad (4)$$

where S_{po} and S_{no} are the surface-recombination velocities on degenerate *n*- and *p*-type surfaces, respectively, u_p and u_n are the hole and electron quasi-Fermi levels, and $u_s - u_i$ is the energy level of recombination centers measured from the intrinsic Fermi level. These energy levels are normalized to the thermal voltage $-kT/q$. In Fig. 14 and (4) it is assumed that the change of quasi-Fermi levels across the transition region is negligible but may be appreciable in the channel due to channel resistance. The maximum surface recombination occurs when the surface potential in (4) is

$$u_s = (u_p + u_n - \log_e S_{no}/S_{po})/2. \quad (5)$$

⁹ R. N. Hall, "Germanium rectifier characteristics," *Phys. Rev.*, vol. 83, p. 228, 1951; "Electron-hole recombination in germanium," *Phys. Rev.*, vol. 87, p. 387, July, 1952. W. Shockley and W. T. Read, Jr., "Statistics of recombinations of holes and electrons," *Phys. Rev.*, vol. 87, pp. 835-842, September, 1952. D. T. Stevenson and R. J. Keyes, "Measurements of the recombination velocity at germanium surfaces," *Physica*, vol. 20, pp. 1041-1046; November, 1954.

The position of the maximum surface-recombination rate is shown in Fig. 14(c) as heavy dots. For this example, it is assumed that at zero junction and grid voltage an accumulation layer is formed on the p -type surface under the grid, and an exhaustion layer is formed on the n -type surface under the grid. The formation of accumulation and exhaustion layers might arise due to the work function differences between the silicon, oxide and metal of the grid electrode. Thus, the position of the maximum recombination rate $U_s(\text{max})$ coincides with the center of the junction when the grid voltage is a positive value labeled $V_G=1$ in Fig. 14(c). At zero grid voltage, the point of maximum surface recombination is slightly to the right of the center of the junction or closer to the n region. As the grid voltage is increased from large negative values, the maximum surface recombination point moves from the n region into the junction-transition region and then out of the transition region into the p region.

The surface potential u_s may be related to the grid voltage by an analytical procedure similar to that used for the metal-oxide-silicon capacitors.¹⁰ However, the situation is somewhat different in the present case since there is a large minority-carrier concentration near the surface which is injected by the forward-biased junction. The results of the metal-oxide-semiconductor capacitor may be used as a zeroth approximation, using the carrier concentration in the transition region instead of that in the bulk to obtain the surface potential from the grid voltage.

The surface current may be approximated by assuming a constant recombination rate on the surface of the transition layer. The result is

$$I_{SD} = qW_{ET}U_sL_s, \quad (6)$$

where L_s is the circumference, W_{ET} is the emitter-base transition-layer width in the bulk, and U_s is given by (4) evaluated at the center of the junction-transition layer. Thus, using (4) and (5), (6) has the form given by (3) in which j_{SD} is a function of the grid-base voltage. Furthermore, (6) predicts the observed shape of the junction-current vs grid-voltage characteristics of device 1NP2 shown in Fig. 12. The maximum occurs at a grid voltage corresponding to the surface potential condition given by (5).

In the ideal symmetrical junction considered here the

¹⁰ The problem of the potential variation in a metal-oxide-semiconductor sandwich was analyzed by its inventor, J. L. Moll, in "Variable capacitance with large capacity change," 1959 IRE WESCON CONVENTION RECORD, pt. 3, pp. 32-36, and has since been analyzed by a large number of authors recently. Our notations follow closely that of R. H. Kingston and S. F. Neustader, "Calculations of the space charge, electric field and free carrier concentration at the surface of a semiconductor," *J. Appl. Phys.*, vol. 26, pp. 718-720; June, 1955. More recent papers on the analysis of the oxide capacitor are: R. Linder, "Semiconductor surface varactor," 2nd Interim Rept. on Microwave Solid State Devices, Bell Telephone Labs. (Contract DA 36-039-sc-85325), pp. 13-40, November 30, 1960; and D. R. Frankl, "Some effects of material parameters on the design of surface space-charge varactors," *Solid State Electronics*, vol. 2, pp. 71-76; January, 1961.

shape of the I_{SD} vs V_G plot is symmetrical with respect to the grid voltage corresponding to point of maximum surface recombination or maximum current. In the real emitter-base surface diodes of the n - p - n surface-potential controlled transistors, the surface of the n -emitter is more heavily doped than the surface of the p base. Thus, an asymmetrical junction is usually obtained, and the recombination rate would be asymmetrical with respect to the grid voltage, where the surface-recombination current is a maximum.

The diffusion current along the surface outside the transition region is similar to that in the bulk and is usually small compared with the recombination current in the transition region on the surface if a surface channel or an inversion layer is not formed.⁸ The situation is more complicated if the width of the grid is comparable to the diffusion length.

In the case where the surface diffusion length is very long compared with the width of the grid electrode, the electron Fermi level u_n shown in Fig. 14(c) would be quite horizontal in the p region under the grid, and the entire surface area under the grid electrode in the p region would be important for carrier recombination, for positive grid voltage. An approximate result may be obtained by assuming no voltage drop along the surface under the grid electrode in the p region. The expression for current is in the same form as that given by (6) if W_{ET} , the width of the emitter-base transition layer, is replaced by the half width of the grid electrode $W_G/2$ and the recombination rate U_s is evaluated at the center of the region under the grid electrode on the p side. A similar consideration applies to the n region when the grid voltage is negative.

2) *Channel Current:* As the grid voltage is increased to certain value, such as that corresponding to $v_G=3$, shown in Fig. 14(c), the surface potential is pulled down and coincides with the Fermi level of holes on the surface of the p region outside the junction-transition region under the metal-grid electrode. The surface under the grid in the p region now becomes intrinsic. Further increase of the grid voltage results in the formation of an inversion layer although *not* a channel on the p surface, since the energy band is also lower in the n region. (A surface channel is defined as a region near a p - n junction into which either electrons or holes from the other side of the junction can flow without having to climb a potential barrier. For example, the channel shown in Fig. 10 under the grid in the p region is an electron channel, while the exhaustion surface layer in the p region not under the grid electrode is not an electron channel since the electrons must climb a barrier when they flow from the channel into the exhaustion layer.)

The appearance of a channel on one side of the junction under the grid where the band is flat or lower with respect to the other side of the junction near the surface, such as that shown in Fig. 10, may occur in asymmetrical junctions. The requirement for channel formation is that the grid voltage can change the surface potential or

bend the energy band perpendicular to the surface effectively only on one side of the junction and not on the other side. A channel will be formed on the side where the surface potential can be changed more readily by the grid voltage. The readiness of bending the band may be controlled by the thickness of the oxide, the impurity concentration at the surface and the surface-state densities. In the case where a channel can be formed, it can occur at a grid voltage either before, at the same time, or after the onset of surface inversion. For example, let us consider the case shown in Fig. 15 in which the surface potential on the n side is locked in position and cannot be bent by the grid voltage appreciably. Then, as the grid voltage is increased, the surface potential on the p side will be pulled down and become flat with respect to the n side ($V_G=3$) before the surface potential u_s coincides with the Fermi level for holes u_p ($V_G=4$). Thus, a channel for electrons is formed on the p surface before the onset of surface inversion $u_s = u_p$.

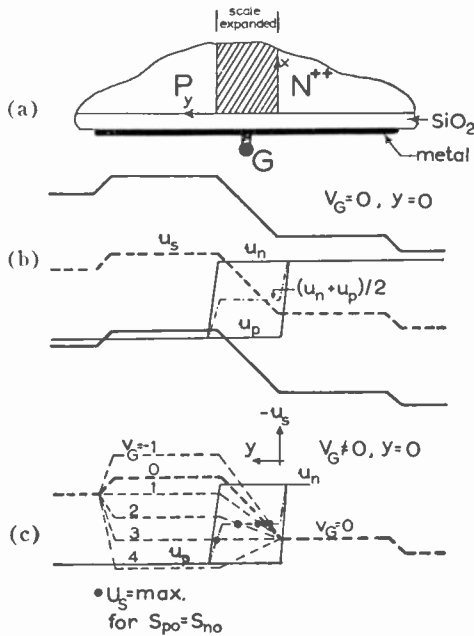


Fig. 15—(a) The cross-sectional view, (b) the energy band diagram at $V_G=0$, and (c) the surface-potential variation along the surface of a hypothetical asymmetrical emitter-base surface diode.

In the practical silicon tetrodes fabricated surface inversion and channel formation appear to be more readily achieved on the p -type than on the n -type surface under the oxide. This is evidenced by the experimental observations that the emitter-base surface-diode current, or the collector current of the tetrode, when plotted as a function of grid voltage, has almost the identical behavior for the n - p - n and the p - n - p tetrodes. Some typical data were shown in Figs. 5 and 6. Since the oxide thickness is fairly uniform and probably slightly thicker on the base side than on the emitter side due to the diffusion sequence, the nonuniformity of the oxide would

probably not account for the same behavior of n - p - n and p - n - p tetrodes. The oxides on the emitter-base junction for the n - p - n and the p - n - p tetrodes are grown in the same way so that it is unlikely that there is high concentration of surface states preferentially located in the n region at the silicon-silicon-oxide interface. The surface-state density required to interpret the similarity of the transfer characteristics of n - p - n and p - n - p tetrodes would be extremely high in order that channel or surface inversion can barely be obtained in the n -type base surface of the p - n - p unit. However, it would still not explain why a channel is easily formed on the emitter surface of the p - n - p unit which is presumably doped to 10^{20} to 10^{21} surface concentration. Thus, it must be concluded that impurity segregation is important so that the n -type impurity is rejected by the oxide during thermal oxidation and forms a degenerate layer near the surface, while the p -type impurity, in this case boron, prefers the silicon oxide under the thermal oxidation condition and thus is depleted at the silicon-silicon-oxide interface. This conclusion seems to be in agreement with the thermodynamic calculation of Thurmond,¹¹ although his estimate of the segregation coefficient of boron between silicon and silicon oxide is not sufficiently accurate (*i.e.*, from 10^{-3} to 10^3) to substantiate the quantitative results obtained for the p - n - p tetrodes.

The formation of the channel or surface inversion layer in the base region or the emitter region may be calculated in a zeroth approximation by neglecting the electrons injected into the channel by the forward-biased emitter-base junction. This assumption is a somewhat better approximation here than when it was applied previously to the surface within the transition region in calculating the surface-recombination current. The results of the metal-oxide-semiconductor capacitor analysis can again be applied.¹⁰

The condition for the onset of surface inversion, *i.e.*, u_s coincides the Fermi level for the majority carriers, is plotted in Fig. 16. Let us consider a numerical example using unit 1W1-3 shown in Fig. 13. The oxide thickness is approximately $L_o=0.6$ micron, and the surface concentrations of the impurity in the base and the emitter regions are approximately $10^{18}/\text{cc}$ and $10^{20}/\text{cc}$. From Fig. 16 one may obtain an approximate effective width of the surface space-charge layer width using the surface concentration instead of the true profile of the diffused emitter or base layers. In the base region Fig. 16 gives $x_s=0.02$ micron indicating that the surface-inversion layer is very thin and concentrated near the surface so that the use of the surface concentration instead of the

¹¹ C. D. Thurmond, "Distribution coefficients of impurities distributed between Ge or Si crystals and ternary alloys or surface oxides," *Proc. Metallurgical Soc. Conf.*, vol. 5, "Properties of Elemental and Compound Semiconductors," H. C. Gatos, Ed., Interscience Publishers, pp. 121-140; 1960. M. M. Atalla and E. Tannenbaum, "Impurity redistribution and junction formation in silicon by thermal oxidation," *Bell. Sys. Tech. J.*, vol. 39, pp. 933-946; July, 1960.

true impurity concentration profile is a good approximation. From Fig. 16 the electric field in the oxide at the onset of surface inversion may also be obtained. In the base region $E_o = 10^6$ v/cm and the voltage drop in the oxide is $V_o = L_o E_o = 60$ volts. The voltage drop in the space-charge region of the semiconductor is approximately 0.4 volt, given by $u_s - u_{s0}$ in Fig. 16. Thus, the total grid voltage required for surface inversion in the p base is about 60 volts, which corresponds well with the observed voltage where there is a rapid rise of I_B shown in Fig. 13.

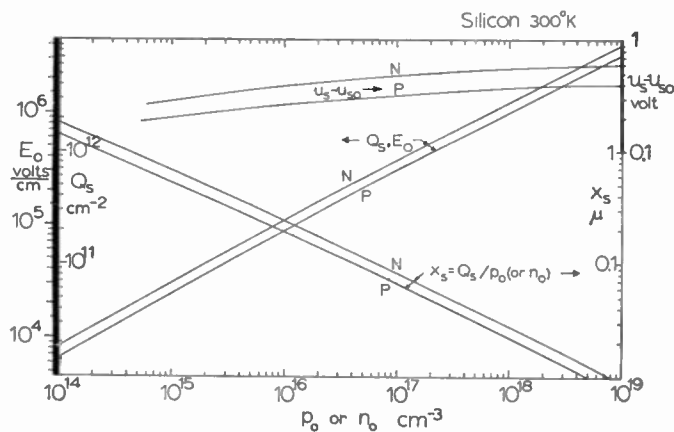


Fig. 16—A chart of the electrical field in the oxide E_o ; the total charge per unit area, Q_s ; the equivalent thickness of the space-charge layer in the silicon; and the voltage drop in the silicon plotted as a function of the carrier concentration in the bulk for both n - and p -type silicon under the condition of surface inversion.

A similar calculation can be made to obtain the required grid voltage for surface inversion in the n emitter. Fig. 16 does not cover the degenerate range; however, a linear extrapolation on the log-log plot may be used for a rough estimate which yields $E_o = 5 \times 10^7$ v/cm or $V_o = 3000$ volts, a value considerably greater than the dielectric breakdown of the oxide.

In order to make a better approximation, it is necessary to include the injected carrier by the forward-biased junction. In the first-order approximation one may replace the carrier concentration in the bulk p_o (or n_o) by $n_i \exp(u_p - u_B) - n_i \exp(u_B - u_n)$, where u_p and u_n are the quasi-Fermi potential for holes and electrons and u_B is the intrinsic Fermi potential in the bulk.

An exact analysis of the recombination current in the channel or the surface-inversion layer is quite complicated since the channel or the inversion layer is quite thin and highly resistive. Consequently, there is a considerable amount of voltage drop along the length of the channel. For example, let us consider the case of an inversion layer and a channel formed at the same time in the p region such as that shown in Fig. 10. As the surface-inversion layer and channel are formed by increasing the grid voltage, a region of high recombination rate given by the condition similar to (5) if u_s is replaced by u appears at the silicon-silicon-oxide interface under the grid. As the grid voltage is further increased, the layer

of high recombination rate moves away from the interface into the interior of the channel. The recombination rate decreases along the channel in the y direction in Fig. 10 due to the voltage drop in the channel. Thus, in calculating the total current flowing into the channel due to carrier recombination in the channel it is necessary to take into account the voltage drop along the channel.

The mathematical analysis of the channel current can be worked out with a procedure very similar to that used by McWhorter and Kingston¹² which was subsequently extended by Culter and Bath¹³ to include the forward-bias region of silicon-alloyed diodes. These authors take into account the voltage drop in the channel. However, they neglected to use the appropriate recombination rate in the channel, which provides the most important voltage dependence of the channel current. For example, Culter and Bath took the diffusion current outside the channel to calculate the total current in the channel for silicon diodes. This approximation is valid only for channels in germanium diodes, since it is well known that the most important current in silicon junctions below or near room temperature comes from minority-carrier recombination in the transition region of the junction.⁸ Consequently, the results of Culter and Bath, when correlated with experimental data in silicon,¹³ require a channel length which is considerably greater than the maximum physical dimension of the silicon wafer of the diode. Furthermore, their theoretical results cannot account for a voltage dependence of $j_{SD} \exp(qV/mkT)$ of the channel current in which m is greater than 2 and j_{SD} has a thermal activation energy less than half of the energy gap. The extension of these analyses to the case appropriate to silicon junctions is fairly obvious if carrier recombination in the transition region in the channel is taken into consideration. The results can then account for a value of m as high as 4 and an activation energy of j_{SD} as low as $\frac{1}{4}$ of the thermal energy gap of silicon.

The calculation of the channel current may be formulated with reference to Figs. 10 and 17. It is assumed that the surface potential is changed by the grid voltage only in the p region and not in the n region, so that a channel will definitely be formed with positive grid voltage, and an equipotential surface similar to that given by Fig. 10 is obtained.

It is also assumed that the quasi-Fermi level for holes u_p is flat and that there is negligible recombination near the surface of the channel so that the total current flow there is entirely carried by electron flowing into the channel from heavily doped n -type emitter. Thus, the hole and the electron currents in the channel are^{6,7}

$$I_p(y) = -qD_p p (du_p/dy) W_L L_S = 0 \quad (7)$$

¹² A. L. McWhorter and R. H. Kingston, "Channels and excess reverse current in grown germanium p - n junction diodes," Proc. IRE, vol. 42, pp. 1376-1380; September, 1960.

¹³ M. Culter and H. M. Bath, "Surface leakage current in silicon fused junction diodes," Proc. IRE, vol. 45, pp. 39-43; January, 1957.

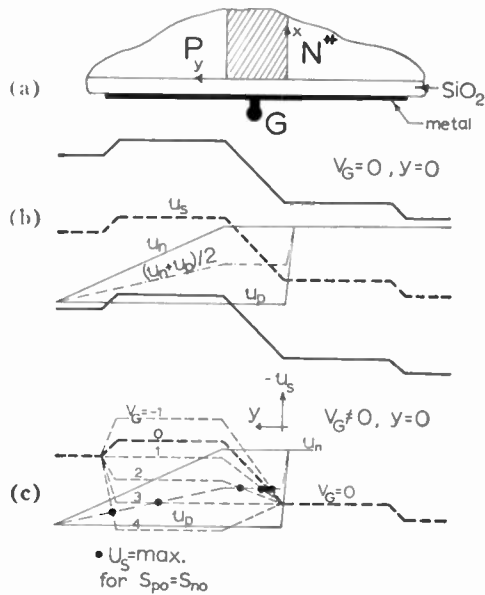


Fig. 17—(a) The cross-sectional view, (b) the energy-band diagram at $V_G=0$, and (c) the surface-potential variation along the surface of a typical asymmetrical emitter-base surface diode.

and

$$I_n(y) = -qD_n n (du_n/dy) W_I L_S, \quad (8)$$

where D_n is the diffusion constant of electrons in the channel, n is the electron concentration in the channel, W_I is the inversion or channel width in the x direction and may be a function of y , and L_S is the circumference. The total current in the channel at a distance y from the emitter-base junction may be obtained (using the continuity relation) and is given by

$$I = I_n(y). \quad (9)$$

It is further assumed that the electron concentration is a constant along the surface of the channel. Thus, the change of the electron quasi-Fermi level u_n is entirely due to the voltage drop in the channel; *i.e.*,

$$n_s = n_i \exp(u_s - u_n) = \text{constant} \quad (10a)$$

or

$$du_s = du_n, \quad (10b)$$

where u_s is the surface potential normalized to the thermal voltage kT/q . The results given by (10a) and (10b), based on the assumption of constant electron concentration on the surface, is consistent with the relation

$$u_p - u_n = v, \quad (11)$$

where v is the normalized voltage drop along the channel. Thus, using (7), (8), (10b) and (11), and replacing n by n_s in (8), the total current flowing in the channel given by (9) may be written as

$$I(y) = qD_n n_s W_I L_S (dv/dy). \quad (12)$$

Another relationship between current and voltage along the channel may be derived by calculating the current flowing out of the channel in the x direction across the surface-potential barrier (see Fig. 10). This current $J_x(v)$ is provided by the electron and hole recombination in the region near the surface where the condition of maximum recombination rate given by

$$u = (u_p + u_n - \log_e S_{no}/S_{po})/2 \quad (13)$$

holds. This condition is similar to that given by (5) for recombination in the transition region on the surface. The recombination current $J_x(v)$ has the form given in Sah, Noyce and Shockley.⁸ With the help of the continuity relation $\text{div } \vec{I} = 0$, the change of the current flow along the channel in the y direction may be set equal to the current flowing out of the channel in the x direction due to electron-hole recombination. Thus,

$$dI(y)/dy = L_S J_x(v), \quad (14)$$

where

$$J_x(v) = qW_I U_I \quad (15)$$

is the recombination current per unit area in the transition region of the surface barrier in the channel. The major variation of $J_x(v)$ with voltage v for positive voltage or forward-bias comes from the term $\sinh(v/2)$ in the recombination-rate expression for U_I which is similar in form to (4).^{6,8} Thus, (15) may be written as

$$J_x(v) = j_{sI} 2 \sinh v/2, \quad (16)$$

where

$$j_{sI} = qn_i W_I f(b)/2\alpha \sqrt{\tau_{po}\tau_{no}} \doteq qn_i W_I /(\tau_{po} + \tau_{no}). \quad (17)$$

Using (16) and (17), (14) may be written as

$$dI(y)/dy = [2qn_i W_I L_S /(\tau_{po} + \tau_{no})] \sinh v/2. \quad (18)$$

The two equations (12) and (18) may be combined to yield

$$\frac{d^2 v}{dy^2} = \frac{2n_i}{n_s D_n (\tau_{po} + \tau_{no})} \sinh \frac{v}{2} \quad (19)$$

if it is assumed that W_I is not a function of y . This assumption is valid inside the channel not too close to the edge of the emitter-base transition region. The solution of (19) may readily be obtained if the channel or the inversion layer is short compared with the width of the grid electrode. Under this condition, it may be assumed that at $y = \infty$, $v(y) = 0$, $I(y) = 0$ and the solution for the current flowing into the surface-inversion layer or channel is

$$I_{sI} = I(0) = 4qW_I L_S \sqrt{\frac{D_n n_i n_s}{\tau_{po} + \tau_{no}}} \sinh \frac{qV_{EB}}{4kT}. \quad (20)$$

Thus, the above result has again the desired form required by the empirical formula given by (3). In particular, (20) shows that m may be as high as 4 if surface-channel or surface-inversion layer current dominates. It also shows that the thermal activation energy of j_{SD} in (3) is that of $\sqrt{n_i}$ in (20) or one fourth the energy gap of silicon. It further shows that the dependence of the channel current on the grid voltage comes from j_{SD} or W_I and n_e . A more accurate solution of (12) may be obtained from (19) if finite boundary conditions are used and the more accurate expression for $J_x(v)$ is used.

IV. SMALL-SIGNAL EQUIVALENT CIRCUIT

The equivalent circuit of the tetrode was obtained in Fig. 9(b) from the physical circuit in Fig. 9(a). The most useful small-signal equivalent-circuit parameters are the hybrid parameters in the grounded emitter connection given by the following equations:

$$V_1 = h_{11}I_1 + h_{12}V_2 + h_{13}V_3 \quad (21)$$

$$I_2 = h_{21}I_1 + h_{22}V_2 + h_{23}V_3 \quad (22)$$

$$I_3 = h_{31}I_1 + h_{32}V_2 + h_{33}V_3 \quad (23)$$

The numerals refer to the electrodes shown in Fig. 9(b): 1 = base, 2 = collector, 3 = grid. Thus, $h_{21} = h_{fe}$, $h_{22} = h_{oe}$, $h_{23} = g_m$, $h_{12} = \mu_{12}$, etc. The hybrid-circuit representation is preferred since it reduces to the usual transistor representation if the base lead is used as input and grid is either dc biased or modulated. If the base lead is ac open circuited and the grid is the input, then the hybrid equations reduce to those similar to the vacuum-tube pentode, thus facilitating the comparison with vacuum pentodes.

The derivation of these h parameters from the equivalent circuit shown in Fig. 9(b) is straight forward with the help of (1) and (2) for the ideal transistor and (3) for the surface diode. The algebra involved is tedious, and only two important parameters will be discussed in the open-base-operation. These are the transconductance $h_{23} = g_m$ and the output admittance $h_{22} = h_{oe}$. The complete expression, neglecting the base resistance r_b , and assuming open base, *i.e.*, I_1 (Base) = 0, are

$$g_m = h_{23} = h_{11} \left[j\omega C_{ge} + g_{SD} \sqrt{\frac{|I_c - I_{co}|}{j_D \alpha_T}} \right] \times \left[|I_c - I_{co}| \frac{q}{kT} - j\omega C_c \right] \quad (24)$$

$$Y_o = h_{22} = j\omega C_c + h_{11}(j\omega C_c + g_c) \times \left[|I_c - I_{co}| \frac{q}{kT} - j\omega C_c \right], \quad (25)$$

where

$$h_{11}^{-1} = \left[g_c + \sqrt{\frac{|I_c - I_{co}|}{j_D \alpha_T}} g_{SD} + h_{fe}^{-1} |I_c - I_{co}| \times \frac{q}{kT} + j\omega(C_c + C_e + C_{gb}) \right] \quad (26)$$

$$h_{fe}^{-1} = \frac{1 - \alpha_T \gamma_N}{\alpha_T \gamma_N} + \frac{(j_{ET} + j_{SD})}{2\sqrt{j_D \alpha_T} |I_c - I_{co}|} \quad (27)$$

and

$$g_{SD} = \frac{\partial j_{SD}}{\partial V_{GB}},$$

which is the transconductance of the surface diode. In this derivation it is assumed that $m=2$ in the surface-diode characteristics.

These relations may be simplified for low and intermediate frequencies. For practical tetrodes, most of the terms in h_{11}^{-1} given by (26) may be neglected, except $h_{fe}^{-1} |I_c - I_{co}| q/kT$. Thus,

$$h_{11}^{-1} \doteq h_{fe}^{-1} |I_{co} - I_c| \frac{q}{kT}. \quad (28)$$

The output admittance becomes

$$Y_o = h_{22} \doteq (1 + h_{fe})j\omega C_c + h_{fe}g_c, \quad (29)$$

and the transconductance is

$$g_m = h_{23} \doteq \left[j\omega C_{ge} + g_{SD} \sqrt{\frac{|I_c - I_{co}|}{j_D \alpha_T}} \right] \times h_{fe} \left[1 - j\omega C_c \cdot \frac{kT}{q} |I_c - I_{co}| \right]. \quad (30)$$

Usually $j_D \alpha_T = 10^{-13}$ amp, $j_{SE} = 10^{-14}$ amp, $C_c = 10$ pf, $C_{ge} \sim 10$ pf and

$$g_{SD} \left[\frac{\alpha_T \gamma_N}{1 - \alpha_T \gamma_N} \right] \sim 10^{-10} \text{ mhos.}$$

Thus, the 3-db frequency of g_m given in (30) is essentially that of h_{fe} , in agreement with that observed in Fig. 7.

The low-frequency transconductance in the intermediate collector-current range may be approximated by

$$g_m = g_{SD} \sqrt{\frac{|I_c - I_{co}|}{j_D \alpha_T}} \frac{\alpha_T \gamma_N}{1 - \alpha_T \gamma_N}. \quad (31)$$

Only the first term in h_{fe}^{-1} given by (27) is retained to obtain (31). The square-root dependence of the transconductance on the collector current is observed in tetrodes in the intermediate collector-current range, and a sample of the experimental data is shown in Fig. 18.

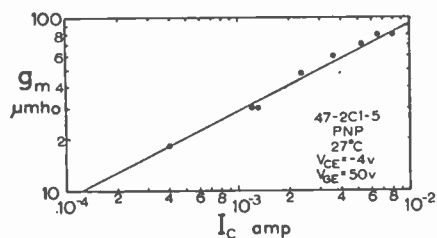


Fig. 18—The low-frequency transconductance plotted as a function of collector current for a $p-n-p$ tetrode.

V. CONCLUDING REMARKS

A new semiconductor tetrode, the surface-potential controlled transistor, has been described. This tetrode employs a field-effect electrode as the grid to modulate the emitter-base surface-diode characteristics of the transistor and thereby the h_{fe} characteristics. The grid features an extremely high input impedance of greater than 10^{15} ohms, and a small capacitance of a few picofarads. Transconductance of 7000 μmhos has been

achieved which is frequency limited by the h_{fe} cutoff.

The elementary theory of the tetrode transistor is worked out, and the theory of the current-voltage characteristics of the emitter-base surface diode is developed in detail.

The development of the surface-potential controlled transistor adds to the transistors and diodes a new family of semiconductor devices which has additional control terminals and which provides additional flexibility and heretofore unobtainable electrical performance.

VI. ACKNOWLEDGMENT

The author is deeply grateful to a number of his colleagues who made the surface-potential controlled transistors a reality. In particular, he is indebted to G. E. Moore and V. H. Grinich for numerous suggestions. He wishes to thank D. A. Tremere and P. S. Flint for fabricating the devices, and H. Bogert for providing the high-frequency data shown in Fig. 7.

CORRECTION

C. V. Freiman, author of "Statistical Analysis of Certain Binary Division Algorithms," which appeared on pp. 91–103 of the January, 1961, issue of PROCEEDINGS, has called the following to the attention of the *Editor*:

- 1) On p. 94, line 11 of the first paragraph, \bar{s}_j replaces s_j .
- 2) On p. 95, (4), $\beta \rightarrow (\alpha\epsilon)$ replaces $\beta \rightarrow (\alpha)$.
- 3) On p. 101, (18), first row of matrix,

6	6	12	42	6	...
6	6	12	42	66	...

 replaces
- 4) On p. 102, fifth line from bottom, drop δ .
- 5) On p. 103, Table IV, each entry of 3–2D should be replaced by 2–2D.

Corrections 4) and 5) were called to the author's attention by Dr. Algirdas Avizienis of the Jet Propulsion Laboratory of the California Institute of Technology.

The Pulsed Ruby Maser as a Light Amplifier*

P. P. KISLIUK† AND W. S. BOYLE†

Summary—A pulsed ruby maser has been operated as a light amplifier using a ruby maser oscillator as a source. A net gain of a factor of two was observed. The dependence of the gain on temperature and pumping power agrees with theory within experimental limits.

INTRODUCTION

USING two pulsed ruby masers, one for the signal source, the other as a light amplifier, we have observed power amplification of a factor of two for visible light. Early observations of line narrowing and the change in the relative intensity of the two R lines in ruby [1], showed that an appreciable part of the fluorescent light at achieved levels of excitation was in fact due to induced emission. The successful operation of maser oscillators [2], [6] leaves no doubt that sufficient gain is attained to overcome the losses [7], but gives no independent measurement of the gain or loss separately. While direct observation of amplification has been obtained in the helium-neon gas device [5], [8] the gain is considerably less than that to be reported herein, and the technique of measurement is different.

The difficulty in observing gain directly is that of distinguishing the signal from the natural fluorescence of the amplifier, *i.e.*, the high noise temperature [7]. By our use of a ruby maser oscillator as a source in these experiments, the signal was made so large that the signal-to-noise ratio was favorable.

PRELIMINARY REMARKS

The intensity I of an electromagnetic wave after traversing a distance x through a medium of absorption coefficient α is

$$I = I_0 e^{-\alpha x}, \quad (1)$$

where I_0 is the incident intensity at $x=0$. At the center frequency of an absorption line [7], [9],

$$\alpha = \frac{2}{\Delta\nu} \sqrt{\frac{\ln 2}{\pi}} \frac{\lambda_0^2}{8\pi\mu^2} \frac{N_1 \left(\frac{g_2}{g_1} \right) - N_2}{\tau}, \quad (2)$$

where $\Delta\nu$ is the width of the absorption line at half maximum (a Gaussian shape is assumed) in cycles per second, λ_0 is the wavelength in cm, g_1 and g_2 are the

statistical weights of the lower and upper states respectively, μ is the refractive index, N_1 and N_2 are the number of atoms per cm^3 of the active species in the lower and upper states, respectively, and τ is the lifetime for spontaneous emission of the upper state in seconds. When $(g_2/g_1) N_1 - N_2$ is negative, one obtains amplification at wavelengths near λ_0 . In solids $\Delta\nu$, λ_0 , μ , and τ may be temperature dependent. For the transition in ruby of interest in this paper, μ and τ are relatively constant, while $\Delta\lambda_0$ and the change in λ_0 are given as functions of temperature in Fig. 1. (These symbols repre-

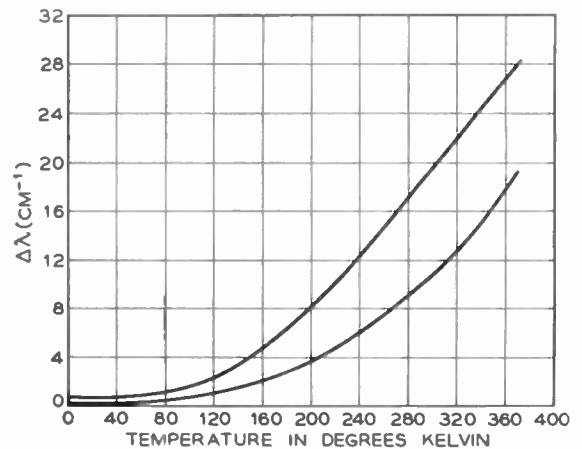


Fig. 1—Upper Curve—Departure of center of R_1 line toward lower wave numbers from an arbitrary zero near $14,418 \text{ cm}^{-1}$ as a function of absolute temperature. At low temperatures where the two components due to the ground state splitting of 0.38 cm^{-1} are resolved, the mean position is plotted. (Data from A. L. Schawlow and G. E. Devlin.)

Lower Curve—Line width at half maximum as a function of absolute temperature [13].

sent the line width and the line position expressed in cm^{-1} .) The maser oscillator yields light in a very narrow range at a wavelength close to that of the center of the natural line at the temperature of the ruby [10]. Therefore, to achieve maximum amplification, the temperature of the amplifier ruby must be close to that of the source ruby. Nevertheless, the optimum condition for a given temperature of the source is reached not when the amplifier is at exactly that temperature, but rather when it is somewhat colder because the narrowing of the line with decreasing temperature causes the gain (or absorption) to be an asymmetric function of the temperature difference between the amplifier ruby and the source ruby. The expected difference is of the order of a few degrees near room temperature for the parameters

* Received by the IRE, July 19, 1961; revised manuscript received, August 30, 1961. This paper was presented at the WESCON Convention, San Francisco, Calif.; August 25, 1961.

† Bell Telephone Labs., Inc., Murray Hill, N. J.

plotted in Fig. 1. As the temperature is lowered, its control becomes more critical because of the narrowing of the line. The exponential dependence of the gain on the departure in frequency from the line center makes the gain appear to be a sharper function of frequency when it is large, which further exaggerates the importance of thermal control at low temperatures.

Consider a three-level maser system with $g_1 = g_2$ in which the time spent in the highest (pumping) state is negligible compared with the normal lifetime in the upper state of the maser transition, τ_u , or with the lifetime—in the presence of the pumping light—of the ground state, τ_g . So long as the average lifetime in the upper maser state is not appreciably shortened by stimulated emission, we have

$$N_2/N_1 = \tau_u/\tau_g. \quad (3)$$

Now τ_g is inversely proportional to the pumping power P .

$$\tau_g = C'/P, \quad (4)$$

whence

$$N_2 - N_1 \equiv -\Delta N = \left(\frac{\tau_u P}{C'} - 1\right) N_1. \quad (5)$$

Furthermore we have

$$N_1 + N_2 = N, \quad (6)$$

the total density of the active species. Therefore,

$$-\Delta N = \left(\frac{CP - 1}{CP + 1}\right) N. \quad (7)$$

Substituting into (1) and (2) and taking the logarithm of both sides,

$$\ln G = \frac{CP - 1}{CP + 1} + K, \quad (8)$$

where G is the gain and K is another constant. For small P , where $CP \ll 1$, the RHS of (8) becomes $\approx (2CP - 1) + K$, and $\ln G$ is a linear function of pumping power, while for $CP \gg 1$ $\ln G$ approaches $1 + K$ asymptotically. One would expect τ_u to be shortened by stimulated emission when $\ln G$ becomes greater than zero, and the asymptote, therefore, to be approached more gradually than indicated by (8). Note that (2) predicts the maximum possible gain at a given temperature to be the inverse of the attenuation at that temperature (for no pumping power) and that if we define the attenuation factor to be A , and $f \equiv \Delta N/N$,

$$\ln G / \ln A = f. \quad (9)$$

For ruby the situation described in this simple treat-

ment is complicated by the fact that the lower state consists, in fact, of two closely spaced levels. At the temperatures of these experiments this can be taken into account by letting the statistical weight of the ground state be twice that of the upper level, *i.e.*, $g_1 = 2g_2$. Furthermore there are two metastable R levels which are populated by the pumping light with appreciable quantum efficiency. When there is maser action evacuating the lower of these levels, the tendency to re-establish a Boltzmann distribution between them occurs so rapidly that a large part of the excitation of the upper state is actually available for induced emission in the maser [11], but the derivation of (3)–(9) requires modification to take the appreciable population of the higher R level into account. Nevertheless, the form of (8) is unchanged and (9) is valid.

APPARATUS

The essential parts of the apparatus are shown in the simplified diagram of Fig. 2. The signal source is a pulsed ruby maser of the conventional type, using a ruby rod 0.2 inch in diameter and 2 inches long, of about 0.05 per cent chromium by weight. The ends are

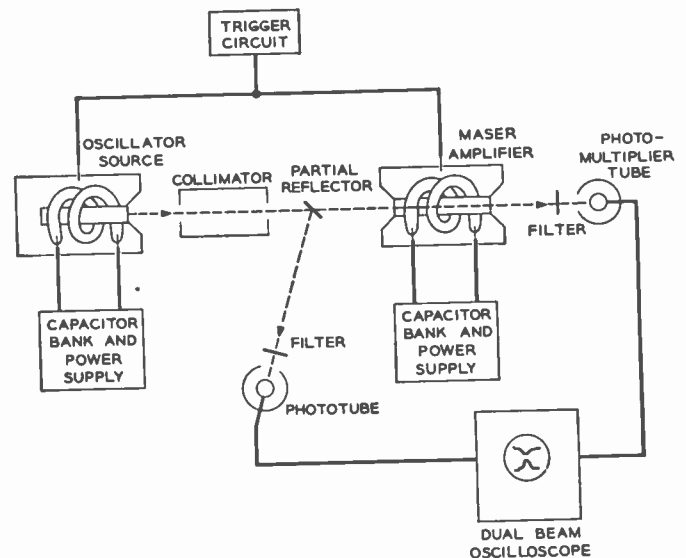


Fig. 2—Simplified diagram of the experimental arrangement.

polished flat and parallel. One end is silvered opaquely; the other silvered to allow a transmission of roughly 5 per cent. The maser light passes first through a filter which cuts down stray light from the oscillator flashtube, then through a collimator, following which a small portion of the beam is reflected out by a microscope cover glass to a phototube which monitors the input signal. A filter in front of this phototube cuts down the stray pumping light from the amplifier flashtube. The main portion of the signal beam then passes through the amplifying ruby which is similar to the source ruby ex-

cept that it is not silvered. The beam from the collimator is small enough in cross section so that no part of it strikes the side of the amplifying ruby or is masked by the amplifier housing. The beam then passes through another filter, and an attenuator, into a photomultiplier tube, which measures the output signal. Both the input monitor and the output signal are displayed on a dual beam oscilloscope. While the GE FT 524 flashtubes which supply pumping power to the two rubies are energized by separate power supplies and capacitors, they are fired simultaneously by a single switch. The housings of the rubies are designed to permit cooling by the flow of cold nitrogen, the temperature of which is measured in both inflow and outflow by means of thermocouples. The housings are lined with magnesium oxide powder in double-walled glass envelopes, providing white surfaces for efficient use of the pumping light. Even with this housing and the filters, a small amount of light from the amplifier flashtube reached the detectors, as well as some of the fluorescent light from the amplifier ruby (the noise referred to above). This is further minimized by masking the entrance to the photomultiplier tube so that it accepts only the solid angle containing the signal beam, but the undesired response is nevertheless easily detected. It is separated from the desired signal by means of its different time dependence.

Gain is measured by comparing the output to input ratio with the amplifier in place, $R_g = I_o/I_m$, to that received when the amplifier is completely removed from the beam, $R_0 = I_o/I_m'$. It is necessary to remove the ruby because the lower state in the transition giving rise to maser action is the ground state. Therefore, if the ruby is in place but not illuminated by the pumping light, it absorbs the signal light. While gain measured in this way, $G = R_g/R_0$, is the net external gain, the true amplification is greater than this because there are losses. The greatest of these losses is a reflection of about 8 per cent as the beam passes through each air-ruby interface.¹

RESULTS

Oscilloscope traces showing gain are exhibited in Fig. 3. The gain and attenuation (both corrected for reflection losses) observed at various temperatures for a constant input energy to the flashtubes are given in Fig. 4 together with theoretical plots of gain or attenuation computed using the parameters plotted in Fig. 1. The theoretical attenuation factor or gain is plotted for various constant values of $-\Delta N$ or ΔN , respectively. Because of inadequate temperature control for the more critical conditions encountered at lower temperature, and because of the difficulty in this region due to frost

on the ruby surfaces, gains were not plotted at lower temperatures. However, it was observed at about -100°C that the amplifier broke into oscillation, and that, therefore, the gain must have been at least a factor of 12.5 to make up for the 92 per cent loss at each end (*i.e.*, only 8 per cent reflected). The gain obtained in this way is also indicated on Fig. 4 to show that it is consistent with the extrapolation from the directly measured gain.

The gain at a fixed temperature is given on a semilog plot as a function of the input energy to the flashtube in Fig. 5.

In both cases the behavior of the measured gain is consistent with the theory outlined earlier. Experimental errors giving rise to the scatter of the experimental points may be due to the crudity of the temperature measurement and control, and possibly also to the unavoidable thermal gradients introduced during the flash. Indeed, the true gains may be somewhat larger than those reported, since all errors outside our control were in the direction of reducing the measured gain, *e.g.*, scattering due to inclusions in the ruby, possible spreading of a small portion of the beam outside of the mask on the detector due to optical inhomogeneity in the ruby, etc. The errors due to these effects are certainly no larger than a few per cent, and are less than the scatter in the experimental points.

The oscilloscope traces of Fig. 3 have been smoothed by the use of long time constants in the detector circuits. If this is not done, the traces are quite ragged because of "spikes" [6], [12] in the output of the maser oscillator.

Because no new spikes appeared in our amplified signal when the long time constant was removed, we conclude that the amplification showed no sudden discontinuities in time, and that the origin of the spikes in maser oscillators lies in the interaction of the amplification and feedback and not in the amplification alone.

The gain of a factor of two at -40°C in the 5 cm long ruby corresponds to an α of -0.14 cm^{-1} for the state of inversion achieved. From (9) we compute f for this condition of pumping to be about 0.18 ± 0.05 consistently for all of the data of Fig. 4. This corresponds to a 26:30.5:43.5 division between the R_2 , R_1 , and ground state levels when the quantum statistical weights are taken into consideration, and the R_1 and R_2 states are assumed to be in thermal equilibrium.

At the highest outputs of the oscillator maser it was possible to saturate the gain so that reduced gain was observed (~ 1.3 where ~ 2.0 was obtained at lower levels). While we observed no saturation of absorption at these levels, it is possible to construct considerably brighter oscillator masers than the one used in this experiment. All the data reported above was taken with such attenuation present that the intensity was at least a factor of four below that where saturation was ob-

¹ This could be minimized by means of antireflection coatings on the ruby faces, but this was not done in the present experiments.

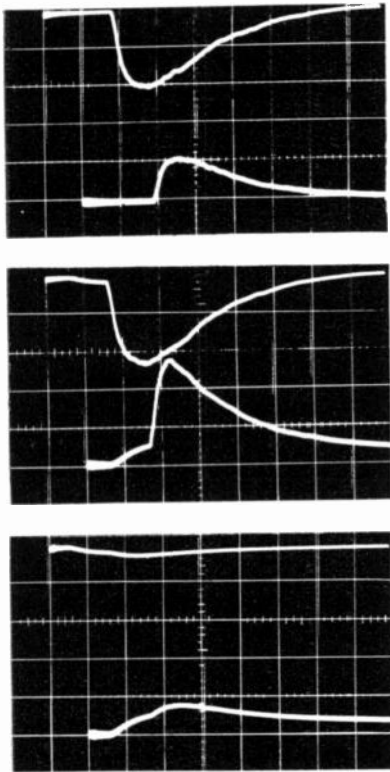


Fig. 3—Oscillograms showing observation of gain. Upper trace in each of the three pairs is response of the input monitor phototube, while lower is signal received at final photomultiplier. Top pair: amplifier ruby removed from beam; middle pair: amplifier ruby present and pumped to exhibit amplified signal; bottom pair: amplifier ruby pumped with no input signal present, showing normal fluorescence and some unavoidable pumping light. Time scale—200 μ sec/div.

The procedure is to subtract the curve of the bottom traces from the corresponding curves of the middle traces, then to compare the ratio of the amplified signal to its monitor with the ratio of the no ruby signal to its monitor.

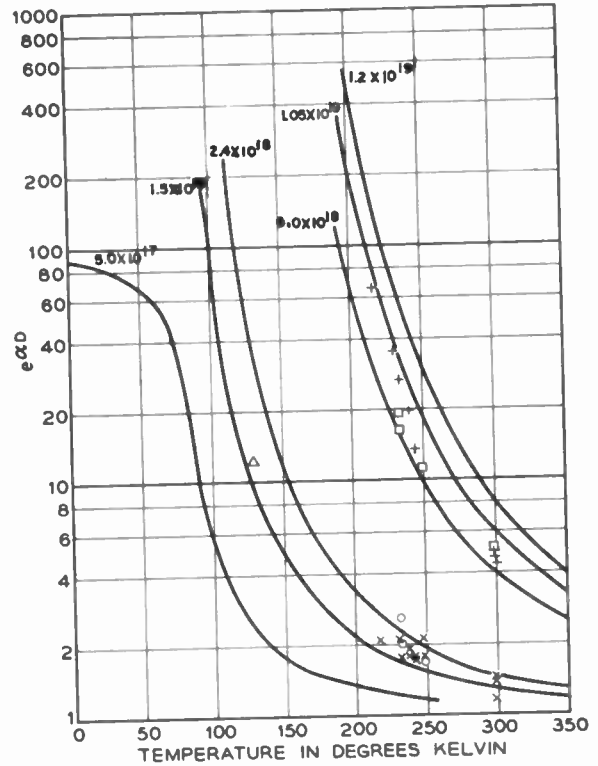


Fig. 4—Solid curves are theoretical values of $e^{\alpha D}$ (i.e., optical density) from (2) for the ruby length $D = 5$ cm, and various indicated constant values of $(N_1 - N_2)$ for attenuation, or $(N_2 - N_1)$ for gain. For the attenuation factor at room temperature $N_1 - N_2 = N$, the number of chromium ions per cm^3 , and the experimental points (+) are for Ruby #1 (nominally 0.05 weight per cent Cr_2O_3) and the points (\square) for Ruby #2 (nominally 0.04 per cent Cr_2O_3). The measured values satisfy (2) for a concentration about 60 per cent of nominal, which is in satisfactory agreement with the true to nominal concentration ratio measured for such rubies [14]. The points (X) and (O) are the measured gains for Ruby #1 and Ruby #2, respectively, at a constant pumping condition, corrected for reflection at the ruby faces. The point (Δ) is the gain obtained from the fact that the amplifier broke into oscillation at that temperature, taking the reflection to be 8 per cent as obtained from the refractive index. The pumping condition is the same as that in the other gain measurements.

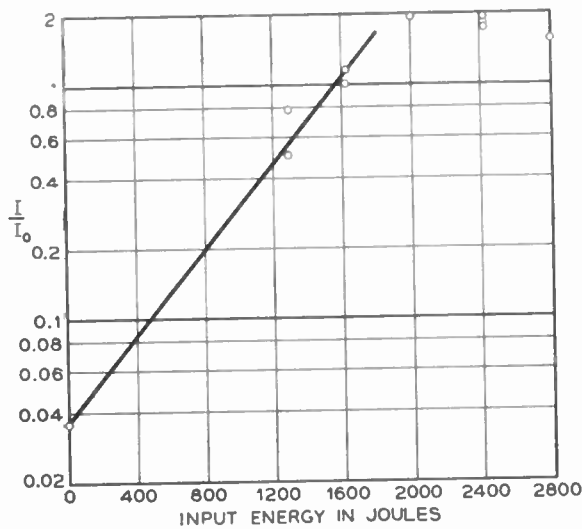


Fig. 5—Gain as a function of input energy to the flashtube at constant temperature.

served, in a region where gain was independent of signal strength within experimental error.

Although the feedback under the conditions of the direct gain measurements was small enough to be ignored, a new problem arises in an amplifier when the feedback is sufficient to nearly cancel the loss. In an oscillator the frequency is automatically that for which the feedback is positive. Since the phase of the feedback is reversed by a change in length of the ruby of only $\lambda_0/4\mu$, where μ is the refractive index, the phase of the feedback in an amplifier for an arbitrary frequency is difficult to control experimentally. The behavior of the amplifier under these conditions would be an interesting experiment in which one might expect large gain for a number of closely spaced extremely narrow frequency bands.

ACKNOWLEDGMENT

Helpful suggestions by D. A. Kleinman and C. G. B. Garrett are gratefully acknowledged. Without the equipment borrowed from a large number of our colleagues this experiment would not have been feasible.

BIBLIOGRAPHY

- [1] T. H. Maiman, "Optical and microwave-optical experiments in ruby," *Phys. Rev. Letts.*, vol. 4, pp. 564-566; June, 1960.
- [2] —, "Stimulated optical emission in ruby," *Nature*, vol. 187, pp. 493-494; August, 1960.
- [3] P. P. Sorokin and M. J. Stevenson, *Phys. Rev. Letts.*, vol. 5, p. 557; 1960.
- [4] —, "Solid state optical maser using divalent samarium in calcium fluoride," *IBM J. Res. & Dev.*, vol. 5, pp. 56-58; January, 1961.
- [5] A. Javan, W. R. Bennett, Jr., and D. R. Herriott, "Population inversion and continuous optical maser oscillation in a gas discharge containing a He-Ne mixture," *Phys. Rev. Letts.*, vol. 6, pp. 106-110; February, 1961.
- [6] R. J. Collins, *et al.*, "Coherence, narrowing, directionality, and relaxation oscillations in the light emission from ruby," *Phys. Rev. Letts.*, vol. 5, pp. 303-305; October, 1960.
- [7] A. L. Schawlow and C. H. Townes, "Infra-red and optical masers," *Phys. Rev.*, vol. 112, pp. 1940-1949; December, 1958.
- [8] A. Javan, W. R. Bennett, Jr., and E. A. Ballik, private communication.
- [9] A. L. Schawlow, "Infra-red and optical masers," *Solid State J.*, vol. 2, pp. 21-27; June, 1961.
- [10] I. D. Abella and H. Z. Cummins, "Thermal tuning of ruby optical maser," *J. Appl. Phys.*, vol. 32, pp. 1177-1178; June, 1961.
- [11] I. Wieder, private communication.
- [12] R. J. Collins, private communication.
- [13] A. L. Schawlow, "Fine structure and properties of chromium fluorescence in aluminum and magnesium oxide," *Advances in Quantum Electronics*, to be published.
- [14] S. V. Grum-Grzhimailo and E. I. Utkina, *Trudy Inst. Krist. Akad. Nauk, U.S.S.R.*, vol. 8, p. 991, 1953; and D. M. Dodd, private communication.

CORRECTION

I. Gerst, co-author of "The Elimination of Intersymbol Interference by Input Signal Shaping," which appeared on pp. 1195-1203 of the July, 1961, issue of PROCEEDINGS, has called the following to the attention of the *Editor*.

On p. 1196, condition c of Theorem 1 should read:

$$c) \quad |G(x+iy)| \leq Ce^{-\alpha x}, \text{ for } x < 0.$$

Inductance in Thin-Film Superconducting Structures*

NORMAN H. MEYERS†, SENIOR MEMBER, IRE

Summary—Thin-film superconducting components and circuits assume the form of coupled strip-transmission lines. The self and mutual inductances of these lines are important to the gain and bandwidth of the circuits. The inductances are influenced strongly by penetration of magnetic fields into the conductors.

This paper gives a field solution which shows that the lowest-order mode on a thin-film superconducting strip line is a TM or E wave because of penetration effects. This mode has a non-negligible axial electric field which makes it incorrect to calculate inductance on a flux-linkage-per-unit-current basis even at low frequencies. However, the low-frequency inductance can be correctly calculated on an energy basis if the kinetic energy of the superelectrons is included in the free energy. This latter method is applied to a structure of current practical interest, that of an arbitrary number of infinitely long, very wide, thin, parallel, superimposed, closely spaced conductors above a common ground plane. All distributed self and mutual inductances with any conductor or combination of conductors in either the super or normal state are evaluated.

INTRODUCTION

CONSIDERABLE work is being done to develop evaporated thin-film superconducting components and circuits for computer applications. This type of circuitry offers the potential advantages of high speed, small size, low-power dissipation, low cost, and logical simplicity. In addition, thin-film superconducting circuitry lends itself readily to batch fabrication by evaporation through masks. Many components and their associated interconnections can be evaporated simultaneously through the same set of masks. The structures thus fabricated assume the form of coupled transmission lines. The components, the thin-film cryotrons, are, in a sense, controlled transmission-line terminations.

Fig. 1 illustrates what is meant here. A control transmission line made of a hard superconductor such as lead passes over a gate transmission line which contains a series section of some softer superconductor such as tin. Suppose that the gate line carries a dc current too small to cause the tin to self-switch into the resistive state. It is possible then, by passing a sufficiently large current pulse along the control line, to cause the associated magnetic field to switch the tin resistive without disturbing the lead. The sudden appearance of a resistive section in the gate line will cause a pair of wavefronts to propagate outward from the tin along the gate line. Eventually, these wavefronts can cause complete transfer of the initial dc gate current into an alternate superconducting path.

Each transmission line of Fig. 1 has a series self-in-

ductance and shunt capacitance per unit length associated with it. In addition, the two lines are inductively and capacitively coupled together. Furthermore, the gate line may contain a series resistance. The resistance, inductance, and capacitance all enter into the dynamic behavior of such structures. The inductance, however, is the most interesting and difficult parameter to calculate since it is influenced by the penetration of magnetic fields into both superconducting and normal conductors. The shunt capacitance and series resistance may be calculated by inspection over a wide range of frequencies, as will be shown.

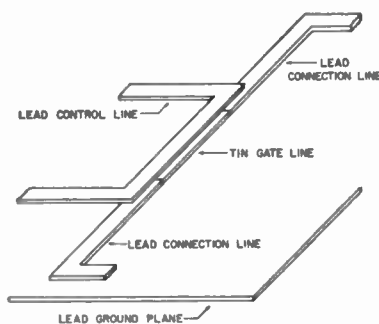


Fig. 1—A thin-film cryotron in the form of coupled strip-transmission lines.

Usually the cryotron gate resistance is small compared with the characteristic impedance of the transmission line in which it is inserted. Under this condition, the transient behavior of the circuit may be adequately characterized in terms of lumped inductance and resistance alone. The shunt capacitance may be neglected in such a case.

There is another reason for emphasizing the role of inductance in the behavior of thin-film superconducting components and circuits. The switching of a superconducting film into the normal state under the influence of an applied magnetic field is governed by magnetic free-energy considerations.¹ The magnetic free energy of a given structure is conveniently expressed in terms of self and mutual inductances. Consequently, the current-gain characteristics of various thin-film cryotrons are related to their inductance parameters. Thus, both the gain and bandwidth of this type of circuitry are dependent on the inductance parameters.

The specific objectives of this paper are as follows.

1) To demonstrate that the lowest-order mode on a superconducting strip line is a TM or E wave because of penetration effects.

* Received by the IRE, April 21, 1961; revised manuscript received, August 28, 1961. The work described in this paper was supported by the Bureau of Ships, U. S. Navy.

† Harvard Business School, Boston 63, Mass. Formerly with Research Center, IBM Corp., Yorktown, N. Y.

¹ F. London, "Superfluids," John Wiley and Sons, Inc., New York, N. Y., vol. 1, p. 130; 1950.

2) To show that the low-frequency field solution has a transmission-line equivalent in terms of a distributed series inductance and resistance and a distributed shunt capacitance. It is further intended to set upper frequency limits on the validity of the equivalent transmission line.

3) To point out that the transmission-line inductance may be correctly calculated by consideration of the static magnetic-field energy only if the kinetic energy of the superelectrons is included as part of the free energy of the structure. It is also intended to show that the familiar *flux-per-unit-current* definition of inductance may not be applied unless the non-negligible axial electric field of the TM mode is taken into account.

4) To demonstrate the important role of the kinetic energy of superelectrons on the inductances of thin-film superconducting structures and to show that this energy leads to an interesting type of lossless slow wave in superconducting strip lines.

5) To apply the method developed for evaluating inductance to the case of an arbitrary number of wide, parallel, superimposed, closely spaced, infinitely long, thin-film conductors above a common ground plane and to calculate all the self and mutual inductances involved with any conductor or combination of conductors, either super or normal.

As early as 1947, Pippard² pointed out that a wave in a superconducting transmission line would be slowed because of penetration of the magnetic field into the conductors. More recently, Young³ suggested that this phenomenon could be exploited in thin-film strip lines to measure penetration depth. Early experiments by Tansal³ agree with predictions. Swihart⁴ has done an exhaustive and excellent analysis of a strip line in which one superconductor is infinitely thick and the other is a thin film. The conductors in Swihart's work are characterized by the two-fluid model, and the dielectric regions inside and outside of the line are treated as lossy. He shows that the velocity is essentially dispersionless at low frequencies and low temperatures where the losses are low. He derives expressions which show the effects on velocity and attenuation as the frequency is raised or the temperature brought close to the critical value.

The field solution given in the Appendix may be regarded as a vast simplification of Swihart's analysis. It is included, however, since it is essential to an understanding of the present paper. The portions of this paper which may be regarded as new contributions are contained primarily in objectives 3) and 5) above. Item 5) is of particular practical significance and is treated at length.

² A. B. Pippard, *Proc. Roy. Soc. (London)*, vol. A191, p. 399; 1947.

³ D. R. Young, J. C. Swihart, S. Tansal, and N. H. Meyers, "Use of a superconducting transmission line for measuring penetration depths," *Bull. Am. Phys. Soc.*, ser. 2, vol. 5, p. 163; 1960.

⁴ J. C. Swihart, "Field solution for a thin-film superconducting strip transmission line," *J. Appl. Phys.*, vol. 32; March, 1961.

SYMBOLS

A complete list of the symbols used in this paper follows. The list is intended to assist the reader in interpreting the equations since, in this particular work, the equations express the salient ideas more clearly than is possible in the text.

Rationalized MKS units are used exclusively throughout this paper.

E	= electric-field intensity
H	= magnetic-field intensity
x, y, z, t	= Cartesian space coordinates and time
I	= amplitude of transmission-line current
V	= amplitude of transmission-line voltage
a	= transmission line, longitudinal propagation constant
j	= square root of minus one
ω	= radian or angular frequency
μ_0	= permeability of free space = $4\pi \times 10^{-7}$ hy/m
σ	= volume conductivity of normal conductor
ϵ	= dielectric constant of transmission-line insulation
ϵ_0	= permittivity of free space = $(1/36\pi) \times 10^{-9}$ fd/m
$\beta_n (n = 1, 2, 3, \dots)$	= reciprocal penetration depth in conductor n
$d_n (n = 1, 2, \dots)$	= thickness of conductor n
$h_n (n = 1, 2, \dots)$	= thickness of insulation layer immediately under conductor n
$\delta = (2/\omega\mu_0\sigma)^{1/2}$	= skin depth in a normal conductor
$F = (j\omega\mu_0\sigma)^{1/2}$	= complex reciprocal skin depth in normal conductor
G	= any complex field or transmission-line quantity
J	= volume density of conduction current (amps/m ²)
Z	= series transmission-line impedance per unit length
Y	= shunt transmission-line admittance per unit length
r	= transmission-line series resistance per unit length
l	= transmission-line series inductance per unit length
c	= transmission-line shunt capacitance per unit length
λ_n	= magnetic flux per unit length linking conductor n
i_n	= conduction current in conductor n
X_1	= an arbitrary but particular value of position coordinate x_1
X_2	= an arbitrary but particular value of position coordinate x_2

situation in detail and has arrived at some helpful conclusions. He has shown that it is possible to define an effective penetration depth such that the spatial variation of magnetic field in a thin film as predicted by the London theory differs by less than $\frac{1}{2}$ per cent from that predicted by the BCS theory. This effective penetration depth, as defined by Ittner, differs from the London penetration depth in that it is a function of film thickness and purity. If either the film thickness or mean-free path becomes less than the coherence length, the effective penetration depth rises rapidly. Using this effective penetration depth, Ittner⁹ has further shown that the measured critical fields of thin tin films are in reasonable agreement with the predictions of London. This last point is significant since it indicates that it makes sense to calculate the field-associated free energy of a film on the basis of the London theory so long as the London penetration depth is replaced by the effective penetration depth. Consequently, one may understand the influence of the nonlocal theories on the inductance formulas derived in this paper simply by using the value of effective penetration depth corresponding to the film thickness and purity in question.

In the Appendix an approximate traveling-wave solution to the field problem just described is given. For parameters and dimensions typical of those currently encountered in practice the solution given is shown to hold over the frequency range from dc up to nearly 1 kMc. This lowest-order field configuration is a TM mode or E wave with non-negligible axial electric field. It may be characterized by an equivalent distributed network consisting of series resistance r , series inductance l , and shunt capacitance c . These per-unit-length transmission-line parameters are shown to be given by the expressions

$$r = (\sigma d_1 W)^{-1} \quad (5)$$

$$l = \mu_0 [h + (d_1/3) + \beta^{-1} \coth \beta d_2] / W \quad (6)$$

and

$$c = \epsilon W / h. \quad (7)$$

The per-unit-length resistance and capacitance are exactly what one expects on the basis of static considerations. However, the inductance is clearly influenced by field penetration into each conductor.

The inductance expression is made up of three parts, one associated with the dielectric region, one associated with the normal conductor, and a final contribution from the superconductor. The contribution to the inductance from the dielectric region is just what one would expect from low-frequency considerations. The contribution from the normal conductor is what one would expect from low-frequency field-energy considerations but differs from what would be predicted on the basis of *flux linkages per unit current*. This will be explained in detail shortly. The contribution to inductance

from the superconductor is very interesting. If the superconductor is thick compared with a penetration depth the strip-line inductance behaves as though the insulation were one penetration depth thicker than it actually is. On the other hand, if the superconductor is made thin compared with a penetration depth, the inductance rises rapidly. This is due to the kinetic energy of the superelectrons which is part of the free electromagnetic energy of the system, as will be shown shortly. This effect of rising inductance with decreasing film thickness is actually enhanced by nonlocal considerations since the effective penetration depth increases with decreasing thickness.

If the normal conductor were replaced by a second superconductor and the field problem solved anew and again reduced to an equivalent transmission line, the capacitance would be unchanged, the resistance would vanish, and the inductance would be modified such that the term $d_1/3$ of (6) would be replaced by the term $\beta_1^{-1} \coth \beta_1 d_1$. The velocity of propagation on such a line would be completely dispersionless, and there would be no attenuation for the frequencies, temperature, and dimensions considered here. The velocity of propagation, normalized with respect to the velocity of a plane unbounded wave in the dielectric, would be

$$v/v_0 = (lc)^{-1/2} / v_0 \\ = [1 + (h\beta_1)^{-1} \coth \beta_1 d_1 + (h\beta_2)^{-1} \coth \beta_2 d_2]^{-1/2}. \quad (8)$$

The velocity can be made small by making d_1 and d_2 small compared with β_1^{-1} and β_2^{-1} , respectively. It can also be made small by making h small compared with a penetration depth in each conductor. Perhaps this lossless slow wave can be utilized eventually in a delay-line memory.

INDUCTANCE BY STATIC-FIELD ENERGY AND BY FLUX-PER-UNIT CURRENT

In the Introduction it was pointed out that emphasis in this paper is to be placed on the inductance parameter. The correct expression for inductance has been established by means of a fairly detailed field analysis, presented in the Appendix, and backed up by Swihart's more extensive treatment. In this section it will be demonstrated that the same inductance can readily be obtained by evaluating the static magnetic-field energy if the kinetic energy of the superelectrons in the superconductor is included. It will also be shown that the flux-linkage-per-unit-current definition of inductance leads to a different and incorrect result. The reason is that the lowest-order mode in the wave-guiding structure under consideration is a TM or E wave rather than the more familiar TEM wave, for which the two inductance definitions are equivalent. By taking the axial electric field into account, the flux-linkage approach can be reconciled with the static-field-energy approach and hence made to agree with the inductance expression obtained from the field analysis.

The static- or low-frequency magnetic-field distribution in the structure of Fig. 2 is sketched in Fig. 3. The field expressions in each region are as follows.

Normal conductor:

$$H_y(x_1) = -I x_1 / W d_1. \tag{9}$$

Dielectric:

$$H_y(x) = I / W. \tag{10}$$

Superconductor:

$$H_y(x_2) = I \sinh \beta x_2 / W \sinh \beta d_2. \tag{11}$$

From the Maxwell equation $\text{curl } \mathbf{H} = \mathbf{J}$, one can obtain the expression for volume density of the supercurrent in the superconductor:

$$J_z(x_2) = \partial H_y(x_2) / \partial x_2 = I \beta \cosh \beta x_2 / W \sinh \beta d_2. \tag{12}$$

In the normal conductor and dielectric regions the magnetic free-energy density is just $\mu_0 |\mathbf{H}|^2 / 2$, while in the superconducting region the magnetic free-energy density is $\mu_0 |\mathbf{H}|^2 / 2 + \mu_0 |\mathbf{J}|^2 / 2\beta^2$,¹⁰ since the kinetic energy of the superelectrons must be included. Integrating these energy-density expressions throughout the thickness and width of the structure and over a unit length gives the total low-frequency magnetic free energy per unit length K :

$$K = \mu_0 I^2 [h + (d_1/3) + \beta^{-1} \coth \beta d_2] / 2W. \tag{13}$$

By requiring that the inductance per unit length l account for this free energy, l may be evaluated.

Since

$$K = l I^2 / 2 \tag{14}$$

$$l = \mu_0 [h + (d_1/3) + \beta^{-1} \coth \beta d_2] / W. \tag{15}$$

This expression agrees with that given in (6) taken from the field analysis in the Appendix.

The magnetic flux linkage per unit length at low frequencies λ is simply

$$\begin{aligned} \lambda / \mu_0 &= \int_0^{d_2} H_y(x_2) dx_2 + \int_{-h/2}^{h/2} H_y(x) dx \\ &+ \int_{-d_1}^0 H_y(x_1) dx_1, \end{aligned} \tag{16}$$

where the various magnetic-field variations are given in (9)–(11). Evaluating the integral and assuming that inductance per unit length is simply flux linkage per unit length per unit current yields the “incorrect” result

$$l = \mu_0 [h + (d_1/2) + \beta^{-1} (\coth \beta d_2 - \text{csch } \beta d_2)] / W. \tag{17}$$

Only the term arising from the dielectric region agrees with the correct result obtained by the energy approach.

¹⁰ London, *op. cit.*, p. 66.

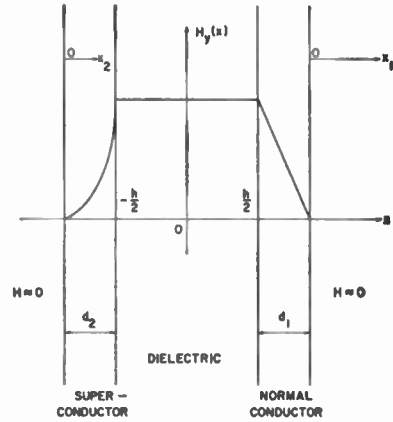


Fig. 3—Low-frequency magnetic-field distribution in a thin-film strip line.

The inconsistency can be reconciled by recognizing that there is a non-negligible axial electric field in both conducting regions. The flux-linkage-per-unit-current definition of inductance cannot be applied without taking this longitudinal E field into account. To demonstrate this, consider the process of converting the Maxwell equation $\text{curl } \mathbf{E} = -j\omega\mu_0 \mathbf{H}$, into the transmission-line voltage equation $dV(z)/dz = -ZI(z)$. In integral form the Maxwell equation is

$$\oint_C \mathbf{E} \cdot d\mathbf{l} = -j\omega\mu_0 \int_A \mathbf{H} \cdot d\mathbf{a}. \tag{18}$$

The contour C to be used is shown in Fig. 2 as the dotted path $abcdefgha$. As pointed out in defining voltage in the Appendix, the contributions to the line integral of electric field along the portions of the path C associated with transverse electric field in the conductors are negligible for a wide range of frequencies and dimensions. Hence, neglect contributions from bc , de , fg , and ha . There remains

$$\begin{aligned} \int_a^b E_x dx - \int_d^c E_z(X_1) dz - \int_f^e E_x dx + \int_g^h E_z(X_2) dz \\ = -j\omega\mu_0 \int_A H_y dx dz. \end{aligned} \tag{19}$$

The right-hand side of (19) is the negative time derivative of the magnetic flux linking the path. If the portion of path C from e to f is assumed to be at z and the portion from a to b is assumed to be at $z+dz$ so that the loop is only dz wide, then the first term on the left side of (19) is $V(z+dz)$, while the third term is $-V(z)$. Furthermore, since the path C is only dz wide, the longitudinal variations of E_x in each conductor along the path may be neglected. Similarly, the longitudinal variations of H_y may also be neglected. Eq. (19) then becomes

$$dV(z)/dz = -j\omega\mu_0 \int_{x_2}^{x_1} H_y dx + E_z(X_1) - E_z(X_2). \tag{20}$$

Comparing (20) with the transmission-line voltage equation shows that the series impedance per unit length is

$$Z = \left[j\omega\mu_0 \int_{X_2}^{X_1} H_y dx + E_z(X_2) - E_z(X_1) \right] I^{-1}. \quad (21)$$

It is now clear that the inductance per unit length cannot be evaluated as the flux linkage per unit current if the axial electric field in either conductor has a non-negligible imaginary part. Eq. (21) can be evaluated in general for arbitrary values of X_2 and X_1 and the resulting impedance can be shown to agree with that derived in the Appendix (76).

INDUCTANCE IN IN-LINE SUPERCONDUCTING STRUCTURES

Thus far it has been shown that the inductance in a thin-film strip-line structure may be evaluated correctly solely by consideration of the static magnetic-field energy, including the kinetic energy of the superelectrons. A sufficiently detailed field analysis has shown this approach to be valid over a wide range of frequencies and dimensions. It is desirable now to extend this approach to a structure of current practical interest. The geometry chosen involves a number of long, parallel, superimposed conductors of equal width above a ground plane, as shown in Fig. 4. The self and mutual inductances in this structure will be calculated in general terms with any conductor or combination of conductors in either the superconducting or normal state.

The assumptions to be made are as follows.

1) All conductors are parallel, of equal width, perfectly registered, and infinitely long.

2) Width W is much greater than the total thickness T , so that fringing is negligible.

3) Width W is narrow compared with a quarter wavelength at the highest frequencies of interest, so that the structure is effectively lumped in the transverse plane and coupled transmission-line notions apply.

4) All excitation currents return in the ground plane.

5) All regions are linear, so that superposition applies.

6) The frequency is low enough so that all the assumptions of the field analysis in the Appendix apply.

In summary they are:

- a) Displacement current is negligible in normal conductors.
- b) Displacement currents and normal conduction currents in superconductors are negligible compared with the supercurrents, so that the *two-fluid* model need not be applied.
- c) Only displacement currents exist in dielectric regions.
- d) Inequalities (60)–(63) of the Appendix are effectively satisfied, and inequality (75) holds in each normal conductor.

Self and mutual inductances must be defined such that they correctly account for the magnetic free energy for any excitation. If the structure shown in Fig. 4 has

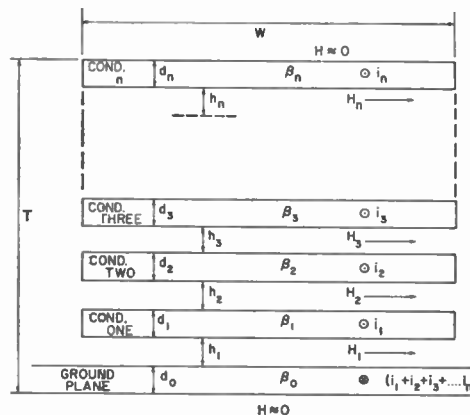


Fig. 4—Cross-sectional view of an in-line superconducting structure of n long, parallel, superimposed conductors. (Distorted scale; actually $W \gg T$.)

3 conductors and a ground plane, it is, in effect, three coupled loops. Under the assumptions made, it may be characterized magnetically by the coupled circuit equations,

$$\left. \begin{aligned} \lambda_1 &= l_{11}i_1 + l_{12}i_2 + l_{13}i_3 \quad (a) \\ \lambda_2 &= l_{21}i_1 + l_{22}i_2 + l_{23}i_3 \quad (b) \\ \lambda_3 &= l_{31}i_1 + l_{32}i_2 + l_{33}i_3 \quad (c) \end{aligned} \right\} \quad (22)$$

The diagonal terms are self inductances per unit length and the off-diagonal terms are mutual inductances per unit length. The reciprocity theorem applies, so that the inductance matrix is symmetrical; *i.e.*, $l_{12} = l_{21}$ etc.

The energy required to build up currents i_1 , i_2 , and i_3 from zero is

$$K = \int_0^{\lambda_1} i_1 d\lambda_1 + \int_0^{\lambda_2} i_2 d\lambda_2 + \int_0^{\lambda_3} i_3 d\lambda_3. \quad (23)$$

Eq. (23) is evaluated by differentiating (22), multiplying each by the appropriate current and carrying out the integrations. Note that the off-diagonal terms integrate in pairs rather than individually, so the result is

$$\begin{aligned} K &= (l_{11}i_1^2 + l_{22}i_2^2 + l_{33}i_3^2)/2 \text{ self-inductance} \\ &\quad \text{energy terms,} \\ &+ (l_{12}i_1i_2 + l_{13}i_1i_3 + l_{23}i_2i_3) \text{ mutual-inductance} \\ &\quad \text{energy terms.} \end{aligned} \quad (24)$$

This magnetic free energy K expressed in network terms can be equated to the magnetic-field and super-electron free-energy densities integrated throughout a unit length of the structure, irrespective of the excitation.

Ampere's circuital law establishes the uniform fields in each dielectric region in terms of the arbitrary excitation currents. These are also the known surface fields for evaluation of the free energy in the superconductors:

$$\left. \begin{aligned} H_1 &= (i_1 + i_2 + i_3)/W \quad (a) \\ H_2 &= (i_2 + i_3)/W \quad (b) \\ H_3 &= i_3/W \quad (c) \end{aligned} \right\} \quad (25)$$

Evaluation of the magnetic free energy per unit length in each dielectric region can now be carried out. The combined result for all dielectric regions is

$$K_h = \int_V k_h dV = \int_V [\mu_0 |H|^2 / 2] dV$$

$$= \mu_0 [h_1 i_1^2 + (h_1 + h_2) i_2^2 + (h_1 + h_2 + h_3) i_3^2] / 2W$$

$$+ \mu_0 [h_1 i_1 i_2 + h_1 i_1 i_3 + (h_1 + h_2) i_2 i_3] / W. \quad (26)$$

Consider next the general problem of an arbitrary superconducting region in the structure under discussion. The situation is shown in Fig. 5. The surface field on one side of the conductor is H^s , while on the other side it is αH^s , where α is a real constant of proportionality which may be either plus or minus. The solution of London's equations at low frequencies gives the field- and current-density distributions in the general superconductor under discussion:

$$H(x) = [(\alpha + 1)H^s / 2 \cosh(\beta d / 2)] \cosh \beta x$$

$$+ [(\alpha - 1)H^s / 2 \sinh(\beta d / 2)] \sinh \beta x, \quad (27)$$

$$J(x) / \beta = [(\alpha + 1)H^s / 2 \cosh(\beta d / 2)] \sinh \beta x$$

$$+ [(\alpha - 1)H^s / 2 \sinh(\beta d / 2)] \cosh \beta x. \quad (28)$$

Using these distributions, one can evaluate the magnetic free energy per unit length, including the kinetic energy of the superelectrons:

$$K_s = \int_V k_s dV = \mu_0 \int_V \{ |H|^2 + \beta^{-2} |J|^2 / 2 \} dV$$

$$= [\mu_0 W (H^s)^2 / 8\beta] [(\alpha + 1)^2 / \cosh^2(\beta d / 2)$$

$$+ (\alpha - 1)^2 \sinh^2(\beta d / 2)] \sinh \beta d. \quad (29)$$

For the various superconducting regions it is clear from Fig. 4 and (25) that the pertinent values of H^s and α are given in Table I.

$$[L_s] = \frac{\mu_0}{W} \begin{bmatrix} (h_1 + b_0 + b_1) & (h_1 + b_0 + c_1) & (h_1 + b_0 + c_1) \\ (h_1 + b_0 + c_1) & (h_1 + h_2 + b_0 + b_2 + 2c_1) & (h_1 + h_2 + b_0 + 2c_1 + c_2) \\ (h_1 + b_0 + c_1) & (h_1 + h_2 + b_0 + 2c_1 + c_2) & (h_1 + h_2 + h_3 + b_0 + b_3 + 2c_1 + 2c_2) \end{bmatrix}. \quad (37)$$

Evaluating (29) for each region,

$$K_{s0} = (\mu_0 / 2W) (i_1 + i_2 + i_3)^2 b_0, \quad (30)$$

$$K_{s1} = (\mu_0 / 2W) [i_1^2 b_1 + 2(i_2 + i_3)(i_1 + i_2 + i_3)c_1], \quad (31)$$

$$K_{s2} = (\mu_0 / 2W) [i_2^2 b_2 + 2i_3(i_2 + i_3)c_2] \quad (32)$$

$$K_{s3} = (\mu_0 / 2W) i_3^2 b_3, \quad (33)$$

where, for convenience,

$$b_n (n = 1, 2, 3 \dots) = \beta_n^{-1} \coth \beta_n d_n \quad (34)$$

and

$$c_n (n = 1, 2, 3 \dots) = \beta_n^{-1} \tanh(\beta_n d_n / 2). \quad (35)$$

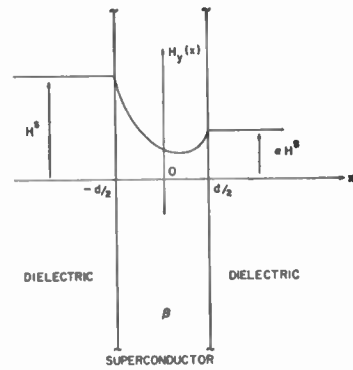


Fig. 5—Sketch of the magnetic-field distribution in an arbitrary conductor of the structure of Fig. 4.

TABLE I

Superconducting Region	H^s	α
0	$(i_1 + i_2 + i_3) / W$	0
1	$(i_2 + i_3) / W$	$1 + i_1 / (i_2 + i_3)$
2	i_3 / W	$1 + i_2 / i_3$
3	i_3 / W	0

All of the magnetic free-energy expressions may now be combined.

$$K = K_h + K_{s0} + K_{s1} + K_{s2} + K_{s3} \quad (36)$$

\uparrow \uparrow \uparrow \uparrow \uparrow
 total free from from from from from
 energy per (26) (30) (31) (32) (33)
 unit length

The total free energy in terms of dimensions and physical constants of materials from (36) may next be equated to the total free energy in terms of inductances from (24). Each self- and mutual-inductance term can readily be identified since the two energy expressions must be equal for any arbitrary combination of independent currents. Thus, with all conductors superconducting, the inductance matrix of the structure of Fig. 4 is

Note that the mutual inductance between any two conductors is close to, but not equal to, the smaller self inductance of the pair.

Careful study of matrix (37) reveals the manner of extending this result to an arbitrary number of conductors without further analysis. The self inductance of the N th conductor, counting upward away from the ground plane, is

$$l_{NN} = \mu_0 \left\{ \sum_{n=1}^N h_n + b_0 + b_N + 2 \sum_{n=1}^{N-1} c_n \right\} / W. \quad (38)$$

The mutual inductance between the M th conductor and the N th conductor when M is less than N is

$$L_{MN} = \mu_0 \left\{ \sum_{n=1}^M h_n + b_0 + c_M + 2 \sum_{n=1}^{M-1} c_n \right\} / W, \quad (39)$$

for $M < N$.

It is interesting to note that this result is independent of N . This is a consequence of the fact that current in the M th conductor produces no appreciable field in the space between conductors M and N , and thus there is no interaction energy associated with this space when both conductors are excited by source currents.

It is now possible to attach some limited physical significance to the terms b_n and c_n . Dimensionally, each is a

Evaluating the integral, one obtains

$$K_{n1} = (\mu_0/2W)d_1 \{ i_1^2/3 + (i_2 + i_3)(i_1 + i_2 + i_3) \}. \quad (42)$$

Comparison of this expression with the free energy in the superconducting state, K_{s1} from (31), is very interesting. The term involving i_1^2 does not correctly pass over from the super to normal states by letting the penetration depth go to infinity ($\beta_1 \rightarrow 0$). All the remaining energy terms, however, do correctly follow in the limit as β_1 vanishes. Hence, all the results except l_{11} follow directly from the superconducting case already calculated, and l_{11} is obtained merely by replacing the term b_1 by the term $d_1/3$.

With conductor one in the normal state the inductance matrix (37) becomes

$$[L_{n1}] = \frac{\mu_0}{W} \begin{bmatrix} (h_1 + b_0 + d_1/3) & (h_1 + b_0 + d_1/2) & (h_1 + b_0 + d_1/2) \\ (h_1 + b_0 + d_1/2) & (h_1 + h_2 + b_0 + b_2 + d_1) & (h_1 + h_2 + b_0 + d_1 + c_2) \\ (h_1 + b_0 + d_1/2) & (h_1 + h_2 + b_0 + d_1 + c_2) & (h_1 + h_2 + h_3 + b_0 + b_3 + d_1 + 2c_2) \end{bmatrix}. \quad (43)$$

distance. The quantity b_n is a penetration distance associated with self current in conductor n . Hence it appears only in the self-inductance term of conductor n . The term b_0 is an exception since every source current always returns through the ground plane. The quantity c_n , on the other hand, is a penetration distance associated with induced current in conductor n . If, for example, conductor two is excited, as it would be in evaluating its self-inductance, the term c_1 appears twice since a field is applied to each face of conductor one and penetrates a distance into each face determined by the induced screening currents. On the other hand, if the mutual inductance between conductors one and two is to be evaluated, think of conductors one and two as each driven by a source current and then ponder over what space to evaluate the energy associated with both loop one and loop two. Evidently it is legitimate to regard the space of loop one, extending a distance c_1 into conductor one from the loop-one side, as the appropriate region over which to evaluate the mutual energy. This same rule, although not rigorous or at all obvious, gives the correct answer in the case of the other mutual-inductance terms.

If one of the conductors, for example conductor one, is in the normal state, its magnetic free energy is different from when it is in the superconducting state. Every surface field is still given correctly in terms of the independent currents by (25). Consequently, the free-energy expressions all remain valid, except for conductor one. In the normal state

$$K_{n1} = \int_V k_{n1} dV = (W\mu_0/2) \int_{x=0}^{x=d_1} |H|^2 dx, \quad (40)$$

where

$$H = (i_2 + i_3 + i_1 x/d_1)/W. \quad (41)$$

Again it is a simple matter to generalize this result to any number of conductors. Furthermore, the case of any number or combination of conductors in the normal state also follows directly. Modifying (37)–(39) to take normal conductors into account is a two-step process. For each normal conductor

- 1) replace b_n by $d_n/3$,
- and
- 2) replace c_n by $d_n/2$.

CONCLUSIONS

Inductances in thin-film superconducting structures can be evaluated up to about 1 kMc simply by consideration of the static magnetic-field energy, including the kinetic energy of the super electrons. The flux-linkage-per-unit-current definition of inductance cannot be used because the lowest-order mode which can exist on the structures in question is a TM or E wave with a non-negligible axial electric field. All the self- and mutual inductances in coupled strip-line structures are strongly influenced by penetration effects. In the case of parallel, superimposed strips above a common ground plane, the mutual inductance between any pair of strips is close to, but not equal to, the smaller self-inductance of the pair.

APPENDIX

REDUCTION OF FIELD SOLUTION TO EQUIVALENT TRANSMISSION LINE

An approximate traveling-wave field solution is first given for the strip-line structure of Fig. 2. At low frequencies this is shown to reduce to an equivalent transmission line. For typical dimensions and parameters, frequency limits are set on the validity of this procedure.

STRIP-LINE FIELD SOLUTION

Eqs. (1)–(3) govern the behavior of the magnetic field in each region. Naturally, the full set of Maxwell equations applies in each region, subject to the assumptions already discussed concerning the relative magnitudes of displacement, normal-conduction, and super-currents.

The sinusoidal steady state is assumed and is characterized by angular frequency ω . The fields are assumed to be driven by a current of complex amplitude I which flows in the positive z direction in the superconductor and in the negative z direction in the normal conductor. A forward traveling-wave solution is sought. Hence, each field component or equivalent transmission-line quantity is assumed to have a longitudinal variation characterized by the factor $\exp(-jaz)$, where a is the complex propagation constant. Thus, one obtains

$$\partial G(z)/\partial z = -jaG(z), \tag{44}$$

where $G(z)$ is any complex field or transmission-line quantity.

Experience shows¹¹ that a solution of the type sought can be obtained if field components E_x , E_z , and H_y are assumed to exist in each region. The axial electric field is necessary in order to account for the flow of field energy into the normal conductor for conversion to Joule heat and also to account for the flow of magnetic-field energy into and out of both conductors because of penetration effects.

The boundary conditions are interesting. First it is assumed that there is no appreciable magnetic field outside the strip line. Hence,

$$H_y = 0 \quad \text{at} \quad x_1 = x_2 = 0. \tag{45}$$

Since displacement currents are negligible in each conductor, the change in magnetic-field intensity with position as one passes through either conductor is just equal to the conduction current per unit width. Hence,

$$H_y = I/W \quad \text{at} \quad x_1 = -d_1. \tag{46}$$

and

$$H_y = I/W \quad \text{at} \quad x_2 = d_2. \tag{47}$$

At the boundaries between the dielectric and the conductors, the tangential components of electric and magnetic-field intensity must be continuous. The normal electric field at these interfaces may be discontinuous since field lines may terminate in or originate from surface charges just inside the conductors. Because the tangential field components must be continuous across the strip-line interfaces there is one and only one longitudinal propagation factor a for the complete structure.

Subject to all these assumptions and boundary conditions, the approximate field solution in the structure of Fig. 2 is shown below.

Low-Frequency Strip-Line Field Solution

Normal Conductor:

$$H_y(x_1) = -I \sinh Fx_1/W \sinh Fd_1 \tag{48}$$

$$E_x(x_1) = -Ija \sinh Fx_1/W\sigma \sinh Fd_1 \tag{49}$$

$$E_z(x_1) = -I(j\omega\mu_0)^{1/2} \cosh Fx_1/W\sigma^{1/2} \sinh Fd_1. \tag{50}$$

Dielectric:

$$H_y(x) = I/W \tag{51}$$

$$E_x(x) = Ia/W\omega\epsilon \tag{52}$$

$$E_z(x) = Ij\omega\mu_0[(\beta^{-1} \coth \beta d_2 - F^{-1} \coth Fd_1) - 2x(\beta^{-1} \coth \beta d_2 + F^{-1} \coth Fd_1)/h]/2W. \tag{53}$$

Superconductor:

$$H_y(x_2) = I \sinh \beta x_2/W \sinh \beta d_2 \tag{54}$$

$$E_x(x_2) = -Ia\omega\mu_0 \sinh \beta x_2/W\beta^2 \sinh \beta d_2 \tag{55}$$

$$E_z(x_2) = Ij\omega\mu_0 \cosh \beta x_2/W\beta \sinh \beta d_2 \tag{56}$$

where

$$F = (j\omega\mu_0\sigma)^{1/2} \tag{57}$$

and

$$a = \omega(\mu_0\epsilon)^{1/2}[1 + (Fh)^{-1} \coth Fd_1 + (\beta h)^{-1} \coth \beta d_2]^{1/2}. \tag{58}$$

Remember that the notation used here assumes the sinusoidal steady state in time, and that the longitudinal dependence is characterized by the complex propagation factor, so that each instantaneous field quantity is obtained from (48)–(56) in the following manner:

$$H_y(x_1, z, t) = \text{Re} \{ H_y(x_1) \exp j(\omega t - az) \}. \tag{59}$$

The field solution given here is readily seen to satisfy the prescribed boundary conditions. Note, however, that the axial electric field E_z does not vanish at $x_1 = x_2 = 0$. Consequently, the assumption that there is no field outside the strip-line structure is not completely valid. It is not too difficult, however, to take external fields into account in a more nearly exact solution, as Swihart has done. The results at low frequencies are essentially unaltered from the simpler version given in this paper.

If the field quantities of (48)–(56) are substituted into the Maxwell equations and into (1)–(3) identities are obtained subject to the following approximations.

Normal Conductor:

$$a^2/\omega\mu_0\sigma \ll 1. \tag{60}$$

Dielectric:

$$\omega^2\mu_0\epsilon h\beta^{-1} \coth \beta d_2/2 \ll 1 \tag{61}$$

and

$$\omega^2\mu_0\epsilon hF^{-1} \coth Fd_1/2 \ll 1. \tag{62}$$

Superconductor:

$$a^2\beta^{-2} \ll 1. \tag{63}$$

¹¹ Ramo, *op. cit.*, p. 323.

Assume the following typical dimensions and parameters:

$$d_1 = d_2 = 5000 \text{ \AA}$$

$$\epsilon/\epsilon_0 = 4$$

$$\sigma = 4.26 \times 10^6 \text{ mhos/cm (for tin film at } 4.2^\circ\text{K)}$$

$$\lambda = \beta^{-1} = 1500 \text{ \AA.}$$

Using these values, and assuming that much less than unity means equal to or less than 0.01, one can show that inequalities (60)–(63) are satisfied for the range of frequencies from dc up to about 10^{13} cps.

EQUIVALENT TRANSMISSION LINE

A well-defined series conduction current was assumed to exist in each conductor in the preceding field solution. This current $I(z)$ was used to establish boundary conditions on magnetic field H_y in each region. Consequently, the axial variation of the conduction current must be characterized by the same propagation factor a as the field quantities.

$$I(z) = I \exp(-jaz). \tag{64}$$

In order to reduce the approximate field solution to an equivalent transmission-line representation, it is necessary to be able to define unambiguously a voltage $V(z)$. Toward this end let us examine the transverse electric field E_x in the structure. Voltage must be defined as the line integral of this transverse electric field across the strip-line structure. There is some uncertainty as to just what two points should be chosen as the end points of the integration. If one integrates only across the dielectric,

$$V = \int_{-h/2}^{h/2} E_x(x) dx = Iah/W\omega\epsilon. \tag{65}$$

The line integral of transverse electric field through each conductor can be separately evaluated and compared with (65). Using the parameter values already assumed, it is found that the contribution to voltage arising from transverse electric field in the normal conductor is completely negligible over a wider frequency range than that for which inequality (62) is satisfied. Similarly, the contribution to voltage arising from transverse electric field in the superconductor is negligible compared with the voltage of (65) over a wider frequency range than that for which inequality (61) is satisfied. If, however, the insulation thickness should become very small compared with a penetration depth in the superconductor or compared with the skin depth in the normal conductor, then the frequency range over which a voltage can be defined unambiguously is reduced.

Having suitably defined a voltage and current, one can determine the per-unit-length series impedance Z and shunt admittance Y of the equivalent transmission

line. This is done by substituting the voltage and current expressions into the transmission-line equations.

$$dV(z)/dz = -ZI(z)$$

or

$$jaV(z) = ZI(z) \tag{66}$$

and

$$dI(z)/dz = -YV(z)$$

or

$$jaI(z) = YV(z). \tag{67}$$

Substituting (64) and (65) into (66) and (67),

$$Z = ja^2h/\omega\epsilon W \tag{68}$$

and

$$Y = j\omega\epsilon W/h. \tag{69}$$

The admittance is clearly that due to the capacitance between conductors and is independent of any penetration effects. The series impedance can be put in a more meaningful form by reference to (58).

$$Z = j\omega\mu_0(h + F^{-1} \coth Fd_1 + \beta^{-1} \coth \beta d_2)/W. \tag{70}$$

The impedance has both real and reactive parts since the second term in brackets, involving F , is complex. This term may be separated into its real and imaginary parts. With the aid of (57),

$$F^{-1} \coth Fd_1 = \delta \left\{ \frac{\sinh \gamma - \sin \gamma}{\cosh \gamma - \cos \gamma} - j \frac{\sinh \gamma + \sin \gamma}{\cosh \gamma - \cos \gamma} \right\} \tag{71}$$

where

$$\gamma = 2l_1/\delta \tag{72}$$

and

$$\delta = (2/\omega\mu_0\sigma)^{1/2}, \tag{73}$$

the normal skin depth. For sufficiently low frequencies δ becomes large, γ becomes small, and the power series expansions of the various functions in (71) converge rapidly. It can be shown directly that

$$F^{-1} \coth Fd_1 = (d_1/3) - j(\omega\mu_0\sigma d_1)^{-1} \tag{74}$$

if

$$d_1^4(\omega\mu_0\sigma)^2/30 \ll 1. \tag{75}$$

Using the values previously assumed, this inequality will be satisfied from dc up to a frequency of nearly 1 kMc. Under these conditions, the per-unit-length series impedance may be written as

$$Z = (\sigma d_1 W)^{-1} + j\omega\mu_0[h + (d_1/3) + \beta^{-1} \coth \beta d_2]/W. \tag{76}$$

ACKNOWLEDGMENT

The author is indebted to N. Rochester and Dr. J. C. Swihart for their stimulation and encouragement.

Reduction of the Frequency-Temperature Shift of Piezoelectric Resonators by Mechanical Stress*

E. A. GERBER†, FELLOW, IRE, AND M. H. MILES†

Summary—A method is described which allows a reduction of the frequency-temperature shift of piezoelectric crystals by the use of bimetal elements applying temperature-dependent pressure to selected spots on the circumference of the resonator disk. A decrease in the frequency change from ± 15 to ± 1 parts per million can be achieved for the AT cut of quartz over a wide temperature range by using one pair of bimetallic elements for the upper and one pair for the lower temperature range. This is accomplished without any increase in the resonance resistance of the crystal. Equations and curves are developed which enable one to obtain the optimum parameters of the bimetallic elements for a given frequency-temperature curve of the crystal. An experimental device, and results achieved with it under various conditions are described in detail. It is expected that in many cases this technique will make power- and space-consuming crystal ovens unnecessary.

INTRODUCTION

IT HAS been known for some time that the frequency of piezoelectric resonators is affected by externally applied stress. Bottom¹ reports that the frequency change of a quartz resonator plate is proportional to a compressional stress applied in one specific direction in the plane of the plate. The frequency change is positive for AT-cut and negative for BT-cut plates. Bottom further observed that a quartz plate compressed along its X-axis exhibits a much larger frequency change than if compressed along its Z'-axis. Michels and Pérez² have studied the effects of hydrostatic pressure upon the frequency of AT- and BT-cut plates. Their results are similar in several aspects to those obtained by the application of linear tensile stresses. More complete measurements of the frequency change of quartz resonators vibrating in thickness shear as a function of the orientation of the mechanical stress have been published by Gerber³ and Ballato and Bechmann.⁴ Fig. 1 shows the effect of compressional force on an AT-cut resonator. The relative frequency change per Newton is plotted as a function of the azimuth. When the compressional force, measured from the X-axis, is applied at about 60°, the frequency change

is zero. The frequency change reaches the extreme values of $+17 \cdot 10^{-6}$ per Newton for a force parallel to the X-axis and $-8 \cdot 10^{-6}$ per Newton for a force parallel to the Z'-axis. As has been shown,^{5,6} the stress sensitivity of vibrating quartz crystals can be used to reduce their frequency-temperature shift considerably if the applied force is made temperature-dependent and applied to selected spots on the circumference of the crystal plate. The necessary force can be supplied, for instance, by bimetal strips, as shown in Fig. 2 and discussed previously.⁵ This technique will enable one to dispense, in many cases, with power- and space-consuming crystal ovens, an important factor in the light of requirements for higher degrees of frequency stability coupled with the trend towards the utmost in miniaturization. It is the purpose of this paper to expand the preliminary results given previously^{5,6} and to discuss the possibilities

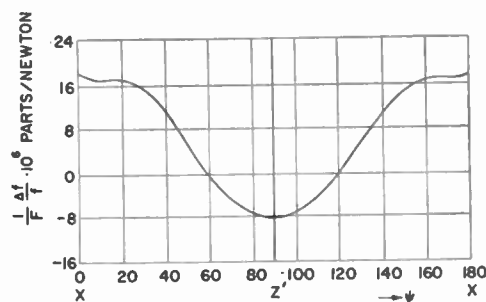


Fig. 1—Relative frequency change per unit of applied force of an AT-cut plate as a function of the azimuth ψ .

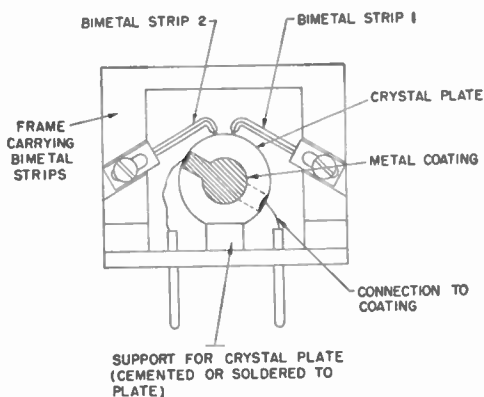


Fig. 2—Quartz crystal unit with two compensating bimetal strips.

* Received by the IRE, July 18, 1961; revised manuscript received, August 30, 1961.

† U. S. Army Signal Research and Development Lab., Fort Monmouth, N. J.

¹ V. E. Bottom, "Mounting techniques for improved heat dissipation in quartz crystal units," Physics Dept., Colorado Agricultural and Mechanical College, Fort Collins, Colorado, Final Rept. on Contract No. DA36-039 SC-5485; February 28, 1951, to February 29, 1952.

² A. Michels and J. P. Pérez, "Déplacement de la fréquence piézoélectrique du quartz sous haute pression," *Physica*, vol. 17, pp. 563-564; May, 1951.

³ E. A. Gerber, "Precision frequency control for guided missiles," *Proc. 1st IRE Natl. Convention on Military Electronics*, pp. 91-98; June 17-19, 1957.

⁴ A. D. Ballato and R. Bechmann, "Effect of initial stress in vibrating quartz plates," *Proc. IRE*, vol. 48, pp. 261-262; February, 1960.

⁵ E. A. Gerber, "Reduction of frequency-temperature shift of piezoelectric crystals by application of temperature-dependent pressure," *Proc. IRE*, vol. 48, pp. 244-245; February, 1960.

⁶ E. A. Gerber and J. M. Havel, "Precision frequency control for military applications," *IRE TRANS. ON MILITARY ELECTRONICS*, vol. MIL-4, pp. 424-437; October, 1960.

and limits of this compensation method analytically and experimentally.

ANALYSIS

The well-known frequency-temperature characteristics of an AT-cut quartz resonator are shown in Fig. 3.⁷ The minimum frequency change which can be obtained for a temperature range from -40° to $+100^{\circ}\text{C}$ is approximately ± 15 parts per million. This total frequency change can easily be compensated for by using bimetals, applying a force of approximately 1.9 Newtons at high temperatures and 0.9 Newtons at low temperatures, respectively. The difficulty is, however, that the frequency change effected by the bimetals is a linear function of the applied force, and therefore of the temperature, whereas the dependence of frequency upon temperature for an AT cut is represented by a polynomial of the third order. Therefore, in order to obtain a better compensation, it is desirable to use two, or even more, bimetals on the warm and on the cold end of the temperature range, in order to approach the polynomial by a group of straight lines. Obviously, it is conceivable that other orientations (YXl) θ of the quartz plate could be selected which would exhibit a linear relationship between frequency and temperature and which would use only one bimetal to compensate for the entire temperature range. However, the disadvantages of this arrangement would be that: 1) extremely large forces in the order of 20 Newtons would be required, and 2) accuracy of the crystal would be influenced by the stability of the bimetal. On the other hand, in the AT cut the necessary forces are much lower and compensation is only effected at the two ends of the temperature range, whereas the frequency at the center of the curve, close to the inflection point, is not influenced by the bimetals at all. Thus, the accuracy of the crystal is not changed by using bimetal compensation since only a corrective action takes place near the upper and lower temperature extremes.

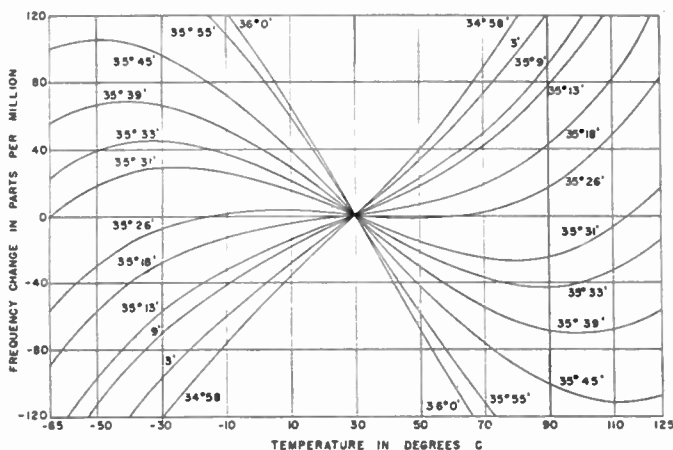


Fig. 3—Frequency-temperature characteristics of a fifth overtone, 29-Mc AT-cut resonator.

⁷ D. L. Hammond, A. R. Chi, and J. M. Stanley, "Effects of Impurities on the Resonator and Lattice Properties of Quartz," Signal Corps Engrg. Labs., Fort Monmouth, N. J., Engrg. Rept. E-1162; November 3, 1955.

The relationship between frequency and temperature of an AT-cut crystal can be described by a polynomial containing only linear and third-order terms, if the inflection point is chosen as the origin:⁸

$$\frac{\Delta f}{f} = a_0 T + c_0 T^3. \tag{1}$$

The constant a_0 is a function of the orientation angle θ , whereas c_0 changes very little with the angle. Its value is $+109.5 \times 10^{-12} (\text{C})^{-3}$.⁹ It is therefore possible to determine the shape of AT frequency-temperature curves for different values of the constant a_0 (or for different orientation angles) and calculate the equations for the bimetals represented by straight lines which match the polynomial closest for a given maximum permissible frequency deviation $\pm (\Delta f/f)_m$. Polynomial (1) is used in the normalized form

$$y = kx + x^3, \tag{2a}$$

where

$$y = \frac{\Delta f}{f} \cdot \frac{1}{|a_0|} \sqrt{\frac{c_0}{|a_0|}},$$

$$x = T \cdot \sqrt{\frac{c_0}{|a_0|}}, \text{ and } k = +1, 0, \text{ and } -1. \tag{2b}$$

Fig. 4 shows a plot of (2a) for $x \geq 0$ and $k = -1$. This case is considered first and solved for the application of two bimetals. Since the inflection point of the curve is in the origin, the solution is also valid for $x < 0$ (lower temperatures). It also can be applied for the case of one bimetal only. Since we have, with increasing x , first a negative frequency deviation in the amount of $y = 2/3\sqrt{3}$, the first bimetal will be set to start operating at the point $x = 2/\sqrt{3}$, which gives the same amount of frequency deviation but with a positive sign. The equations for the two bimetals will then be chosen in such a way that the frequency deviation from zero does not exceed the value of $\pm (2/3\sqrt{3})$ anywhere in the prescribed operating range. If the equations for the two straight lines (see Fig. 4) are

$$y_1 = d \left(x - \frac{2}{\sqrt{3}} \right) \tag{3}$$

and

$$y_2 = b(x - c), \tag{4}$$

then the values for the constants b , c , d , and a (the latter being the maximum value for the abscissa), can be obtained by equating

$$\frac{2}{3\sqrt{3}} = |\alpha|, = |\beta|, = |\gamma|, = |\delta|.$$

⁸ R. Bechmann, "Frequency-temperature-angle characteristics of AT-type resonators made of natural and synthetic quartz," Proc. IRE, vol. 44, pp. 1600-1607; November, 1956.

⁹ R. Bechmann, "Frequency-temperature-angle characteristics of AT- and BT-type quartz oscillators in an extended temperature range," Proc. IRE, vol. 48, p. 1494; August, 1960.

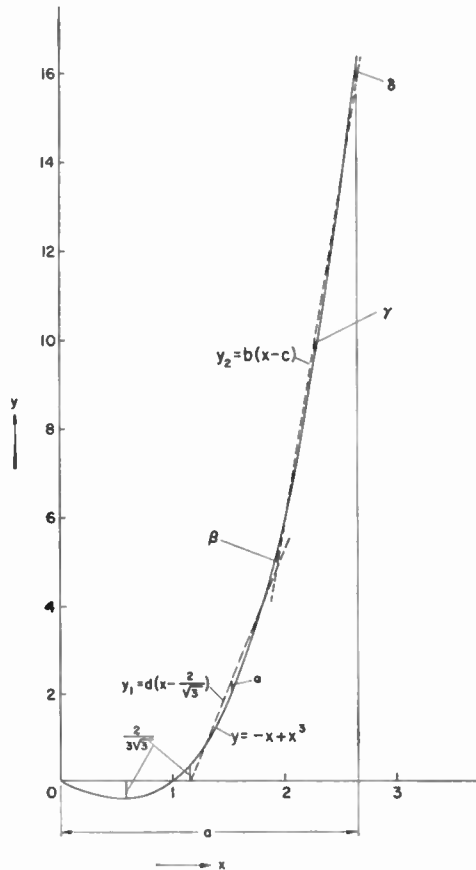


Fig. 4—Plot of the polynomial $y = -x + x^3$ and of the two straight lines which approximate it with an error $\leq (2/3\sqrt{3})$.

α and γ are obtained by setting the first derivatives of the functions $y - y_1$ and $y - y_2$ equal to zero. β is obtained by calculating the coordinates of the intersection of y_1 and y_2 , and the difference between y and the ordinate of the intersection. δ is the difference between y and y_2 at $x = a$. The equations for these four quantities are

$$|\alpha| = \frac{2}{3\sqrt{3}} (1 + d)^{3/2} - \frac{2}{\sqrt{3}} d, \tag{5}$$

$$|\beta| = -\frac{\frac{2}{\sqrt{3}}d - bc}{d - b} + \left(\frac{\frac{2}{\sqrt{3}}d - bc}{d - b} \right)^3 - bd \frac{\frac{2}{\sqrt{3}} - c}{d - b}, \tag{6}$$

$$|\gamma| = \frac{2}{3\sqrt{3}} (1 + b)^{3/2} - bc, \tag{7}$$

$$|\delta| = a(a^2 - 1) - b(a - c), \tag{8}$$

$$|\alpha| = |\beta| = |\gamma| = |\delta| = \frac{2}{3\sqrt{3}}. \tag{9}$$

These equations are solved numerically for a, b, c and d with the help of a computer. The values of a_0 used for the computation are listed in the right-hand table of Fig. 5. The relationship between $-a_0, (\Delta f/f)_m$ and θ has been calculated according to Bechmann.⁸ The constants b and d give information as to the necessary sensitivity of the bimetals. However, since bimetal 1 con-

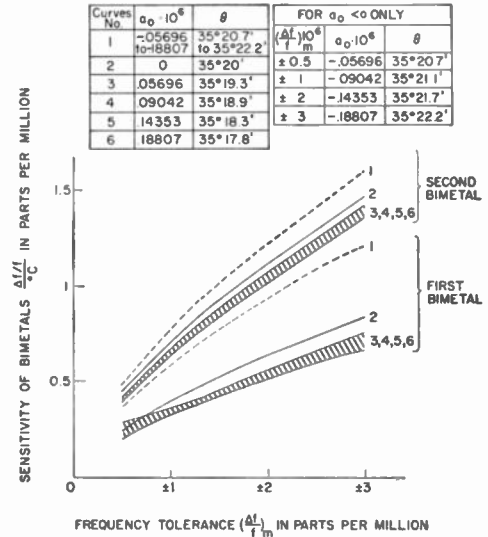


Fig. 5—Sensitivity of bimetals as a function of the desired frequency tolerance. Parameter of the curves is the orientation angle θ of the crystal plate.

tinues to operate after bimetal 2 has made contact, the sensitivity of bimetal 2 must actually be $b - d$. The abscissa value ($=\xi$) of the intersection of the two straight lines, which corresponds to the temperature at which the second bimetal has to make contact, is obtained by

$$\xi = c \frac{b - d/c}{b - d}. \tag{10}$$

The calculated data enable us finally to draw curves which give the sensitivity of the two bimetals (Fig. 5), the maximum temperature range obtainable, and the contact temperatures of the bimetals (Fig. 6), as a function of a maximum permissible frequency deviation $\pm (\Delta f/f)_m$. The parameter is the constant $-a_0$ which, in turn, is a function of the angle of orientation θ . Note that for each value of $\pm (\Delta f/f)_m$, a different orientation θ is required, since $(\Delta f/f)_m$ is given by the minimum ordinate value of (1) which changes with the orientation angle θ . In examining the No. 1 curves of Fig. 6, it is noted that a frequency tolerance $(\Delta f/f)_m$ of ± 1 part in 10^6 can be maintained for a temperature range of $\pm 56^\circ\text{C}$ by using one bimetal each at the higher and lower temperature, and of $\pm 75^\circ\text{C}$ by using two bimetals each. Compared with the best uncompensated curve, this represents an improvement by the factor 15.

The data for the bimetals in the cases of $a_0 = 0$ and $a_0 > 0$ are calculated in a similar manner. They are likewise plotted in Figs. 5 and 6. In these two latter cases, however, different values of $(\Delta f/f)_m$ can be chosen for each different crystal orientation, since no negative ordinate values exist above $x = 0$.

Finally, dimensional data for the bimetals can be obtained by combining the fundamental force-temperature relation⁹

$$\frac{F}{\Delta T} = A \frac{wl^2}{l} \tag{11}$$

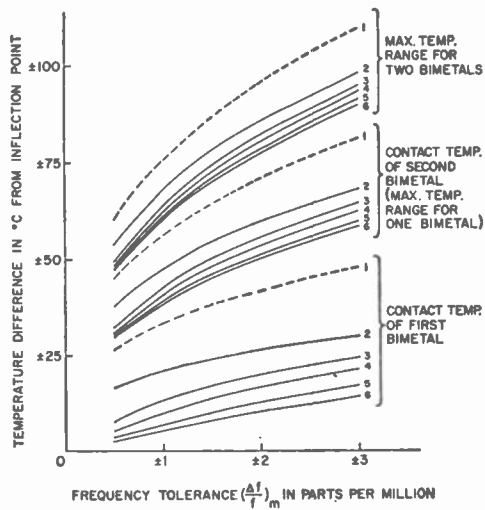


Fig. 6—Maximum temperature range obtainable and contact temperatures of the bimetals as a function of the desired frequency tolerance. Parameter is the orientation angle θ of the crystal plate. Refer to Fig. 5 for the meaning of the numbers ascribed to curves.

with the force-frequency coefficient $(\Delta f/f)/F$ (Fig. 1)

$$\frac{\Delta f/f}{F} \cdot A \frac{wt^2}{l} = \frac{\Delta f/f}{\Delta T} \quad (12)$$

F is the force applied to the crystal plate by the bimetal; t , w , and l are the thickness, width, and length of the bimetallic element; the factor A contains Young's modulus, and the expansion coefficients of the bimetallic materials. $(\Delta f/f)/F$ and $(\Delta f/f)/\Delta T$ can be taken from the graphs in Figs. 1 and 5.

EXPERIMENTAL RESULTS

Fig. 7 shows the crystal holder that was used in the experiments. It is made entirely of brass and has three main parts: the base on which the crystal is mounted, the vise-like frame on which the bimetal holders are mounted, and a cover (not shown) to seal the entire unit. The crystal is mounted in the channel of the base with silver bonding cement. This insures that the crystal will remain stationary under pressure of the bimetals. The bimetals are soldered into holders which are held tightly by the vise grip of the frame. A projecting arm from the bimetal holder allows the use of a screw to set the gap between the first bimetal and the crystal. The gap between the two bimetals is adjusted by lapping after the two bimetals have been soldered into the bimetal holders.

Some difficulty has arisen in the mounting operation of the crystal. The bonding cement is placed at the two points where the crystal touches the edges of the channel. This cement, when dried, sets up a stress between the two points and causes the temperature-frequency characteristic curve of the crystal to change slightly. However, after the initial change due to the bonding cement has taken place, no additional change occurs. At the present time, a new crystal base is under development which will prevent stresses from forming in the crystal due to the bonding cement.

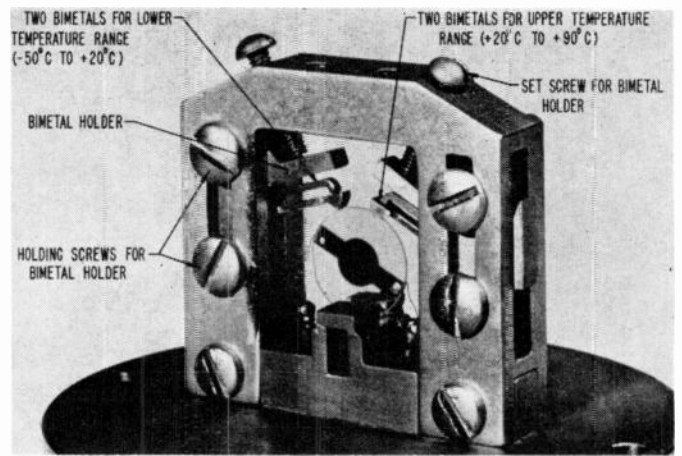


Fig. 7—Experimental crystal holder.

For the experiments, 29-Mc third-overtone AT-cut crystals with an orientation angle θ of $35^{\circ}20'$ and a diameter of 0.45 inch were mounted, with the X -axis 77° off the center line of the holder. The bimetal used was "Highflex."¹⁰ It was chosen among other samples because it combines relatively high sensitivity with a high elastic limit. The dimensions of all the bimetals were 0.33 inch, 0.056 inch, and 0.031 inch in length, width, and thickness, respectively.

Fig. 8 shows how the reduction in the frequency-temperature shift is varied by changing the temperature at which the bimetal makes contact. The measurement has only been made above the inflection point since the behavior below the inflection point is identical. The rate of compensation for each gap setting is constant, due to the fact that the azimuth angle ψ (angle between the X axis and the line of applied force, 82° in this case) is the same for each run. The temperature at which the bimetal makes contact with the crystal can be predetermined by adjusting the gap setting with a measuring microscope. As can be noted from the curve, a variation in gap setting of ± 5 microns will result in a deviation of approximately ± 1.5 parts per million from the desired compensation.

The variation in compensation resulting from a change in the azimuth angle, keeping the gap between the first bimetal and the crystal constant, is shown in Fig. 9. The width of the gap was 10 microns at 25°C . For this test, one pair of bimetals was used in the upper temperature range. The gap was set so that compensation began at the same temperature for each run. The setting of the azimuth angle is not as critical as the gap setting. A tolerance of $\pm 2^{\circ}$ in the range of $\psi = 80^{\circ}$ to $\psi = 90^{\circ}$, and $\pm 1^{\circ}$ between $\psi = 60^{\circ}$ and $\psi = 80^{\circ}$, will result in no appreciable error. By using a shadowgraph for setting the bimetals, tolerances can be maintained within $\pm \frac{1}{2}^{\circ}$.

The results of compensation over the temperature range of -30°C to $+80^{\circ}\text{C}$ are illustrated in Fig. 10. For this test, two pairs of bimetals were used (see Fig. 7).

¹⁰ H. A. Wilson Co., Div., of Engelhard Industries, Inc., Union, N. J.

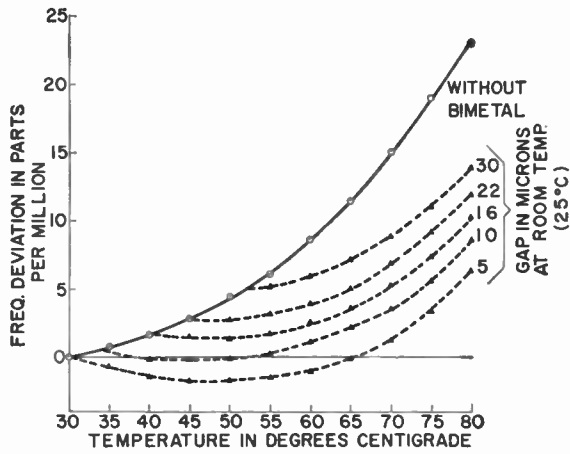


Fig. 8—Frequency-temperature curves of a crystal with and without compensation by one bimetallic element. Parameter of the curves is the gap between tip of bimetal and edge of crystal at 25°C.

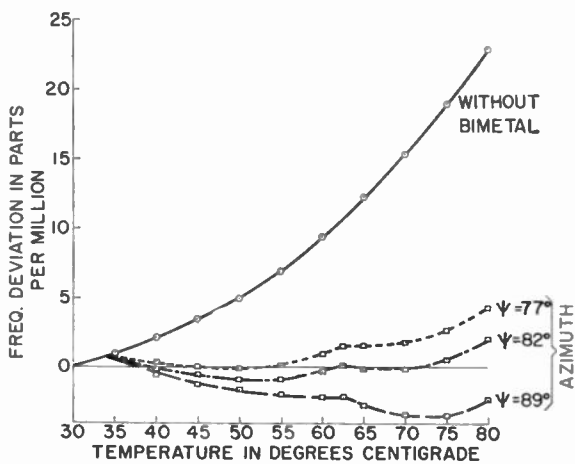


Fig. 9—Frequency-temperature curves of a crystal with and without compensation by a pair of bimetals. Parameter of the curves is the azimuth angle ψ .

The frequency deviation is reduced from ± 25 parts per million to ± 2.5 parts per million, *i.e.*, by a factor of 10. The theoretical results given in Fig. 6 would yield, for a maximum temperature range of 110°C ($\pm 55^\circ\text{C}$ with the inflection point at 25°C) and an a_0 value of 0.134×10^{-6} (curve No. 5 in Fig. 6), a frequency tolerance $(\Delta f/f)_m$ of ± 0.75 part per million. The measured data in Fig. 9 show that this optimum result was obtained for the upper temperature range while the lower temperature range fell short of the optimum. To have achieved optimum results in the lower temperature range, the second bimetal should have made contact at approximately -10°C rather than at 0°C . Also, the second bimetal should have had increased width to give greater sensitivity $(\Delta f/f)/^\circ\text{C}$, whereas, for the sake of simplicity of the experiment, all bimetals were made with identical dimensions.

In order to test the reproducibility of the bimetal compensation, a rerun of the upper temperature range was made (see Fig. 11) and the reproducibility obtained was well within 3 parts in 10^7 .

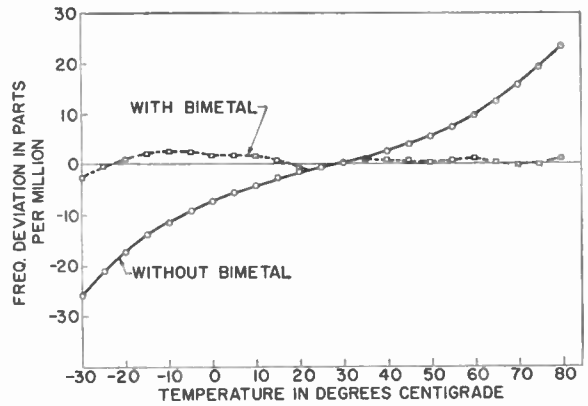


Fig. 10—Compensation by two pairs of bimetals over a temperature range of -30° to $+80^\circ\text{C}$.

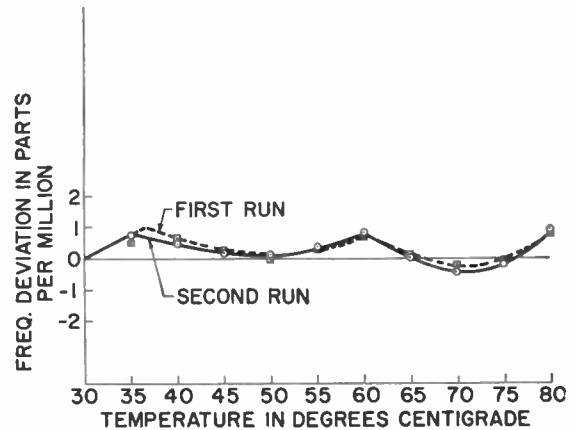


Fig. 11—Reproducibility of compensation with one pair of bimetals.

The resonance resistance of the crystal was measured as a function of temperature during all tests, and there was no change observed which was not within the accuracy of measurement of the crystal impedance meter, type TS-683/TSM.

CONCLUSIONS

It has been shown that the frequency-temperature shift of piezoelectric crystals can be drastically reduced by mechanically applied pressure. This pressure must be a function of the environmental temperature and is applied by bimetallic strips at selected spots on the circumference of the crystal disk. Ahead lies the task of reducing the experimental devices to production-line models by decreasing the size of the entire holder, by working out simple methods for setting the bimetals, and by studying the aging of the device and its behavior under rugged environmental conditions.

ACKNOWLEDGMENT

The authors wish to thank Joseph Weinstein and Dr. Richard K. Brown of the U. S. Army Signal Research and Development Laboratory, Fort Monmouth, N. J., for their assistance in the computations leading to Figs. 5 and 6.

Fundamental Limitations to Optical Doppler Measurements for Space Navigation*

R. H. NORTON† AND R. L. WILDEY‡

Summary—Theoretical consideration is given to the problem of optical Doppler velocity determination of the high accuracy (about 1 ft/sec) required to be useful for space navigation. From the physical theory of line-broadening and -shifting mechanisms in stellar atmospheres, it is concluded that an intrinsic variability of ± 200 ft/sec may be expected in the measurement of an observer's Doppler velocity. Examination of the current state of the art in measuring equipment suggests that it does not set the limits on accuracy.

INTRODUCTION

IT has been suggested that a useful portion of the information needed to make orbit corrections for a spacecraft undergoing the maneuvers of midcourse or approach guidance can be obtained from the determination of the spacecraft's velocity, by measuring the Doppler shift of absorption lines in the spectra of astronomical objects.¹ Noton has shown that the present state of the art for injection guidance is sufficient to permit the treatment of departures of the spacecraft's true orbit from the standard trajectory by linear perturbation theory.² He computed that an error in the range rate determination of 1 ft/sec during midcourse guidance would lead to a 4000-mile miss at Mars. Hence, velocity information, in order to be useful, must be accurate to about 1 ft/sec. For a representative wavelength of 4000 angstroms, the corresponding Doppler shift is 4×10^{-6} angstroms.

The physical mechanisms affecting the shapes and positions of spectral lines will be discussed, and limitations on the accuracy of observed Doppler velocities will be found to be caused by the inconstancy of these mechanisms. Of the available celestial sources to be considered, the only practical one is the sun, since the flux from the brightest star is only 10^{-10} that from the sun.

In addition, present spectroscopic techniques and instrumentation will be discussed, with emphasis upon the accuracy obtainable within the state of the art as imposed by the restrictions encountered in space-borne missions.

* Received by the IRE, April 10, 1961; revised manuscript received, July 21, 1961. This paper presents results of one phase of research carried out at the Jet Propulsion Lab. under Contract NASw-6, sponsored by the Natl. Aeronautics and Space Admin.

† Guidance and Control Research Section, Jet Propulsion Lab., Calif. Inst. Tech., Pasadena, Calif.

‡ Formerly with the Guidance and Control Research Section, Jet Propulsion Lab., Calif. Inst. Tech., Pasadena, Calif.

¹ R. G. Franklin and D. L. Bix, "A study of natural electromagnetic phenomena for space navigation," *Proc. IRE*, vol. 48, pp. 532-541; April, 1960.

² A. R. M. Noton, "Interplanetary Post-Injection Guidance," presented at Am. Rocket Soc. Meeting, San Diego, Calif., June 10, 1959, Jet Propulsion Lab., Pasadena, Calif., External Publication No. 653; June 4, 1959.

PHYSICAL NATURE OF STELLAR ABSORPTION LINES

Absorption lines in stellar spectra, for example as in the spectrum of the sun, are fundamentally affected by the physical conditions existing in the region of the stellar atmosphere where the absorption takes place. The general result of these effects is to broaden an otherwise monochromatic absorption line into a feature from which the physical conditions in the star's atmosphere may be induced. Line-broadening mechanisms may be divided into two classes: those that produce symmetric broadening, and those that produce asymmetric lines. It is the latter class that is of particular interest for the line profile for an asymmetric line will exhibit a wavelength difference between the line centroid and the point of greatest absorption. It will be wise to investigate whether these mechanisms are constant with time, for if not, a natural variability will be introduced in the observer's Doppler velocity which cannot be removed.

Symmetric Line-Broadening Mechanisms

Let us briefly discuss those line-broadening mechanisms which produce symmetric lines; they are:

- 1) Doppler broadening, characterized by a bell-shaped absorption coefficient $\exp[-\text{const} (\Delta\lambda)^2]$. Fig. 1(a) illustrates the line profile of Ca II, $\lambda_0 = 3934$ angstroms, for varying abundances in the solar atmosphere.
- 2) Radiation and collisional broadening, characterized by an absorption coefficient with a deep, narrow core and broad wings, in accordance with the dispersion formula $A/[B + (\Delta\lambda)^2]$. Fig. 1(b) illustrates the line profile for radiation damping only, for 1.8×10^{18} atom/gm of Ca II, $\lambda_0 = 3934$ angstroms. The line profile for collisional broadening will be similar to radiation damping. Fig. 2 shows the line profile (computed and observed) for the Ca II K line in the sun, with $T = 5700^\circ$ and $N = 1.8 \times 10^{18}$ atom/gm.
- 3) Linear Stark effect, which produces components spaced symmetrically about the unperturbed line center.
- 4) Hyperfine structure, which, though not necessarily symmetric, is the same for a reference laboratory source as for a stellar source.
- 5) Linear Zeeman effect, which can be derived from a linear perturbation of the Hamiltonian in Schrodinger's equation, is symmetric for weak magnetic fields, both in line splitting and intensity distribution.

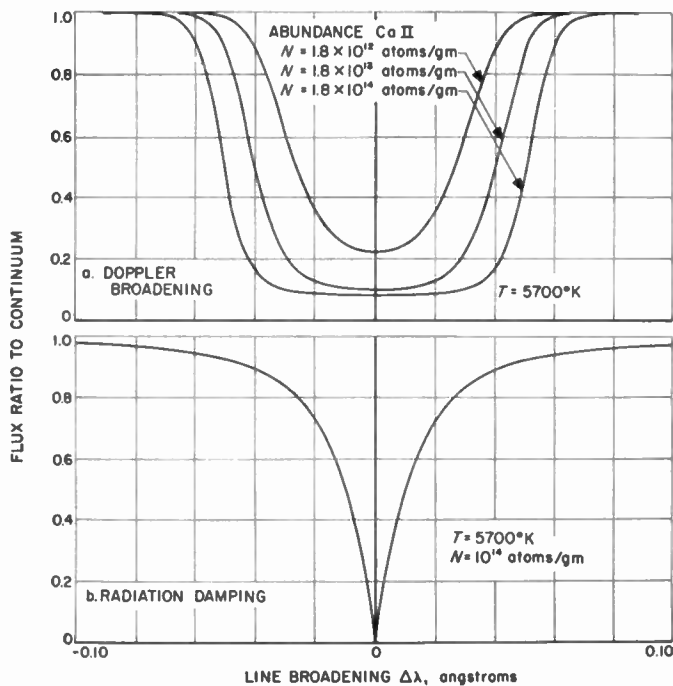


Fig. 1—Computed spectral line profiles for Ca II, 3934 angstroms.

- 6) Rotational broadening, from rapidly rotating stars, which produces a broad, shallow dish-shaped line profile, symmetric about the line center.

Asymmetric Line-Broadening Mechanisms

There is no direct information on the variation of average solar electric fields, but if we adopt, as an average field, the field of a single ion at a distance equal to the mean separation of particles at the mean level of absorption in the solar atmosphere and allow a relative variation in this field equal to the relative variation observed in the general solar magnetic field, we obtain a variation of approximately 1 to 9 v/cm. The interaction energy in a hydrogen-like atom is given by³

$$\Delta T = 6.42 \times 10^{-5} n(n_2 - n_1) F + 5.22 \times 10^{-16} n^4 \{ 17n^2 - 3(n_2 - n_1) - 9m_l^2 + 19 \} F^2 + \dots \quad (1)$$

where ΔT represents the shift in the energy level in wave numbers from the field-free state due to the presence of the electric field, and F is the field strength in v/cm. n is the usual total quantum number, and n_1 , n_2 , and n_l are electric quantum numbers subject to the condition

$$m_l = n - n_1 - n_2 - 1. \quad (1a)$$

The first observations of the second-order Stark effect in hydrogen were made by Takamine and Kokubu in the Stark pattern of $H\gamma$ when the spectrum was produced in a field of 147,000 v/cm, and they observed a shift to the red of the middle component of $H\gamma$ of 0.8 angstrom.⁴ Therefore, we would expect for the assumed

³ H. E. White, "Introduction to Atomic Spectra," McGraw-Hill Book Co., New York, N. Y., p. 402; 1934.

⁴ T. Takamine and H. Kokubu, "Further studies on the Stark effect in Helium and Hydrogen," *Proc. Tokyo Math. Phys. Soc.*, vol. 9, pp. 394-404; August, 1918.

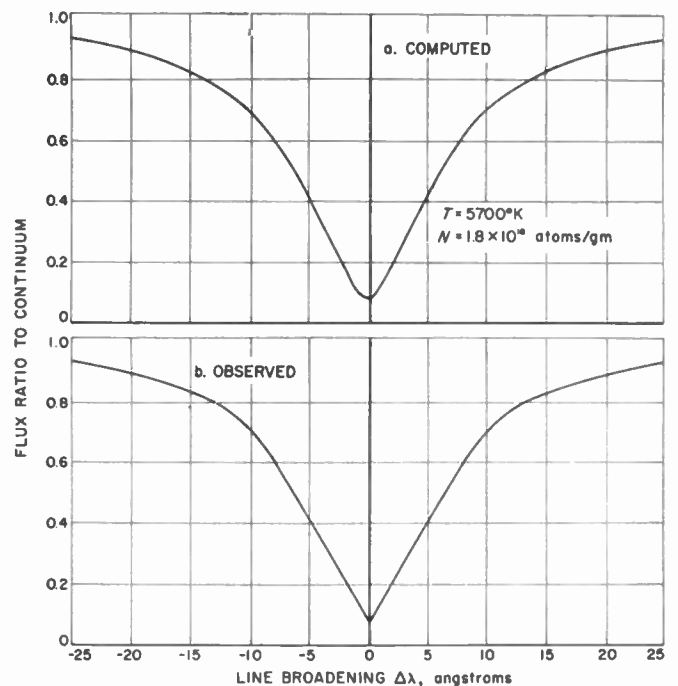


Fig. 2—Computed and observed solar line profiles for Ca II, 3934 angstroms, including Doppler broadening, radiation damping, and collision damping.

variation of the general solar electric field a maximum shift of the centroid wavelength of $H\gamma$ of 3×10^{-9} angstroms. It appears that the quadratic Stark effect, at least in this form, will not prevent measurements of optical Doppler velocities to 1 ft/sec.

However, the other form of quadratic Stark effect, known as pressure shift, has a much more appreciable effect. Due to the polarization of one atom by the close approach of another, an excited or outer state will be lowered more than a tightly-bound lower state. The frequency distribution during this time of close approach is added to the collision damping distribution, with the result that the observed spectral line is spread out more on the long wavelength side than on the short. The shift observed depends on the foreign gas used; it is also proportional to the relative density, defined as the ratio of the density under existing conditions to the density at STP.

For an order of magnitude example, consider as a typical line the mercury resonance line $\lambda = 2537$ angstroms. The empirical pressure-shift relationship with H_2 as the foreign gas (atomic hydrogen would be the most abundant foreign gas in all but the hottest stars) is:⁵

$$\Delta\lambda = 0.004 \left[\frac{\rho}{\rho_0} \right] \quad (2)$$

where $\Delta\lambda$ is in angstroms and ρ_0 = density at STP.

⁵ White, *op. cit.*, p. 433.

If we assume that this relationship holds for atomic hydrogen as the foreign gas and extrapolate to densities in the solar atmosphere, taking as an example the density at about the level of formation of a moderately strong line from the model solar atmosphere of Chandrasekhar and Munch:⁶

$$\begin{aligned}\tau &= \text{optical depth} = 0.3 \\ P_0 &= \text{antilog } 4.67 = 4.68 \times 10^4 \text{ dyne/cm}^2 \\ T &= 5850^\circ \text{ K} \\ \frac{\rho}{\rho_0} &= \frac{P}{P_0} \frac{T_0}{T} = 2.2 \times 10^{-3} \\ \Delta\lambda &= 9 \times 10^{-6} \text{ angstroms.}\end{aligned}\quad (2a)$$

We must also consider the variability of this effect. Flares, sunspots, plages, and other phenomena exhibiting markedly different densities from their surroundings will have profound effects over limited regions of the sun, but they are most unpredictable. In addition, for that small part of the absorption line formed in the chromosphere or outer atmosphere, the variation of the spicule pattern, those hot and dense spire-like cells of photospheric material thrusting up into the chromosphere, will have an appreciable effect. Also, the granule pattern in the photosphere, which is closer to the mean level of absorption, is not constant. It is, therefore, estimated that the above shift can vary by about its own magnitude, or produce a variability in the observed velocity of 0 to 4 ft/sec.

Let us now consider the second-order Zeeman effect. A linear perturbation of the Hamiltonian in Schroedinger's equation yields, for light circularly polarized perpendicular to the magnetic field,

$$\nu = \nu_0 \pm \frac{eH}{4\pi mc^2} + \frac{e^2 H^2 a_0 n^4}{4mc^3} \quad (3)$$

The second-order term, giving the shift in the line centroid relative to the unperturbed line centroid, is

$$\Delta\nu = \frac{e^2 H^2 a_0 n^4}{4mc^3} = 1.24 \times 10^{-32} H^2 \quad (4)$$

where $\Delta\nu$ is in wavenumbers, cm^{-1} , and all physical constants are in electrostatic cgs units. H is the magnetic-field strength in oersteds, and n is the refractive index in the solar atmosphere. It is obvious that no reasonable variation in the general solar magnetic field will produce a centroid shift sufficient to preclude optical Doppler velocity measurement accurate to 1 ft/sec.

Turning now to the variability of stars, we can, upon making simple assumptions, estimate the contribution of this effect to the variability of a measured Doppler velocity. At present, it is not possible to measure the brightness of a star to better than about 1 per cent, and

it has been suggested that all stars are variable to some degree, the vast majority having a variability of less than 1 per cent. When a star varies in brightness, its radius and temperature change, giving rise to a true Doppler shift. The change in radius and temperature also have profound effects upon the pressure and density in its outer layers, in turn affecting all line broadening mechanisms.

Let us estimate the magnitude of the Doppler shift due to the change of radius of a star similar in mass, radius, and temperature to the sun. For such a small variation, less than 1 per cent, we may assume that the pulsation is an adiabatic process; further, we will assume the perfect gas law, and these assumptions are embodied in the two relations:

$$\begin{aligned}P &= K\rho^\gamma \\ P &= \frac{k}{\mu H} \rho T\end{aligned}\quad (5)$$

where K = constant, γ = ratio of specific heats (5/3 for a monatomic perfect gas), μ = mean molecular weight in units of the mass of a hydrogen atom, and H = mass of hydrogen atom. We will also employ the relation between the luminosity, radius, and effective temperature of a star:

$$L = 4\pi R^2 \sigma T^4. \quad (6)$$

For a variation in brightness $\delta L/L$, we have

$$\frac{\delta L}{L} = 2 \frac{\delta R}{R} + 4 \frac{\delta T}{T}. \quad (7)$$

It can easily be shown that the temperature and radius variations for a monatomic perfect gas undergoing an adiabatic pulsation are given by

$$\frac{\delta T}{T} = -2 \frac{\delta R}{R}. \quad (8)$$

Hence,

$$\frac{\delta L}{L} = -6 \frac{\delta R}{R}. \quad (9)$$

If, for a star like the sun, the brightness changes by 0.1 per cent, the radius variation will be

$$\delta R = 1.2 \times 10^7 \text{ cm} = 3.8 \times 10^5 \text{ ft.}$$

The theory of adiabatic pulsations predicts that the product of the period of pulsation and the square root of the mean density of the star be a constant, and this is substantiated by observation. If we adopt the value of this constant as determined observationally, we have:⁷

$$p \left[\frac{\bar{\rho}}{\bar{\rho}_\odot} \right]^{1/2} = 0.04 \quad (10)$$

⁶ S. Chandrasekhar and G. Munch, "The continuous spectrum of the sun and the stars," *Astrophys. J.*, vol. 104, pp. 446-457; November, 1946.

⁷ G. H. Herbig, Ed., "Non-Stable Stars," IAU Symp. No. 3, Cambridge University Press, Cambridge, Eng., p. 187; 1957.

where p = period in days, and $\bar{\rho}_{\odot}$ = mean density of the sun. Thus, for a star similar to the sun, the period of pulsation is approximately one hour. It then follows that the mean velocity of the pulsation wave will be 210 ft/sec. The observed shift in the spectral lines, however, is made up of contributions from all points on the disk, so that the observed velocity will be related to the pulsation wave velocity by

$$v_{\text{obs}} = 0.707 v. \quad (11)$$

Here we also included the effects of limb darkening.

Thus we may expect, if the sun has a variation in brightness of 0.1 per cent, a mean shift in an observer's measured velocity of ± 150 ft/sec. Of course, the maximum velocity of the pulsation will be higher than the mean velocity.

The fourth source of line asymmetry to be considered is the "sunspot effect." The largest sunspot group ever observed covered 0.0054 of the visible solar surface.⁸ The effect of such a spot group as the one above can be estimated from the following simple model. The best compromise, in the maximization of line shift, between the component of velocity in the observer's line of sight and the projected area of the spot group, places the spot group 0.707 of the way from the center of the disk to the limb. The radial velocity here, at the equator, is 4700 ft/sec. We assume the solar disk to be evenly illuminated; in fact, it shows pronounced limb darkening, but not enough to effect order of magnitude estimates. By the same token we assume the sunspots to be completely black; we can compute the effect of the sunspot group on the centroid wavelength due to Doppler effect alone. It will be the zero shift of the vast majority of the disk weighted by its intensity, which would be $[1-2(0.0054)]$ plus the shift of 4700 ft/sec of the portion of the disk on the opposite side of the disk from the sunspot group, which the group fails to balance in oppositely shifted radiation, weighted by its intensity of 0.0054. The shift of the centroid of the line in the emergent solar flux is ± 25 ft/sec.

The effects of the foregoing mechanisms are summarized in Table 1, from which one may conclude that a natural variation in the measurement of a spacecraft's optical Doppler velocity of approximately ± 200 ft/sec may be expected.

TABLE I

Effect	Expected Maximum Optical Doppler Variation
Second-order Zeeman effect	10^{-24} ft/sec
Quadratic Stark effect	10^{-3} ft/sec
Pressure shift	4 ft/sec
Sunspot effect	25 ft/sec
Variability of radius	150^* ft/sec

* Mean value given; maximum value incalculable, since explicit mathematical form of variation is not presently known.

⁸ S. B. Nicholson and J. Hickox, "The great sunspot group of February, 1946," *Pubs Astron. Soc. Pacific*, vol. 58, pp. 86-88; April, 1946.

It must be emphasized here that the values given in the tabulation represent the maximum expected Doppler variations, under certain assumptions. In the case of the variability in the luminosity of the sun, it may be argued that the sun is not variable. However, we are here dealing with a change in brightness an order of magnitude less than the precision with which the observations can at present be made. This phenomenon has such a profound influence on the accuracy of optical Doppler velocity measurements that the question of its existence should provide sufficient heuristic grounds for a program whose objectives are to settle the issue.

Minimum values of the expected Doppler variations for each phenomenon can be set equal to zero, but the conditions necessary to obtain minimum values are considered extremely improbable.

The question now remaining is whether these variations can be averaged to zero by a suitable integration time. From the observations that the granule pattern presents a randomly changing appearance over a period of a few minutes, it seems likely that the variability due to pressure shift could be smoothed in a matter of minutes. For the Doppler variation arising from a true variability of the sun, the expected period is of the order of an hour, which appears to be too long an integration time for a mid-course guidance maneuver. Finally, since the period of rotation of the sun is 27 days, a sunspot group remains visible for 12-13 days, during which time the associated Doppler shift will swing its full value. It is expected that at most times the general sunspot pattern will create an average Doppler shift less than the maximum value which has been computed, but the possibility of such a large variation which cannot be removed still remains.

INSTRUMENTATION STATE OF THE ART

The state of the art in optical Doppler shift measurements today is exemplified by the Babcock magnetograph at the Mt. Wilson observatory. A 17-in image of the sun is formed by an off-axis Cassegrain reflecting system with a focal length of 150 ft located in a large steel tower.⁹ The spectrograph, a vertical Littrow instrument employing a large plane grating, is located in a 75-foot pit under the tower, obtaining a dispersion in the green of 11 mm/angstrom with a 75-ft-focal-length lens. The grating, used in the fifth order, has a ruled area of $5\frac{1}{4} \times 8$ in, with 15,000 grooves/in and a resolving power in the green of 600,000. Using the Rayleigh criterion for resolution, two sharp lines 0.009 angstrom apart may just be resolved in the green, but by working into the diffraction pattern much better precision is obtained in centroid measurements.

In front of the entrance slit to the spectrograph is placed an electro-optic retardation plate in the form of a Z-cut crystal of ammonium dihydrogen phosphate.

⁹ H. W. Babcock, "The solar magnetograph," *Astrophys. J.*, vol. 118, pp. 387-396; November, 1953.

Upon the application of an alternating voltage the retardation oscillates at the applied frequency, 120 cps, between plus and minus a quarter wave. A Nicol prism follows this plate, the two fixed elements thus constituting an oscillating circular analyzer.

Two slits are used at the exit of the spectrograph just before the detectors, each slit being placed at the point of steepest slope on each side of a spectral line. Thus, as the retardation of the quarter wave plate is oscillated, one measures the difference between the two exit slits first for the right-hand and then the left-hand circularly polarized components of solar line radiation. Magnetic fields of one gauss, causing a Zeeman splitting of 10^{-5} angstroms, can be measured accurately, and the rms shot noise of the system corresponds to about 0.1 gauss.

However, it is readily apparent that such an instrument as the Babcock magnetograph, capable of measuring an optical Doppler velocity with a precision of perhaps 3 to 5 ft/sec, is hardly practical from the standpoint of space-borne missions, because of its enormous weight and size. Limitations of instruments have been discussed by Franklin and Birx;¹ the best velocity resolution to be hoped for on the basis of detector noise considerations is 60 ft/sec. Possibilities exist for the use of

interferometric techniques in order to obtain high dispersion and narrow instrumental profiles with non-bulky equipment; such an instrument might consist of a fixed-plate Fabry-Perot interferometer crossed with a small spectrograph, whose function is to separate the orders. It is interesting to note, however, that the original Fabry-Perot interferometer designed for the Babcock magnetograph was replaced by the present plane grating spectrograph because it was found impossible to maintain the temperature equilibrium necessary. Such an instrument would have to withstand the rigors of space-borne guidance maneuvers.

CONCLUSIONS

Calculations have been made on the assumption that the physical characteristics of stellar electromagnetic sources, as for example the sun, vary in such a manner that a variability of approximately ± 200 ft/sec may be expected in the observer's measured optical Doppler velocity. It is the authors' opinion that it is this that imposes a fundamental limitation on the accuracy with which Doppler measurements may be made optically, rather than the instrumentation.

Timing Potentials of Loran-C*

R. H. DOHERTY†, SENIOR MEMBER, IRE, G. HEFLEY†, AND R. F. LINFIELD†, SENIOR MEMBER, IRE

Summary—The Loran-C navigation system is capable of synchronizing and setting clocks to a relative accuracy of better than 1 μ sec throughout the system's service area. A Loran-C receiver functions as a slaved oscillator and a trigger generator. The generated triggers bear a time relationship to the triggers at the master transmitter, which is known to within a microsecond. Clocks operating from these sources are compared with clocks operating from independent free-running oscillators.

A fundamental relationship between time and position is considered. Loran-C as a navigation and timing system can provide both position and time simultaneously. The East Coast Loran-C chain will be time synchronized. The national frequency standards and uniform time source located at Boulder will be used to monitor these signals. Time synchronization and time distribution have been demonstrated on the Atlantic Missile Range. Inter-range time synchronization and precise time for large areas of the world could be provided in the future.

Appendix I describes briefly the results of ground wave measurements made on the Loran-C (Cytac) system. Appendix II describes the results of sky wave measurements made with the system.

* Received by the IRE, June 30, 1960; revised manuscript received, August 28, 1961.

† Radio Systems Division, National Bureau of Standards, Boulder, Colo.

I. INTRODUCTION

IN the majority of timing applications a problem exists in setting two or more clocks to agree with one another. The greater the requirement for precise agreement between these clocks, the more difficult the problem becomes and, if the clocks are in widely separated locations, the difficulty is further increased. The reading of a single clock is meaningful only as it relates to its own frame of reference. For example, a clock may gain or lose with respect to the periodicity of the earth as it revolves about its own axis or about the sun.

Accurate astronomical time depends on long-term observations, but is ultimately limited by unpredictable variations in the earth's rotation. Furthermore, any astronomical time can be determined only to an accuracy of several milliseconds for a single set of observations. The initial settings of individual clocks may, therefore, differ by amounts of the order of milliseconds. These differences combined with the gains or losses of individual clocks are of such magnitude that

independently operating clocks or clocks synchronized by existing radio timing signals are unable to make measurements more precise than a millisecond at different locations.

When it is necessary to measure time at two or more locations to an accuracy of $1 \mu\text{sec}$ or better, such measurements must all be made within the same frame of reference, that is within a single clock system. The term "clock system" as used in this paper means a master clock at a convenient central location and other clocks at widely separated locations which are slaved to the master in such a way that each will track the master. Such a clock system must also provide for a means to synchronize or set each slave clock to agree accurately with the master clock. A number of Loran-C clocks will function as such a clock system with initial setting or synchronizing accuracies of $1 \mu\text{sec}$ or better using ground wave reception. Accuracies of $10 \mu\text{sec}$ or better should be obtainable using sky wave reception. Other methods may be used to set remote clocks, such as flying atomic standards from place to place, but they do not offer the convenience or reliability of Loran-C.¹

The National Bureau of Standards at Boulder, Colo., maintains the nation's primary frequency standard. A fail safe clock operating from this standard would provide an extremely uniform time source that could be related in retrospect to any astronomical time measurements. This uniform time source is the proposed means for monitoring the aforementioned master clock.

II. LORAN-C OPERATION AND ITS TIMING APPLICATION

Loran-C² is a pulse navigation system operating on a basic frequency of 100 kc and normally consisting of a master station and two or more slave stations. Several Loran-C chains are operational or under construction. The presently operating U. S. East Coast Loran-C chain, and the previously operated Cytac (later named Loran-C) chain are shown in Fig. 1. The master station is located at Cape Fear, N. C., and the two slave stations at Martha's Vineyard, Mass., and Jupiter Inlet, Fla. The area over which a ground wave could be received for timing purposes would extend approximately 3000 km seaward or 2000 km landward from any one transmitter.

The Loran-C system utilizes synchronous detection techniques for measuring phase, and methods for determining a fixed sampling point early on the pulse, independent of pulse amplitude. By this means the ground wave is completely resolved from the sky waves. See Fig. 2. To a first approximation the ground wave transmission time is proportional to distance. Secondary corrections, however, usually have a magnitude in the range of 1 to $10 \mu\text{sec}$. These corrections are determined

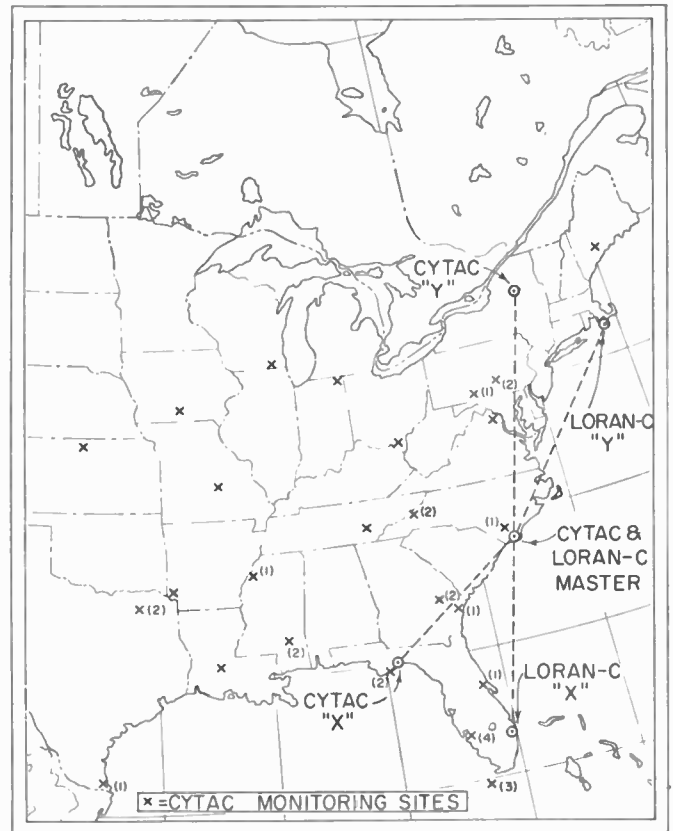


Fig. 1—Loran-C and Cytac locations.

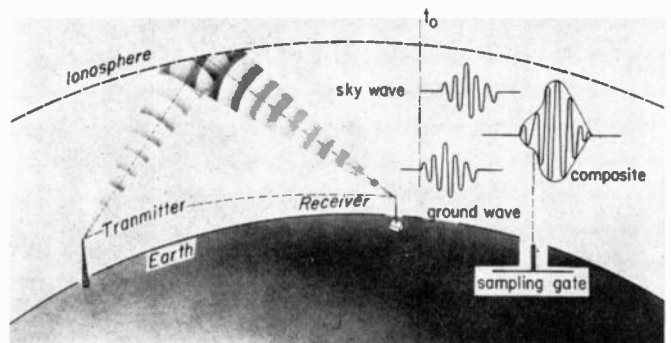


Fig. 2—Ground wave resolution with Loran-C.

largely by the conductivity of the path and to a much smaller extent by the dielectric constant and the index of atmospheric refraction.^{3,4} Both the conductivity and the dielectric constant of sea water are accurately known. Consequently, the transmission time over sea water can be computed accurately. Transmission times over paths involving land cannot be as accurately calculated since the conductivity of land is not well known. However, by correlating time difference measurements⁵

³ J. R. Johler, W. J. Kellar and L. C. Walters, "Phase of the Low Radiofrequency Ground Wave," Natl. Bureau of Standards, Boulder, Colo., NBS Circular No. 573; June, 1956.

⁴ K. A. Norton, "The propagation of radio waves over the surface of the earth and in the upper atmosphere," Proc. IRE, vol. 25, pp. 1203-1236; September, 1937.

⁵ All time difference measurements are determined by phase differences at 100 kc.

¹ F. H. Reder, M. R. Winkler and C. Vickart, "Results of a long range clock synchronization experiment," Proc. IRE, vol. 49, pp. 1028-1042; June, 1961.

² W. P. Frantz, W. Dean and R. L. Frank, "A precision multipurpose radio navigation system," 1957 IRE NATIONAL CONVENTION RECORD, pt. 8, pp. 79-97.

with generalized assumptions of ground conductivity, individual path conductivities may be deduced. For example, it has been demonstrated that the best single value of conductivity which can be assigned to the eastern half of the U. S. is 0.005 mho/meter. The average error between time differences computed using this conductivity and those measured in a test program (see Appendix I) was approximately $0.8 \mu\text{sec}$. The algebraic average was nearly zero and the maximum error among all sites was $2.5 \mu\text{sec}$. The largest errors were associated with sites located in mountainous terrain. Until better prediction methods are developed it must be assumed that systematic errors of the order of $1 \mu\text{sec}$ may exist for land and mixed paths unless the transmission time has been measured by the use of two transmitters, such as is done over the Loran-C baselines.

The East Coast Loran-C chain operates on a basic repetition rate of twenty pulse groups per second.⁶ A pulse group consists of eight phase coded pulses with a uniform spacing of 1 msec. The Loran-C system, as presently operated, does not resolve time increments larger than the repetition period or 50 msec. Larger increments could be resolved without interference to the system, but at this time there appears to be no pressing requirement for such a change. The 50-msec interval between pulse groups can be resolved conveniently by the WWV seconds' pulses. In order to use WWV and Loran-C in such a manner the two transmitting systems must be synchronized, as they would be since WWV is transmitting uniform time.⁷ See Fig. 3.

The Loran-C navigation system operating on a basic frequency of 100 kc performs the vitally important function of slaving all oscillators in the system to the oscillator at the master transmitter. By virtue of the technique of slaving a number of relatively cheap oscillators to a master oscillator, all clocks operated from such oscillators will, by definition, have an average drift rate of zero. The instantaneous deviation of any one clock from the average is primarily determined by the factors listed below:

- 1) Signal-to-noise ratio.
- 2) Relative and absolute quality of slave and master oscillators.
- 3) Integration time.
- 4) Tightness of coupling of the slave oscillator.

The positioning system requires a means for selecting a given cycle and a point on that cycle. It is obvious that this criteria for the positioning system satisfies the requirements for synchronizing a timing system. The instrumentation being utilized in the navigation system has a resolution of a few hundredths of

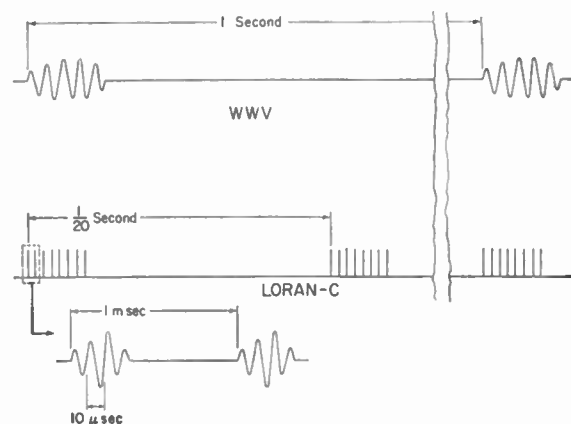


Fig. 3—Synchronization of Loran-C with WWV time signals.

$1 \mu\text{sec}$. The time variations in propagation due to changes in refractive index, conductivity, etc. are substantially less for all times than the previously mentioned prediction capability. Standard deviations of 0.2 to $0.3 \mu\text{sec}$ may be expected. (See Appendix I.)

In order to relate the Loran-C system to the primary frequency standard it has been proposed that an extremely high quality secondary frequency standard be installed at the Loran-C master station, and that the master transmissions be monitored at Boulder and that corrections be published periodically.

Measurements of Loran-C sky wave signals from the East Coast made in Boulder in 1955 and 1961 (Appendix II) showed that the propagation time can be determined to an absolute accuracy of about $1 \mu\text{sec}$ with an integration time of less than one minute. The standard deviation of such measurements (daytime) is less than $0.5 \mu\text{sec}$. A better receiving antenna has made it possible to use the ground wave signal and achieve a substantially better measurement of the Loran-C master oscillator frequency.

III. SETTING A LORAN-C CLOCK

In order to set a slave clock to agree with the master clock it is first necessary to determine the amount by which the apparent time at the slave is slow with respect to the master.

After the signal has reached the antenna, additional time is required for it to pass through the receiver and produce a trigger suitable for starting or synchronizing the clock. This time depends solely on the receiver design. For timing purposes the Loran-C receiver should be designed in such a way that the transmission time through it remains constant over a wide range of environmental conditions.

The apparent time at the receiver is slow by the amount of time required for the signal to propagate from the master transmitter and through the Loran system to the receiver, plus the transmission time through the receiver plus any additional systematic delays such as the coding delay normally used in a Loran system. This is illustrated by the following example:

⁶ Fractional Loran rates can also be used for the operation of a clock by gating the received pulses and using only those transmitted on the second to set the clock.

⁷ A. H. Morgan, "Precise Time Synchronization of Widely Separated Clocks," Natl. Bureau of Standards, Boulder, Colo., NBS Tech. Note No. 22; July, 1959.

- Given: 1) Receiver 2000 km from slave transmitter.
 2) Sea water path.
 3) Receiver delay 25.0 μ sec.

Propagation time 2000 km sea water	6,675.3
Propagation time Master to Slave	2,711.8
Slave coding delay	12,000.0
Receiver delay	25.0
Total Delay	21,412.1

It is assumed that a pulse is transmitted from the master station precisely at each second. The corresponding pulse from the slave station would produce a time trigger at the receiver output 21,412.1 μ sec later. Therefore, the clock at the receiver should read 0.021412 second when this time trigger is used as a read command. The calibration of this clock to read the correct fraction of a second is accomplished by adding counts to the divider chain, and the clock will maintain the same uniform time as the master clock. A one second or one minute output from the clock will occur within 1 μ sec of the respective output from any other Loran-C clock in the system.

Fig. 4 is a front view of the developmental model of a Loran-C clock.⁸ The panel immediately above the oscilloscope contains a 15-digit visual display covering from 1 μ sec to 1000 days. When the clock is given a read command this display reads out the time and holds the reading until the next read command is received.

IV. SLAVED CLOCKS VS INDEPENDENT CLOCKS

The comparison of Loran-C clocks (slaved clocks) with independent clocks running from oscillators of different qualities is shown in Fig. 5. This comparison assumes that two independent clocks are drifting apart at a drift rate equal to the maximum rate indicated. The independent clocks must be initially synchronized and must run continuously without interruption. The Loran-C clocks may be interrupted and resynchronized at random without affecting the accuracy.

If a clock operating from the slaved oscillator of a Loran-C receiver is correctly set and if that clock and receiver are moved a distance of 300 meters toward the Loran-C transmitter, the clock will then be 1 μ sec fast. Similarly, if the clock is moved 300 meters in the opposite direction it will be 1 μ sec slow. In contrast, if the same clock were operating from an independent oscillator it would neither gain nor lose as a result of motion.

If a Loran-C clock is used in a moving vehicle its position must always be taken into account. In either ships or aircraft the fixes available from the Loran-C navigation system can provide the necessary information. However, the computations required to convert the time difference readings to distance from the transmitters are rather involved and may necessitate the use of a separate computer. An independent clock may be

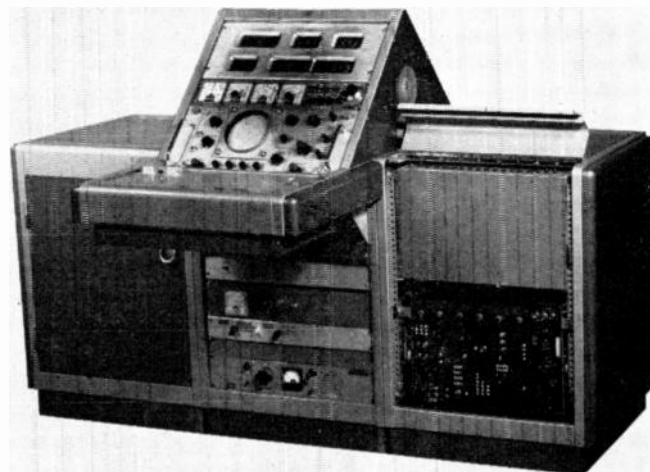


Fig. 4—Loran-C clock.

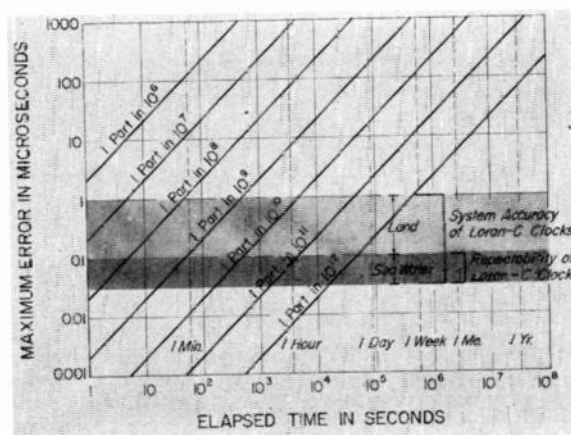


Fig. 5—Comparison of slaved and independent clocks.

more satisfactory than a slaved clock in a moving vehicle if the clock does not have to maintain the correct time for a long period. Even the best clocks (or oscillators) will drift with respect to other clocks. In cases where drifts of the order of a microsecond are important, the slaved clock is a virtual necessity.

As the accuracy of clocks within a timing system is increased, the location of each clock becomes correspondingly more important. Fig. 6 illustrates this simple relationship. The timing precision of Loran-C and WWV are also shown for an integration time of approximately one minute. Much longer integration times would improve the accuracies obtainable with WWV.⁷

V. MISSILE RANGE TIMING

The National Bureau of Standards demonstrated Loran-C timing potentials on the Atlantic Missile Range in October, 1960. These tests were conducted using two experimental Loran-C clocks and a UHF timing distribution system.⁸ The clocks were rather complex devices consisting of modified Loran-C receivers and counting and read-out circuits. The two clocks were synchronized on two separate transmitters and an external read command was used to check any variation

⁸ T. L. Davis and R. H. Doherty, "Widely separated clocks with microsecond synchronization and independent distribution systems," IRE TRANS. ON SPACE ELECTRONICS AND TELEMTRY, vol. SET-6, pp. 138-146; December, 1960.

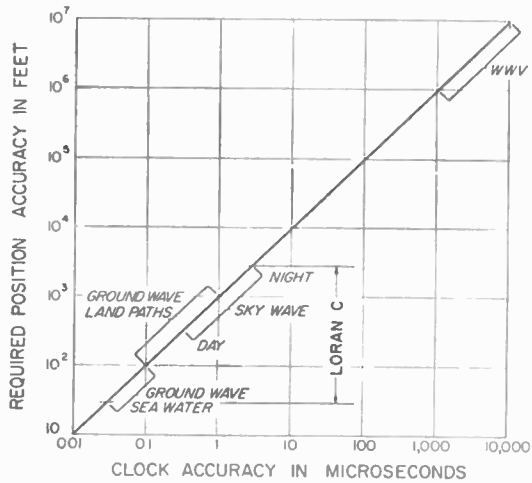


Fig. 6—Time-position accuracy relationship.

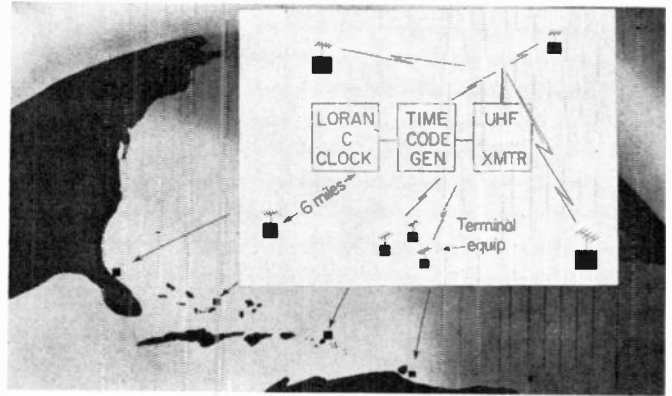


Fig. 7—UHF time distribution system.

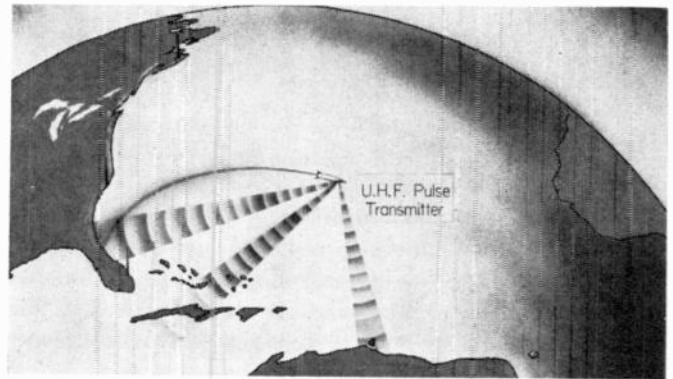


Fig. 8—Trajectory determination by precise timing.

between the clocks. When a large number of equipments requiring time are operated in close proximity, a single clock can serve them all by means of an appropriate UHF timing distribution system.⁸ This basic system of time measurement and distribution could be duplicated at any number of locations within the coverage area of a Loran-C chain. See Fig. 7.

Loran-C ground wave coverage extends down range as far as Trinidad. The various down-range sites to that distance can be provided with absolute timing accuracy of approximately $1 \mu\text{sec}$. Beyond Trinidad and down to Ascension Island the Loran-C clocks must be synchronized on sky waves. It is important to note that the absolute accuracy involves an allowance for *systematic* propagation errors which cannot be measured independently by any existing system or method. The repeatability of time measurements at any one station, however, will in general be better than $0.1 \mu\text{sec}$. In some cases, repeatability may be at least as important as absolute accuracy. For example, the trajectory of a missile or the position of a satellite⁹ could be determined by transmitting very short pulses at UHF or microwave frequencies from the missile and recording their time of arrival at a number of time synchronized stations. See Fig. 8. Systematic time errors among the observing stations would result in a corresponding error in the absolute position of the trajectory, but the changes from reading to reading would be influenced only by the stability of the individual clocks and the stability of the propagation medium between the missile and the ground stations.

On the basis of theory¹⁰ and measurements (Appendix II) there is little doubt that Loran-C clocks can be

quite accurately synchronized even on second and/or third hop sky waves. Second hop sky wave time differences from the Cytac (Loran-C) transmitters (Forestport, N. Y., Cape Fear, N. C., and Carrabelle, Fla.) were measured at distances up to 5000 km. Standard deviations of these differences were less than $2 \mu\text{sec}$ day or night. Sunrise and sunset effects corresponding to 18 to 20 km change in ionospheric height were observed. When only the first reflected signal was utilized these sunrise and sunset effects rarely lasted more than 30 minutes. The height variations agree well with other observations for oblique incidence.^{11,12} At distances beyond ground wave range there is no satisfactory way to accurately measure sky wave delays. But there is no reason to distrust computed values based on theoretical calculations, former observations and recent electron density rocket information.¹⁰⁻¹³ Based on this information, it should be possible to establish time at ranges from 2000 to 8000 km at least within $10 \mu\text{sec}$.

The Atlantic and Pacific missile ranges can be linked with a common timing system which will provide $1 \mu\text{sec}$ accuracy. The link between the two ranges requires the

¹¹ J. R. Wait, "Diurnal change of ionospheric heights deduced from phase velocity measurements at VLF," *Proc. IRE (Correspondence)*, vol. 47, p. 998; May, 1959.

¹² J. M. Watts, "Oblique incidence propagation at 300 kc using pulse techniques," *J. Geophys. Res.*, vol. 57, pp. 487-498; December, 1952.

¹³ A. H. Waynick, "The present state of knowledge concerning the lower ionosphere," *Proc. IRE*, vol. 45, pp. 741-749; June, 1957.

⁹ G. Hefley, R. F. Linfield and R. H. Doherty, "Timing and Space Navigation with an Existing Ground Based System," presented at AGARD 10th General Assembly, Istanbul, Turkey, October, 1960, Pergamon Press Inc., New York, N. Y.; 1961.

¹⁰ J. R. Johler and L. C. Walters, "On the theory of reflection of low and very-low radiofrequency waves from the ionosphere," *J. Res. NBS*, vol. 64D, pp. 269-285; May-June, 1960.

installation of additional Loran-C stations in a generally east-west direction across the Continental U. S. Possible locations for these stations are shown in Fig. 9. Such a configuration would provide inter-range synchronization as well as excellent navigational coverage over the Continental U. S.

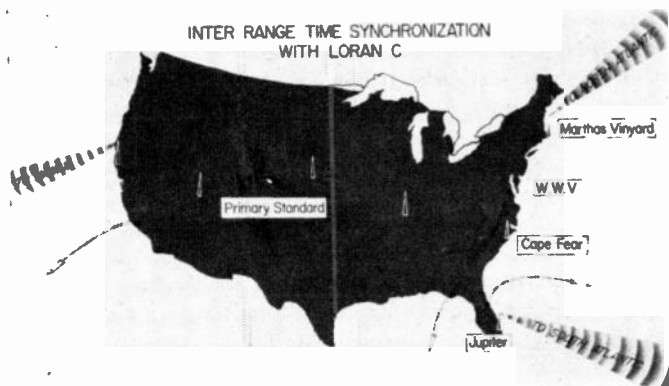


Fig. 9—Possible transmitter locations.

The inter-range synchronization only could be obtained on a very reliable basis by providing a transmitter in Illinois and another transmitter and secondary frequency standard near the West Coast. The western transmitter would be located within ground wave range of Boulder and could be steered by the primary frequency standard. If a number of Loran-C chains were synchronized, one to another, in order to provide coverage over very long ranges, the synchronization accuracy would be degraded to some extent. As far as is known, synchronization errors are of a random nature and therefore can be expected to add as the root-sum-square. For example, if the synchronization error in each transmitter is $0.03 \mu\text{sec}$, the accumulated error in synchronizing six stations would be $\sqrt{6(0.03)^2}$ or $0.073 \mu\text{sec}$.

The synchronization accuracy of the present Loran-C system could be improved by the use of better oscillators and longer integration times. It is not obvious, however, how much improvement could be achieved before reaching the point of diminishing returns.

The total noise or synchronization errors which can be expected in synchronizing a chain in the Hawaiian Islands from the U. S. should be substantially less than the prediction error in a land or mixed path.

VI. ADDITIONAL USES OF PRECISE TIME

Some scientific and commercial uses of a precise timing system that may have direct or indirect military applications are:

- 1) The positioning of high-altitude aircraft from the ground by using the UHF pulse technique.
- 2) The location of thunderstorms by precisely measuring the location of the lightning discharge.
- 3) The accurate position-fixing of nuclear detonations by a similar means.
- 4) A precise evaluation of the fluctuations of the periodicity of the earth's rotation and other astronom-

ical phenomena by relating observations made at widely separated points.

5) The precise measurement of time variations on high-frequency transmissions such as WWV as an aid to better understanding of propagation phenomena.

6) Similar measurements on forward scatter communication links and other types of communication could also be made.

7) The surveying of offshore islands and remote areas.

8) The investigation of Loran-C sky waves to give a better understanding of ionospheric conditions.

9) The precise time from a single Loran-C clock could be made economically feasible for a variety of users in industry and research by the application of a VHF or UHF distribution system. Relatively inexpensive distribution would result if sufficient users were located within range of the distribution system. Existing facilities such as television transmitters could be utilized for this purpose.

APPENDIX I

LORAN-C GROUND WAVE MEASUREMENTS

The data presented in this appendix have been abstracted from a report concerned with the position fixing aspects of the Loran-C (formerly Cytac) system.¹⁴

The data were obtained primarily in the service area (see Fig. 1) during 1954 and 1955. The data are presented in the form of time difference measurements, since the position-fixing information was of prime concern. Although individual propagation paths were not resolved, these measurements were entirely consistent with the individual round-trip paths observed at the transmitters. Since no appreciable differences were detected, the time difference data in the service area were considered to be representative of single path propagation times. Data presented in Appendix II, comparing various sky wave time modes with the ground wave signal, are also consistent with this assumption.

These time-difference (TD) measurements were made in two stages. An envelope measurement was made automatically by subtracting the derivative of the envelope from the envelope and detecting an axis crossing with a servo loop. A cycle measurement was made automatically using synchronous detection techniques and a null seeking servo system. In all cases, the master signal was used to control the reference frequency, and the time differences ($X - M$ and $Y - M$) were measured with respect to the master. The difference between the envelope TD readings and the cycle TD readings was denoted as the discrepancy. If this discrepancy did not exceed plus or minus $5 \mu\text{sec}$, cycle identification was assured by the envelope reading. A typical plot of the cumulative distribution of this reading is illustrated in Fig. 10. Within ground wave recep-

¹⁴ R. F. Linfield, R. H. Doherty, and G. Hefley, "Evaluation of the Propagation Aspects of the Cytac System," private communication; March 18, 1957. (Originally classified confidential.)

tion, the discrepancy was always well within reasonable limits.

The differences between observed and predicted readings were either position dependent or time dependent. The variations related to the position are thought to be caused by an incorrect assumption of the value of the conductivity. Fig. 11 shows a plot of data from locations where the signals arrived over land path. It appears that 0.005 mho/meter is a good average for the M-X pair, but that a higher value of conductivity from the Y transmitter would better approximate the M-Y paths.

The mean of the observed phase readings was compared to predicted phase readings calculated using an assumed conductivity of 0.005 mho/meter for land and 5 mhos/meter for sea water. Differences between

the mean and the calculated readings are listed in Table I. Also shown are the distances from the transmitters, the hours of observation, and the standard deviations of the two time differences. The hours of observation were distributed randomly, day or night, throughout the period of operation at each location.

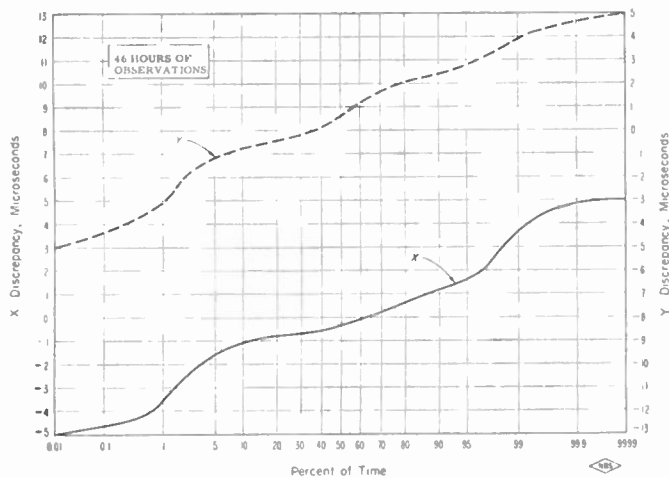


Fig. 10—Cumulative distribution of discrepancy readings—Wisconsin.

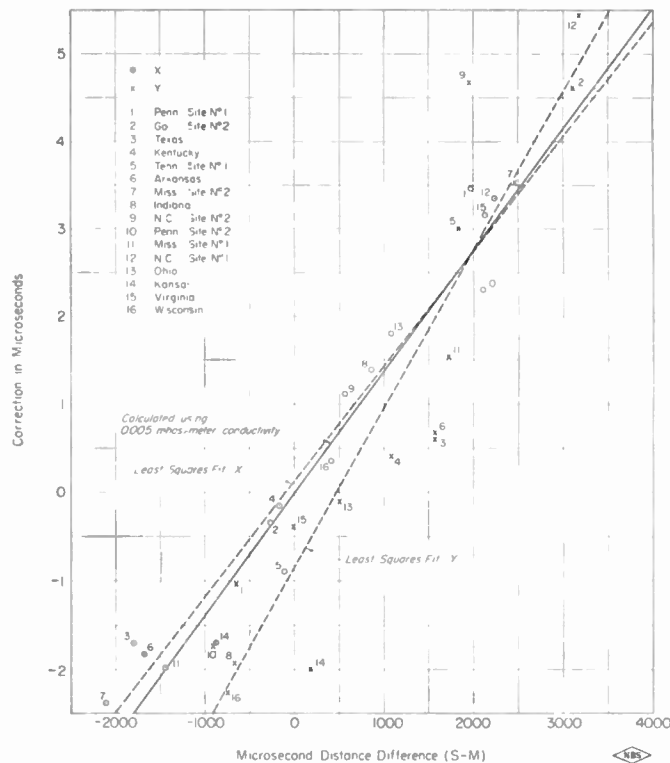


Fig. 11—Comparison of theoretical phase of secondary field difference corrections and measured data.

TABLE I
RESULTS OF CYTAC MONITORING PROGRAM

Receiver Location	Distance to Transmitters km			Total Observations (hours)	Days At Site	Mean (all Observations) Minus Predicted (μsec)		Std. Deviation of the Observations	
	M	X	Y			M-X	M-Y	M-X	M-Y
Miss.—1	1187	753	1704	800	341	+0.10	-0.47	0.11	0.47
N. C.—1	84	756	1028	750	316	+0.35	+1.01	0.16	0.53
Ohio	670	993	825	200	102	+0.48	-1.20	0.10	0.21
Texas—1	2055	1312	2781	98	64	-1.25		0.15	
Maine	1322	2051	437	92	11		-0.07		0.23
Tenn	663	630	1214	58	5	-0.76	+0.78	0.10	0.24
Missouri	1339	1120	1556	52	5	-0.04	-2.88	0.14	0.25
Penn.—1	666	1252	472	52	3	+1.30	-0.09	0.12	0.05
Indiana	1039	1294	839	51	5	+0.29	-1.04	0.07	0.09
Wisconsin	1324	1430	1101	46	5	-0.13	-1.33	0.11	0.13
Florida	656	401	1717	34	7	-0.51	+0.89	0.16	0.27
Kansas	1939	1696	2010	30	5	-0.60	-2.22	0.17	0.19
N. C.—2	499	670	1084	27	2	+0.54	+2.24	0.05	0.09
Iowa	1573	1469	1542	22	2	+0.28	-1.58	0.11	0.10
Penn.—2	681	1314	409	17	3	-0.15	-0.43	0.09	0.07
Virginia	545	1184	544	16	2	+0.63	-0.33	0.26	0.06
Georgia—1	412	368	1408	16	3	+0.32	+0.14	0.12	0.15
Georgia—2	440	359	1371	14	2	-0.05	+0.38	0.11	0.07
Florida—2	816	37	1754	9	1	-0.01	+0.65	0.06	0.17
Louisiana	1414	780	2063	9	2	-0.81	-1.59	0.05	0.23
Arkansas	1519	1015	1990	8	2	+0.48	-1.37	0.04	0.22
Florida—3	1118	655	2182	8	2	-0.03	-0.03	0.08	0.12
Miss.—2	1079	449	1818	8	2	+0.43	+0.07	0.10	0.18
Florida—4	927	454	1983	7	2	+0.02	+0.02	0.06	0.10
Texas—2	1669	1133	2141	7	1	+0.80	-1.19	0.03	0.16

The standard deviation of the mean minus the predicted values listed in Table I for the M-X pair is 0.5 μsec , the mean deviation is 0.43 μsec and the algebraic average is +0.06 μsec . For the M-Y pair the standard deviation is 1.17 μsec , the mean deviation is 0.92 μsec , and the algebraic average is -0.41 μsec . The Millington¹⁵ method for combining conductivities was used for evaluating predictions for 13 sites, but this did not appreciably improve the standard deviations. However, the only conductivity values¹⁶ that were available were measured at broadcast frequencies and over limited areas and are, therefore, not considered applicable at 100 kc. By assuming conductivities for the Y path ranging from 0.004 to 0.008 mho/meter, the standard deviation of the mean-predicted values for the M-Y pair was reduced to 0.69 μsec , and the average error was reduced to 0.51 μsec . Even though the two paths (receiver to M and receiver to X or Y) cannot be separated this method could provide a means for empirically evaluating conductivity at 100 kc in areas where Loran-C measurements are available.

Figs. 12-16 present cumulative distributions of the time difference readings taken at 2.5 minute intervals for sites where the total observation time was limited. Figs. 17-20 present cumulative distributions of the daily average readings for sites where observations were made for several months.

From these figures it can be seen that variations were within 1 μsec during a very high percentage of the time. It may be noted that the M-Y (northern) pair generally had greater deviations than the M-X (southern) pair. This is also quite obvious from Figs. 21-24 where the daily averages are plotted for the fixed sites. Figs. 25 and 26 indicate some typical diurnal variations on the M-X and M-Y pairs. Again it can be seen that the M-Y variations were greater than the M-X variations.

The reason for the larger time variation associated with the northern path was never completely resolved although many contributing factors can be listed. Errors of this magnitude do not exist on the northern pair of the present east-coast Loran-C system.

Most of the data presented here were obtained from signals that were not phase coded. Multihop sky wave contamination was not eliminated and could contribute toward time variations (see Fig. 27). During the first few months of operation some variations were probably due to inexperience of operating personnel.

The operation was not continuous and evidently instabilities accompanied shut down periods. Fig. 28 shows such changes recorded at four stations when the operating periods were compressed into a single plot. Correlation coefficients were calculated using simul-

taneous data from these four sites. The correlation coefficients are shown in Table II.

In a further investigation, the variations were divided into two categories or components: 1) purely random variations and 2) variations which would produce correlation at the observation points. Since servos in the different pieces of equipment were not adjusted to have identical damping characteristics, the data were normalized to the average characteristics of the four equipments. The results indicated in Table III demonstrate that the maximum variations that could positively be attributed to propagation did not exceed 0.03 to 0.04 μsec .

Although the time fluctuations have sometimes been shown to correlate with weather phenomena, particularly temperature, it has not been conclusively established that the variations were not partially within the antenna system. The typical Loran-C installation includes a 600-foot top loaded transmitting antenna, and a 30- to 90-foot receiving whip within a few hundred meters of the transmitting antenna. Impedance changes of the transmitting antenna would affect the phase characteristics of the receiving antenna. An attempt to check this effect was made by using a receiver on the base-line extension. Any effect due to the antenna impedance change was evidently masked by larger variations.

The large time variations on the northern pair (M and Y) were probably the result of a combination of multihop sky wave contamination, and the first-hop sky wave contamination. The first-hop contamination could occur if the signal were sampled too late, that is, after the first-hop sky wave had started to arrive. The base-line path of the northern pair during the Cytac tests was quite long (over 1000 km); it was all over land (causing maximum delay of the ground wave), and it was at a high geomagnetic latitude.

A subsequent Loran-C chain located in the arctic (high geomagnetic latitude) has encountered trouble with very short first-hop sky wave delays because of the lower ionospheric heights at these latitudes. This situation was encountered even though the base lines were over sea water.

The Loran-C chain located on the East Coast of the United States has been relocated since 1955. The northern base line is now partially over sea water and the northern station is at a slightly lower geomagnetic latitude. With continuous operation and the new locations, the variations have been reduced by an order of magnitude.

Amplitudes of the ground wave signal out to ranges as great as 3700 km are shown in Fig. 29. The paths that the signals traversed were partially land, but primarily sea water. The agreement between predicted and measured values is fairly good in the range of 2400 to 3700 km. The deviation from the predictions at ranges less than 2400 km is greater than can be explained by experimental error.

¹⁵ G. Millington, "Ground wave propagation over an inhomogeneous smooth earth," *Proc. IEE*, vol. 96, pt. III, pp. 53-64; January, 1949.

¹⁶ R. S. Kirby, *et al.*, "Effective Radio Ground Conductivity Measurements in the United States," Natl. Bureau of Standards, Boulder, Colo., NBS Circular No. 546; February, 1954.

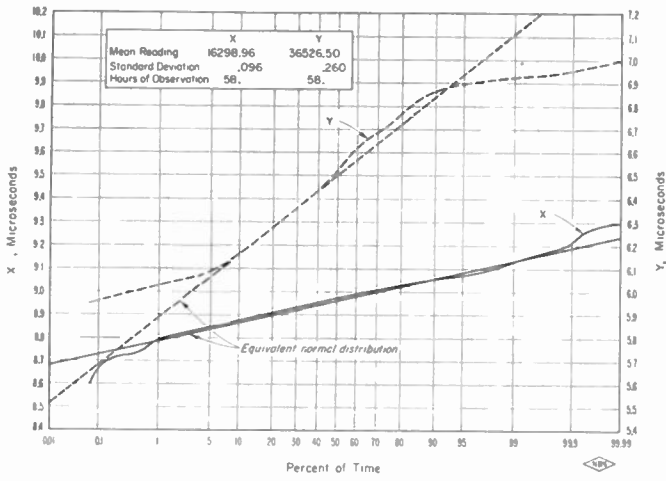


Fig. 12—Cumulative distribution of time difference readings—Tennessee Site 1 (2.5 minute intervals).

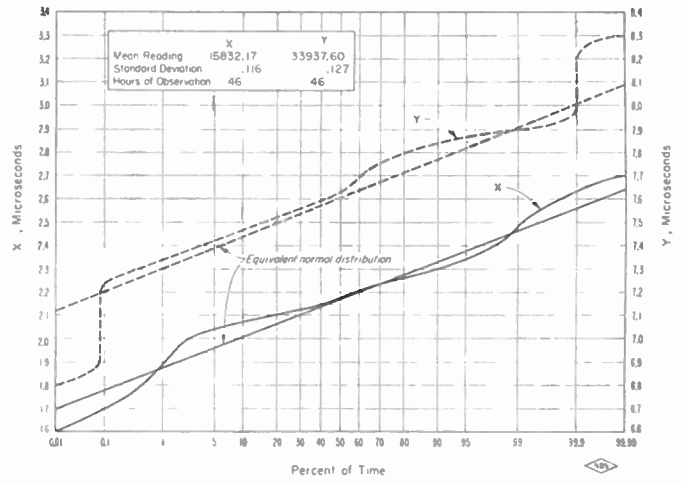


Fig. 13—Cumulative distribution of time difference readings—Wisconsin (2.5 minute intervals).

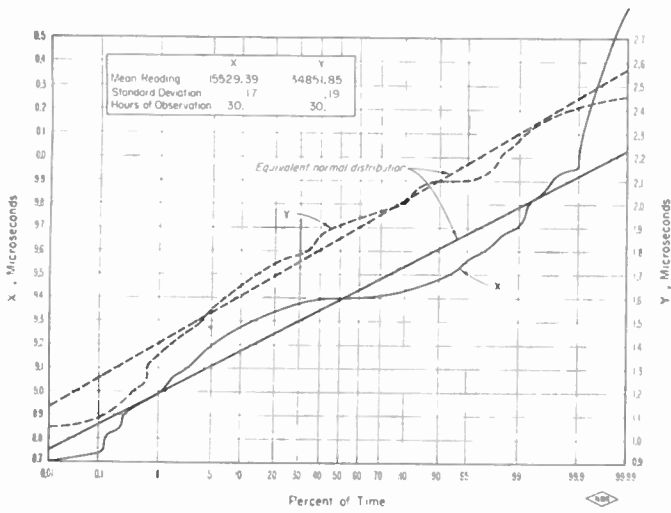


Fig. 14—Cumulative distribution of time difference readings—Kansas (2.5 minute intervals).

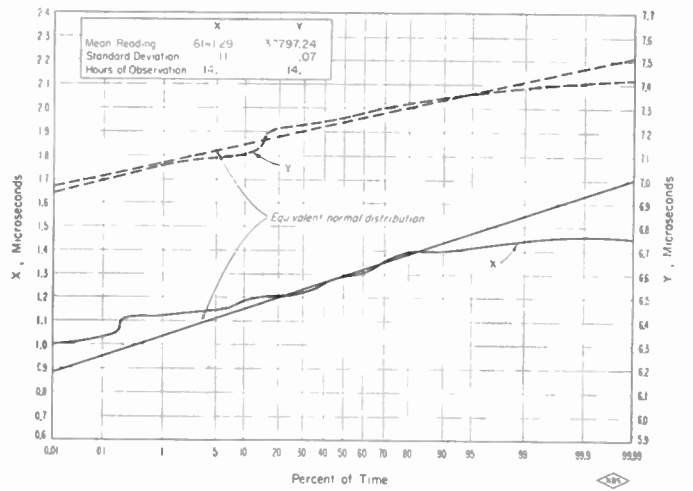


Fig. 15—Cumulative distribution of time difference readings—Georgia Site (2.5 minute intervals).

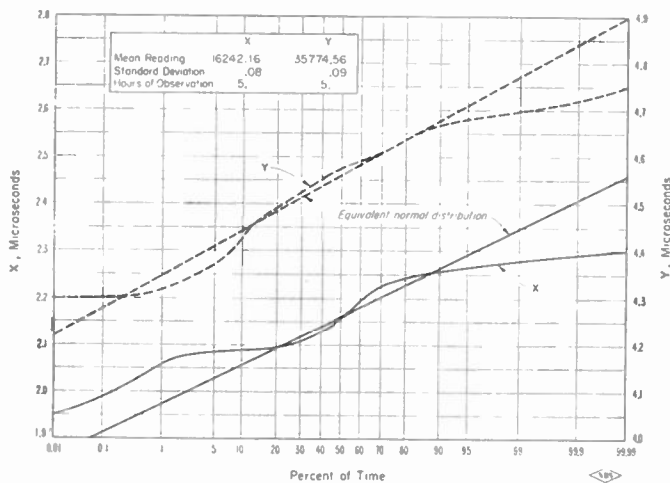


Fig. 16—Cumulative distribution of time difference readings—Kentucky (2.5 minute intervals).

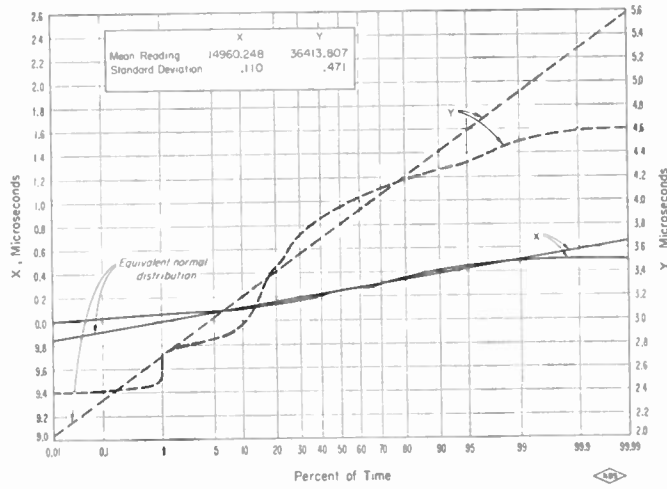


Fig. 17—Cumulative distribution of daily averages—Mississippi Site 1 (November 1954–1955).

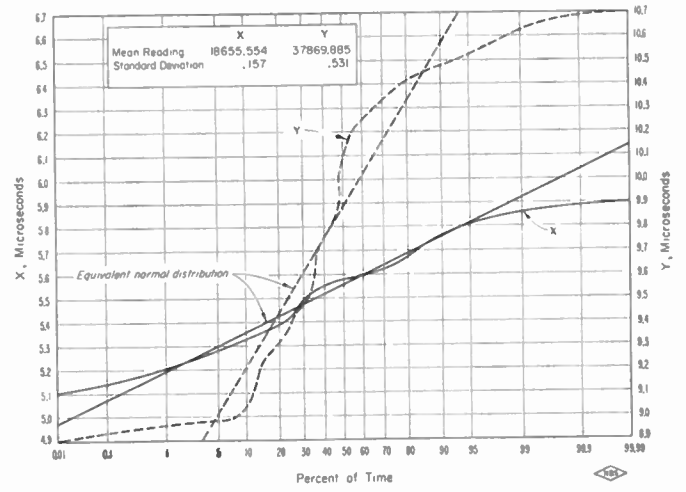


Fig. 18—Cumulative distribution of daily averages—North Carolina Site (January–October 1955).

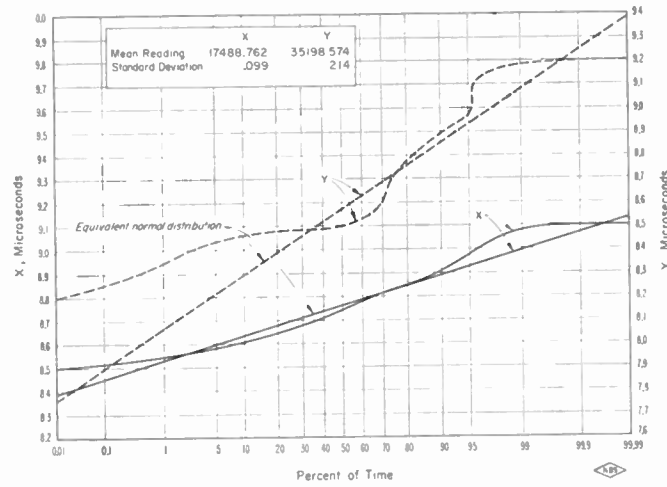


Fig. 19—Cumulative distribution of daily averages—Ohio (January–February 1955).

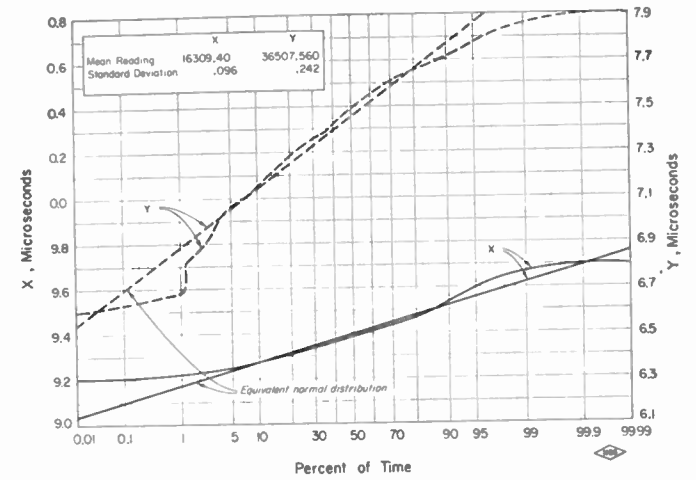


Fig. 20—Cumulative distribution of daily average—Tennessee Site 1 (March–November 1955).

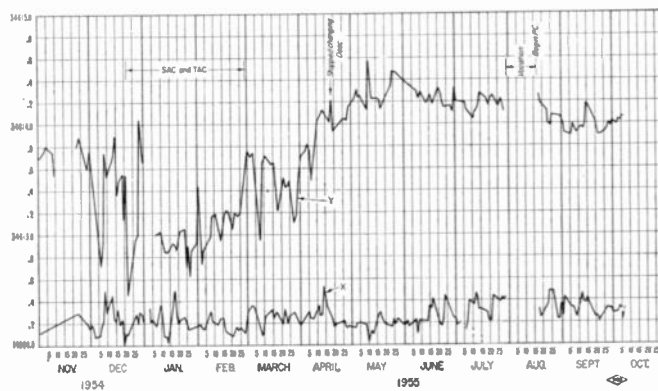


Fig. 21—Daily average X and Y cycle readings—Mississippi Site 1.

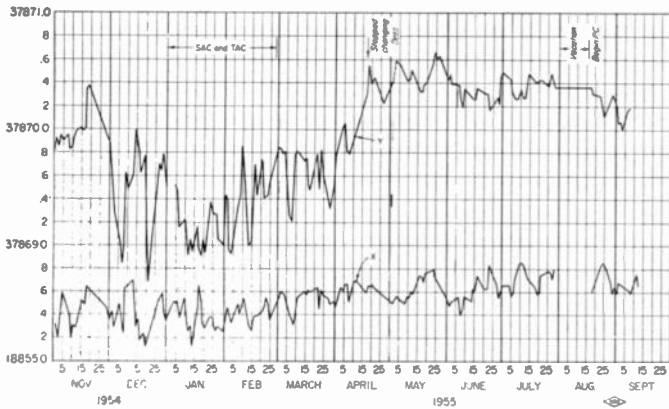


Fig. 22—Daily average X and Y cycle readings—North Carolina Site 1.

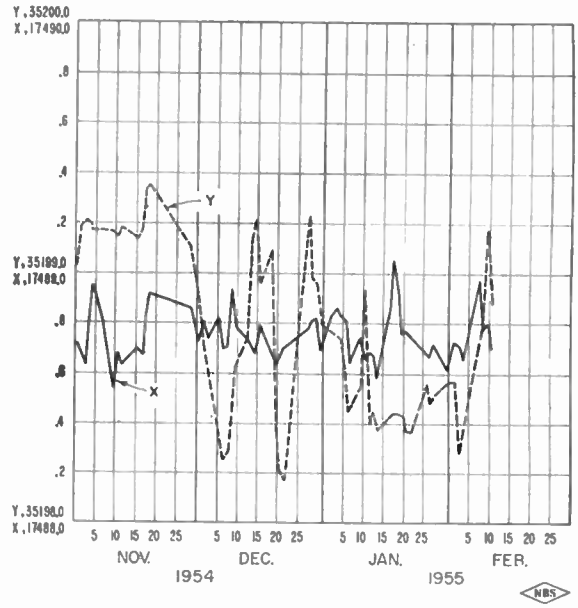


Fig. 23—Daily average X and Y cycle readings—Ohio.

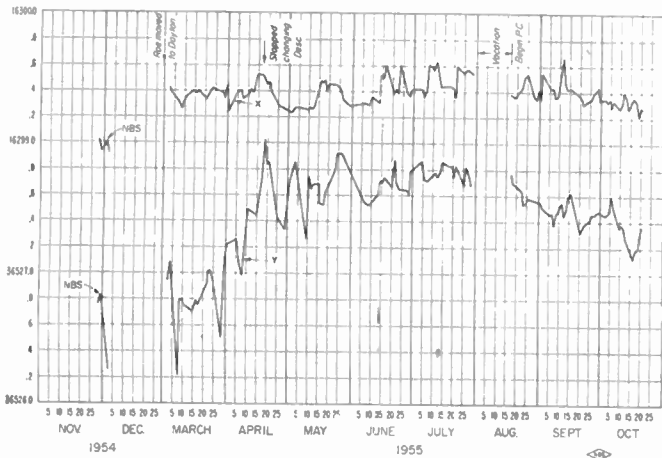


Fig. 24—Daily average X and Y cycle readings—Tennessee Site 1.

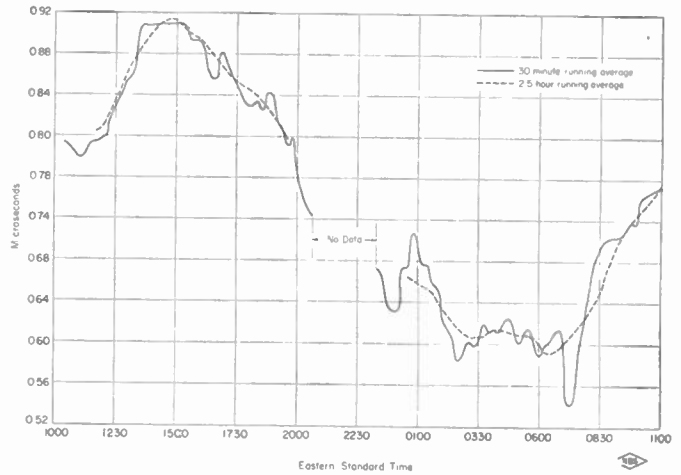


Fig. 25—Running average of Y time difference—North Carolina Site 1 (November 30–December 1, 1954).

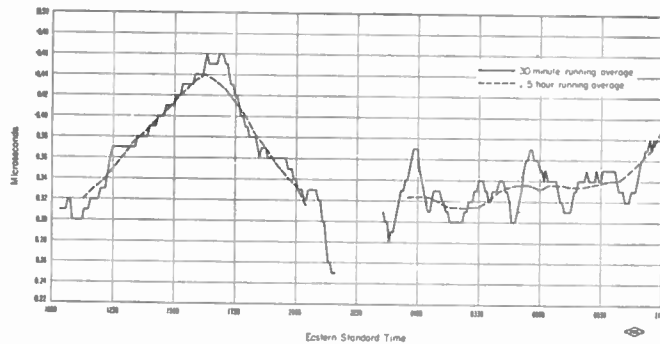


Fig. 26—Running average of X time difference—North Carolina Site 1 (November 30–December 1, 1954).

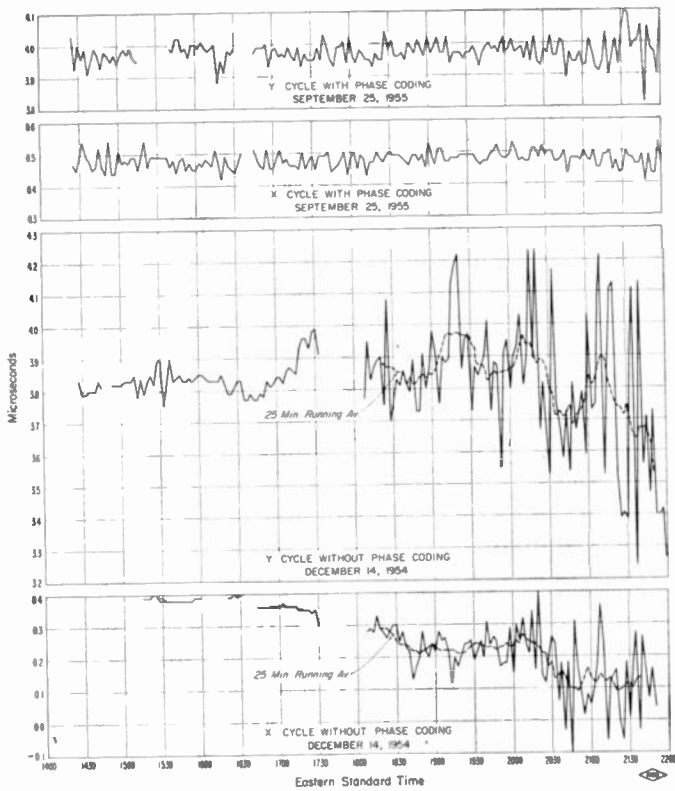


Fig. 27—Cycle readings with and without phase coding—Mississippi Site 1.

TABLE II
CORRELATION OF S_1 PAIR

	Tenn. Site 1	Tenn. Site 2	Miss. Site 1	N. C. Site 1
Tenn. Site 1		0.930	0.934	0.901
Tenn. Site 2	0.930		0.934	0.855
Miss. Site 1	0.934	0.934		0.870
N. C. Site 1	0.901	0.855	0.870	

CORRELATION OF S_2 PAIR

	Tenn. Site 1	Tenn. Site 2	Miss. Site 1	N. C. Site 1
Tenn. Site 1		0.526	0.658	0.620
Tenn. Site 2	0.526		0.543	0.442
Miss. Site 1	0.648	0.543		0.669
N. C. Site 1	0.620	0.442	0.669	

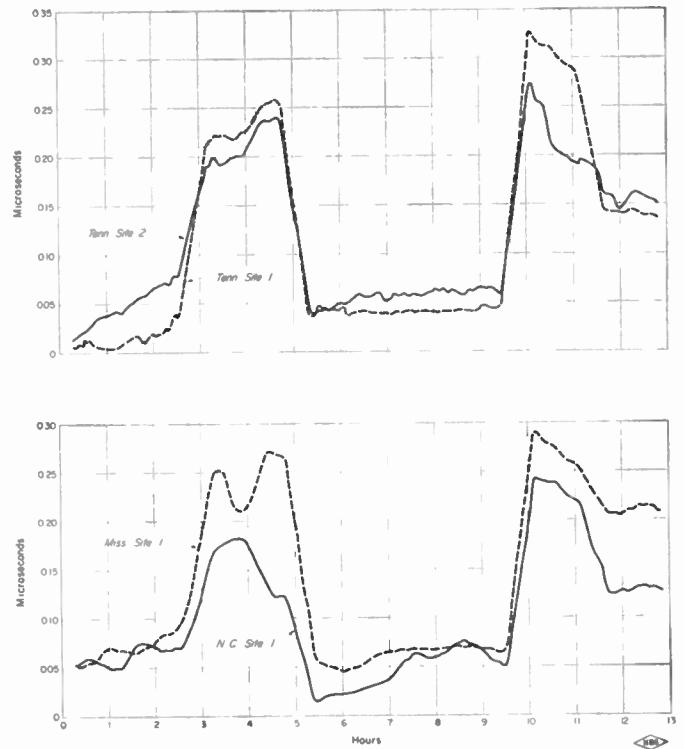


Fig. 28—37.5 minute running averages of X readings (13.1 hours of data, September 1-13, 1955).

TABLE III

	Measured	Normalized	Noise Component	Synchronous Component
S_1 PAIR				
Tenn. Site 1	0.107	0.077	0.011	0.076
Tenn. Site 2	0.081	0.081	0.009	0.076
Miss. Site 1	0.092	0.081	0.003	0.076
N. C. Site 1	0.068	0.082	0.032	0.076
S_2 PAIR				
Tenn. Site 1	0.057	0.038	0.024	0.029
Tenn. Site 2	0.043	0.043	0.032	0.029
Miss. Site 1	0.043	0.035	0.019	0.029
N. C. Site 1	0.105	0.037	0.022	0.029

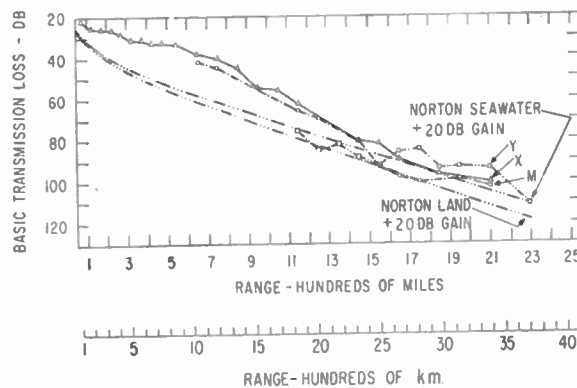


Fig. 29—Predicted and measured ground wave signal amplitude.

APPENDIX II

LORAN-C SKY WAVE MEASUREMENTS

Loran-C is a pulse navigation system utilizing sampling techniques to select the ground wave and discriminate against the sky wave signal. These same sampling techniques can be utilized to select one sky wave signal and discriminate against all other sky wave signals at ranges beyond ground wave reception. This provides a means for measuring the phase and amplitude of a particular sky wave time mode rather than a composite signal as is done in CW measurements. Many measurements that have been made with Loran-C indicate that the phase of a particular time mode is very stable, but the amplitude of that time mode is quite unstable. Furthermore, the variations occurring on one time mode do not necessarily correlate with variations occurring on another time mode.

If a number of vectors of different fixed phases but of variable amplitudes are added together, the phase of the resultant will change as a result of the amplitude variations. Similarly, the phase of a CW signal varies in accordance with the amplitudes of the different time modes. Consequently, the phase variations do not nec-

TABLE IV

Mode	Distance (Kilometers)	Time (Day or Night)	Delay (μ sec)	σ Standard Deviation (μ sec)
BELIZE, BRITISH HONDURAS				
X Gnd. Y Gnd.	1425 3133	D	- 0.4	0.944
X Gnd. Y 1st	1425 3133	D	+ 29.9	1.012
X Gnd. Y 1st	1425 3133	N	+ 43.1	1.219
X Gnd. Y 3rd	1425 3133	D	+102.8	0.541
X Gnd. Y 2nd	1425 3133	N	+103.9	1.460
X Gnd. Y 4th	1425 3133	N	+267.7	0.904
KINGSTON, JAMAICA				
M Gnd. X Gnd.	1786 1539	D	- 0.7	0.551
X Gnd. Y Gnd.	1539 3829	N	+ 0.3	0.366
M Gnd. Y Gnd.	1786 3829	D	+ 1.0	0.356
PUERTO CABEZAS, NICARAGUA				
X Gnd. Y Gnd.	1763 3356	D	- 2.21	1.235
X Gnd. Y 1st	1763 3356	D	+ 30.0	1.436
X Gnd. Y 1st	1763 3356	N	+ 49.7	1.234
X Gnd. Y 3rd	1763 3356	D	+211.4	1.018
M Gnd. X Gnd.	2286 1763	N	- 1.9	0.255
BUENAVENTURA, COLOMBIA				
M Gnd. X Gnd.	3339 2983	D	- 2.64	0.590
M 1st X 1st	3339 2983	N	- 2.06	0.415
M 1st Y 1st	3339 4385	N	+ 0.0	0.936
M Gnd. Y 2nd	3339 4385	D	+ 37.5	1.864
M Gnd. Y 3rd	3339 4385	D	+105.3	0.909
X 1st Y 4th	2983 4385	D	+222.7	1.309
X Gnd. Y 4th	2983 4385	D	+235.9	1.015
GUAYAQUIL, ECUADOR				
M 1st X 1st	4024 3574	N	- 1.98	0.299
M 1st Y 2nd	4024 5086	N	+ 56.6	0.527
M 1st X 1st	4024 3574	D	- 0.50	1.812

essarily indicate phase changes in the individual time modes nor changes in ionospheric height.

At ranges beyond ground wave reception the first signal arriving via the ionosphere was normally observed. At shorter ranges uncontaminated higher order multihop sky wave signals were observed. Sky wave signals have been observed at distances as great as 12,000 km (Johannesburg, S. A. from Jupiter, Fla.). A large number of measurements listed in Table IV have been made between 3000 and 5000 km. Multihop measurements listed in Table V have been made at ranges as short as 500 km.

Figs. 30-31 illustrate typical daytime first-hop sky waves observed at Boulder, Colo. (about 3000 km from the transmitters). All of the data available suggest an excellent sky wave phase stability when a single propagation mode is studied. The Boulder data recorded over a period of more than one month had short term variations of only 0.25 μ sec and day to day variations of only 0.5 μ sec. This data was obtained by comparing a first-hop sky wave from one transmitter with the ground wave from another (southern pair). Nighttime measurements were not made in 1955 because the transmitters did not operate on a 24-hour basis during September and October. Similar measurements made at Boulder in 1961 indicate nighttime stabilities to be at least within 5 μ sec (see Fig. 32).

TABLE V

Distance Kilometers	Transmitter	Total Delay (μ sec)	Amplitude (in μ v/m)	Most Probable Hop	Corresponding Layer Height km
WOODSTOCK, KENTUCKY					
817	X	304	9.6	3rd	65.0
817		Nothing could be observed for 4th			
817	X	784	10.3	5th	65.5
817	X	1024	10.8	6th	63.6
1051	Y	285	19.2	3rd	69.5
1051	Y	505	14.4	4th	71.8
1051	Y	753	11.2	5th	71.7
1051	Y	993	9.6	6th	69.6
SPRING CREEK, NORTH CAROLINA					
496	M	815	24.4	4th	68.0
496	M	1050	20.0	5th	64.0
676	X	454	—	3rd	74.2
676	X	752	13.2	4th	74.0
1078	Y	1083	—	6th	74.0
BOULDER, COLORADO					
2526	Y	32	—	1st	*
2526	Y	448	—	5th	78.8
2526	Y	618	—	6th	78.3
2518	Y	34	—	1st	*
2518	Y	298	2.0	4th	77.4
2518	Y	440	—	5th	77.5
2510	M	34	—	1st	*

* Since the apparent heights are obtained from a graph based on geometrical-optical considerations, and the distance for first-hop sky wave is far beyond that obtainable by geometrical-optical theory, any apparent heights assigned to these first-hop reflections would be completely meaningless.

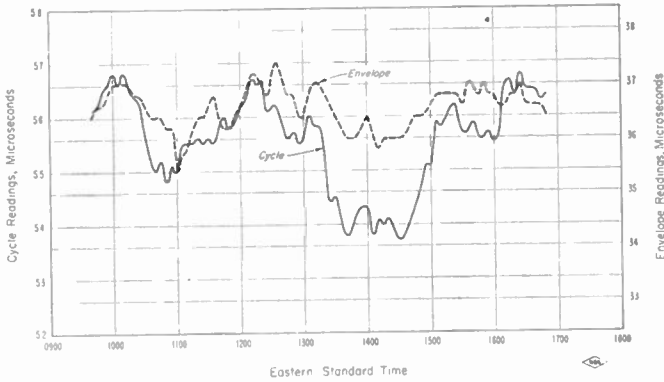


Fig. 30—Envelope and cycle readings, first-hop sky wave—Boulder, Colo. (September 13, 1955).

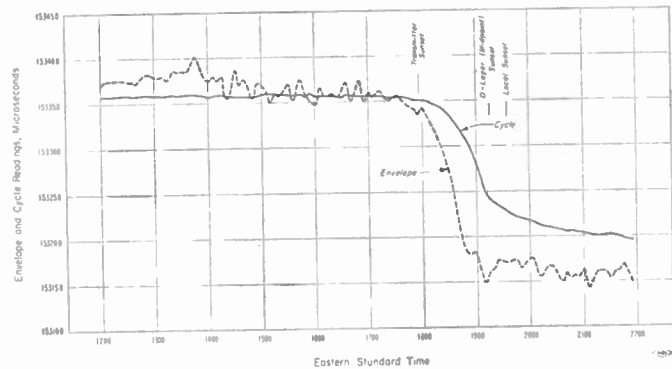


Fig. 31—First-hop sky wave measurements—Boulder, Colo. (October 6, 1955).

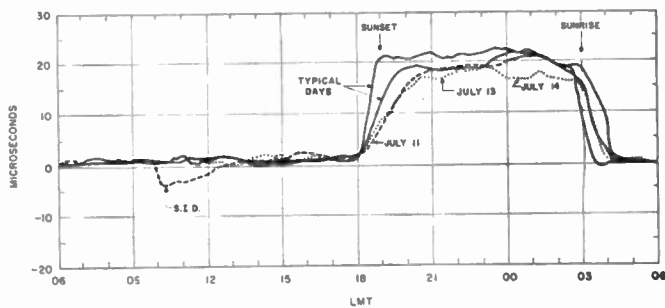


Fig. 32—First-hop sky wave from Cape Fear, N. C.—Boulder, Colo. (1961). Approximately 3000 km.

The standard deviations listed in Table IV were typical of observations for an entire day or night made in Central and South America in 1956. These standard deviations again suggest excellent stability of the sky wave phase. The delays listed are delays as compared to the predicted arrival time of the ground wave signal. These delays seem to be quite reasonable for the propagation mode being measured. Fig. 32 illustrates the phase change resulting from an S.I.D. occurring on July 11, 1961. The event was rated at about $3\frac{1}{2}$ on a scale of 4. VLF records indicated a change of up to 30 μ sec. This first-hop sky wave signal showed a total phase change of 4.5 μ sec. This phase decrease was ac-

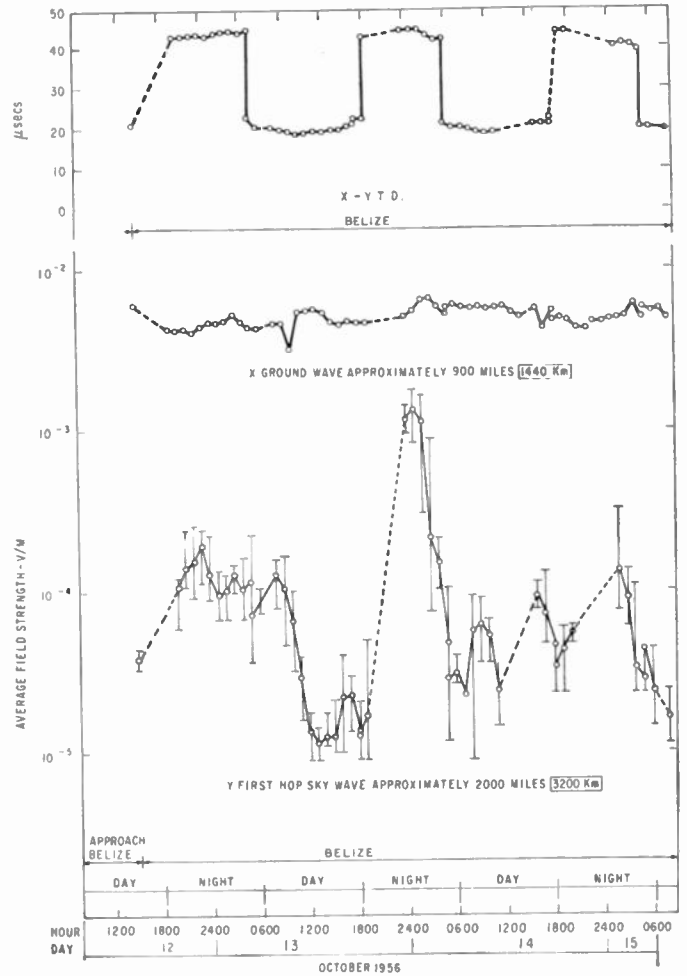


Fig. 33—Phase and amplitude of Loran-C sky wave referred to ground wave.

companied by an amplitude increase of more than 12 db. The slower sunset effect seems to be related to the flare and the magnetic storm that followed the event. On July 13th and 14th (dotted curves) a magnetic storm occurred that disturbed the phase of VLF CW measurements.

Fig. 33 presents a three-day plot of both the phase and amplitude of a first-hop sky wave signal, the upper plot representing the T.D. between a first-hop sky wave signal from 3200 km and the ground wave signal from 1440 km. Again rather good phase stability is suggested. The lower plots are the measured amplitudes of the two signals. The amplitude of the sky wave signal is quite variable and not obviously correlated with any phase changes.

The amplitudes of the various time modes present vary relative to one another, often quite rapidly. Fig. 34 illustrates several time modes of the Loran-C master pulses observed at Boulder. The relative amplitudes of the several time modes obviously do not correlate. A CW measurement made at this frequency would show phase changes due to these relative amplitude changes alone.

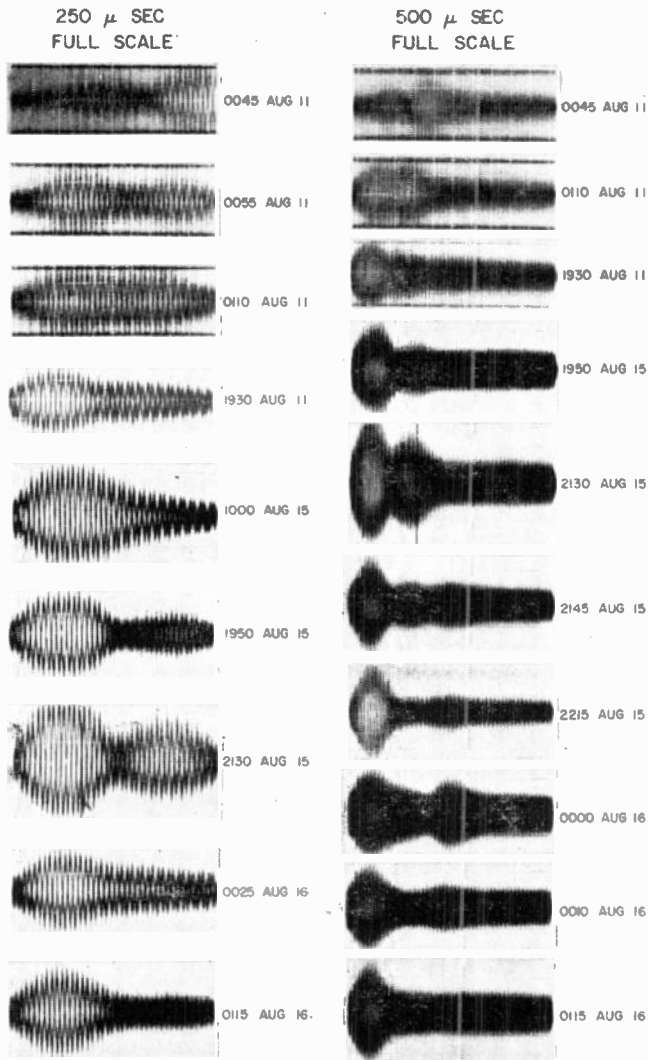


Fig. 34—Multihop sky waves master signal observed at Boulder, Colo.

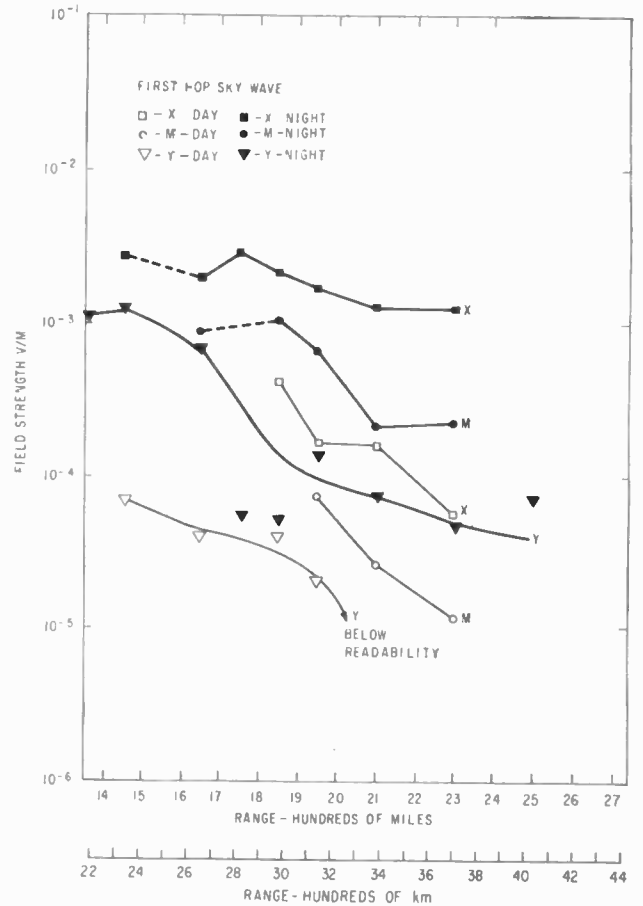


Fig. 35—Field strength of Loran-C sky wave on north-south paths.

multihop sky waves were present at most locations. It was further noted as can be seen from the tabulations that often the amplitude of the n th hop would be as great as or greater than the amplitude of the n th-1 hop. Assumptions made as to predominant time modes or negligible time modes for CW measurements may be somewhat questionable in view of these observations.

VII. ACKNOWLEDGMENT

Special acknowledgment is given to P. J. Kiser, of the Air Force Eastern GEEIA Region, for his engineering contributions to the Loran-C clock and his assistance in the preparation of this paper.

The entire Loran-C clock and UHF distribution system has been developed by the National Bureau of Standards, Boulder Laboratories under the sponsorship of Headquarters, Eastern GEEIA Region.

Fig. 35 represents average amplitudes observed on a predominantly north-south path. Since these plots are strictly amplitude versus distance and the Y transmitter was about 15° farther north than the X transmitter, a strong latitude effect on signals propagated by the ionosphere is suggested. The average nighttime sky wave field intensity was about 20 db larger than the average daytime field intensity.

Table V presents other interesting observations made at relatively short ranges. It was noted that high-order

A Provisional Ground Conductivity Map for Canada*

G. CLEMENT IRELAND†, MEMBER, IRE

Summary—The Department of Transport promulgated a new ground conductivity map for Canada as of January 1, 1961. The derivation of this map is discussed. Included is a brief account of propagation measurements at broadcast frequencies carried out by the Department in the Great Lakes region.

accurate picture of ground conductivity in Canada and to derive an up-to-date map. In this regard, the procedure used in deriving the current U. S. map was noted.¹

INTRODUCTION

CONDUCTIVITY VALUES FOR LAND AREAS

AS OF January 1, 1961, a new ground conductivity map for Canada was promulgated by the Department of Transport. This map replaces the one promulgated in 1948 as part of the Department's Broadcast Specification No. 14 and subsequently included in the North American Regional Broadcasting Agreement (NARBA) of 1950. Although derived from the best available data existing at the time, the old map had proved to contain many inaccuracies since it had been based on a few field measurements generalized for fairly large areas. With respect to the allocation of standard radio broadcasting stations, these inadequacies were responsible for extra administrative work since many notifications had to be cleared by individual field measurements.

One of the main concepts used in deriving the current U. S. ground conductivity map was to have an "effective" map giving values of conductivity which would "result in the over-all median field strength for the path or segment of path under consideration when used in conjunction with groundwave field strength versus distance curves." Considering the variables that are present when measuring conductivity over any given path, there appeared to be no point in having a map with conductivity classifications closer than 2 to 1. The following conductivity classes were therefore established for land areas: 0.5, 1, 2, 4, 8, 15 and 30 millimhos per meter. The range of conductivities for each class was determined by calculating the geometric mean with adjacent values in the scale.

Since 1948, additional ground conductivity data has been acquired by the Department in the radial path field measurements submitted in proofs of performance which, in Canada, are required for both directional and omnidirectional standard radio antenna systems. When submitting the radial measurements for these proofs, the Department's specifications require sufficient field intensity readings to determine not only the efficiency

After some consideration, it was decided to draw up a Canadian map using much the same concept. However, the field measurement data in the Department and the nature of the terrain in certain large areas of Canada where average values of 40 millimhos per meter can be expected, favored the adoption of a somewhat different conductivity scale. This scale, with the ranges of conductivity for each class, is given in Table I.

TABLE I

Conductivity Class (millimhos per meter)	Range of Conductivities
1	1.414
2	1.414-2.828
4	2.828-4.889
6	4.889-7.746
10	7.746-14.14
20	14.14-28.28
40	28.28-56.56

of the antenna, but the day-time and night-time protected contours as well. As a result many radials have been run for a considerable distance giving an indication of the conductivity in the immediate vicinity of the station and any trend to a change at the greater distances. Soon after joining the Department in 1957, the author began a study of this data to determine a more

Although some overlap of a 2 to 1 ratio occurs in the "4-6-10" portion of the scale, graph values for NARBA field intensity curves are used throughout. While the actual values of conductivity may vary over the indicated range in any one conductivity area, the theory would indicate that these values should average out to approximately the scale value for any given distance.

In order to arrange the available data in a form

* Received by the IRE, March 31, 1961; revised manuscript received, July 5, 1961.

† Radio Regulations Division, Department of Transport, Ottawa, Ontario, Canada.

¹ H. Fine, "An effective ground conductivity map for continental United States," Proc. IRE, vol. 42, pp. 1405-1408; September, 1954.

which could be interpreted, map overlays for various sections of the country were prepared. By means of a system of color coding in which specific conductivity values were assigned different colors, the radials from all outstanding proofs of performance in the Department were plotted. Any one color, or a group of colors, on the overlay which seemed to predominate in a particular area gave some indication of the measured conductivity in that area.

As may be expected, there were areas where field measurement data was sparse. In an attempt to find a basis for suitable values in these areas, the overlays were compared with different types of maps, *i.e.*, geological, forest classification, gravity anomaly, soils, topographical, etc., to see if any correlation could be determined. This approach left much to be desired and no definite findings could be established. Nevertheless, predicting values on soil data appeared to have some merit and this method was used in areas where little or no field measurement information was available.

To avoid too much "extrapolation" and to allow for additional data becoming available in the future, three types of conductivity designations are used. In a section of the country along the United States boundary, where almost all of the Canadian broadcasting stations are concentrated, the conductivity values have been predicted either solely on a basis of field measurement data or on a combination of field measurement data and soil data. Field intensity calculations based on these values should be of an accuracy sufficient to fulfill international treaty obligations and domestic regulations. In a second section the conductivity values have been predicated almost wholly on soil studies alone. The values shown in these areas have been encircled. While there appears to be some justification for the values assigned, they are to be regarded as an approximation only, and if used, must be confirmed. In a third section, which consists for the most part of the far northern areas, the values of conductivity are designated as being "unknown" since there appears to be no field measurement data or soil data upon which values can be predicated. If values for these areas are required, they will have to be determined.

CONDUCTIVITY VALUES FOR BODIES OF WATER

Although the generally accepted value of conductivity for fresh water is 10 millimhos per meter, few propagation measurements at broadcast frequencies have been made over any sizeable fresh water bodies. Since Canada contains many large fresh water lakes, a problem is presented in assigning them conductivity values. This problem is accentuated in the Great Lakes, where the Federal Communications Commission and the Department have used different conductivity values over the American and Canadian sectors respectively.

In view of the lack of data, it was decided in the Department to take propagation measurements over Lake Ontario to determine how close the accepted values

were to actual conditions. The National Research Council's motor vessel "Radel II" was made available for this purpose, position fixes being obtained by means of the ship's radar. Since the transmitter of Radio Station CFRB, Toronto, was ideally located at one end of the lake, it was used as the source of radiation, CFRB kindly agreeing to operate with an omnidirectional pattern for the duration of the measurements. With this arrangement, a radial was run the length of the lake.

The results of these measurements indicated the conductivity of Lake Ontario to be about 15 millimhos per meter, which was higher than any value previously used in allocations. It was concluded that contamination could be responsible for this high value since Lake Ontario was the lowest lake in the system. It was therefore arranged for the "Radel" to make quick conductivity checks on the remainder of the Great Lakes (excluding Lake Michigan), a mobile broadcast transmitter being used as the source of radiation. These results showed that the conductivity from lake to lake tended to vary in accordance with position in the system.

In an attempt to determine the validity of the contamination theory, water samples were taken from the four lakes concerned for analysis by the National Research Council. This analysis indicated that the lakes having the higher measured conductivities also had the higher amounts of contamination.

As a result of these tests, values have been assigned to the Canadian sectors of these lakes as follows:

Lake Ontario—	15 millimhos per meter
Lake Erie—	10 millimhos per meter
Lake Huron and Georgian Bay —	10 millimhos per meter
Lake Superior—	8 millimhos per meter

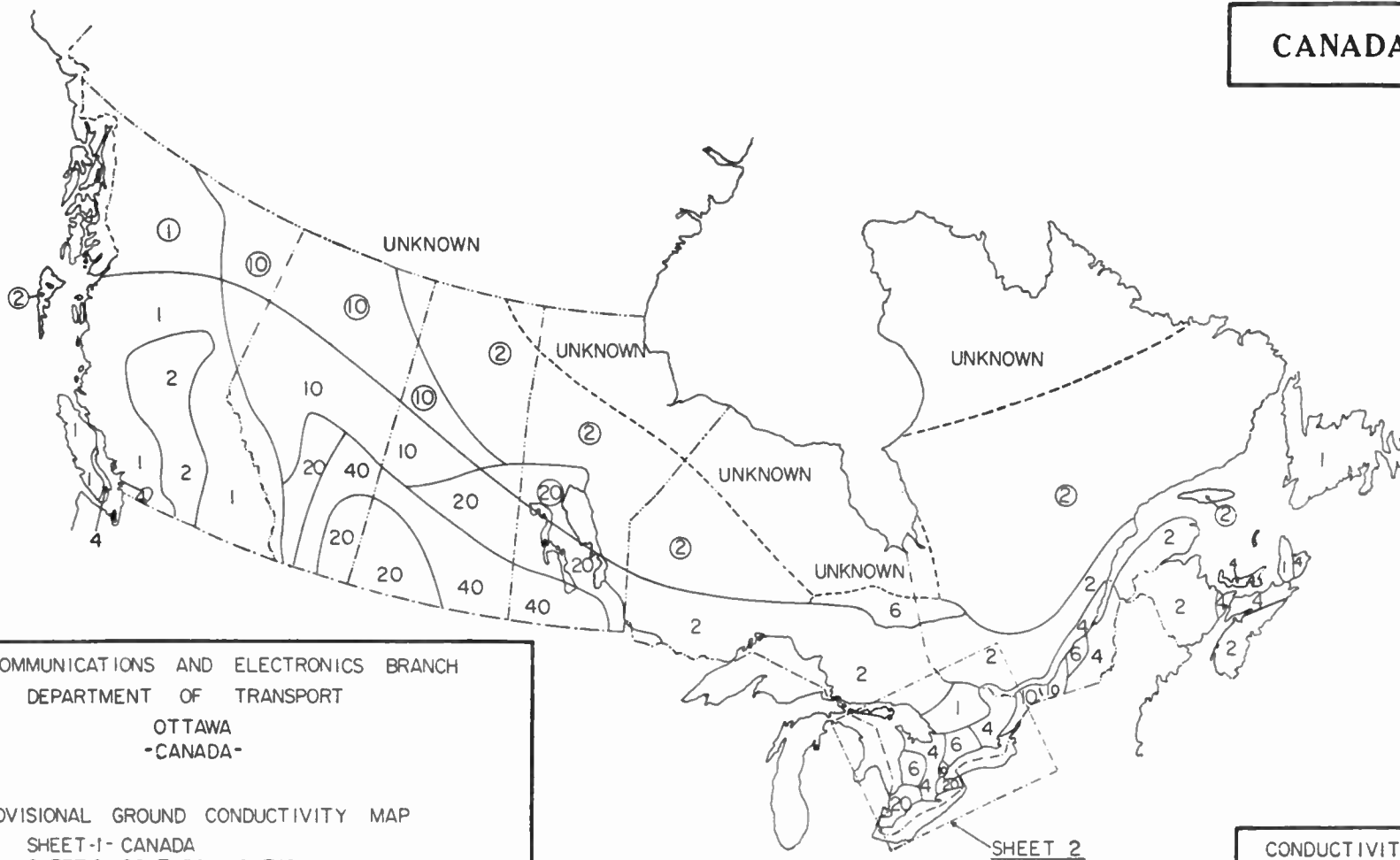
For other Canadian fresh water bodies, a value of 10 millimhos per meter is used. For sea water the value is 5000 millimhos per meter.

DISCUSSION

Determining conductivity over land areas by field measurement is subject to some approximation due to the effect of climate and terrain. Therefore, any conductivity map based on this type of information could give a general conductivity picture only. In addition, the density of field measurements will vary widely in different parts of the country resulting in a tendency for the map to vary in accuracy to the same extent. Even where the density of measurements is fairly high, *i.e.*, southwestern Ontario, it is often necessary to define conductivity areas somewhat arbitrarily. The main value of this type of map is as an acceptable standard upon which satisfactory allocations may be made.

Within the above-mentioned limitations, it is considered that the new Canadian map gives a good general outline of conductivity as it exists in the country. Too much approximation is avoided by having the three types of conductivity designations. The map as a whole has been accepted by the Canadian Association of Broadcast Consultants as being fairly indicative of

CANADA



TELECOMMUNICATIONS AND ELECTRONICS BRANCH
DEPARTMENT OF TRANSPORT
OTTAWA
-CANADA-

PROVISIONAL GROUND CONDUCTIVITY MAP
SHEET-1- CANADA
SHEET-2- SOUTHERN ONTARIO
IN THE APPLICABLE AREA, SHEET 2 WILL
TAKE PRECEDENCE.

WHERE CONDUCTIVITY VALUES ARE NOT
CIRCLED, INDICATED VALUES WILL APPLY.
WHERE CONDUCTIVITY VALUES ARE CIRCLED,
INDICATED VALUE IS BASED ON LIMITED
DATA ONLY AND SHOULD BE CONFIRMED
WHERE CONDUCTIVITY VALUE IS INDICATED
AS UNKNOWN, NO ACCURATE INFORMATION
IS AVAILABLE AT PRESENT

JUNE 1, 1960

CONDUCTIVITY OVER WATER	
SEA WATER	5000
FRESH WATER LAKES (EXCEPT GREAT LAKES)	10
<u>GREAT LAKES:</u>	
LAKE SUPERIOR	3
LAKE HURON AND GEORGIAN BAY	10
LAKE ERIE	10
LAKE ONTARIO	15

Fig. 1.

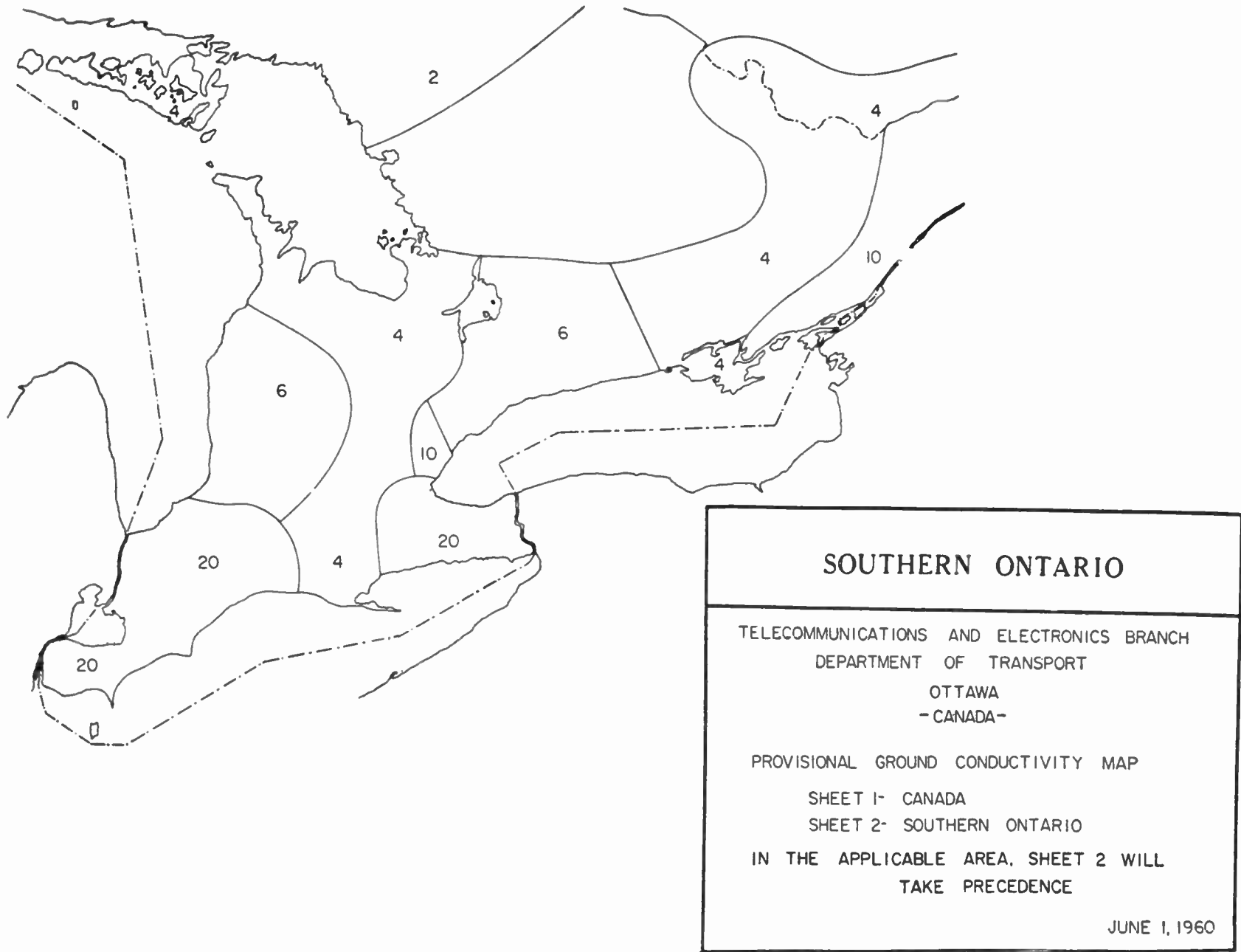


Fig. 2.

actual conditions. The unit, millimhos per meter, is used for values of conductivity throughout.

Since a body of water is practically homogeneous and there is very little scattering effect on a radio wave at broadcast frequencies, it seemed a reasonable assumption that conductivities over water could be measured more accurately than a 2 to 1 ratio. This was confirmed in the radials obtained on the lakes which followed the theoretical propagation curves very closely. Thus, the binary scale was abandoned for over-water propagation and the values as measured were assigned.

The new map is published in two sheets. The first sheet (Fig. 1) is on a scale of 1:6,336,000 and includes Canada as a whole. This scale was used because it appeared to be adequate and a base map was already available, thus facilitating immediate promulgation. However, a large portion of Canada's broadcasting stations are located in Southern Ontario and it had been past experience that a special need existed for agreed values in this area. Therefore, a second sheet (Fig. 2) showing Southern Ontario on a scale of 1:1,000,000 is also published. This sheet takes precedence over the first sheet in the applicable area. Specimens only of the two sheets are shown in Figs. 1 and 2.

It is admitted that use of this new Canadian map, in conjunction with the U. S. map, produces anomalous situations along the international boundary. This is a result of the two maps being drawn up by two different agencies evaluating information independently of one another. (It may be noted that other types of maps, *i.e.*, soil maps, contain similar anomalies.) While it may be argued that conductivity anomalies of this nature are impossible in a practical sense, satisfactory allocations

should result if the anomalies are treated simply as conductivity boundaries. It is anticipated that, eventually, negotiations between the F.C.C. and the Department of Transport will result in these anomalies being removed or minimized; this is why the present map is designated as "provisional." Until such time as these negotiations are completed and promulgated, the provisional designation will apply.

Due to the provisional status of the map, wide circulation will not be encouraged. However, agencies and individuals who have a need for copies may obtain them at \$5.00 per copy (one copy comprising both sheets) by writing the Controller of Radio Regulations, Department of Transport, Ottawa, Canada. Checks or money orders should be made payable to the Receiver General of Canada.

ACKNOWLEDGMENT

The author wishes to thank the following persons for their generous assistance and co-operation: W. B. Smith and J. T. Chrome of Radio Regulations Engineering Section, Department of Transport; Radio Station CFRB, Toronto; Clive Eastwood, Chief Engineer, CFRB; J. F. Edwards, Civil Defence Division, Department of National Health and Welfare, for arranging the loan of a mobile transmitter for the "over-water" measurements; Captain H. Ross Smyth, Navigational Aids Section, National Research Council, for arranging the use of Radel II for the over-water measurements; Dr. L. H. Doherty, National Research Council, for arranging the chemical analysis of the Great Lakes water samples, and for many helpful suggestions; Captain J. A. Hehir, Master of "Radel II," and his crew.

Correspondence

Tunnel-Diode Series Resistance*

The purposes of this note are 1) to describe a source of large error in the usual method of measuring the tunnel-diode series resistance, and 2) to indicate alternative measuring techniques.

The series resistance r_s of a tunnel diode is determined generally by measuring the incremental slope of the V - I characteristic at some large value of reverse current. The diode resistance actually measured r_m is the sum of r_s and the incremental resistance for the p - n junction r_d :

$$r_m = r_s + r_d. \quad (1)$$

Typical characteristics of r_m , r_d , and r_s as a function of reverse bias current I are shown in Fig. 1.

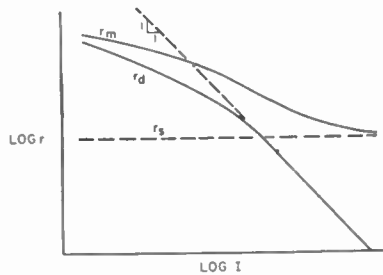


Fig. 1

GENERALLY USED TECHNIQUE FOR DETERMINING r_s

With increasing reverse current, the incremental resistance for the p - n junction r_d decreases (see Fig. 1). Therefore, for some large value of reverse current, the measured incremental resistance r_m is essentially equal to r_s . This is the basis of the usual technique for determining r_s . But frequently an insufficiently large value of measuring current is used, either because of unfamiliarity with what is involved or because an adequately large value of reverse current will cause excessive heating of the diodes. As is evident from Fig. 1, the measurement actually determines r_m , and this may be many times larger than r_s for the particular measuring current.

One common error is to define the value of measuring current in terms of the forward peak current I_p . However, it is our experience that the required measuring current cannot be related generally to I_p and that such an attempt only blankets the type of error described.

In many cases heating of a diode is a limitation of the test circuit and not of the diode. When reverse bias is established with a narrow current pulse of low duty cycle, excessive heating usually can be avoided by simply reducing the width of the current pulse. If heating occurs and the width of the pulse cannot be conveniently reduced, then

r_s may not be accurately determined by the generally used technique.

TECHNIQUES FOR DETERMINING r_s WITH REDUCED CURRENTS

For values of reverse current smaller than required in the above technique, r_s may be accurately determined only by correcting for r_d .

Except for small currents, conduction in the reverse-bias region is by Zener emission, for which Chynoweth, *et al.*,¹⁻³ have suggested the following equation. Neglecting series resistance,

$$I = AV^p(V_i + V)^{q/2} \exp[-B/(V_i + V)^{1/2}], \quad (2)$$

where I is the measured current, V is the voltage applied to the p - n junction, being positive for reverse bias, V_i is the built-in voltage (internal-contact potential), and A , B , p , and q are constants (p is usually about unity).

From the derivative of (2) we may solve for $r_d (=dV/dI)$, the incremental resistance of the V - I characteristic for the p - n junction:

$$r_d = \frac{1}{I \left[\frac{p}{V} + \frac{B + q(V_i + V)^{1/2}}{2(V_i + V)^{3/2}} \right]}. \quad (3)$$

Two-Measurement Technique

With increasing reverse current, the voltage V applied to the p - n junction approaches a constant value. From (3) we see that, with V essentially constant, r_d is inversely proportional to current. The measured incremental resistance is then given by

$$r_m = r_s + \frac{k}{I}, \quad (4)$$

where k is a dimensional constant. Since in (4) there are two unknowns (r_s and k), r_s may be determined with measurements of r_m at two currents for which this equation holds.

Multiple-Measurement Technique

Alternatively, for a range of relatively small currents, the quantity $(V_i + V)$ is essentially constant, so that the value of the second term within the brackets of (3) may be considered constant. For this range of current the measured incremental resistance is given by

$$r_m = r_s + \frac{1}{I \left(\frac{p}{V} + N \right)}, \quad (5)$$

¹ A. G. Chynoweth, *et al.*, "Internal field emission at narrow silicon and germanium P-N junctions," *Phys. Rev.*, vol. 118, pp. 425-434; April 15, 1960.

² A. G. Chynoweth and R. A. Logan, "Internal field emission at narrow P-N junctions in indium antimonide," *Phys. Rev.*, vol. 118, pp. 1470-1473; June 15, 1960.

³ A. G. Chynoweth, "Physics of Esaki Diodes," Special Summer Session on New Devices for Amplification and Switching, The Moore School of Elec. Engrg., University of Pennsylvania, Philadelphia; 1960.

where N is a constant. Since in (5) there are three unknowns (r_s , p , and N), r_s may be determined with measurements of the incremental resistance r_m and the total voltage applied to the device $V_M (=V+r_s I)$ at three values of current. Calculation is especially easy if $p=1$, which fortunately is a reasonably valid assumption for most diodes.

MEASUREMENTS

The series resistance of several experimental GaAs tunnel diodes was measured by the three techniques described with good agreement between results of each measurement for most diodes. In some cases results for a diode with the multiple-measurement technique differed from results with the other techniques by more than 10 per cent. This was possibly due to incorrectly assuming $p=1$ to simplify the calculations.

While the latter two techniques require additional and more accurate measurements, this in many cases more than offsets the requirement of a large measuring current for the single-measurement technique.

E. L. BONIN

J. R. BIARD

Research and Engineering Dept.
Components Division
Texas Instruments, Inc.
Dallas, Tex.

Some Measurements on an Iris Beam Waveguide*

The resonance in a parallel plate resonator which has first been investigated by King, Scheibe, and Tatsuguchi,¹ led to the conclusion that an array of uniformly spaced identical irises should guide a wave beam with relatively little diffraction loss, provided the apertures of the irises are sufficiently large compared to the wavelength. Assuming circular irises and uniformly directed field, one can formulate the condition for a beam whose field repeats from iris to iris by the following integral equation:

$$f(x) = q \int_0^a f(\xi) J_0(x\xi) e^{-j/2(x^2+\xi^2)} \xi d\xi \quad (1)$$

with

$$x = \sqrt{k/D} \rho, \quad \xi = \sqrt{k/D} \eta,$$

$$a = \sqrt{k/D} R, \quad k = \frac{2\pi}{\lambda}$$

* Received by the IRE, July 26, 1961; revised manuscript received, August 22, 1961.

¹ For references to the literature see E. Scheibe, "Measurements of resonators formed from circular plane and confocal paraboloidal mirrors," *Proc. IRE (Correspondence)*, vol. 49, p. 1079; June, 1961.

* Received by the IRE, August 28, 1961.

where J_0 is the Bessel function of zero order, R the aperture radius of the irises, and D their spacing. ρ, η are radial coordinates at two adjacent irises. The eigenfunctions describe the radial distribution of the field and the eigenvalues q the amplitude ratio between the fields at two successive irises.

Early measurements by the authors with irises of 20 cm aperture and various spacings at a frequency of 25 Gc indicated that a large number of irises is necessary to obtain a repetitive field. However, when a phase transformation was introduced at each iris which removed the phase term $e^{-j/2(\alpha^2 + \xi^2)}$ in the integral equation, only a few passages were necessary to obtain a substantially repetitive field. Furthermore, the loss was much smaller for the same size of aperture and iris spacing. The results were in good agreement with the then available solution of (1) with compensated phase term.²

Recently, Fox and Li³ have evaluated (1) with the inclusion of the phase term. If the derivation of the equation is based upon Huygens' principle, one makes the assumption that $(R^4/\lambda D^3) \ll 1$. The equation can also

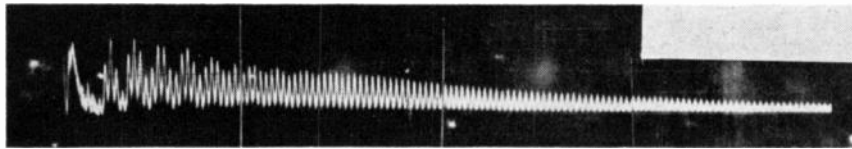


Fig. 2—Multiply-reflected pulse train from experimental setup.

be derived by expressing the field in terms of a bundle of plane waves whose directions of propagation are limited to small angles θ against the beam axis.⁴ In this case, the limitation $D/\lambda(\theta/2) \ll 1$ applies. Therefore, one should expect that the restriction $R^4/\lambda D^3 \ll 1$ is not necessary for the validity of (1) if the reiterative beam comprises only small propagation angles.

In order to verify this, pulse measurements have been performed with a setup consisting of two plane aluminum reflector plates approximately 56 cm square and facing each other at a distance S . Various numbers of identical plywood frames, with square apertures of the size of the reflectors were aligned equally spaced between the reflectors as indicated in Fig. 1. The reflectors were provided with a small coupling hole in the center for injecting and receiving the multiply-reflected pulse. Measurements were first made at a frequency of 35 Gc with a reflector spacing of 2.2 m. Since the travel time of the pulses was much shorter than the pulse duration, the pulses overlapped. The attenuation of the fundamental beam mode was determined from the rate of decay of the oscilloscope display. The results, plotted in Fig. 1 as squares, show the diffraction loss caused by one frame

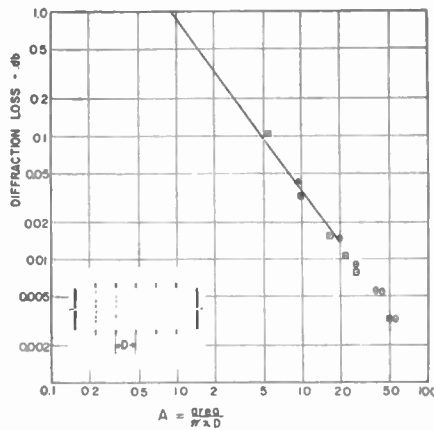


Fig. 1—Measured diffraction loss per iris in an iris beam waveguide:

□ = measured at 35 Gc.
 ○ = measured at 70 Gc.
 △ = measured by Scheibe, King, and Tatsuguchi¹ from measurements on a parallel plate resonator with circular reflector plates.
 Curve = theoretical curve by Fox and Li³ for a parallel plate resonator of circular reflector plates.

as a function of a quantity A which is defined as aperture area divided by $\pi\lambda D$.

A second set of measurements was made at 70 Gc. The spacing S was increased to about 10 m so that the multiply-reflected pulses were separated in time. A typical pulse trail observed with this setup is shown in the photograph (Fig. 2). Each pulse represents a round trip down the line and back. Since there were 16 frames equally spaced between the reflectors the number of iterations between two successive pulses was 34. Almost 2500 iterations were required before all the higher beam modes were damped out and the exponential decrease of the pulse train was established. The results are indicated in Fig. 1 as circles. The triangular point in the plot is the value obtained by Scheibe, *et al.*,¹ from resonance measurements on a parallel plate resonator with circular reflector plates. The curve shown in the figure has been calculated by Fox and Li³ for the parallel plate resonator but with circular reflector plates.

Although our measurements have been made with irises of square aperture, while the calculated curve by Fox and Li applies to circular reflectors, it can be concluded from the results that the condition $R^4/\lambda D^3 \ll 1$ is not required for the validity of (1), at least so far as the lowest mode is concerned. The values of $R^4/\lambda D^3$ in the measurements range from 0.07 to 11.

J. R. CHRISTIAN
 G. GOUBAU
 Institute for Exploratory Research
 U. S. Army Signal Research
 and Development Labs.
 Fort Monmouth, N. J.

Ionospheric Contributions to the Doppler Shift at VHF from Near-Earth Satellites*

The ionospheric contributions to the Doppler shift at VHF arising from satellites sensibly above the ionosphere have been considered to $O(1/f_s^3)$, where f_s is the satellite transmitter frequency, and the vacuum Doppler shift is considered of $O(f_s)$. To this order, the phase (whose time derivative is the Doppler shift) cannot be approximated by the usual Fermat integral of geometrical optics. Through a consideration of the characteristics of an ideal Doppler tracking receiver, boundary conditions can be imposed upon the solution of the wave equation containing an arbitrary ionosphere electron contribution to the refractive index (including the earth's magnetic field) such that the solution is valid to $O(1/f_s^2)$ in the phase. The resulting nonrelativistic refracted Doppler shift corresponding to circularly polarized radiation is

$$\Delta f(t) = -\frac{f_s}{c} \frac{d}{dt_0} \phi(f_s, t_0) + O\left(\frac{v^2}{c^2}\right),$$

$$\phi(f_s, t_0) = \int_0^{\omega_s^*(t_0)} d\vec{r}' \cdot \hat{s}(\vec{r}') \cdot N(\vec{r}', t_0 | f_s) + O\left(\frac{1}{f_s^3}\right),$$

$$t_0 = t - \frac{\partial}{\partial f_s} \left[\frac{f_s}{c} \phi(f_s, t) \right] + O\left(\frac{v^2}{c^2}\right),$$

where

$\vec{r}_s(t_0)$ = satellite position vector at the time t_0 in a coordinate system where the receiving station is at the origin,
 $\hat{s}(\vec{r}')$ = unit vector tangent to the path at \vec{r}' which makes $\phi(f_s, t_0)$ an extremum,
 $\hat{R} = \frac{\vec{r}_s(t_0)}{|\vec{r}_s(t_0)|}$,
 $\hat{\xi}(R)$ = normal to $\vec{r}_s(t_0)$ and is the vector difference between the extremum path and the geometric path, $\hat{\xi}(0) = \hat{\xi}(R) = 0$,
 $\vec{r}' = R\hat{R} + \hat{\xi}(R), 0 \leq R \leq |\vec{r}_s(t_0)|$ = vector from origin to extremum path,
 $N(\vec{r}', t_0 | f_s) = n(\vec{r}', t_0 | f_s) + \frac{2\pi^2 c^2}{f_s^2} \frac{\hat{R} \cdot \nabla n + \hat{\xi} \cdot \frac{d\hat{\xi}(R)}{dR}}{R} + O\left(\frac{1}{f_s^3}\right)$,
 $n(\vec{r}', t_0 | f_s)$ = ionospheric refractive index appropriate to the circularly polarized component received.¹

* Received by the IRE, September 8, 1961. This work was supported by the U. S. Dept. of the Navy, Bureau of Naval Weapons, under Contract NORD 7386.

¹ J. A. Stratton, "Electromagnetic Theory," McGraw-Hill Book Co., Inc., New York, N. Y., pp. 327 ff.; 1941.

² J. R. Christian and G. Goubau, "Experimental studies on a beam waveguide for millimeter waves," IRE TRANS. ON ANTENNAS AND PROPAGATION, vol. AP-9, pp. 256-263; May, 1961.

³ A. G. Fox and T. Li, "Resonant modes in an optical maser," PROC. IRE, vol. 48, pp. 1904-1905; November, 1960.

⁴ G. Goubau and F. Schwering, "On the guided propagation of electromagnetic wave beams," IRE TRANS. ON ANTENNAS AND PROPAGATION, vol. AP-9, pp. 248-263; May, 1961.

The above equations express the fact that to $0(1/f_s^2)$, the phase is given by a modified Fermat principle in which the index of refraction n is replaced by the function N given above. Since ∇n and the deviation of the extremum path from the geometric path ξ are of $0(1/f_s^2)$, the difference between n and N is of $0(1/f_s^4)$.

After expanding the index of refraction in a power series in $1/f_s$, the above equations for the refracted Doppler shift were used to estimate upper bounds on the various contributions. First, it was found that, while the contribution of the difference $N-n$ is of $0(1/f_s^2)$, its magnitude was sufficiently small to be negligible in all cases of interest in the VHF region. Consequently Fermat's principle and the consequent optical approximation are valid to $0(1/f_s^2)$ at VHF. Second, numerical upper bounds were established for the various orders in $1/f_s$ using the above equations. The results are summarized in Table I. During periods where the ionosphere is not seriously disturbed, the magnitude of the various refraction terms are most likely a factor of 3-10 lower. It can be seen that for frequencies above about 100 mc the use of two frequency Doppler data to eliminate refraction effects is adequate.²

TABLE I
MAXIMUM IONOSPHERIC CONTRIBUTIONS TO
THE SATELLITE DOPPLER SHIFT
(ENTRIES ARE IN CPS)

f_s (Mc)	Vacuum Doppler	$0(1/f_s)$	$0(1/f_s^2)$	$0(1/f_s^3)$
50	1200	20	0.6	2
100	2500	10	0.2	0.3
150	3700	6.7	0.07	0.04
200	5000	5	0.04	0.03
300	7500	3.3	0.02	0.01
400	10000	2.5	0.01	—
500	12500	2	—	—

A detailed report is being submitted for publication.

WILLIAM H. GUIER
Applied Physics Lab.
The Johns Hopkins University
Silver Spring, Md.

² W. H. Guier and G. C. Weiffenbach, "A satellite Doppler navigation system," Proc. IRE, vol. 48, pp. 507-516; April, 1960.

WWV and WWVH Standard Frequency and Time Transmissions*

The frequencies of the National Bureau of Standards radio stations WWV and WWVH are kept in agreement with respect to each other and have been maintained as constant as possible with respect to an

improved United States Frequency Standard (USFS) since December 1, 1957.

The nominal broadcast frequencies should for the purpose of highly accurate scientific measurements, or of establishing high uniformity among frequencies, or for removing unavoidable variations in the broadcast frequencies, be corrected to the value of USFS, as indicated in the table below. The corrections reported have been arrived at by means of improved measurement methods based on LF and VLF transmissions.

The characteristics of the USFS, and its relation to time scales such as ET and UT2, have been described in a previous issue,¹ to which the reader is referred for a complete discussion.

The WWV and WWVH time signals are also kept in agreement with each other. Also they are locked to the nominal frequency of the transmissions and consequently may depart continuously from UT2. Corrections are determined and published by the U. S. Naval Observatory. The broadcast signals are maintained in close agreement with UT2 by properly offsetting the broadcast frequency from the USFS at the beginning of each year when necessary. This new system was commenced on January 1, 1960. A retardation time adjustment of 20 msec was made on December 16, 1959; another retardation adjustment of 5 msec was made at 0000 UT on January 1, 1961; and a time advancement of 50 msec was made at 0000 UT on August 1, 1961.

WWV FREQUENCY
WITH RESPECT TO U. S. FREQUENCY STANDARD

August, 1961	Parts in 10^{10} †
1	-150.6
2	-150.3
3	-150.1
4	-150.0
5	-150.1
6	-149.6
7‡	-149.6
8	-150.9
9	-151.0
10	-151.5
11	-151.4
12	-151.5
13	-151.5
14	-151.5
15	-151.4
16	-151.3
17	-151.2
18	-151.2
19	-151.1
20	-150.9
21	-150.8
22	-150.7
23	-150.9
24	-149.5
25§	-149.8
26	-151.2
27	-151.4
28	-151.7
29	-151.9
30	-152.2
31	-152.1

† A minus sign indicates that the broadcast frequency was low. The uncertainty associated with these values is $\pm 5 \times 10^{-11}$.

‡ The frequency was adjusted -1.3×10^{-10} on August 7.

|| The frequency changed $+1.7 \times 10^{-10}$ on August 23.

§ The frequency was adjusted -0.9×10^{-10} on August 25.

NATIONAL BUREAU OF STANDARDS
Boulder, Colo.

¹ Refer to "National Standards of Time and Frequency in the United States," Proc. IRE (Correspondence), vol. 48, pp. 105-106; January, 1960.

Persistent-Current Memory Circuit*

Crittenden, *et al.*, state (page 1244)¹ that lead films have "large critical currents at working temperatures (2° to 5°K), and large heat evolution occurs in the normal state. This leads to long recovery times determined by thermal relaxation and tends to make lead unsuitable for Persistor switch elements." Experiments with persistatron² circuits made entirely from evaporated lead and operating at 4.2°K have demonstrated that this opinion is pessimistic. We have observed complete switching (denoting total reversal of the magnetic flux linking a superconducting circuit) in less than 10 nsec, several times faster than in the tin and indium persistor circuits. Fig. 1 shows a lead persistatron on a 1-inch \times 0.4-inch glass substrate.

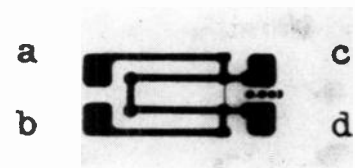


Fig. 1—Thin-film persistatron made of lead evaporated onto a glass substrate. Terminals *ab* are for current input; *cd* are for voltage sense. The self-inductance of the loop is $0.02 \mu\text{h}$.

Our results are quite reasonable in light of a circuit analysis that includes the conservation of flux in a multiply-connected superconductor.³ The persistor (or persistatron, the same circuit by a different name) is considered to be a superconducting loop, rather than a nonlinear resistor and inductor driven in parallel. The flux linking the loop may change only when some portion of the loop becomes normally conducting. This analysis does not restrict the switch element to a smaller self inductance than the remaining part of the loop.

If one assumes that there is negligible electric field within the superconducting portion of the loop—the usual low-frequency approximation to one of London's equations—then the output voltage developed across the switch element is comprised of two parts:

- 1) $L(dI/dt)$ voltage from the inductance seen across the current input terminals, even though the net flux linking the loop remains constant.
- 2) $d\phi/dt$ voltage arising from a change in the net flux linking the loop and appearing as an IR drop across the switch element, even though input current is constant.

* Received by the IRE, August 28, 1961. This work was performed under AEC Contract No. AT-(40-1)-2430.

¹ E. C. Crittenden, Jr., J. N. Cooper and F. W. Schmidlin, "The 'persistor'—a superconducting memory element," Proc. IRE, vol. 48, pp. 1233-1246; July, 1960.

² M. J. Buckingham, "The persistatron—a superconducting element for computers," Proc. 5th International Conf. on Low Temperature Physics and Chemistry, Madison, Wis., August, 26-30, 1957; University of Wisconsin Press, Madison, 1958.

³ F. London, "Superfluids," John Wiley and Sons, Inc., New York, N. Y.; 1950.

* Received by the IRE, September 25, 1961.

As Crittenden, *et al.*, pointed out, it is the $d\phi/dt$ portion of the output signal that is significant in determining the sense of the stored flux. Fig. 2 shows the superposition of switching and nonswitching output waveforms from a persistatron.

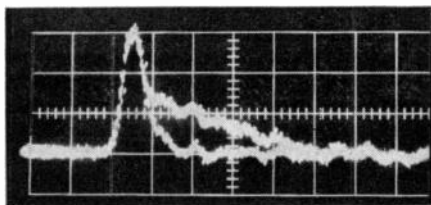


Fig. 2—Two superimposed output waveforms from a persistatron showing LdI/dt nonswitching signal (lower trace), and the switching signal plus LdI/dt (upper trace). The large deflection on the left corresponds in time to the leading edge of the 250-ma input current pulse. Vertical scale is 0.5 v per large division; horizontal scale is 2 nsec per large division.

The amount of energy dissipated as heat during switching depends *only* upon the quantity of flux that is changed, and not upon the resistance of the switch element. The switching speed (for a given circuit configuration and stored flux level) will be faster for a switch element that develops high resistance in a short time—a characteristic of thin lead films—with a correspondingly larger output signal. The relatively large critical current of a lead film provides higher stored flux levels and also yields an increase in output signal level.

Our analysis shows further that it is *not* necessary to terminate the input current pulse immediately after switching occurs in order to establish a persistent current. A lead persistatron has stored the same quantity of flux with current pulses of 10-nsec duration and of 1- μ sec duration. The necessity for terminating input pulses just after switching, as reported by Crittenden, *et al.* (page 1234), suggests that thermal relaxation may be a more serious problem in tin and indium switch elements operated only slightly below critical temperature.

W. C. STEWART
H. A. OWEN
M. S. P. LUCAS
C. R. VAIL

Superconducting Circuits Laboratory
Electrical Engineering Department
Duke University
Durham, N. C.

A C-Band Parametric Amplifier with Large Bandwidth*

A bandwidth of 700 Mc has been obtained from a nondegenerate parametric amplifier built to operate at C band. This amplifier, utilizing a single silicon-varactor

diode, has a measured gain of 13 db and a noise figure of 2.4 db. Band-pass response of the amplifier is shown in Fig. 1; other operating conditions obtained are pictured in Figs. 2-4.

To enhance bandwidth, multituning techniques¹ similar to those used with good success on degenerate parametric amplifiers²⁻⁵ were employed. The approximate equivalent circuit for the signal and idler frequencies is depicted in Fig. 5. The elements used to double-tune the circuit (represented by C_1 and L_1), while not physically located at the diode terminals, do present, to the first approximation, the same impedance function to the terminals. The manner

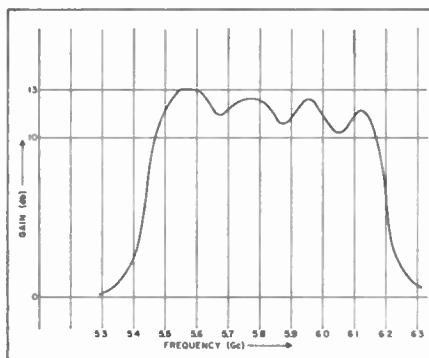


Fig. 1.

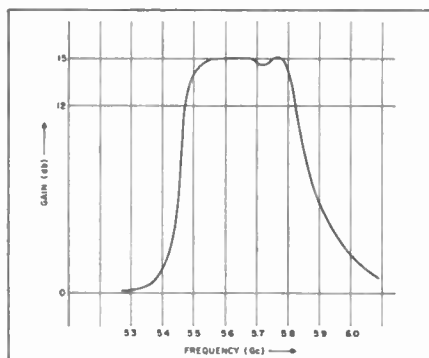


Fig. 2.

amplifier was a broad-band 3-port circulator with isolation of 25 db and insertion loss of 0.3 db maximum.

Both the unusually large bandwidth and the good noise-figure performance of the amplifier are attributed in part to large C_1/C_0 values, presumably explained by the phenomenon of multiplication of stored carriers.⁶ The sensitivity of amplifier gain to pump-power variations is dependent upon circuit adjustments and the value of C_1/C_0 realized. Under most adjustments this amplifier appeared more sensitive to changes in pump power than amplifiers incorporating GaAs diodes. This is believed due to circuit detuning, which is caused by the average

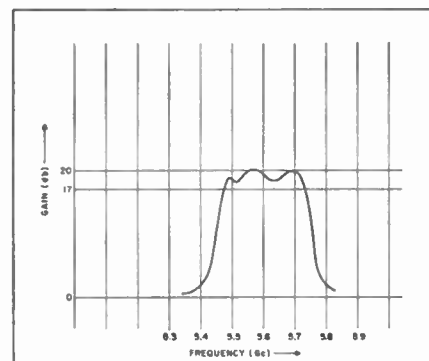


Fig. 3.

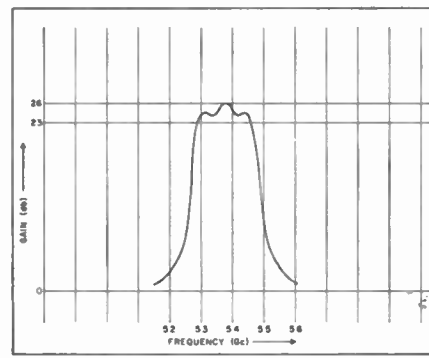


Fig. 4.

in which the idler susceptance is made to transform into the signal circuit is believed to account for the quadruply tuned response indicated in some of the band-pass sketches. The L_2, C_2 combination was resonant at approximately 8 Gc; this was also the approximate self-resonant frequency of the diode (which had a junction capacitance of 0.63 pf). The pump frequency was approximately 16.6 Gc. The circulator used with the

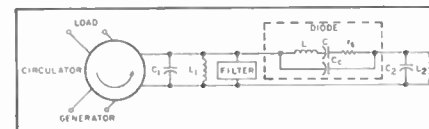


Fig. 5.

capacitance of the silicon varactor being a stronger function of pump power at high C_1/C_0 values than the GaAs varactor.

The author wishes to thank K. M. Johnson for his many helpful comments and suggestions.

B. T. VINCENT, JR.
Apparatus Div.
Texas Instruments, Inc.
Dallas, Tex.

* Received by the IRE, August 21, 1961. Research sponsored by Bureau of Naval Weapons, Contract No. N0w 61-0283-d.

¹ H. Seidel and G. F. Herman, "Circuit aspects of parametric amplifiers," 1959 IRE WESCON CONVENTION RECORD, pt. 2, pp. 83-90.

² A. G. Little, "A wide-band single-diode parametric amplifier using filter techniques," PROC. IRE, vol. 49, pp. 821-822; April, 1961.

³ Advertisement, Airborne Instrument Lab., "C-band degenerate parametric amplifier," PROC. IRE, vol. 49, p. 4A; February, 1961.

⁴ M. Gildden and G. L. Matthaeci, "A nearly optimum wide-band degenerate parametric amplifier," PROC. IRE, vol. 49, pp. 833-834; April, 1961.

⁵ B. T. Vincent, "A high-performance X-band parametric amplifier," PROC. IRE, vol. 49, pp. 511-512; February, 1961.

⁶ K. Siegel, "Comparative figures of merit for available varactor diodes," PROC. IRE, vol. 49, pp. 809-810; April, 1961.

Multiple Reflections of Microwaves Propagating Through a Semiconductor Medium*

In considering the transmission of microwave energy through a semiconductor medium such as high-resistivity germanium or silicon, an analysis has been made of the role of absorption and multiple internal reflections in the medium. In this problem the microwave radiation is assumed to be propagated through three media: air, a semiconductor slab, and air. The physical arrangement is suggested in Fig. 1.

As a result of this study, a new family of devices, useful as modulators, has been suggested. In this case, excess carriers are injected by forward-biased contacts made to the semiconductor. Carrier densities could alternatively be increased by incident light.

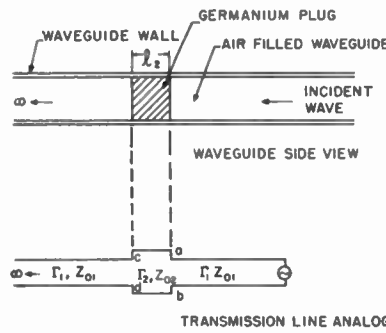


Fig. 1—Equivalent circuit for microwave propagation in three media. The regions indicated by the propagation constant and impedance Γ_1 and Z_{01} represent the waveguide in air. The terms Γ_2 and Z_{02} represent the waveguide completely filled with a semiconductor plate, l_2 being the thickness of this plate.

TABLE I
NORMALIZED CONSTANTS FOR PROPAGATION OF MICROWAVES THROUGH SEMICONDUCTORS*

Experimental Conditions	A Wavelength in the Medium in Millimeters	B Thickness of Sample for Maximum Change in Attenuation by Transmission per a Unit Change in Conductivity	C Transmission Mode, Thickness for No Phase Shift as Conductivity is Changed	D Reflection Mode, Thickness for No Change in Reflection Amplitude as Conductivity and Reflection-Coefficient Phase is Varied	E Reflection Mode, Thickness for No Change in Reflection Coefficient Phase as Conductivity and Reflection Amplitude is Varied
I. Air, Germanium Slab, Air Unbounded $f = 10^{10}$ $(l_2/\lambda) \rightarrow$	7.5	0.5, 1.0, 1.5	0.28, 0.51, 0.64	0.45, 0.64, 1.15	0.32, 0.51, 0.82, 1.0
II. Air, Germanium Slab, Air all in X-Band Waveguide $f = 10^{10}$ $(l_2/\lambda) \rightarrow$	7.6	0.5, 1.0, 1.5	0.31, 0.49, 0.76		
III. Air, Silicon Slab, Air Unbounded $f = 10^{10}$ $(l_2/\lambda) \rightarrow$	8.6	0.5, 1.0, 1.5	0.31, 0.51, 0.77	0.39, 0.65	0.27, 0.50, 0.76
IV. Air, Silicon Slab, Air all in X-Band Waveguide $f = 9.549 \times 10^9$ $(l_2/\lambda) \rightarrow$	9.2	0.5, 1.0, 1.5	0.31, 0.50, 0.77, 1.0		
V. Air, Germanium Slab, Air Unbounded $f = 2.4 \times 10^{10}$ $(l_2/\lambda) \rightarrow$	3.1	0.5, 1.0, 1.5	0.32, 0.50, 0.77		
VI. Best Estimate		0.5, 1.0, 1.5	0.31, 0.50, 0.77, 1.0	0.39, 0.65, 1.15	0.29, 0.50, 0.79, 1.0

* All thickness constants are in terms of l_2/λ . The term l_2 refers to the thickness of the semiconductor plate. For free-space propagation, λ is the wavelength in a large lossless semiconductor plate. In the case of the waveguide filled with the semiconductor, λ is the guide wavelength in the material. The constants are more precise as the conductivity σ becomes smaller.

In changing the conductivity of the semiconductor, the transmission, reflection and absorption of carrier-frequency energy can be significantly changed. Modulation experiments have been previously described as well as detailed computer calculations for waveguide and free-space conditions¹ at carrier frequencies of 10,000 Mc.

The results of further calculations at various frequencies have now been tabulated in normalized form and it appears that there may be several dimensionless constants, which having been determined, will allow a simplified design procedure for devices such as described above.

* Received by the IRE, February 8, 1961; revised manuscript received, July 10, 1961.

¹ H. Jacobs, F. A. Brand, J. D. Meindl, M. Benanti and R. Benjamin, "Some device aspects of multiple microwave reflections in semiconductors," 1960 IRE WESCON CONVENTION RECORD, pt. 3, pp. 42-48.

H. Jacobs, F. A. Brand, J. D. Meindl, M. Benanti and R. Benjamin, "Electrodeless measurement of semiconductor resistivity at microwave frequencies," PROC. IRE, vol. 49, pp. 928-932; May, 1961.

For slightly lossy material ($\sigma \ll \omega\epsilon$) it is well known that at one-half wavelength in thickness maximum transmission is attained. In this case, we refer to the wavelength in the nonlossy medium. In germanium, where $\epsilon_R = 16$, the wavelength in the semiconductor medium is one-fourth the wavelength in air. In a waveguide, the wavelength is further modified and given by

$$\lambda_p = \frac{\lambda_1}{\sqrt{1 - \left(\frac{\lambda_1}{\lambda_0}\right)^2}}, \quad (1)$$

where λ_p is the wavelength in the medium in the waveguide, λ_1 is the wavelength in the infinite, lossless dielectric and λ_0 is the cut-off wavelength for the waveguide.

What has not been established to date is the role of multiple internal reflections on the phase shift of the transmitted or reflected waves. From the calculated data, if one considers the ratio of the thickness of the semiconductor (medium 2) to the guide wave-

length in the lossless medium l_2/λ , constant values exist for which there is no change in the phase of the transmission coefficient E_o/E_{in} . The constant ratios are still maintained even if waveguides are not present, as in the case of air, large area semiconductor plate, and air, if one considers λ as the wavelength in the infinite lossless dielectric medium. This would be useful in the design of devices which provide amplitude modulation with little or no change in phase shift. With respect to the reflection coefficient E_R/E_{in} , other nearly constant values of l_2/λ exist where amplitude modulation can occur with no phase shift. In Table I we see the results of calculations which support the thesis that there are specific critical values of the ratio of thickness of the semiconductor to the wavelength in the lossless medium, where nodes occur such that the phase shift of the reflected wave does not vary even as

the conductivity of the semiconductor is varied, and the amplitude of the reflected wave is caused to change. Similarly, at other critical thicknesses, the amplitude of the reflected wave is constant as the conductivity of the material and phase of the reflected wave is changed.

The values have been determined for germanium and silicon in free space and in a waveguide at various frequencies. It is hopefully expected that the constants will hold for all semiconductors in a similar physical arrangement. The range of frequencies for which this effect occurs would be determined as follows. The lower frequency limit would exist at the condition $\sigma \ll \omega\epsilon$. That is, the conductivity must be less than the product of the angular frequency and the permittivity of the dielectric in medium 2. The upper-frequency limit for which the table of constants may be applied depends upon ϵ remaining constant and $\omega\tau \ll 1$, as was assumed in the calculations. Experimental evidence at room temperature indicates that,

for high-resistivity germanium and silicon, this assumption is generally valid throughout the microwave region² with rare exceptions.³

Acknowledgments should be made to Dr. Leonard Hatkin and Dr. G. Goubau for theoretical discussions, to Mrs. M. Tate in the application of the computer and calculation of numerical values, and to Charles LoCascio for his part in the experimental work involved in checking parts of the theoretical predictions at the frequency of 10,000 Mc with high-resistivity germanium plates of various thickness.

H. JACOBS

F. A. BRAND

J. D. MEINDL

U. S. Army Signal Res. and Dev. Lab.

Fort Monmouth, N. J.

R. BENJAMIN

Monmouth College

West Long Branch, N. J.

² A. F. Gibson, "Infrared and microwave modulation using free carriers in semiconductors," *J. Sci. Instr.*, vol. 35, p. 274; August, 1958.

³ A. C. Baynham, A. F. Gibson and J. W. Granville, "On the dielectric constant of germanium at microwave frequencies," *Proc. Phys. Soc.*, vol. 75, pt. 2, pp. 309-311; February, 1960.

Correlation Optical Radar*

Recently, considerable attention has been given to ranging systems which employ optical masers as pulsed oscillators.¹ To date, the devices have used a fluorescent line in ruby of wavelength 6943 Å (in the visible red) which corresponds to a frequency of about 4.3×10^{14} cps. The standard practice has been to pulse the maser in such fashion that the output is a narrow beam which, as measured, radiates one or a few joules of the desired frequency in a period, typically of order 10^{-4} to 10^{-3} seconds. This energy at the red wavelength corresponds to 10^{19} photons. Of course, a millisecond pulse radar is of rather restricted use but could be considered quasi-CW for many tactical situations. In ruby the light output during this rather long quasi-CW pulse actually consists of many random spikes of about 10^{-7} to 10^{-6} seconds duration. This randomness of the spikes evidences the difficulty in designing a coherent radar, since the spike-to-spike uncertainty allows no single value of phase to be remembered for coherent detection unless it is decided to use one or a few individual spikes. Under these circumstances, the only efficient way to achieve coherent data processing is to delay a portion of the transmitted wave and beat it with the echo before integrating; in short, it is desirable to build a correlation optical radar.

In a correlation optical radar the mixing may occur at photosensitive surfaces illuminated by the diffraction pattern from

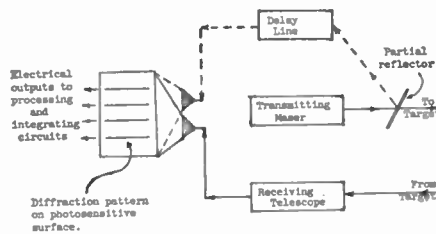


Fig. 1.

two slits. One slit projects a delayed portion of the emitted light, and the other projects light reflected from targets (Fig. 1). The photosensitive surface will be made up of a mosaic of several segments per fringe. It is easily seen that a change in target range of $\lambda/2$ will reverse positions of light and dark fringes. Thus, two segments per light fringe will detect target motion, and four segments per light fringe will provide information as to increase or decrease in range. It should be pointed out that the scheme could suffer from too much information. For example, with a carrier of 4.3×10^{14} cps, the radar Doppler is about 1.3×10^6 cps for a 1-mph target. Thus, moving target indication will require more involved processing and detection than microwave radars where display of the Doppler output may require no more than a pair of earphones.

An additional problem will be to provide a low-loss delay mechanism for the replica of the transmitted pulse. Losses here will, at least until better systems are achieved, limit the range more severely than beam spreading—the ultimate limit in ranging systems. One possible storage device for such a radar is a fiber optic waveguide of optical path length equal to the round trip target distance. Present fiber optic waveguide is reported to have losses of nearly 10 db in 20 feet,² or round trip (radar) losses of about a db/foot for wavelengths in the visible region. This will be somewhat improved by the actual slowing of the light by the waveguide. However, if we assume 10^{19} photons are available for signal processing at the transmitter, and find that 10^4 photons are needed to beat the echo, we obviously have a range limited to not much more than 150 feet. The choice of 10^4 photons is based on the number of quanta required to remove an eightfold uncertainty about the target at the output of the signal processing and integrating circuitry. Thus, a fourfold uncertainty must be resolved to get phase information adequate for velocity determination, that is, to 90°, and a further twofold uncertainty as to the existence of a target must be removed at any given phase. Treating this signal from a wave standpoint requires 8^4 photons.³ Of these 4×10^3 photons, 2×10^3 are from the target and 2×10^3 are the delayed and attenuated portion of the emitted pulse. Therefore, 10^4 photons should be adequate, assuming photoelectric surfaces of good quantum efficiency and low system noise. Improving the loss factor by one

order of magnitude⁴ gives a radar range in the order of 1500 feet, which begins to look interesting tactically. Inserting fiber optic amplifiers² or other negative resistances along the delay path will allow for a small increase in range. Our calculations indicate that one or two octaves may be expected if spurious responses produced by reflections in the system are kept to 10 db or more below the desired signal. If the system can be approached from a coded pulse rather than from a quasi-CW basis, the spurious response due to reflections may be reduced by gating the negative resistances. The development of unilateral light amplification will, it is hoped, result in devices limited in range only by the conventional radar range equation.

In summary it is felt that optical maser radars can be built which will accurately measure target velocity as well as range, and which will accomplish this by a coherent radar technique. This method will resemble an interferometer in which one path will be through an optical path in dielectric waveguide of known length. Although the losses in present fiber optics at 6943 Å severely limit range capabilities, it may be possible to develop tactical optical maser radars with ranges of one to a few miles.

M. KATZMAN

E. FROST

U. S. Army Signal Research

and Development Lab.

Fort Monmouth, N. J.

⁴ E. Snitzer, "Optical Dielectric Wave-Guides," presented at 2nd Internatl. Conf. on Quantum Electronics, University of California, Berkeley; March 23-25, 1961. (To be published.)

Unidirectional Lower Sideband Parametric Amplifier Without Circulator*

A method is presented of obtaining the characteristics of a traveling-wave parametric amplifier, *i.e.*, matched input and nonreciprocity of amplification, using a structure containing only two variable reactance units operating in the lower sideband mode.¹ A circulator is not required.

The matched input in a negative conductance traveling-wave device can be attributed to the cancellation of the backward waves excited by successive sections of the line. In a lumped structure this can be achieved simply by using a quarter wave separation of the negative conductance units. Fig. 1 illustrates one section of a ladder network matched to a load of $G-G_n$.

The nonreciprocity of a traveling-wave parametric amplifier is determined by the direction in which the pump power is sup-

* Received by the IRE, July 21, 1961; revised manuscript received, August 29, 1961.

¹ Since this letter was submitted, it has come to the attention of the author that a similar device has been described by L. D. Baldwin, "Nonreciprocal parametric amplifier circuits," *Proc. IRE (Correspondence)*, vol. 49, p. 1075; June, 1961. A somewhat differing layout has also been disclosed independently, by K. H. Locherer and R. Mauer, *Electronics*, vol. 34, p. 21; March, 1961.

² E. Snitzer, "Proposed fiber cavities for optical masers," *J. Appl. Phys.*, vol. 32, pp. 36-9; January, 1961.

³ D. Gabor, "Communication theory and physics," *Phil. Mag.*, vol. 41, pp. 1161-1187; November, 1950.

* Received by the IRE, August 28, 1961.

¹ D. A. Budenz, *et al.*, "An experimental laser ranging system," 1961 IRE INTERNATIONAL CONVENTION RECORD, pt. 5, pp. 185-193.

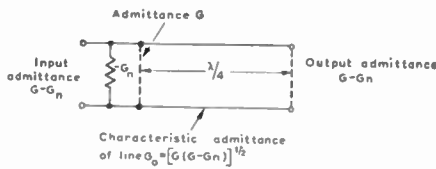
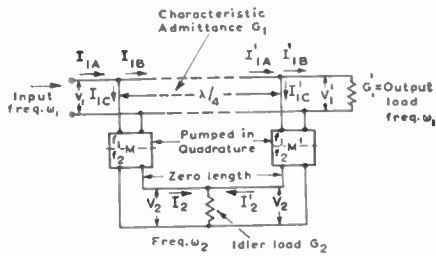
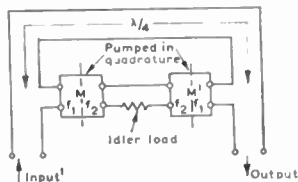


Fig. 1—Section of repetitive negative conductance amplifier.



(a)



(b)

Fig. 2—Unidirectional twin varactor parametric amplifiers. (a) Shunt-tuned parametric units (schematic). (b) Series-tuned parametric units.

plied. The condition that the sum of the propagation coefficients of the signal and the idler waves be equal to that of the pump can usually only be satisfied in one direction. However, if parametric elements are situated at intervals of half the pump wavelength there is no means of sensing the direction of the pump supply. For maximum nonreciprocity with the fewest number of elements, the separation should be a quarter wavelength at the pump frequency, or approximately an eighth of a wavelength at the signal and idler frequencies.

Although similar principles can be used in a twin-diode amplifier, the transition from many diodes to only two is not perfectly straightforward. The difficulty lies in the fact that, ideally, for uniform operation a traveling-wave device should be supplied with power at both the signal and idler terminals. In a multi-element device any unbalance in the supply disappears after a few sections. This obviously does not apply when only two elements are present.

A circuit (and its dual) which gets over the difficulty is illustrated in Fig. 2. Parametric units M_1 and M_2 are represented by two terminal pair junctions with a line dividing the terminal pairs to indicate that frequency conversion takes place between them. It must be understood that these junctions are assumed to contain all the filters and tuning elements necessary for the operation of the amplifier.

To obtain maximum nonreciprocity the pump supply is applied in quadrature to the two units, and the condition that the sum of the phase changes of the signal and the idler should equal that of the pump is satis-

fied by making the idler phase change zero (i.e., by connecting the two pairs of idler terminals) and by introducing a quarter wave separation at the signal. This arrangement is susceptible to simple analysis and a simple matching procedure because no reactive effects are introduced by the parametric units. The quadrature phase of the signal voltage at the terminals of the parametric units, in conjunction with the quadrature phase of the pump, ensure that the idler currents generated in each are in phase for forward propagation and in antiphase for backward propagation (analysis shows that they are equal and opposite in the latter case). The common voltage at the two pairs of idler terminals means that equal current will be supplied to the signal terminals of each unit with a quadrature phase delay, or phase advance, determined by the relative pump phases. Analysis shows that for forward operation the current is of the correct phase to produce amplification and that for reverse operation the current is zero since the idler voltage is zero. The latter result means that the amplifier produces no effect on the backward wave, which passes without amplification or attenuation. The forward wave is amplified, and it is easy to show that equal currents injected in quadrature at a quarter wave interval couple no energy in the reverse direction, and therefore introduce no mismatch. Analysis shows that the amplification is identical to what would be obtained using one of the parametric units as a reflection amplifier on one arm of a circulator with input and output loading of the same characteristic impedance as for the twin diode layout.

It can also be shown that the noise power contributed by losses in the diodes is the same as in the circulator layout. It will be assumed that the noise appears to come from a generator in shunt with the diode with admittance G_i . Noise contributed by the second diode will not be amplified, passing back through the device in the same way as a signal injected in the reverse direction. If the source admittance is G_1 noise current from the first diode, of magnitude $2(kTBG_i)^{1/2}$, is loaded by $2G_1$ when the amplifier is matched, and therefore produces a voltage at the input of $(kTBG_i)^{1/2}/G_1$ compared with the voltage of $(kTB/G_1)^{1/2}$ produced by noise in the input signal (assuming the same temperature). The noise figure is therefore $1 + G_i/G_1$ which is the same as for a similar diode in the circulator layout. In single-sideband operation the inevitable idler noise will, of course, also be present.

The amplifier therefore reproduces the behavior of the circulator unit in respect to match, amplification, noise figure, and nonreciprocity, but is inferior in respect to bandwidth because of the frequency sensitivity of the quarter wave line.

Note: Since submitting this note, it has come to the author's attention that a similar device has been described by L. D. Baldwin, "Nonreciprocal parametric amplifier circuits," Proc. IRE (Correspondence), vol. 49, p. 1075; June, 1961. A somewhat differing layout has also been independently disclosed by Locherer and Maurer.¹

G. H. B. THOMPSON
Standard Telecommunication Labs. Ltd.
London, England

One-Tunnel-Diode Flip-Flop HF Behavior*

In a note by Kaenel¹ and subsequent comments by Flowerday and McKibbin,² the one-tunnel-diode flip-flop was discussed. It is the purpose of this paper to offer an analysis of the approximate switching speed of the circuit and thereby show that this type of circuit may be used as a frequency divider with a fixed pulse length output, that is to say, that the normal scale of two divisions associated with a flip-flop will be modified to a much higher value under suitable trigger conditions (Fig. 1).

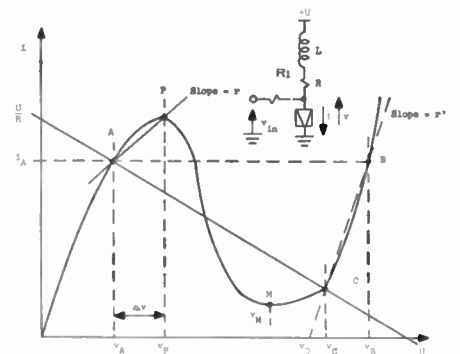


Fig. 1.

It is assumed that the triggering signal is injected through R_1 long enough to shift the diode from A to P along AP . The value of L is chosen so that the current i_A remains essentially constant. The equivalent during triggering is then approximately as shown in Fig. 2, so that the voltage across the diode is given by (1).

$$v = v_A + \frac{rv_{in}}{r + R_1} \left(1 - \exp \left\{ - \frac{t}{\frac{R_1 r}{R_1 + r} C} \right\} \right) \quad (1)$$

$\tau_p \geq \tau \geq \tau_A$

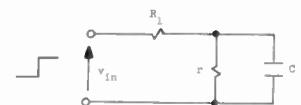


Fig. 2.

In most applications the inequality $R_1 \gg r$ is satisfied, which yields a time constant $\tau = rC$, or a waiting time of about 200 μsec for a fast tunnel diode. After obtaining the peak current the diode will switch. Since the triggering signal is removed the current i will be very nearly i_A so that conditions are given by point B . The characteristic will now be approximated by (2).

$$i = \frac{1}{r'} \quad v = \frac{1}{r'} v_0 \quad (2)$$

* Received by the IRE, August 23, 1961.
¹ R. A. Kaenel, "One-tunnel-diode flip-flop," Proc. IRE (Correspondence), vol. 49, p. 622; March, 1961.
² T. W. Flowerday and D. D. McKibbin, "Tunnel diode one-shot and triggered oscillator," Proc. IRE (Correspondence), vol. 49, p. 1315; August, 1961.

This yields a current response of the form:

$$i = \frac{U - v_0}{R + r_1} (1 - e^{-(R+r_1)/L t}) + i_1 e^{-(R+r_1)/L t} \quad (3)$$

The relaxation time is therefore controlled by the time constant L/R . The implication is that the sensitivity to the negative voltage reset trigger is modified from $v_c - v_M$ to a value as high as $v_B - v_M$, so that a circuit with a negative input only slightly higher than $v_c - v_M$ will act as a frequency divider. The division ratio for a given input signal depends therefore on the time constant and the amount of input signal.

The assertions of the preceding analysis were tested experimentally with some very fast tunnel diodes. It was found that the circuit operated for frequencies up to 3000 Mc; 100 per cent modulation of the RF input yielded an output which could be used to recover the audio signal. The circuit, with perhaps slight modification, therefore offers the additional uses of RF detector and high scale counter, which indeed is surprising for such a simple arrangement.

HENRY GUCKEL
Digital Computer Lab.
University of Illinois
Urbana, Ill.

Additional Information on "An Interaction Circuit for Traveling-Wave Tubes"

The purpose of this note is to present several important facts regarding the class of traveling-wave tube interaction structures described by Crepeau and Itzkan.¹ These additional observations are as follows: 1) circuits of the type described by Crepeau and Itzkan can support a multiplicity of propagating modes in the lowest pass band which may interfere with proper circuit operation in linear beam tubes. 2) The Crepeau and Itzkan structures (which might be termed "ring-line" circuits) can be made entirely self-supporting and can also be effectively cooled by the substitution of conducting plates for the wire lines which connect successive rings. The resulting circuits might be called "ring-plane" circuits. 3) Low-velocity circuits of this family can be fabricated conveniently from plane-supported helices ("helix-plane" circuits).

The most crucial observation is the first, the existence of several modes having nearly equal phase velocities in the lowest pass band. Two modes have been observed in circuits similar to the two-wire circuits of Crepeau and Itzkan, three modes in a three-wire version, and so on. These modes were observed in cold tests several years ago at

the General Electric Traveling-Wave Tube Product Section and at the University of California at Berkeley.² In recent hot tests of an X-band plane-supported helical structure at the University of California, backward-wave oscillation was obtained by interaction with the spatial harmonics of the two distinct modes.

Several members of the plane-supported ring family are shown in Fig. 1. The lowest-

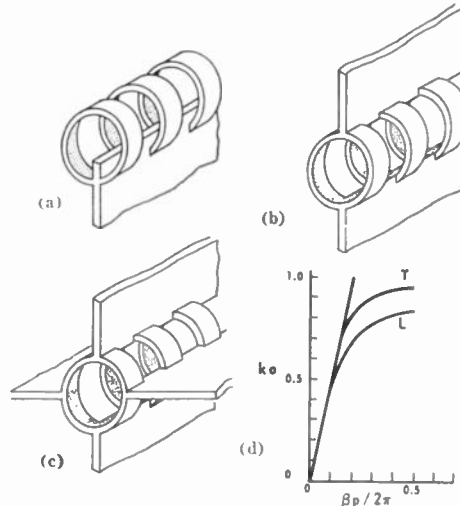


Fig. 1—Several members of the family of plane-supported ring circuits. Axial electric field dependence on the angular coordinate is as $\sin(n\phi)$. For circuit (a), $n = \frac{1}{2}$; for (b), $n = 1$; for (c), $n = 2$. Fig. 1(d) shows the ω - β diagram for the plane-supported ring ($n = 1$) circuit of Fig. 1(b). The circuit pitch is p , the inside ring diameter is a ; the straight line represents propagation at the velocity of light. The transverse and longitudinal modes are represented by curves T and L , respectively.

order ($n = \frac{1}{2}$) member is the plane-supported ring structure of Fig. 1(a). On this circuit,^{3,4} a single mode propagates in the z direction; it has primarily z -directed electric fields having their maximum amplitude at the top of the rings, and a zero amplitude at the plane itself. The angular dependence of the field is $E_z \sim \sin(n\phi)$, where $n = \frac{1}{2}$, and ϕ is the angular coordinate. The next-higher-order plane-supported ring circuit, the $n = 1$ member, is similar in behavior to the ring-line circuit previously mentioned.¹ The circuit, shown in Fig. 1(b), has a vanishing electric field along the support planes which serve both as mechanical supports and as thermal conductors. Two modes have been observed on this circuit [as indicated in Fig. 1(d)], both having an angular dependence $|E_z| \sim |\sin \phi|$. In one mode, both wires at any transverse section are excited in phase, so that predominantly longitudinal electric fields exist between successive rings and on the axis. In the other mode, the "transverse" mode, the two wires at any cross section are oppositely charged, and

C. K. Birdsall and D. E. Chaffee, work supported in part under contract AF 33(616)6139.

² H. Heffner, "Traveling-Wave Amplification of Millimeter Waves," Stanford University, Stanford, Calif., Tech. Rept. No. 51, Contract N6our251, ERL; July 31, 1952. See especially Fig. 57 for $n = \frac{1}{2}$ circuit.

³ C. K. Birdsall and T. E. Everhart, "Modified Contra-Wound Helix Circuits for High-Power Traveling-Wave Tubes," Hughes Aircraft Co., Culver City, Calif., Tech. Memo. No. 909, 1955. See especially Fig. 19 for $n = \frac{1}{2}$ circuits; Fig. 14 for $n = 1$ circuits.

strong transverse electric fields cross the center of the circuit. In this second mode there are also longitudinal fields between successive rings.

Support of this general mode picture was obtained at the GE Traveling-Wave Tube Product Section in cold tests of the four-wire structure of Fig. 2. This structure,

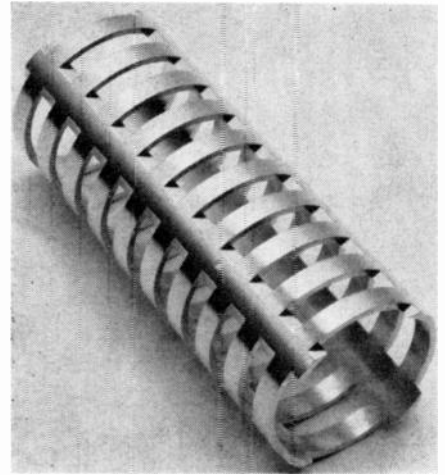


Fig. 2—Photograph of a four-ring (or four-ladder) circuit.

when tested without any supporting planes, showed clearly that there were at least three modes closely spaced in frequency; it is possible that a fourth mode went undetected because of the close mode spacing. At certain frequencies, a length of this circuit resonated with strong fields on two opposing slots and zero fields at the centers of the slots on either side of the excited slots. At other frequencies, only three of the four sets of slots were excited, the set nearest the exciting probe being the most strongly excited. These tests indicated the need for great care in measuring propagation characteristics and in evaluating mode suppression schemes applied to these circuits.

The upper cutoff frequency for the longitudinal mode of circuits of this sort can be calculated approximately by assuming that cutoff occurs when the circumferential length of a slot is one-half a free-space wavelength. Such a simple consideration is plausible if one considers these circuits as members of the ladder structure family which obey this rule very well.⁵ This family includes the Easitron, on which strong electric fields exist at only the frequency for which the ring length is exactly equal to $\lambda_0/2$, the unsupported slotted plane, the Karp circuit, and the ring structures described here. To be sure, additional inductance in the conducting member which joins successive rings alters the cutoff condition somewhat. However, the entries in Table I show that this simple condition is adequate for estimation of the upper cutoff frequency, and hence, approximation of the ω - β diagram.

⁵ R. M. White, C. K. Birdsall, and R. W. Grow, "Multiple ladder circuits for millimeter wavelength traveling-wave tubes," Proc. Symp. Millimeter Waves, Brooklyn Polytech. Inst., Brooklyn, N. Y.; March 31-April 2, 1959.

* Received by the IRE, April 17, 1961; revised manuscript received, May 1, 1961.

¹ P. J. Crepeau and I. Itzkan, "An interaction circuit for traveling-wave tubes," Proc. IRE (Correspondence), vol. 49, p. 525; February, 1961.

TABLE I

Comparison of calculated and observed upper cutoff frequencies f_c of the longitudinal mode for various ladder-type circuits. Calculated value obtained by assuming the length of the conduction path for one element of the periodic circuit equals $\lambda_0/2$ at the upper cutoff frequency.

Circuit	Reference	Calculated Upper f_c
		Observed Upper f_c
Easitron	4	1.00
Plane ladder	4	1.12
Double ring-on-wire	1 [Fig. 2(a)]	1.09
Double ring-on-wire	1 [Fig. 2(b)]	1.08
Double ring-on-wire	1 [Fig. 2(c)]	0.93
Quadruple ring-on-meander line	1 [Fig. 2(d)]	0.83

To summarize, even though these circular ladder structures can support undesired modes of propagation, they still represent an excellent means of making well-cooled and well-supported periodic structures having both a large interaction impedance and a diameter comparable with or larger than $\lambda_0/2$.

R. M. WHITE
Traveling-Wave Product Section
General Electric Co.
Palo Alto, Calif.
C. K. BIRDSALL
D. E. CHAFFEE
University of California
Berkeley, Calif.

Authors' Reply⁶

The comments of White, Birdsall, and Chaffee are correct; however, the problem of interfering modes is more acute in circuits with rings connected to planes or straight wires than in circuits with rings connected to meandered wires. Fig. 1(d) shows the transverse and longitudinal modes for rings connected to planes. For rings connected to meander lines, the transverse mode is essentially unaffected, but the upper cutoff frequency of the longitudinal mode is appreciably decreased. [This decrease of the longitudinal mode can be seen by comparing curves (a) and (b) of Fig. 2 in Crepeau and Itzkan.¹]

In practical traveling-wave tube applications, the interaction circuit is usually surrounded by a cylindrical conducting shell. There is strong coupling between the transverse circuit mode and the TE_{11} circular cylindrical waveguide mode; this is a result of the similarity between the field configurations for these two modes. The coupling raises the lower cutoff frequency of the transverse mode from zero to very nearly that of the TE_{11} cutoff. This is shown in Fig. 3.

The composite transverse electric mode intersects the velocity line for an operating beam at a frequency greater than 1.5 times the upper cutoff of the useful band. This condition makes mode suppression easy, and, in fact, a high-power broad-band tube

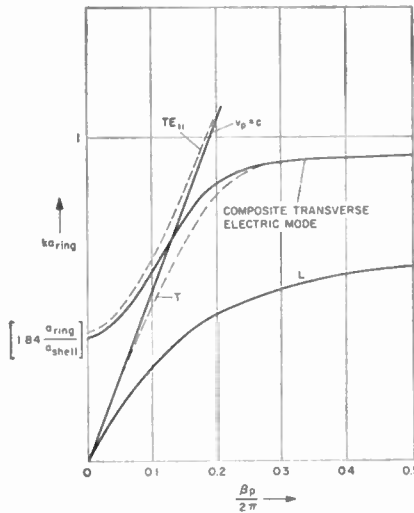


Fig. 3—Dispersion curve for ring-loaded meander line with outer conducting shell.

has been operated with absolutely no interference from competing modes.⁷

The essential virtue of the ring-loaded meander line is this freedom from interfering modes. The authors, however, in no way wish to imply that this is an inherent property of all "ring-line" circuits.

P. J. CREPEAU
I. ITZKAN
Electronic Tube Div.
Sperry Gyroscope Co.
Great Neck, N. Y.

⁷ C. Burkund, "A broadband megawatt TWT using a ring-loaded meander line interaction circuit," to be published.

Comments on "Design Theory of Optimum Negative-Resistance Amplifiers"*

In a recent article¹ Kuh and Patterson state in the second paragraph of the Introduction that, prior to their work which was first submitted to the IRE on December 8, 1960, and finally on February 27, 1961, no general theory had been found for the limitations and synthesis of amplifiers incorporating tunnel diodes.

We wish to point out that in this respect they are in error since the three papers,

- 1) "Network Synthesis with Negative Resistors," by H. J. Carlin and D. C. Youla,
- 2) "Optimum Negative-Resistance Amplifiers," by D. C. Youla and L. I. Smilen,
- 3) "Gain Bandwidth Performance of Maximally Flat Negative-Conductance Amplifiers," by E. W. Sard,

* Received by the IRE, June 21, 1961.

¹ E. S. Kuh and J. D. Patterson, *PROC. IRE*, pp. 1043-1050; June, 1961.

which were submitted to the Brooklyn Polytechnic Symposium on Active Network and Feedback Systems and read April 19-22 1960, predated their efforts by at least seven months. These later appeared in the published Polytechnic Institute of Brooklyn Symposium Proceedings. Moreover, the paper,

- 4) "Exact Theory and Synthesis of a Class of Tunnel Diode Amplifiers" by L. I. Smilen and D. C. Youla,

appeared in complete printed form in the *Proc. NEC*, vol. 16, October, 1960, this time predating them by two months.

The second paper quoted gave: 1) A complete, rigorous and systematic account of the gain-bandwidth limitations of amplifiers constructed with either one or many tunnel diodes embedded in a lossless, passive-reciprocal or nonreciprocal environment, together with appropriate synthesis procedures. 2) Exact and explicit formulas were presented for both Butterworth and Tchebicheff insertion-loss characteristics of arbitrary order for both optimum-nonreciprocal and transmission amplifiers employing a single diode. 3) The stability, noise figures and sensitivities of the various configurations were also explicitly determined and discussed.

Some of these results were also obtained by Sard³ using an entirely different approach.

The NEC paper 4) contains a careful study of the reflection amplifier. Its gain-bandwidth performance is summarized in (133), its noise figure in (147) and (150), its sensitivity and stability in (161) and (152), and (153), respectively. Again a full account of the associated synthesis procedures is given. Section II of this paper also includes an exhaustive treatment of the transmission amplifier [Figs. 1(a) and (b)]. Its gain-bandwidth restriction appears in (16), the gains of the Butterworth and Tchebicheff responses in (20) and (23) and the sensitivity and stability formulas (44), (45), (47), (86) and (88), respectively. The noise figure relations are compactly expressed in (68) and (82). As before the pertinent synthesis techniques are treated fully.

We also wish to take issue with some of the technical statements which appear in the Kuh-Patterson paper. In their treatment² these authors find it necessary to describe their 3-port N_a in terms of a scattering matrix normalized to G_S at port #1, C at port #2 and Y_0 at port #3, where Y_0 is an arbitrary passive admittance at their disposal. Then they proceed to assert on the following page that since S_{21a} , S_{31a} and S_{32a} are the scattering coefficients of a lossless network with passive reference admittance their magnitudes must all be bounded by unity. The normalization technique they employ is implied to be the one developed in their [6]. Unfortunately their assertion is false, as a simple counterexample shows. Let Y be an arbitrary Foster function and any passive admittance. According to the definition in their [6] [p. 215, (146)], the scattering coefficient s of the lossless 1-po-

⁶ Received by the IRE, July 14, 1961.

⁷ *Ibid.*, p. 1403, Fig. 2.

Y normalized to y is

$$s = \frac{Y - y}{Y + y} \tag{1}$$

For $p=j\omega$ set $Y=jB$ and $y=g+jb$. Then

$$|s(j\omega)|^2 = \frac{(B - b)^2 + g^2}{(B + b)^2 + g^2}$$

Clearly, if $B > 0$ and $b < 0$, $|s(j\omega)| > 1$. Their statement is also incorrect even if Y is passive but not Foster.

Actually, the correct way to normalize is by means of the old and familiar Bode formula,

$$s = \frac{Y - \bar{y}}{Y + \bar{y}} \tag{2}$$

where \bar{y} is the complex conjugate of y . A proper normalization procedure for n -ports is also available and automatically leads to a unitary scattering matrix S whenever these structures are lossless.³ Eq. (1) only succeeds when y is real and positive. Thus the authors' artifice of inserting a parallel-tuned circuit for the purposes of making Y_{22} real (p. 1044) may be dispensed with if it is understood that the normalization has been carried out in the correct manner.

Nevertheless, the entire question of complex normalization may be completely avoided by the simple and natural expedient of lumping the diode parasitic capacitance C in with the 3-port equalizer and normalizing port #1 to G_S , port #2 to G_L and port #3 to $G = 1/R$, where $-R$ is the negative resistance appearing in the tunnel-diode equivalent circuit. This leads immediately to the transducer power-gain expression

$$G_T(\omega^2) = \left| \frac{s_{12}(j\omega)}{s_{22}(j\omega)} \right|^2 \tag{3}$$

and involves only magnitudes. Formula (3), which appeared for the first time as (16) in Youla and Smilen [2], p. 250], should be contrasted with Kuh and Patterson's (3), (p. 1044) which is both magnitude and phase sensitive.

Lastly, Kuh and Patterson fail to mention that the main advantage of optimum nonreciprocal over-reciprocal equalization is not the additional gain, which can never exceed 6 db, but the significantly reduced noise figure. It has been shown in Youla and Smilen [2], (160), p. 292] that, for equal load and generator temperatures, $(F_{opt})_{recip} = 2(F_{opt})_{non\ recip}$, i.e., a difference of 3 db.

H. J. CARLIN
L. I. SMILEN
D. C. YOULA
Electrophysics Dept.
Polytechnic Inst. of Brooklyn
Brooklyn, N. Y.

Authors' Comment⁴

We wish to thank Carlin, Smilen and Youla for their comments on our paper. The omission of the references is unfortunate.

³ D. C. Youla, "Solution to the Problem of Complex Normalization," *Microwave Res. Inst., PIBMRI-891-61*; January 30, 1961. Polytechnic Inst. of Brooklyn, N. Y.

⁴ Received by the IRE, July 10, 1961.

However, some of the results in our paper were disclosed to Professor Carlin in August, 1960, when none of the papers quoted were available. Our paper was first submitted in early September, 1960, to the *Journal of Applied Physics*. The reviewer of *JAP* recommended in December that the paper should be published in PROCEEDINGS OF THE IRE. References 1), 2), and 3) quoted above did not appear until April, 1961.

The paper of Youla and Smilen 2) contains certain results we have obtained. However, the proof of the optimum-gain bandwidth and the synthesis procedures are completely different. We feel that our presentation is simpler, and we include amplifier configurations and synthesis procedures not treated elsewhere.

Their comments on the normalization of the scattering matrix is immaterial as far as the proof of the optimum-gain bandwidth is concerned. The arbitrary passive admittance Y_0 is introduced as one of the reference admittances only in the preliminary step. It is then justified that Y_0 can be made real without losing any generality. The unitary property of the scattering matrix with real reference admittance is used to prove the optimum-gain bandwidth formula. Youla's conjugate impedance normalization would be helpful, but was not needed in the proof.

We appreciate their pointing out the sentence regarding the boundedness of the scattering coefficient as being correct only in terms of the conjugate impedance normalization, but incorrect in terms of the usual impedance normalization.

Finally, following the suggestion of the reviewer, we did not include a section on noise figure. However, it is mentioned in the introduction that, except for the circulator and hybrid types, other amplifiers have large reflection coefficients at the input and output.

E. S. KUH
J. D. PATTERSON
Dept. of Elec. Engrg.
University of California
Berkeley, Calif.

Noise in Tunnel-Diode Mixers*

An expression for the noise figure of the tunnel diode mixer, derived by Breitzer,¹ includes the noise of the load conductance of the mixer. It is the aim of this note to modify Breitzer's result and obtain the noise figure of the mixer itself. The results are of interest for the following reasons:

1) Since the noise of the load is only part of the IF amplifier noise, it is often undesirable to count its noise as part of the tunnel diode mixer circuit.

2) Friis' formula for stages in cascade, if it can be applied, uses the noise figure of the mixer itself, not that of the mixer plus the load.

3) Friis' formula cannot be applied if the output conductance g_{out} of the mixer circuit is negative. Nevertheless, it is still not right to ignore the noise of the first IF stage unless the gain of that stage is large.

4) The results can be put in a simple form if $g_{out} > 0$.

The noise figure of the tunnel diode mixer stage itself can be obtained by eliminating the contribution of the load conductance g_L to the noise figure in Breitzer's result.² This yields

$$F = 1 + \frac{e}{2kT} \frac{I_{e0}}{g_1^2} \left[g_s + \frac{1}{g_s} (g_0^2 - 2g_0g_1 \frac{I_{e1}}{I_{e0}} + g_1^2) + 2(g_0 - g_1 \frac{I_{e1}}{I_{e0}}) \right] \tag{1}$$

In (1), e is the electronic charge, k is Boltzmann's constant, T is room temperature, g_s is the source conductance, I_{e0} and I_{e1} are Fourier components of the instantaneous equivalent shot noise current $I_{en}(t)$, and g_0 and g_1 are Fourier components of the instantaneous conductance $g(t)$ of the tunnel diode, defined by the equations

$$I_{en}(t) = I_{e0} + 2I_{e1} \cos \omega t + \dots \tag{2}$$

$$g(t) = g_0 + 2g_1 \cos \omega t + 2g_2 \cos 2\omega t + \dots \tag{3}$$

Eq. (1) shows that the correlation between the RF and IF noise currents can either enhance or decrease the noise figure of the mixer depending upon both the magnitude and the sign of the parameters I_{e0} , I_{e1} , g_0 and g_1 .³ Eq. (1) has the minimum value

$$F = F_{min} = 1 + \frac{e}{2kT} \frac{I_{e0}}{g_1^2} \left[2\sqrt{g_0^2 - 2g_0g_1 \frac{I_{e1}}{I_{e0}} + g_1^2} + 2(g_0 - g_1 \frac{I_{e1}}{I_{e0}}) \right] \tag{4}$$

for

$$g_s^2 = (g_s^2)_{opt} = g_0^2 - 2g_0g_1 \frac{I_{e1}}{I_{e0}} + g_1^2 \tag{5}$$

The right-hand side of (5) is always positive since $I_{eq}(t) > 0$ at all times; this implies $|I_{e1}| \leq I_{e0}$.

If $g_{out} > 0$, the over-all noise figure F_{tot} of the system can be obtained by Friis' formula

$$F_{tot} = F_{min} + \frac{(F_{IF} - 1)}{G_{av}} \tag{6}$$

¹ $r_L = 1$ r_2 in Breitzer's paper. Our (1) can be obtained by omitting the third term of (5) in Breitzer's paper and substituting the notations $I_{e0} = I_{0f} + I_{0r}$, $I_{e1} = I_{1f} + I_{1r}$, $g_s = 1/r_1$, $e = q$ and $T = T_1$.

² Neglecting the correlation means putting $I_{e1} = 0$; (1) then becomes

$$F = 1 + \frac{e}{2kT} \frac{I_{e0}}{g_s} + \frac{e}{2kT} \frac{I_{e0}}{g_s} \left(\frac{g_0 + g_1}{g_1} \right)^2$$

This equation is identical to (26) of the paper: K. K. N. Chang, G. H. Heilmeyer, and H. J. Prager, "Low-noise tunnel-diode down converter having conversion gain," *Proc. IRE*, vol. 48, pp. 854-858, May, 1960, if this equation is modified as follows:

Omit the noise contributions due to the loss conductances G_1 and G_2 and the load conductance G_L , and substitute $T_0 = T$, $G_0 = g_s$, $G_1 = g_0$, $G_2 = g_1$ and $G = eI_{e0}/2kT$.

* Received by the IRE, July 31, 1961.

¹ D. I. Breitzer, "Noise figure of tunnel-diode mixer," *Proc. IRE*, vol. 48, pp. 935-936; May, 1960.

here F_{IF} is the noise figure of the IF amplifier and G_{av} is the available gain of the mixer. It is difficult to give a general expression for F_{tot} if $g_{out} < 0$; especially since one has to satisfy the condition $(g_{out} + g_L) > 0$ in that case in order to have stability.

The output conductance g_{out} of the mixer is

$$g_{out} = g_0 - \frac{g_1^2}{g_0 + g_s} \quad (7)$$

and the power gain of the mixer is

$$G = \frac{4g_s g_L g_1^2}{[(g_0 + g_s)(g_0 + g_L) - g_1^2]^2} \quad (8)$$

If g_{out} is positive, G can be optimized by putting $g_L = g_{out}$; one then obtains the available gain

$$G_{av} = \frac{g_s}{g_{out}} \left(\frac{g_1}{g_0 + g_s} \right)^2 \quad (9)$$

The conditions $g_s = (g_s)_{opt}$ and $g_{out} > 0$ are not always satisfied simultaneously. If one keeps $g_s = (g_s)_{opt}$, the relation $g_{out} > 0$ is only satisfied if g_0 and g_1 meet certain requirements.

If $g_1^2 > g_0^2$, the mixer circuit is not unconditionally stable, since G can be made infinitely large by proper choice of g_s and g_L . The circuit is unconditionally stable if $g_1^2 < g_0^2$ and $g_0 > 0$; G can then be optimized as a function of g_s and g_L .

The latter is the case for the ordinary diode mixer,⁴ for which

$$\frac{I_{e1}}{I_{e0}} = \frac{g_1}{g_0} \quad (10)$$

The optimized values of F and G ,

$$G = G_{max} = \frac{g_1^2/g_0^2}{(1 + \sqrt{1 - g_1^2/g_0^2})^2} \quad (11)$$

$$F = F_{min} = 1 + \frac{e}{2kT} \frac{I_{e0}}{g_1^2} 2\sqrt{g_0^2 - g_1^2} \cdot \left(1 + \sqrt{1 - \frac{g_1^2}{g_0^2}} \right) \quad (12)$$

are then obtained for

$$g_s = g_L = g_0 \sqrt{1 - \frac{g_1^2}{g_0^2}} \quad (13)$$

It is seen that $G_{max} \leq 1$, since $g_1^2 \leq g_0^2$; G_{max} and F_{min} approach unity if g_1^2 approaches g_0^2 . This is generally not the case for the tunnel diode mixer because the relation (10) is not satisfied here, so that the condition $|g_1| \rightarrow |g_0|$ does not lead to $F_{min} \rightarrow 1$.

The case $g_{out} < 0$ will be dealt with in another paper. A study is under way to determine the influence of the correlation effect on the noise figure.

Very sincere thanks are due Prof. A. van der Ziel for his constant advice and encouragement.

SHIH-FANG LO
Elec. Engrg. Dept
Univ. of Minnesota
Minneapolis, Minn.

⁴ A. van der Ziel, "Noise," Prentice-Hall, Inc., Englewood Cliffs, N. J., pp. 247-250; 1954.

Comments on "Tunnel-Diode Microwave Oscillators"*

We have read with great interest the above paper.¹ We would draw attention to an apparent error (printing or otherwise) in (25) and suggest that the imaginary part of this should be rewritten as

$$\left[\tan \beta l_2 + \frac{\{1 - (Z_0/Z_R)^2\} \sin \beta l_1 \cos \beta l_1}{(Z_0/Z_R)^2 \sin^2 \beta l_1 + \cos^2 \beta l_1} \right]$$

While initially calculating values for a practical circuit, some rather improbable solutions resulted which lead us to investigate the derivation of (25) and the subsequent realization that the brackets had been omitted from the numerator.

We are indebted, however, to the authors of this paper for their invaluable contribution to this new field of microwave oscillators.

G. FULLER
G. W. H. WOODING
Radar Div.
Elliott Brothers, Ltd.
Rochester, Kent, Eng.

Author's Comment²

The authors wish to thank Fuller and Wooding for pointing out the omission of brackets in (25). It should be noted that the correct form of (25) was used in plotting Fig. 14.

Another error occurs in (6): the plus sign before I in the left-hand side of the equation should be changed to a minus sign. This error does not affect the following equations.

We regret any inconvenience which has been caused by these errors.

D. STERZER
D. E. NELSON
Electron Tube Div.
RCA Labs.
Princeton, N. J.

* Received by the IRE, June 12, 1961.

¹ F. Sterzer and D. E. Nelson, Proc. IRE, vol. 49, pp. 744-753; April, 1961.

² Received by the IRE, July 13, 1961.

Gravitational Fields*

Interest in the general theory of relativity has recently been renewed especially since the advent of the artificial earth satellites. It is well-known that there are gravitational analogies to the electromagnetic field in that theory. A recent paper in this journal¹ contains a good survey of the literature and the work done in that field.

However, it is interesting to notice that the gravitational and the "protational" field,

obtained by linearizing the equations of the general theory of relativity are not completely analogous to the electric and the magnetic field. Namely, the Maxwell equations cannot be obtained strictly from the general theory of relativity.

Suppose now that the existence of the "protational" field, which may also be called the "antigravitational" field, since it acts in certain cases opposite to the gravitational field, is experimentally established by some means to a certain degree of accuracy. The "protational" field of a moving point mass must have the form

$$h = \frac{1}{c^2} v \times g, \quad (1)$$

where g is the gravitational field. Eq. (1) is completely formally analogous to the Biot-Savart law for the magnetic field. The gravitational field of a point mass is given by the Newton law

$$g = km \frac{r}{r^3} \quad (2)$$

The sign in this equation is chosen positive intentionally to stress the analogy, and, therefore, different symbols for the gravitational and the "protational" field are used here from those used in the paper mentioned; k is the gravitational constant. The force on a moving mass particle m in the gh field is

$$F = -m'g - m'v' \times h, \quad (3)$$

which is, except for the sign, completely formally analogous to the Lorentz force in the electromagnetic field.

In the case of the mass distribution ρ , we have instead of (1) and (2) the following equivalent field equations:

$$\nabla \cdot g = 4\pi k \rho, \quad \nabla \times h = \frac{4\pi k}{c^2} \rho v. \quad (4)$$

Provided now that in the general nonstationary case the equation of continuity

$$\frac{\partial \rho}{\partial t} + \nabla \cdot (\rho v) = 0 \quad (5)$$

holds, (4) may be generalized for the nonstationary case into the following set of equations:

$$\nabla \times h = \frac{4\pi k}{c^2} \rho v + \frac{1}{c^2} \frac{\partial g}{\partial t}, \quad \nabla \times g = -\frac{\partial h}{\partial t} \quad (6)$$

$$\nabla \cdot h = 0 \quad \nabla \cdot g = 4\pi k \rho,$$

and those are the Maxwell equations for the gh field.

The conclusion from the above is that if someone experimentally proves the existence of the "protational" field, then it will be only the proof of the Maxwell equations, which are already proved for the electromagnetic field. It will not be a sufficient proof of the general validity of the general theory of relativity.

JOVAN DJURIĆ
Institute Mihailo Pupin²
Belgrade, Yugoslavia

* Received by the IRE, June 30, 1961.

¹ R. L. Forward, "General relativity for the experimentalist," Proc. IRE, vol. 49, pp. 892-904; May, 1961.

² On leave of absence 1961-1962; teaching in the Dept. of Elec. Engrg., University of New Mexico, Albuquerque, N. Mex.

The *gh*-Field Theory*

The *gh*-field theory has been defined in a recent communication¹ by the present author. It has been shown there that the *gh* field is defined by the Maxwell equations

$$\nabla \times \mathbf{h} = \frac{4\pi k}{c^2} \rho \mathbf{v} + \frac{1}{c^2} \frac{\partial \mathbf{g}}{\partial t}, \quad \nabla \times \mathbf{g} = -\frac{\partial \mathbf{h}}{\partial t}, \tag{1}$$

$$\nabla \cdot \mathbf{h} = 0 \qquad \nabla \cdot \mathbf{g} = 4\pi k \rho.$$

To these equations boundary conditions must be attached which are formally completely analogous to the boundary conditions of the electromagnetic theory.

It is obvious that the *gh*-field theory is a very close approximation to the classical mechanics and the Newton theory of gravitation with a straightforward physical meaning of all the quantities involved.

We shall now put forward a working hypothesis that light is of the *gh* nature instead of the electromagnetic nature. The consequence of this hypothesis is indeed a striking one.

It must be emphasized that due to the formal identity of the electromagnetic theory and the *gh*-field theory, numerous formulas, but by no means all, from the electromagnetic theory of light can be immediately transferred into the *gh*-field theory of light with a proper change of symbols.

It is well known that the classical electromagnetic theory of light breaks down at the fact that an atom, e.g., a hydrogen atom to take the simplest form, does not radiate light in the stationary state. Even after the introduction of the quantization, that theory cannot explain this fact, unless further assumptions are introduced.

However, if we assume that the introduced hypothesis of the *gh* nature of light is correct, then we immediately arrive at the conclusion that a self-closed system of masses, subject only to internal forces, cannot radiate in a stationary state a time-varying *gh* field, provided that the forces which are acting between the masses of such a system are conservative. For such a system of masses the principle of the conservation of momentum is valid, and if one mass is accelerated in one direction, then the remaining masses are accelerated in the opposite direction to such an extent, so that the net effect is that the total radiation outside will cancel, since the partial radiations which leave the system will be out of phase. A static gravitational field will be observed outside the system, superimposed with an "induction" field which decreases much faster than the gravitational field, so that at a sufficient distance from the system only the static gravitational field will be observable.

A "naively" imagined atom approximates very closely a self-closed system of masses mentioned above, and the conclusion is that such an atom cannot radiate, in its stationary state, a time-varying *gh* field which is presumably light, unless that atom is excited by some external forces. Such a

situation is exactly observed experimentally, and this is a direct consequence of the presumed *gh* nature of light. It provides a plausible explanation of a riddle which is a stumbling block in the classical physics, and corroborates the basic hypothesis. It is, however, obvious that the introduction of the quantization into the *gh*-field theory is imperative, if that theory is to be applied to various other problems of light.

It is interesting to point out that the gravitational deflection of light also corroborates the basic hypothesis of the *gh* nature of light. The actual difficulty lies, however, in the fact that even the *h* field is hypothetical. Nevertheless, the fact that molecules, i.e., matter, radiate light if excited, gives credence to the basic hypothesis. The future research in that direction must give further evidence of the presumed validity, or incogency of the *gh*-field theory of light.

JOVAN DJURIC
Institute Mihailo Pupin²
Belgrade, Yugoslavia

² On leave of absence 1961-1962; teaching in the Dept. of Elec. Engrg., University of New Mexico, Albuquerque, N. Mex.

X-Band Electronically-Variable Attenuator*

An electronically variable attenuator has been developed and successfully operated in the X-band frequency range using a symmetrical stripline structure. The attenuator circuit is illustrated in Fig. 1. It consists of a 3-db branch-line hybrid with a balanced pair of Sylvania 1N832 diodes mounted on arms of equal length. The diodes were matched to a 50-ohm stripline as detectors of 9-kMc energy with no external bias applied. By applying an external bias in the negative direction, the reflection coefficient of the diodes and their power detection can be controlled over a wide range. At a power level of 1 mw, the voltage reflection coefficient of a stripline 1N832 diode mount can be varied from approximately 0 to 90 per cent by varying the external bias from 0 to -3.0 volts. (See Fig. 2.)

The operation of the attenuator of Fig. 1 is as follows:

1) At any bias setting, the reflected energy from the diodes will emerge from Arm 4 if Arms 2 and 3 are equal in length. Thus Arm 1 will be matched at the center frequency of the device.

2) With the control voltage *V* set to -3.0 V, the diodes are back biased and maximum output signal is obtained at Arm 4. As *V* is varied from -3.0 to 0 V, the diode reflection decreases, the power absorbed by the diodes increases, and the output signal is attenuated.

The insertion loss of the device at the minimum attenuation setting, i.e., at -3.0

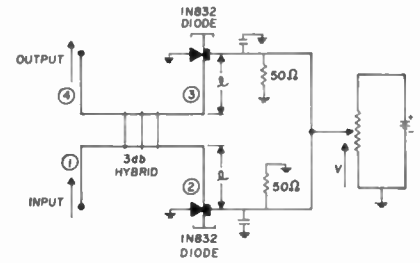


Fig. 1—Attenuator circuit.

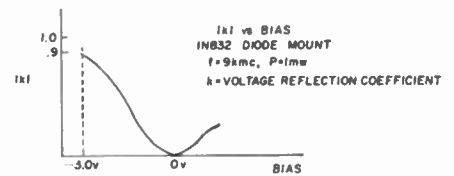


Fig. 2—Voltage reflection vs bias.

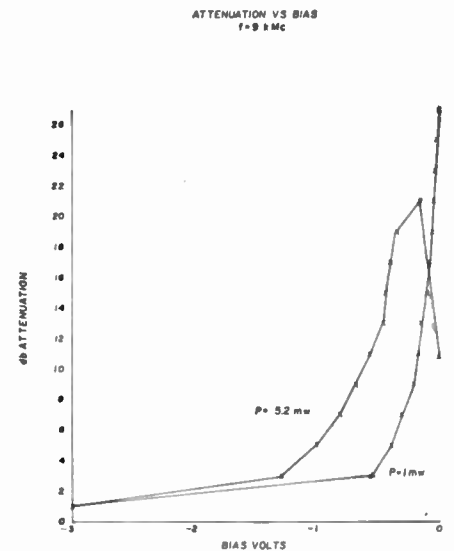


Fig. 3.

TABLE I
MEASURED DATA ON THE ATTENUATOR AT 9 KMC

Input	Bias Change	Attenuation Range
1-mw CW signal	-3.0 v to 0 v	26 db
5.2-mw CW signal	-3.0 v to 0 v	20 db
1-mw peak pulse (1 nsec)	-3.0 v to +0.12 v	15 db

V, is approximately 1 db. The attenuation characteristic of the device at 9 kMc is illustrated in Fig. 3 for input powers of 1.0 and 5.2 mw. A summary of measured data on the attenuator is given in Table I.

The pulse measurement was made using a 9-kMc carrier pulse whose half-power width is 1 nsec. The detection of the pulse is accomplished by the use of a special-purpose sampling oscilloscope.¹ The results of the

¹ A. S. Farber, "Sampling oscilloscope for millimicrosecond pulses at a 30-Mc repetition rate," *Rev. Sci. Instr.*, vol. 31, no. 1, pp. 15-17; January, 1960.

* Received by the IRE, July 26, 1961.
¹ J. Djuric, "Gravitational fields," *Proc. IRE* (Correspondence), this issue, p. 1689.

* Received by the IRE, July 26, 1961

pulse measurements indicate that the device is usable for at least a 10 per cent bandwidth. In addition, the control voltage can be a very fast waveform since the low-pass filter at the video terminals of the diode mount was designed for transmission of 1-nsec video pulses.

P. L. FLEMING
Res. Center IBM Corp.
Yorktown Heights, N. Y.

A Method of Displaying Ultra-Fast Limit Cycles or Three-Parameter Trajectories*

In studying the operation of nonlinear circuits with complex loads, there is often a need for determining trajectories of the instantaneous operating point when the circuit is in a dynamic state. The effects of different device parameters or circuit element values are usually such that computation of the trajectories is extremely tedious and time-consuming without the use of simplifying piece-wise approximations or the use of an electronic computer. Even with the aid of computers, however, it is desirable to check the solutions with experiment. Further, if the trajectories could be determined simply and accurately by experiment, experiment itself could serve as a useful design tool for many cases of interest. This correspondence describes a method of displaying,

on an X-Y scope, trajectories for circuits switching as fast as 0.2 nanosecond. This method (Fig. 1) was devised in the course of a study to develop means of accurately predicting switching times of diodes, transistors and tunnel diodes. For present purposes, the method will be illustrated by the specific example of displaying I-V trajectories of a tunnel diode switch.

This author had independently derived the same solutions as Schuller and Gärtner¹ for switching of tunnel diodes, and used the circuitry of Fig. 1 to verify the results. The reader is therefore referred to Schuller and Gärtner's paper for the theory and background for the example to follow. For the same circuit as Fig. 3 of the reference, and conditions between cases 4 and 6 in Fig. 4, the I-V trajectories displayed by the circuit of Fig. 1 are shown in Fig. 2. Here the tunnel diode was pulsed with a triangular wave-shape having a base width of 2.5 nsec. Using the methods discussed in the reference and superimposing the static current-voltage characteristics of the tunnel diode, these traces can aid considerably in detailed transient analysis.

An especially useful feature of the newer sampling scopes is the provision for shifting,

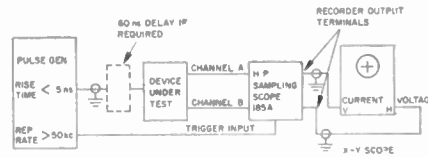


Fig. 1—Test setup for display of I vs V plot of a tunnel diode.

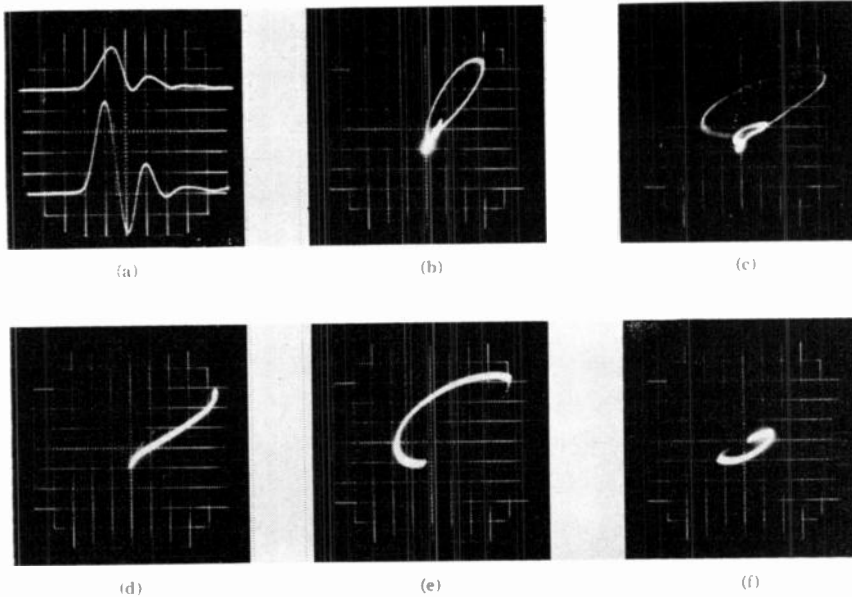


Fig. 2—Trajectories on a I-V plot. (a) Top curve: current through the diode, 5 ma/cm. Bottom curve: voltage across the diode, 100 mv/cm. Time scale; 5 nsec/cm. The diode inductance was increased to 150 mμh by adding a small inductor to show ringing. Rise time and fall time of applied pulse ~1 nsec. (b) I (2.5 ma/cm) vs V (100 mv/cm) without inserted inductance. (c) I (2.5 ma/cm) vs V (100 mv/cm) with 150 mμh series diode inductance. (d) I (2.5 ma/cm) vs V (100 mv/cm) for the first 5 nsec, with L = 150 mμh. (e) I (2.5 ma/cm) vs V (100 mv/cm) for the second 5 nsec, with L = 150 mμh. (f) I (2.5 ma/cm) vs V (100 mv/cm) for the third 5 nsec, with L = 150 mμh.

under direct manual control, a "window" along the sweep and expanding time within the window. Thus one can examine any particular portion of a trajectory down to picosecond times. This is shown in Fig. 2(d)-(f) where the trajectory of Fig. 2(c) is broken into 5-nsec segments to provide a very clear insight into the dynamic processes in the circuit.

WILLIAM T. RHOADES
Ground Systems Division
Hughes Aircraft Company
Fullerton, Calif.

An Extension of Newtonian Relativity to Include Electromagnetic Phenomena*

The Newtonian relativity, together with the Galilean Transformation (the G.T.), when extended to include electromagnetic phenomena, predicts that the velocity of light with respect to the observer is not always a constant, but instead is a quadratic function of the purely relative velocity of its source. To understand this, we must consider the equivalence of two inertial frames of reference, X and Y, in terms of line elements in a Euclidean 4-space:

$$\delta_{ij}dx^i dx^j = \delta_{ij}dy^i dy^j, \tag{1}$$

where

$$(\delta_{ij}) = \begin{pmatrix} 1 & 0 & 0 & 0 \\ 0 & 1 & 0 & 0 \\ 0 & 0 & 1 & 0 \\ 0 & 0 & 0 & 1 \end{pmatrix}.$$

On account of the equivalence, the observer can arbitrarily be stationed in either isotropic frame; therefore, let $y_4 = ict/\alpha_{xy}$ and let $x_4 = itc/\alpha_{xy}$, where α_{xy} is to be regarded as a refractive index for light originating in the X frame when viewed by an observer stationary in the Y frame. In accordance with the G.T., and with Newton's definition, the time t is independent of the metrical considerations, and distances are invariant under the transformation.

Now a minimal statement of Poincaré's principle of relativity is that the relative space of any arbitrarily selected observer whatsoever shall possess only a quadratic optical isotropy. There is no physical justification for including linear optical effects in this principle, and recently several tests have been suggested whereby this matter may be more closely examined.¹⁻⁴ Regardless of the out-

* Received by the IRE, July 18, 1961.
¹ P. M. Rapier, "A proposed test of the constancy of the velocity of light," Proc. IRE (Correspondence), vol. 49, p. 1322; August, 1961.
² J. Palacios, "The postulates of a new theory of relativity," Rev. Roy. Acad. Exact. Sci. Madrid, vol. 54, pp. 313-330; July, 1960.
³ M. Ruderfer, "Relativity: blessing or blindfold?" Proc. IRE, vol. 48, pp. 1661-1662; September, 1960.
⁴ H. Dingle, "Relativity and electromagnetism: an epistemological appraisal," Phil. Sci., vol. 27, pp. 233-253; July, 1960.

¹ M. Schuller and W. Gärtner, "Large-signal circuit theory for negative-resistance diodes, in particular tunnel diodes," Proc. IRE, vol. 49, pp. 1268-1278; August, 1961.

* Received by the IRE, August 25, 1961.

come of these experiments, however, the conditions for quadratic isotropy for the assumed observer in the Y frame must be

$$\sum_1^3 dy_i^2 = 0, \quad \text{and} \quad \alpha_{yy} = 1,$$

with the latter requirement necessary because it has been well established that every observer will measure the two-way velocity of light from a source rigidly connected with his frame as the universal constant c . With these substitutions, (1) has a unique solution for the effect of relative motion upon the refractive index of free space

$$\alpha_{xy} = 1/(1 + V^2/c^2)^{1/2}. \quad (2)$$

The velocity of the light received from a relatively moving source, therefore, turns out to be c/α_{xy} , which is not a constant at all, but is a symmetrical quadratic function of the relative velocity. If this quantity is designated by C_{mn} , where m and n are dummy indices, (2) becomes

$$\alpha_{mn} = \alpha_{nm} = (1 - V^2/C_{mn}^2)^{1/2}, \quad (3)$$

so that when m equals n , α_{mn} equals unity. Now under the Lorentz Transformation, (the L.T.), α_{mn} is written as $(1 - v^2/c^2)^{1/2}$, wherein v/c should have been written V/C_{mn} , or $V\alpha_{mn}/c$. Hence, it turns out that v , the relativistic velocity appearing in Einstein's equations, actually equals $V\alpha_{mn}$; since by definition of a velocity, $V \equiv dX/dt$, it follows that $v \equiv \alpha_{mn}dX/dt$, which is not a velocity at all, but is simply a mathematical abstraction.⁴ Therefore, one result of the L.T. is to cause real physical quantities to appear as variants and purely abstract notions to appear as invariants in the physical equations. This might appear to be good mathematics, but it is certainly not good physics. In any satisfactory physical theory, we expect only those quantities to be invariant that have an objective significance, e.g., that can be identified directly with the real properties of real bodies.

If we let β_{mn} equal V/C_{mn} , we can employ the 4-vector addition of velocities, *viz*,

$$\beta_{xz} = (\beta_{xy} + \beta_{yz})/(1 + \beta_{xy}\beta_{yz}), \quad (4)$$

whereby a single G.T. takes the place of two separate ones. This theorem explains at once Fizeau's results with moving liquids, Fresnel's dragging coefficient, $1/n^2$, and Airy's experiment. In the case of Ruderfer's experiment,⁵ Townes' maser experiment,⁶ and the Michelson-Morley experiments, the apparatus is moving along in space with the observer with an absolute velocity

$$\left(\sum_1^3 dy_i^2 \right)^{1/2} / dt.$$

⁵ M. Ruderfer, "First order terrestrial ether drift experiment," *Phys. Rev. Lett.*, vol. 5, pp. 191-192; September 1, 1960.
⁶ C. H. Townes and J. Cedarholm, "A new experimental test of special relativity," *Nature*, vol. 184, pp. 1350-1351; October 31, 1959.

However, because of the isotropy of this frame we have already seen that

$$\sum_1^3 dy_i^2$$

equals zero. Since this is a vector, it vanishes identically in all coordinate systems, along with all effects of the absolute motion on the apparatus. For these, and for all similar experiments, Newtonian relativity predicts precisely null results.

An important consequence of the principle of relativity presented herein is that it requires the existence of an aether which has a velocity-dependent index of refraction. The principle also admits the possibility that relative space may be linearly anisotropic with respect to the propagation of electromagnetic waves. Thus, experiments yielding first-order positive results, such as the Sagnac experiment, the aberration of starlight, Courvoisier's observations,³ and the Pound-Rebka experiments,⁷ which contradict Einstein's principle, are explained under Newtonian concepts in a classical manner. It is obvious from the foregoing discussion that the concepts presented herein do not admit the possibility of "action at a distance." Finally, they do not pretend to explain everything upon the elusive basis of two mutually contradictory postulates, as is the fad with modern theoreticians, but instead possess an inner consistency that renders them completely free from paradoxes.

The basic consequence that the velocity of light in the aether is a quadratic function of the relative velocity of its source has only recently been verified in a series of experiments by electronic techniques that will be the subject of a separate communication.

PASCAL M. RAPIER
 Newtonian Science Found.
 Richmond, Calif.

⁷ C. W. Sherwin, "Some recent experimental tests of the clock paradox," *Phys. Rev.*, vol. 120, pp. 17-21; October 1, 1960.

Maser Terminology*

I would like to suggest a change in terminology for stimulated emission devices. Since devices operating in the optical and infrared spectra have been demonstrated recently, the terminology has become unwieldy and confusion reigns. At present there are masers, mosers, losers, lasers, irasers, presumably irosers, optical masers, infrared masers, etc., ad infinitum.

Since the term *maser* represents *Micro-wave Amplification by Stimulated Emission of Radiation*, it is a mistake to designate a device which does not amplify and does not operate in the microwave spectrum an *optical maser*. The term *loser* has been objec-

tionable because no one wants to *lose*. In addition to these objections it would be much better to have a common name for devices which are identical in principle.

I believe the following names would be comprehensive enough to cover the entire group of devices, would be simple, and would show enough similarity to present terminology to permit recognition by persons not yet acquainted with the change.

- E^mma'ser for *Electromagnetic amplification by stimulated emission of radiation*.
- E^mmo'ser for *Electromagnetic oscillation by stimulated emission of radiation*
- Or, to misquote Dr. A. L. Schawlow, Emaser can represent "Extensive money acquisition schemes for expensive research."

WILLIAM R. MALLORY
 G.E. Advanced Electronics Ctr.
 Ithaca, N. Y.

Technique for Amplitude Modulating a Van Atta Radar Reflector*

In Bauer's recent communication,¹ he discussed the possibility of designing a satellite which, through use of a Van Atta radar reflector and radar absorber material, would be undetectable by enemy radars. At the same time, this satellite could be tracked by friendly radars through illumination "with the appropriate coded signal which would be answered by coding the modulation of the Van Atta array. During the time when no interrogation was being effected the array would be biased to a zero state to reduce the radar cross section to a minimum."

The analysis of amplitude modulation of the reflector concerned itself with a monostatic radar illuminating the array from an arbitrary direction. By varying phase shift in the interconnecting transmission lines of the array, one can modulate the signal radiated in the direction of the illuminating radar. The modulation is in fact the result of varying the direction of the reradiated signal and not its total energy. While it is easy to adjust phase shift so that monostatic echo in a given direction is minimized, it is impossible to do this for all incidence angles simultaneously. Unless energy incident on the array was absorbed in some manner, it always would be possible to choose positions for an illuminating radar which would provide the radar with the maximum echo of which the array was capable.

WILLIAM F. BAHRET
 Reconnaissance Laboratory
 Aeronautical Systems Div.
 Wright-Patterson AFB, Ohio

* Received by the IRE, May 3, 1961.
¹ L. H. Bauer, *Proc. IRE (Correspondence)*, vol. 49, pp. 634-635; March, 1961.

* Received by the IRE, July 26, 1961.

Some Ladder Networks Representing Certain Transcendental Numbers—Classroom Note*

The numerical computation of important irrational and transcendental numbers such as $\sqrt{2}$, π , e and $\log 2$ has been the subject of historical mathematical investigations. It may be of some recreational and possibly practical interest to scientists and engineers to suggest sequences of simple resistive circuits whose resistances asymptotically approach the values of such numbers.

For an applied voltage of 1 volt, the input current of the circuit of Fig. 1, asymptotically approaches the value of $1/\sqrt{2}$ amperes if a larger and larger number of ladder sections are considered.

Similarly, the input resistances of the networks in Figs. 2-4 approach the values of $\pi/2$, e and $\log 2$, respectively. In all four cases, appropriate continued fractions have been chosen leading to familiar grounded ladder circuits. It was thought that the suggested network realization might be considered as an electrical engineering method for the evaluation of these basic numbers. The students in a laboratory course, for instance, may find this an interesting exercise. In each of the given four cases, the mathematical computation involved is rather trivial, but it can be further pursued by referring to classical work on continued fractions.^{1,2} The derivation of the foregoing expansions are given in Wall or Perron. Admittedly, we have selected expansions leading to resistive grounded ladder with simple numerical values for resistors. No effort has been made to arrive at particularly rapidly converging resistive structures. This can be done by selecting faster converging expansions if so desired.

The more enthusiastic reader may wish to pursue this matter further by synthesizing other well-known expansions in resistor-capacitor or resistor-inductor ladder

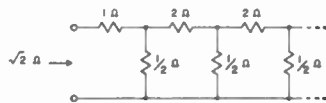


Fig. 1— $\sqrt{2} = 1 + \frac{1}{2 + \frac{1}{2 + \frac{1}{2 + \dots}}}$

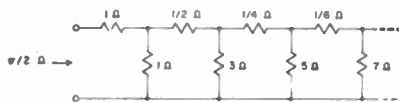


Fig. 2— $\frac{\pi}{2} = 1 + \frac{1}{1 + \frac{1.2}{1 + \frac{2.3}{1 + \frac{3.4}{1 + \dots}}}}$

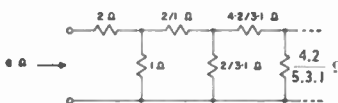


Fig. 3— $e = 2 + \frac{2}{2 + \frac{3}{3 + \frac{4}{4 + \frac{5}{5 + \dots}}}}$



Fig. 4— $\log 2 = \frac{1}{1 + \frac{1}{1 + \frac{4}{1 + \frac{9}{1 + \frac{16}{1 + \dots}}}}}$

circuits. The following expansions are cited for those who wish to undertake such exercises. The pertinent mathematical discus-

sions (convergence, etc.) can be found in Wall.¹

F. REZA
Dept. of Elec. Engrg.
Syracuse University
Syracuse, N. Y.

Performance Degradation of Linear FM-Pulse-Compression Systems Due to the Doppler Effect*

In a recent correspondence¹ Cook has presented an analysis of linear FM pulse compression. It is possible to perform a similar analysis based on a more exact model of the Doppler effect. In doing so, a fundamental limitation of the linear FM pulse-compression technique becomes apparent.

Using the transmitted waveform as it leaves the antenna for phase and time reference, one can write for the transmitted waveform

$$S(\omega) = \text{rect} \frac{\omega - \omega_c}{\Omega} \exp j[a(\omega - \omega_c)^2] \quad (1)$$

In (1), $\text{rect} (\omega - \omega_c/\Omega)$ denotes a rectangular amplitude spectrum centered around ω_c having a bandwidth Ω . The corresponding phase-matched² filter (the compression filter) is described by

$$F(\omega) = \text{rect} \frac{\omega - \omega_c}{(1 + \epsilon)\Omega} \cdot \exp j[b_0 + b_1(\omega - \omega_c) - a(\omega - \omega_c)^2] \quad (2)$$

The factor $1 + \epsilon$ implies that the phase-matched filter is wide enough to accept Doppler-shifted signals without reducing the signal bandwidth.

When a moving target is radar-illuminated, each frequency component in the transmitted waveform suffers a frequency shift due to the Doppler effect. A frequency ω is, upon return, observed as a frequency

$$\omega \frac{1 + \nu/2}{1 - \nu/2}$$

The quantity ν equals $2v_r/c$, where v_r is the relative velocity between radar and target along their connecting line and c is the speed of light. The expression given above for the Doppler-shifted return is exact except for relativistic effects. Since ν , however, is always much smaller than 1 even for orbital velocities, one can write for the Doppler effect, $\omega(1 + \nu)$ or, as well, $\omega/(1 - \nu)$. In many cases it is sufficient to treat the return as if it were translated in frequency by an amount $\omega_d = \nu\omega_c$, the Doppler shift of the center frequency. This was the procedure used by Cook. The present analysis takes into account that in fact each frequency component is shifted by an amount $\nu\omega$, and thus an expression for the radar return from a moving target is

* Received by the IRE, July 14, 1961; revised manuscript received, July 25, 1961.

¹ C. E. Cook, "General matched-filter analysis of linear FM-pulse compression," *Proc. IRE* (Correspondence), vol. 49, p. 831; April, 1961.

² H. O. Ramp and E. R. Wingrove "Principles of pulse compression," *IRE TRANS. ON MILITARY ELECTRONICS*, vol. M1L-5, pp. 109-116; April, 1961.

* Received by the IRE, July 26, 1961.
¹ H. S. Wall, "Analytic Theory of Continued Fractions," D. Van Nostrand Co., Inc., New York, N. Y.; 1948.
² O. Perron, "Die Lehre von den Kettenbrüchen," B. G. Teubner, Leipzig and Berlin, Ger., 2nd ed.; 1929.

$$\log(1+s) = \frac{s}{1 + \frac{1^2 s}{2 + \frac{1^2 s}{3 + \frac{2^2 s}{4 + \frac{2^2 s}{5 + \frac{3^2 s}{6 + \dots}}}}}$$

$$\int_0^\infty \frac{e^{-nu} du}{(1+su)^a} = \frac{1}{1 + \frac{1 \cdot s}{1 + \frac{(a+1)s}{1 + \frac{2 \cdot s}{1 + \frac{(a+2)s}{1 + \frac{3 \cdot s}{1 + \dots}}}}}$$

$$R(\omega) = \text{rect} \frac{(1 - \nu)\omega - \omega_c}{\Omega} \cdot \exp j\{c_0 + c_1[(1 - \nu)\omega - \omega_c] + a[(1 - \nu)\omega - \omega_c]^2\}. \quad (3)$$

The output, given by $R(\omega) \cdot F(\omega)$, is

$$O(\omega) = \text{rect} \frac{\omega - (1 + \nu)\omega_c}{(1 + \nu)\Omega} \cdot \exp j\{d_0 - d_1\omega_c + (d_1 - c_1\nu + 2a\nu\omega_c)\omega - a\nu(2 - \nu)\omega^2\}, \quad (4)$$

where $d_0 = b_0 + c_0$ and $d_1 = b_1 + c_1$. Interpreting (4), one finds that

- 1) The center frequency of the output spectrum is $(1 + \nu)\omega_c$, compared to $(1 + \nu/2)\omega_c$ in Cook's treatment. This difference occurs because different receiving filter bandwidths were assumed in each case.
- 2) The bandwidth of the signal has changed to $(1 + \nu)\Omega$, *i.e.*, is wider or narrower, depending on the sign of ν (ν is positive for decreasing range, negative for increasing range).
- 3) The constant phase is the same as in the case of a stationary target.
- 4) The coefficient of the linear term, $(d_1 - c_1\nu + 2a\nu\omega_c)$, gives the position of the output signal on the time axis. In particular d_1 is the round-trip time to target plus phase-matched filter delay and $-c_1\nu$ is a range- and velocity-dependent time shift, encountered with any radar waveform. The latter term is very small and can for all practical purposes be neglected. The term $2a\nu\omega_c$ is a time shift dependent on the waveform parameters and carrier-frequency Doppler shift. This shift is typical for linear FM pulse-compression systems and was also noted by Cook.
- 5) The last term, $-a\nu(2 - \nu)\omega^2$, is of particular interest. It indicates that a phase-slope dispersion² exists in the output signal. A consequence of this dispersion is a widening of the output pulse, *i.e.*, the output pulse due to a moving target is wider than the output pulse due to a stationary target.

Time did not permit continuing the above analysis to obtain the pulse widening quantitatively. An estimate can be obtained quickly, however, by performing a similar analysis³ starting with a transmitted waveform having a Gaussian-amplitude spectrum and parabolic-phase spectrum $S(\omega)$, with corresponding phase-matched filter response $F(\omega)$; thus

$$S(\omega) = e^{-b\omega^2} e^{j\omega^2} \\ F(\omega) = \text{rect} \frac{\omega}{(1 + \epsilon)\Omega} e^{-ja\omega^2}. \quad (5)$$

The analysis yields a compressed pulse length (between $1/e$ -points) of

$$\bar{\tau} = 4\sqrt{b} \sqrt{1 + \left(\nu \frac{\pi K}{2}\right)^2}, \quad (6)$$

where $2\pi K = T \cdot \Omega$, with T and Ω the phase-

slope dispersion and bandwidth of $S(\omega)$ between $1/e$ -points. Investigation of (6) shows the following: 1) $4\sqrt{b}$ is the shortest possible output pulse length and is obtained in case of ideal pulse compression, *i.e.*, for $\nu = 0$. 2) The pulse widening factor,

$$w = \sqrt{1 + \left(\nu \frac{\pi K}{2}\right)^2} \quad (7)$$

depends, as expected, on ν ; furthermore, it depends on only one more variable K , the compression ratio.

Eq. (7) can be used to obtain numerical values for the pulse widening due to the dispersive effects of target velocity. Assuming the case of two earth orbiting vehicles on collision course, v_r can approach 31,000 knots, *i.e.*, ν becomes 10^{-4} . For this speed and a compression ratio $K = 10,000$, the pulse widening factor is found to be 1.87. This means the actual compression ratio is $K_{\text{act}} = 5900$, which is a sizeable reduction from the original $K = 10,000$. With the pulse widening there also occurs an amplitude reduction, thus the SNR is reduced. This numerical example is based on a special waveform, but for other linear FM waveforms widening effects of the same order of magnitude can be expected.

The above analysis shows that a degradation of the performance of linear FM pulse-compression systems takes place when moving targets are illuminated. The degradation, which is in form of a pulse widening and loss in SNR is minor for present-day systems and targets. However, for advanced pulse-compression systems in a space environment, the degradation can become serious.

H. O. RAMP
E. R. WINGROVE, JR.
Electronics Lab.
General Electric Co.
Syracuse, N. Y.

Doppler-Shift Effects in Space Propagation*

Space propagation involves propagation within an ionosphere for great distances. Unlike common experience, however, the ionosphere is the ionosphere of the sun, and the ion and electron concentration is very low near the earth's orbit.

"Steady-state" propagation in this type of field has been examined in several papers.¹ This note examines approximately the effect of non-steady-state conditions on Doppler shift to obtain an estimate of the magnitude of possible effects. The non-steady-state conditions may result from a change in electron concentration, or from the motion of a plasma stream, or from both, these being characteristic of disturbed solar conditions.

* Received by the IRE, July 26, 1961.
¹ C. N. Lee, "Space-to-space propagation phenomena," in "Advances in Astronautical Sciences," vol. 3, Plenum Press, New York, N. Y., 1958.
² G. Kuiper, "The Sun," University of Chicago Press, Chicago, Ill., 1953.

The dielectric constant in the presence of free electrons is

$$k^2 = 1 - \frac{81N}{f^2} \quad (1)$$

where N = concentration, electrons per cc, f = frequency, kc. The phase of a radio signal at a receiver, referred to the transmitter, is

$$\varphi_r = \omega t - \frac{2\pi}{\lambda_0} \int_T^R k dx, \quad (2)$$

where ω = transmitter frequency, and λ_0 = vacuum wavelength.

The instantaneous received frequency is

$$2\pi f_r = \frac{d\varphi_r}{dt} = \omega - \frac{2\pi}{\lambda_0} \frac{d}{dt} \left(\int_T^R k dx \right), \quad (3)$$

which may be written as

$$\frac{\Delta f}{f} = \frac{1}{C} \frac{d}{dt} \left(\int_T^R k dx \right) \quad (4)$$

for straight-line propagation. R and T are receiver and transmitter locations. C is the velocity of light.

In order to evaluate this expression, consider several specific cases.

Case 1): Moving constant-width and constant-density electron cloud between R and T . Let x_1 , x_2 be the boundaries of the cloud. Then (4) becomes

$$\frac{\Delta f}{f} = \frac{1}{C} \frac{d}{dt} \left[\int_T^{x_1} dx + \int_{x_2}^R k dx + \int_{x_1}^{x_2} dx \right]. \quad (5)$$

Since the sum of the first and last terms is constant, and the middle term is also constant, there is no Doppler shift.

Case 2): Moving constant-density electron cloud surrounding R . Let x be the position of the edge of the cloud. Then (4) may be written as

$$\frac{\Delta f}{f} = \frac{1}{C} \frac{d}{dt} \left[\int_T^x dx + \int_x^R k dx \right]. \quad (6)$$

The magnitude of the term in brackets changes linearly with the velocity of the edge of the cloud, the slope being equal to $(1 - k)$. Therefore,

$$\frac{\Delta f}{f} = \frac{1}{C} (1 - k) \frac{dx}{dt}. \quad (7)$$

Case 3): Stationary, constant-width cloud of variable density. In this case the middle term in brackets of (5) is not a constant, and (5) becomes

$$\frac{\Delta f}{f} = \frac{1}{C} (x_2 - x_1) \frac{dk}{dt} \\ = \frac{x_2 - x_1}{C} \frac{81}{2f^2} \frac{dN}{dt}. \quad (8)$$

Case 4): Expanding cloud of constant density between R and T . This can be evaluated by assuming that an auxiliary receiver-transmitter unit is located at the center of the cloud. Then, assuming that both edges are moving at the same rate,

$$\frac{\Delta f}{f} = \frac{2}{C} (1 - k) \frac{dx}{dt}. \quad (10)$$

Case 5): An electron cloud expanding so that the total number of electrons is con-

³ H. A. Wheeler, "The solution of unsymmetrical-sideband problems with the aid of the zero-frequency carrier," Proc. IRE, vol. 29, pp. 446-458; August, 1941.

stant. This may be solved by introducing the linear assumption

$$\Delta f \text{ (total)} = \Delta f \text{ (width change)} \\ + \Delta f \text{ (density change)}, \quad (11)$$

which combines cases 2) and 3).

The magnitude of these effects is of interest. Assume that

$$f = 10^8 \text{ kc} \\ N = 1000 \text{ electrons/cc} \\ dN/dt = 1 \text{ electron/sec} \\ x_2 - x_1 = 300,000 \text{ km} \\ C = 300,000 \text{ km/sec} \\ dx/dt = 50 \text{ km/sec.}$$

Then the Doppler shifts for the various cases are

$$\text{Case 1) } f = 0 \text{ cps} \\ \text{Case 2) } f = 70 \text{ cps} \\ \text{Case 3) } f = 40 \text{ cps} \\ \text{Case 4) } f = 140 \text{ cps} \\ \text{Case 5) } f = 110 \text{ cps.}$$

These appear to be negligible, except in single-sideband transmission, or in precision tracking. Closer to the sun, where the electron concentration is greater and the gas clouds move more rapidly, the various effects of changes in the propagation medium would appear to become very important in most modes of communication.

R. P. HAVILAND
Missile and Space Vehicle Dept.
General Electric Co.
Philadelphia, Pa.

Comment on Shot-Noise Smoothing Mechanism Proposed by LaRosa and Wilhelmsen*

In a recent note to this department,¹ La Rosa and Wilhelmsen (L. and W.) advance a theory of noise smoothing in tunnel diodes. The theory is based on the argument that the tunneling probability p is approximately $\frac{1}{2}$, and therefore a binomial rather than a Poisson distribution should be used to describe the number of electrons tunneling during an interval of observation (θ , T). This change in distribution leads, according to L. and W., to a reduction of shot noise by a factor of $(1-p) \approx \frac{1}{2}$.

Although noise measurements of tunnel diodes^{2,3} show full shot noise, the possibility of reduced shot noise would be of great theoretical and practical interest. We therefore wish to present arguments that the mechanism suggested by L. and W. will not lead to shot noise smoothing.

* Received by the IRE, April 11, 1961.

¹ R. La Rosa and C. R. Wilhelmsen, "Theoretical justification for shot-noise smoothing in the Esaki diode," *Proc. IRE (Correspondence)*, vol. 48, p. 1903; November, 1960.

² J. Tieman, "Shot noise in tunnel diode amplifiers," *Proc. IRE*, vol. 48, pp. 1418-1423; August, 1960.

³ C. A. Lee and H. Montgomery, *Bull. Am. Phys. Soc.*, vol. 5, p. 160; 1960.

Consider an electron in the conduction band; it is rapidly being scattered by its interaction with the lattice, and every so often its momentum, after a scattering process, is such as to permit it to tunnel. In this manner we may speak of the electron impinging on the barrier so many times per second. Now if the probability of tunneling is of the order of $\frac{1}{2}$, as suggested by L. and W., then a binomial distribution is indeed appropriate to describe the number of successes resulting from a given number of trials. Unfortunately, measurement of the current is only sensitive to the number of successes in a given interval of observation, and we have no way of knowing how many failures there were or when they occurred. To observe the second moment of the binomial distribution, as suggested by L. and W., would require that this knowledge of the total number of trials at least be implicit in the measurement.

The quantity from which the power spectrum is correctly obtained is the correlation function of the current

$$\psi(\tau) = \langle I(t)I(t + \tau) \rangle.$$

Then, making the usual assumption that the current may be expressed as a superposition of impulses occurring independently at random times t_i ,

$$I(t) = \sum_i F(t - t_i),$$

and if we also assume that the probability of the occurrence of an impulse in the interval dt is a constant independent of the time, it can be shown that⁴

$$\psi(\tau) = \nu \int_{-\infty}^{\infty} F(t)F(t + \tau)dt.$$

This expression for the correlation function⁵ involves an average over the arrival times of the impulses and an average over the distribution of the number of impulses arriving in an interval of observation (θ , T). It should be noted that these assumptions are sufficient to determine uniquely a Poisson sequence for the times t_i . We now observe that only the first moment ν (the average number of particles per second) appears, and that white noise will be observed up to frequencies comparable to the inverse width of a current pulse.

It is consistent with the present view of direct tunneling processes that individual pulses should be uncorrelated (*i.e.*, the times t_i) for "intervals" much greater than the dielectric relaxation time of the semiconductor material. By "interval" we mean the time between successive particles within a volume where the space charge of a particle which has just made a tunneling transition will alter appreciably the tunneling probability of the succeeding particle.

It is now apparent that for independent tunneling events, full shot noise will be observed regardless of the magnitude of the tunneling probability⁶ p . A large value of p can only lead to reduced noise insofar as

⁴ S. O. Rice, *Bell Sys. Tech. J.*, vol. 23, pp. 282-332; July, 1944.

⁵ The term giving the dc power has been neglected.

⁶ Estimates of the tunneling probability for the types of junctions described in the literature are many orders of magnitude less than $1/2$.

it might induce a correlation between the times t_i ; for example, the "interval" between particles may become comparable to the dielectric relaxation times.

An exception to these remarks probably should be made for "excess" current where tunneling involves intermediate states. Associated with this type of tunneling transition, time constants of the order of 10^{-8} to 10^{-9} seconds have been observed.⁷ At frequencies whose periods are equal to or less than these time constants, something less than full shot noise might be observed, depending, of course, on the nature of the correlation between successive events which is associated with these time constants.

The authors wish to thank H. C. Montgomery and J. P. Gordon for helpful discussions.

C. A. LEE
A. YARIV
Bell Telephone Labs.
Murray Hill, N. J.

⁷ F. F. Fang, paper presented at Symp. on Electron Tunneling in Solids, Philadelphia, Pa.; January, 1961 (unpublished). A symposium report by E. O. Kane is to be published which contains Fang's remarks.

Vacuum-Tube Networks*

Some years after the paper by Llewellyn and Peterson under the above title was published,¹ I discovered an error in the equation for the anode current in a triode. At my suggestion, the senior author reviewed the derivation and found himself in agreement with my result. At that time I was outlining a paper in which the equation questioned would be used, and by agreement with Dr. Llewellyn the error was to be pointed out in my paper and the revised expression employed. The paper became too long, and before publication it was shortened by omitting any discussion of transit time effects. Meanwhile, my intention of calling attention to the necessary change was forgotten.

In view of the continued basic importance of the Llewellyn-Peterson paper, the equation mentioned should be corrected. Reference is to the last term in the denominator of (50a). As published, this is

$$- \zeta_2 \left(1 - \frac{\theta_2}{2\theta_1} + \frac{\theta_1}{2\theta_2} \right),$$

but should be

$$- \frac{\zeta_2}{2\theta_1\theta_2} (\theta_1 + \theta_2)^2.$$

The meanings of the letter symbols are the same as in the original paper.

GEORGE D. O'NEILL
General Telephone &
Electronics Labs. Inc.
Bayside, N. Y.

* Received by the IRE, August 10, 1961.

¹ F. B. Llewellyn and L. C. Peterson, "Vacuum-tube networks," *Proc. IRE*, vol. 32, pp. 144-166; March, 1944.

Flow Graphs and Tapered Transmission Lines*

If a transmission line with continuous taper is approximated by a cascade of short, separately uniform segments, the determination of the reflection coefficient is a problem in linear algebra; hence, the signal flow-graph technique¹ may be applied. In this instance, as in so many others, the flow graph reveals the "structure" of the problem clearly.

Suppose that a continuously nonuniform transmission line is approximated by a line with n uniform segments. The j th segment, centered at x_j , is to have a uniform characteristic impedance Z_j equal to $Z(x_j)$ of the original line. The reflection coefficient $r_{j,j+1}$ between the j th and $j+1$ st segments is obtained from the Fresnel reflection formula

$$r_{j,j+1} = \frac{Z_{j+1} - Z_j}{Z_{j+1} + Z_j} \quad (1)$$

which, for short segments and moderate taper, becomes

$$r_{j,j+1} \cong \frac{\Delta Z_j}{2Z_j} \quad (2)$$

The phase change across the j th segment is given by

$$\exp\{-\gamma_j(x_{j+1} - x_j)\} = \exp\{-\gamma_j \Delta_j x\}, \quad (3)$$

The behavior of a cascade of uniform segments is described by a set of linear simultaneous equations relating the forward and backward wave values at the segment boundaries. The signal flow-graph representation of this set of equations is shown in Fig. 1.

This graph may be simplified by noting that all "looped" paths (those which pass through any node more than once) are at least two orders higher in the reflection coefficients than the "direct" paths. Under the assumption that $|r_{jk}| \ll 1$, the looped paths may be ignored, which means that all of the upward-pointing transmittances may be removed. The resulting simplified graph is shown in Fig. 2.

The over-all reflection coefficient for n uniform segments,

$$R_n = \frac{E_{\theta}^-}{E_{\theta}^+} \quad (4)$$

is found by summing all possible paths in Fig. 2 from node E_{θ}^+ to node E_{θ}^- . For this situation a further simplification of the graph is obtained by noting that every path except r_{01} involves at least one pair of transmittances of the form $1+r_{jk}$ (going across the top of the graph) and $1-r_{jk}$ (coming back across the bottom). Since these transmittances occur in pairs, whose product $1-r_{jk}^2$ is approximately unity for short segments, all transmittances of the form $1 \pm r_{jk}$ on the top and bottom of the graph may be replaced by unity. The resulting graph is shown in Fig. 3.

* Received by the IRE, April 3, 1961; revised manuscript received, August 14, 1961.

¹ S. J. Mason, "Feedback theory—some properties of signal flow graphs," *Proc. IRE*, vol. 41, pp. 1144-1156; September, 1953.



Fig. 1—Signal flow-graph for n -section transmission line.

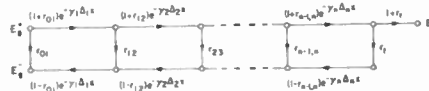


Fig. 2—Simplified flow-graph.

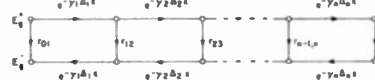


Fig. 3—Flow-graph for computation of reflection coefficient.

All paths from the E_{θ}^+ -node to the E_{θ}^- -node are now summed, giving

$$R_n = r_{01} + [r_{12} \exp\{-2\gamma_1 \Delta_1 x\} + r_{23} \exp\{-2(\gamma_1 \Delta_1 x + \gamma_2 \Delta_2 x)\} + \dots + r_{n-1,n} \exp\{-2(\gamma_1 \Delta_1 x + \dots + \gamma_{n-1} \Delta_{n-1} x)\} + r_t \exp\{-2(\gamma_1 \Delta_1 x + \dots + \gamma_n \Delta_n x)\}; \quad (5)$$

hence,

$$R_n = r_{01} + \sum_{j=1}^{n-1} \left[r_{j,j+1} \exp\left\{-2 \sum_{i=1}^j \gamma_i \Delta_i x\right\} \right] + r_t \exp\left\{-2 \sum_{k=1}^n \gamma_k \Delta_k x\right\} \quad (6)$$

The number of segments is now permitted to increase in such a manner that the largest $\Delta_j x$ becomes vanishingly small; therefore, from (2),

$$r_{j,j+1} \rightarrow r(x) = \frac{dZ(x)}{2Z(x)} = \frac{1}{2} \frac{d}{dx} (\ln Z) dx \quad (7)$$

and

$$-r_{j,j+1} \rightarrow -\gamma(x) dx.$$

Hence, from (6) and the definition of the Riemann integral,

$$R = \lim_{n \rightarrow \infty} R_n = r_{01} + \left[\int_0^l \frac{1}{2} \frac{d}{dx} (\ln Z) \cdot \exp\left\{-2 \int_0^x \gamma(s) ds\right\} dx \right] + \left[r_t \exp\left\{-2 \int_0^l \gamma(x) dx\right\} \right]. \quad (8)$$

This result is the same as that obtained by Bolinder,² differing only in the presence of terms to account for the input and terminating discontinuities.

FRANK M. BROWN

Captain, USAF

Dept. of Elec. Engrg.

Institute of Technology

Wright-Patterson AF Base, Ohio

Large Signal Interaction Between a Spiraling Electron Beam and the TE₁₀ Rectangular Waveguide Mode*

In the attempt to push microwave devices to higher power levels and frequencies, several workers have proposed the use of periodic beams and smooth circuits (waveguides) rather than smooth beams and periodic circuits. The smooth circuits have greater power dissipation capabilities which are required for high powers or frequencies. One of the simplest embodiments of this proposal is that of a beam spinning about an axial dc magnetic field in a rectangular waveguide propagating the TE₁₀ mode. This case will be considered here.

The success of a device of this sort depends on whether good bunching of the beam can be obtained. The bunching was investigated using the method of Webber¹ and Phillips,² where electron motion is observed in the presence of a constant RF circuit field. The equations of motion are used to find the position and velocity of injected electrons. Knowing the velocity of a group of electrons in an RF cycle, the efficiency can then be calculated using

$$\eta(t) = 1 - \frac{\sum_{i=1}^{N_0} v_i^2(t)}{N_0 v_0^2},$$

where v_0 is the initial electron velocity, $v_i(t)$ is the velocity of the i th electron at time t , and N_0 is the number of electrons considered per cycle. The equations were programmed on the Datatron 205-digital computer where eight electrons were considered under synchronous conditions at a 500-kw power level in S-band waveguide. The helical bunching described by Chow and Pantell³ was not observed, because the transverse electric fields completed the energy exchange with the electrons before the transverse magnetic fields could accomplish any bunching. The efficiency was negative, reaching -36 per cent after three cycles. The large negative efficiency was due to the predominant effect of the unfavorable electrons.

If a device of this sort is to work at higher power levels, some method must be found to quickly move these unfavorable electrons into a favorable phase. Looking at the axial and transverse equations of motion separately, conditions can be set up where the electrons move very quickly through the accelerating phase and are trapped in the decelerating phase. A second computer run was made for these conditions, with a power level in the guide of 4 megw. The transverse velocity was 0.7 c , and the axial velocity was 0.2 c , corresponding to a considerable

* Received by the IRE, August 11, 1961.

¹ S. E. Webber, "Electron bunching and energy exchange in a traveling-wave tube," *IRE TRANS. ON ELECTRON DEVICES*, vol. ED-4, pp. 87-91; January, 1957.

² R. M. Phillips, "The Ubitron, a high power traveling-wave tube based on a periodic beam interaction in unloaded waveguide," *IRE TRANS. ON ELECTRON DEVICES*, vol. ED-7, pp. 231-241; October, 1960.

³ K. K. Chow and R. H. Pantell, "The cyclotron resonance backward-wave oscillator," *Proc. IRE*, vol. 48, pp. 1865-1870; November, 1960.

² E. F. Bolinder, "Fourier transforms and tapered transmission lines," *Proc. IRE* (Correspondence), vol. 44, p. 557; April, 1956.

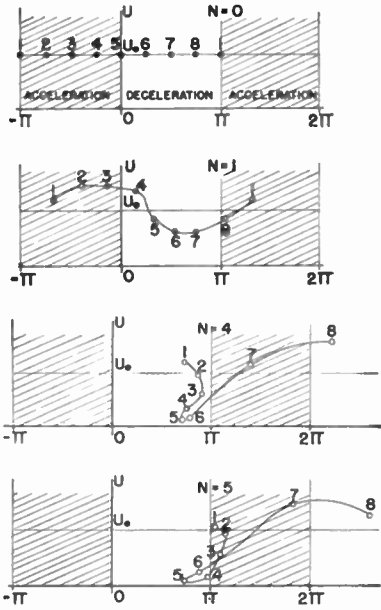


Fig. 1.

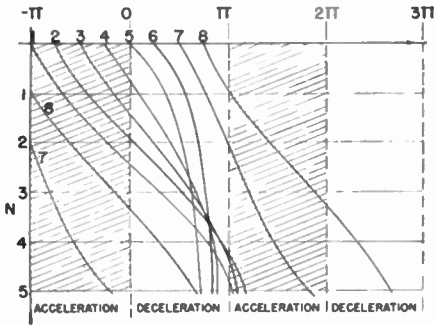


Fig. 2.

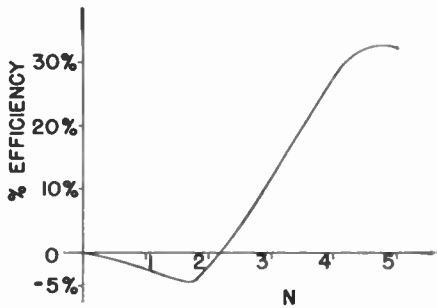


Fig. 3.

amount of over-velocity. The total electron kinetic potential U is shown vs phase position in Fig. 1 for $N=0, 1, 4,$ and 5 cycles. After one cycle the electrons have gained or lost energy according to their phase position. At four cycles a bunch has been formed and much energy has been extracted. At five cycles a saturation effect is expected as the bunch has now moved into the accelerating phase. An Applegate diagram for this process is shown in Fig. 2, where the formation of a bunch in the decelerating phase is evident. The efficiency is shown in Fig. 3. The

curve is as expected from Fig. 1, and a peak efficiency of 35 per cent is obtained.

This large signal bunching mechanism can give good efficiency, but the gain available is limited to something like 10 db due to the initial negative efficiency present. Higher efficiencies and gains may be possible as the conditions used in this computer run may not be optimum.

Our results have shown that although helical bunching is not possible at higher power levels, a large signal bunching mechanism is available. This large signal bunching can be obtained for over-velocity conditions where the electrons are trapped in the decelerating phase. Good efficiencies are available with modest gains, indicating an application as a high-power output tube.

W. L. DICKSON
C. C. JOHNSON
R. W. GROW
University of Utah
Salt Lake City, Utah

On Backward-Wave Oscillator Stabilization*

There has been and there will be an increasing need for a stable-tunable microwave source. These two requirements are generally incompatible in common microwave sources. The material herein reports the results of some preliminary work to provide a stable-tunable microwave source.

The experimental problem is specifically to stabilize a backward-wave oscillator (BWO) which is electrically tunable over an octave in S-band. In order to stabilize an oscillator, a frequency reference is needed. For an ideal stabilization system this is equivalent to putting the reference signal frequency through a high-gain amplifier with unity feedback; or, in other words, the stabilized microwave oscillator acts as a transfer network with a gain of one for the microwave reference. See Fig. 1. The loop gain of the stabilized system corresponds to the stabilization factor for the oscillator. The properties of the stabilization system will depend on whether an automatic frequency control (AFC) loop or an automatic phase control (APC) loop is used.¹⁻⁵ One serious limitation that appears to be present in this system is the additive or background noise which is introduced between the microwave mixer and the frequency discriminator or phase detector. See Fig. 2. This appears

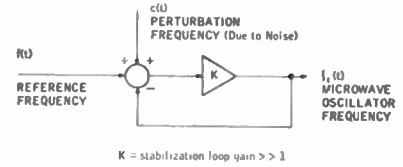


Fig. 1—Block diagram of ideal stabilization system.

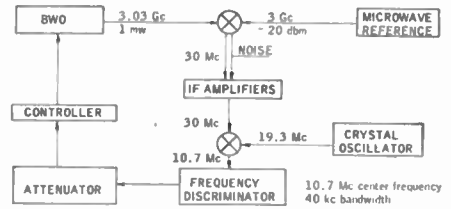


Fig. 2—Block diagram of actual stabilization system using AFC.

as an added input to the ideal system, shown in Fig. 1, and adds directly to the instability already present in the microwave oscillator frequency.

An S-band BWO (Sylvania 4198) with an inherent instability of at least 1 kc rms over a bandwidth of 5 kc, of which 200 cps is contributed by ripple from power supply, has been stabilized. An AFC loop with a bandwidth of 40 kc has been used to reduce the instabilities to 200-300 cps rms. The instabilities have been reduced further to 30 cps rms with the use of a 500 cps bandwidth low-pass filter in the AFC loop.

The reason for the improvement in stability with the addition of the low-pass filter appears to be the reduction of the background noise introduced in the mixer and preamplifier of the AFC loop. This corresponds to the phenomenon cited above as a limitation in the feasibility of providing a stabilized tunable microwave oscillator with a given microwave reference input.

R. B. CLARK
W. D. COMSTOCK
Syracuse Univ. Res. Corp.
Syracuse, N. Y.

Education and Creativity*

What Johnson¹ says bears repeating with great emphasis and not only for electronic engineering education.

In this age of swift and demanding technological progress, the learning of old tricks devised by our predecessors may preserve our present know-how by copy-cat techniques, but it will never advance the state of our science and arts in a world where others, advancing by leaps and bounds, leave us in relative obsolescence.

* Received by the IRE, August 19, 1961.
¹ R. W. Johnson, "Are Electronic Engineers Educated," Proc. IRE, vol. 49, p. 1319; August, 1961.

* Received by the IRE, August 16, 1961.
¹ K. V. Pound, "Frequency stabilization of microwave oscillator," Proc. IRE, vol. 35, pp. 1405-1415; December, 1947.
² W. G. Tuller, et al., "Recent developments in frequency stabilization of microwave oscillators," Proc. IRE, vol. 36, pp. 794-800; June, 1948.
³ M. Peter and M. W. P. Strandberg, "Phase stabilization of microwave oscillators," Proc. IRE, vol. 43, pp. 869-873; July, 1955.
⁴ T. J. Rey, "Automatic phase control: theory and design," Proc. IRE, vol. 48, pp. 1760-1771; October, 1960.
⁵ H. G. Pascalar, "An investigation of frequency stabilization techniques for backward-wave oscillators," M.I.T. Lincoln Lab., Lexington, Mass., Group Rept. No. 48.7; August, 1959.

When the text and reference books provide no answers for the myriads of challenging new problems, only creativity can find the answers. When the facts of science and engineering are taught, not as final dictums of design, but only as stepping stones to new methods and designs, then each student engineer will come to the realization that when he cannot find a way, he must *make* one!

Instead of placing his reliance on knowledge found or created by others in the past, he must learn that nothing man or nature ever created is perfect, that vast room for improvement exists in all things, that entirely new things and methods for accomplishing old ones are being created every day by those no better qualified than he; he must learn to think *synthetically* instead of only analytically, as Johnson suggests.

Creativity has *not* been taught, but I believe firmly that it *can* be. This involves the development of a highly critical state of mind, which sees imperfections in every object with which it comes in contact, instead of accepting these objects as the "last word" of creation by others. Once he has developed a jaundiced eye, he then can begin to synthesize other solutions from his mental and library storehouse of elementary components to meet the purposes of these imperfect designs, and, if some of those components are absent, he must create new ones which fit his purpose.

Student design problems, rather than being planned to test his digestion of previously taught theory, should set entirely new problems which demand exercise of his imagination and which test the variety and number of his "vocabulary" of ideas and elementary building blocks available for synthesis into new and useful objects.

A few self-reliant engineers and scientists develop these abilities early in life, and they expand with use. All creative people have them in varying degrees. All engineers could be trained in their development if our institutions of learning placed strong emphasis on creativity instead of on mimicry in engineering design.

B. F. MIESSNER
 Miessner Inventions, Inc.
 680 N.E. 105th St.
 Miami Shores, Fla.

A Simple Method for the Supervision of the Orbital Period of Artificial Satellites*

Last year U. S. and Russian sources reported that the orbital constants of Sputnik IV (Epsilon 1960) had been altered on May 17, 1960, in an attempt to return this satellite to earth. These efforts failed and the satellite assumed a new orbit. The purpose

* Received by the IRE, August 11, 1961.

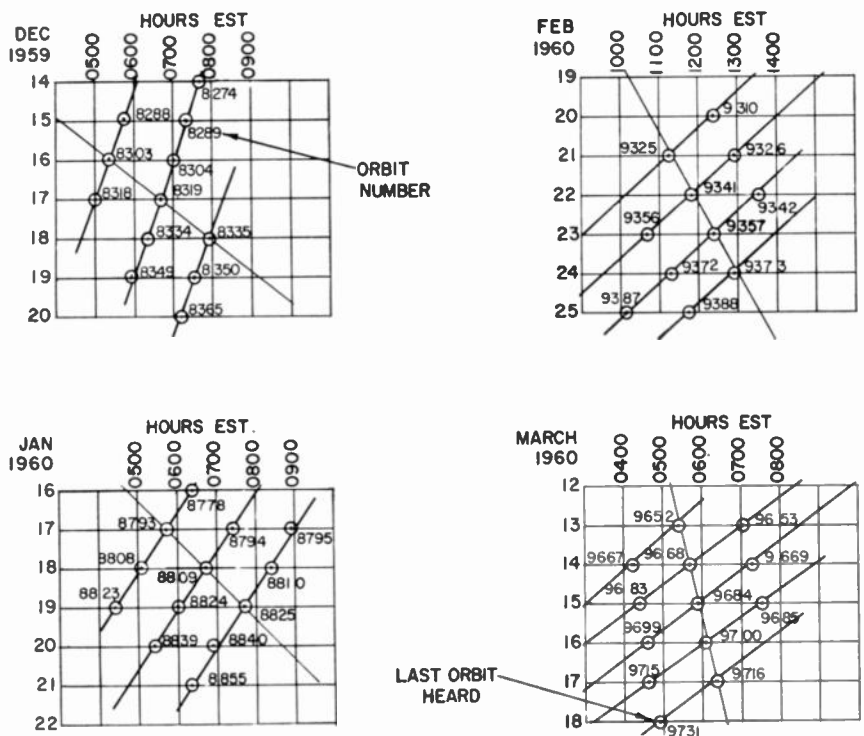


Fig. 1. Progression charts, Sputnik III, Delta 1958.

of this letter is to call attention to a simple method of observing such orbital changes.

Stations that make continuous satellite observations use progression charts, which consist of a time diagram that uses the 24 hours of the day as abscissa and the datum of the days as ordinate. When the passage of a satellite is recorded, the center time of this passage is noted by a point on the progression chart. Thus, the various passages observed on one day form a line of horizontally-distributed points on that date, and the distance between the points is an average measure of the period of the satellite's orbit. The same procedure is repeated on the next day; this new line of points representing the passages observed is shifted in time with respect to the previous day, because the period of the satellite is not a submultiple of the earth's revolution. The equator crossings of corresponding orbits are shifted. As long as the orbital constants of the satellite do not change, however, this shift of equator crossings remains constant, and the picture on the progression chart consists of rows of dots that can be connected by a system of parallel straight lines. The progression charts of long-living, steady satellites are characterized by such a system of straight lines, the slope of which remains constant over many months.

In contrast, the progression charts of short-living satellites and of satellites near the ends of their lives are quite different. The centers of passage times of corresponding orbits of these satellites represent lines of different slopes (see Fig. 1). When a satellite approaches the end of its orbital life, its orbital velocity is increased. The closer the satellite approaches the earth, the higher its velocity becomes, until a dense atmosphere is reached and strong braking effects are

developed, at which time the acceleration is reduced again. Since the radio beacons in most of the satellites become silent long before the re-entry period, the observed changes in the progression charts refer only to the acceleration period mentioned.

Fig. 1 shows the progression charts of Sputnik III, Delta 1958, during the last four months of its life. Because of the increasing orbital velocity, corresponding orbits appear a little earlier in true time each day than predicted by means of a system of parallel lines. The total amount of this shift becomes larger as the satellite comes closer to the earth; consequently, the slope of the connecting lines becomes flatter day by day.

These progression charts cannot be used for precise measurement of the alteration of the orbital period from each orbit to the next one, because the graphical method lacks the precision for such measurement. Moreover, the observation times do not refer to the same position in the orbital trajectory, nor is the apparent altitude accounted for. However, a sudden change in a satellite's orbital constants will obviously be indicated by these progression charts in a manner comparable to the indication given by the continuous alterations during the last weeks of a satellite.

During the early life of the satellite represented in Fig. 2, the progression chart followed the system of straight lines shown in the upper part of the figure. The undisturbed configuration is seen for orbits 5 through 58. However, beginning with orbit 68, we see a new scheme of time sequences working: the inclination of the lines has changed. Thus, after the observation of orbit 69, the station reported a change in the orbital behavior. Confirmation was later received that the Russian attempt to return

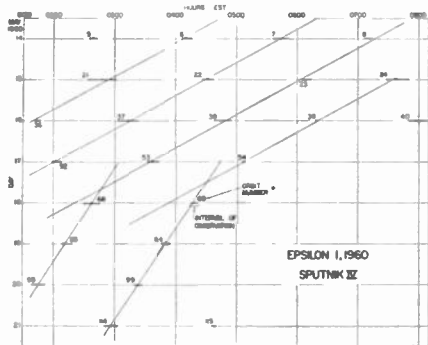


Fig. 2—Progression chart, Sputnik IV, Epsilon 1, 1960.

the satellite to earth had been made between orbits 58 and 68, namely during orbit 63, which was entirely over Russia for its northern part. This change had already been observed by means of the progression chart of Fig. 2, during the second orbit that could have been observed by our station at the Deal Astro-Observation Center, USASRDL.

This simple method of timing the passages of satellites has been found to be a valuable tool for indicating alterations of a satellite's orbital data. In addition, this method is of great practical value in making local predictions of expected passage times and in differentiating between the passages of various satellites that use the same radio frequency.

P. R. ARENDT
L. H. MANAMON
Institute for Exploratory Research
U. S. Army Signal Research and
Development Lab.
Fort Monmouth, N. J.

Comment on "A Theoretical Comparison of Average- and Spot-Noise Figure in Transistor Amplifiers"*

Ekiss and Halligan¹ make use of the common error that the high-frequency corner at which a transistor's noise figure starts rising at 6 db per octave is given by $\sqrt{1-\alpha_0}fab$. Cooke² has shown the serious errors resulting from the use of this approximation. The results of Case 2 in Ekiss and Halligan are therefore not generally correct.

PAUL J. BÉNÉTEAU
Analog Circuits Group
Fairchild Semiconductor Corp.
Mountain View, Calif.

* Received by the IRE, July 30, 1961.
¹ J. A. Ekiss and J. W. Halligan, "A theoretical comparison of average- and spot-noise figure in transistor amplifiers," Proc. IRE (Correspondence), vol. 49, p. 1216, July, 1961.
² H. F. Cooke, "Transistor upper noise corner frequency," Proc. IRE (Correspondence), vol. 49, p. 648; March, 1961.

The Directional Coupler Core of an Arbitrary, Lossless, Reciprocal 4-Port*

The arbitrary, lossless 4-port was the subject of an early study by one of the authors.¹ The result of this study was the demonstration that "any arbitrary junction of four transmission lines (lossless reciprocal 4-port) can be represented either as a directional coupler with transformers in three of the lines or as a junction consisting of two-interconnected 'T-junctions.'" The ideal directional coupler which might lurk within a particular 4-port has appeared somewhat reluctant in the sense that no formula was available which would yield the characteristics of this coupler in terms of the conventional parameters of the given 4-port. We now present the necessary formulas, and note the generalizations of the original result which become apparent in the derivation.

A 4-port, Fig. 1, may be described by its normalized voltage-scattering matrix, $S = [S_{ij}]$,

$$b_i = \sum_j S_{ij} a_j \quad (1)$$

or, equivalently, by a scattering-transfer matrix, $T = [T_{ij}]$,

$$\begin{bmatrix} b_3 \\ a_3 \\ b_4 \\ a_4 \end{bmatrix} = T \begin{bmatrix} a_1 \\ b_1 \\ a_2 \\ b_2 \end{bmatrix} \quad (2)$$

Both Fig. 1 and (2) indicate a particular grouping of the four ports of (1) into in-ports and out-ports; other groupings are, of course, possible; one formal way of obtaining these is a simple renumbering of terminals.

Now consider the scattering-transfer matrix representation (2) of an ideal directional coupler. There are three possible

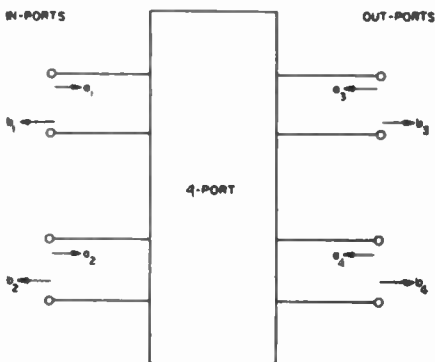


Fig. 1—General 4-port.

combinations of decoupled ports. Corresponding to the three possible forms of the scattering matrix for these ideal cases (at suitable reference planes),

$$\begin{aligned} S_1 &= \begin{bmatrix} 0 & 0 & \alpha & j\beta \\ 0 & 0 & j\beta & \alpha \\ \alpha & j\beta & 0 & 0 \\ j\beta & \alpha & 0 & 0 \end{bmatrix}, \\ S_2 &= \begin{bmatrix} 0 & \alpha & 0 & j\beta \\ \alpha & 0 & j\beta & 0 \\ 0 & j\beta & 0 & \alpha \\ j\beta & 0 & \alpha & 0 \end{bmatrix}, \\ S_3 &= \begin{bmatrix} 0 & j\beta & \alpha & 0 \\ j\beta & 0 & 0 & \alpha \\ \alpha & 0 & 0 & j\beta \\ 0 & \alpha & j\beta & 0 \end{bmatrix}; \end{aligned} \quad (3)$$

one has three forms of T .

$$T_1 = \begin{array}{c|c} \begin{matrix} \alpha & 0 \\ 0 & \alpha \end{matrix} & \begin{matrix} j\beta & 0 \\ 0 & -j\beta \end{matrix} \\ \hline \begin{matrix} j\beta & 0 \\ 0 & -j\beta \end{matrix} & \begin{matrix} 0 & \alpha \\ \alpha & 0 \end{matrix} \end{array}$$

$$T_2 = \begin{array}{c|c} \begin{matrix} 0 & -j\frac{\alpha}{\beta} \\ j\frac{\alpha}{\beta} & 0 \end{matrix} & \begin{matrix} j\left(\beta + \frac{\alpha^2}{\beta}\right) & 0 \\ 0 & -j\frac{1}{\beta} \end{matrix} \\ \hline \begin{matrix} j\left(\beta + \frac{\alpha^2}{\beta}\right) & 0 \\ 0 & -j\frac{1}{\beta} \end{matrix} & \begin{matrix} 0 & -j\frac{\alpha}{\beta} \\ -j\frac{\alpha}{\beta} & 0 \end{matrix} \end{array}$$

$$T_3 = \begin{array}{c|c} \begin{matrix} \alpha^2 + \beta^2 & 0 \\ \alpha & 1 \end{matrix} & \begin{matrix} 0 & j\frac{\beta}{\alpha} \\ -j\frac{\beta}{\alpha} & 0 \end{matrix} \\ \hline \begin{matrix} 0 & j\frac{\beta}{\alpha} \\ 0 & \alpha \end{matrix} & \begin{matrix} \alpha^2 + \beta^2 & 0 \\ \alpha & 1 \end{matrix} \end{array} \quad (4)$$

Conservation of energy would imply $\alpha^2 + \beta^2 = 1$. Now it is clear that on interconnection with 2-ports at each port a transfer matrix, partitioned as shown,

$$T_i = \begin{array}{c|c} \begin{matrix} t_{11} & t_{12} \\ \hline \hline \end{matrix} & \begin{matrix} \hline \hline \end{matrix} \\ \hline \begin{matrix} \hline \hline \end{matrix} & \begin{matrix} t_{21} & t_{22} \end{matrix} \end{array} \quad (5)$$

* Received by the IRE, June 27, 1961; revised manuscript received, July 18, 1961.
This work was supported in part by the U. S. Army Signal Corps, the Air Force Office of Scientific Res., and the Office of Naval Res.; Contract AF-18(600)-1505.
¹ C. G. Montgomery, et al., "Principles of Microwave Circuits," McGraw-Hill Book Co., Inc., New York, N. Y., ch. 9, pp. 303-306; 1948.

$$\frac{1}{S_{13}S_{24} - S_{14}S_{23}} \begin{pmatrix} + S_{21} S_{13} S_{24} & + S_{23} S_{24} & + S_{22} S_{13} S_{24} & - S_{23} S_{14} \\ - S_{21} S_{14} S_{23} & - S_{24} S_{23} & - S_{22} S_{14} S_{23} & + S_{24} S_{13} \\ - S_{11} S_{33} S_{24} & & - S_{12} S_{23} S_{24} & \\ + S_{11} S_{34} S_{23} & & + S_{12} S_{34} S_{23} & \\ + S_{21} S_{33} S_{14} & & + S_{22} S_{33} S_{14} & \\ - S_{21} S_{34} S_{13} & & - S_{22} S_{34} S_{13} & \\ - S_{24} S_{11} & + S_{24} & - S_{24} S_{12} & - S_{14} \\ + S_{14} S_{21} & & + S_{14} S_{22} & \\ \hline + S_{41} S_{13} S_{24} & + S_{43} S_{24} & + S_{42} S_{13} S_{24} & - S_{43} S_{14} \\ - S_{41} S_{14} S_{23} & - S_{44} S_{23} & - S_{42} S_{14} S_{23} & + S_{44} S_{13} \\ - S_{11} S_{43} S_{24} & & - S_{12} S_{43} S_{24} & \\ + S_{11} S_{44} S_{23} & & + S_{12} S_{44} S_{23} & \\ + S_{21} S_{43} S_{14} & & + S_{22} S_{43} S_{14} & \\ - S_{21} S_{44} S_{13} & & - S_{22} S_{44} S_{13} & \\ + S_{23} S_{11} & - S_{23} & + S_{23} S_{12} & + S_{13} \\ - S_{13} S_{21} & & - S_{13} S_{22} & \end{pmatrix}, \quad (8)$$

goes over into

$$T = \begin{pmatrix} A_{11}C & A_{12}D \\ \hline B_{21}C & B_{22}D \end{pmatrix}, \quad (6)$$

wherein A , B , C and D are transfer representations of the 2-ports. Thus, the sub-determinants are invariants provided $\det \{AC\} = \det \{AD\} = \det \{BC\} = \det \{BD\} = 1$. The latter is true for any reciprocal 2-ports, lossless or dissipative.² The invariants are, by inspection,

$$\alpha^2, \beta^2 = 1 - \alpha^2; \quad (7a)$$

$$\left(\frac{\alpha}{\beta}\right)^2 = \frac{\alpha^2}{1 - \alpha^2}, \quad 1 + \left(\frac{\alpha}{\beta}\right)^2 = \frac{1}{1 - \alpha^2}; \quad (7b)$$

$$\frac{a^2 + \beta^2}{\alpha^2} = \frac{1}{\alpha^2}, \quad \left(\frac{\beta}{\alpha}\right)^2 = \frac{1 - \alpha^2}{\alpha^2}. \quad (7c)$$

On the other hand, the absolute value of the determinant of the transfer representation of a lossless $2N$ -port, reciprocal or nonreciprocal, is also unity. Hence, the absolute values of the invariants are significant as well for nonreciprocal lossless tuning in the arms of the 4-port.

Evidently the transfer matrices corresponding to a general scattering matrix have subdeterminants which correspond to the invariants (7). For the grouping of the ports indicated in (2), the transfer matrix T is

from which the determinants of the sub-matrices are

$$\frac{S_{24}S_{31} - S_{21}S_{34}}{S_{24}S_{13} - S_{23}S_{14}}, \quad \frac{S_{14}S_{32} - S_{12}S_{34}}{S_{14}S_{23} - S_{13}S_{24}}, \quad (9)$$

$$\frac{S_{23}S_{41} - S_{21}S_{43}}{S_{23}S_{14} - S_{24}S_{13}}, \quad \frac{S_{13}S_{42} - S_{12}S_{43}}{S_{13}S_{24} - S_{14}S_{23}}$$

These expressions are of the general form

$$\frac{S_{ij}S_{kl} - S_{il}S_{kj}}{S_{ij}S_{lk} - S_{ik}S_{lj}}$$

The above relations are valid for arbitrary 4-ports, but the interpretation in terms of an imbedded ideal directional coupler is limited to the lossless reciprocal case. As previously mentioned, the analogous forms for the different groupings of ports may be obtained formally by permuting the port designations. The new expressions thus obtained are also invariant. The magnitudes of the several invariants in a specific case, in particular whether sums or differences equal unity, determine the proper choice of directional coupler terminals [see (7)].

Of the 2-ports A , B , C , D which convert the lossless, reciprocal 4-port to an ideal directional coupler, one may be chosen arbitrarily. The other three may then be obtained from (6) and the standard forms shown in (4). In particular one port may remain untuned.

W. K. KAHN

Polytechnic Inst. of Brooklyn
Brooklyn, N. Y.

R. L. KYHL

Res. Lab. of Electronics
Mass. Inst. Tech.
Cambridge, Mass.

Spectral Response of a Nonlinear Device*

It is frequently desirable to be able to determine the spectral output of a nonlinear device when it is driven by a periodic input. If the device and the input signal satisfy certain conditions, the output may be specified. These conditions are that 1) the output is a single-valued function of the input which is constant over the frequency range of the input, and that 2) the input may be represented by a finite sum of terms. If the device satisfies these conditions, it may be expanded by a Fourier series over the interval $-e_m \leq e \leq e_m$, where e_m is greater than the maximum absolute value of the input.

$$e_0 = f(e_{in}) = \sum_{n=1}^{\infty} \left[a_n \sin\left(\frac{n\pi e_{in}}{e_m}\right) + b_n \cos\left(\frac{n\pi e_{in}}{e_m}\right) \right] \quad -e_m \leq e \leq e_m \quad (1)$$

where as usual

$$a_n = \frac{1}{\pi} \int_{-\pi}^{\pi} f(e_{in}) \sin\left(\frac{n\pi e_{in}}{e_m}\right) de_{in}$$

$$b_n = \frac{1}{\pi} \int_{-\pi}^{\pi} f(e_{in}) \cos\left(\frac{n\pi e_{in}}{e_m}\right) de_{in}.$$

It is assumed that the input may be represented by a finite sum of terms,

$$e_{in} = \sum_{i=1}^N \alpha_i \sin \omega_i t. \quad (2)$$

Then each term in the Fourier expansion is of the form,

$$\cos\left(\frac{n\pi e_{in}}{e_m}\right) = \cos\left(\frac{n\pi}{e_m} \sum_{i=1}^N \alpha_i \sin \omega_i t\right). \quad (3)$$

The argument of each term in the expansion contains all N harmonics of the input. By repeated use of the trigonometric identity for the sum of two arguments, (3) may be written as a sum of 2^{N-1} terms. Each of these terms will be the product of N factors of the form

$$\prod_{i=1}^N T\left(\frac{n\pi}{e_m} \alpha_i \sin \omega_i t\right), \quad (4)$$

where T may be either sin or cos:

$$\left\{ \begin{array}{l} \cos\left(\frac{n\pi e_{in}}{e_m}\right) \\ \sin\left(\frac{n\pi e_{in}}{e_m}\right) \end{array} \right\} = \sum_{j=1}^{2^{N-1}} \left\{ \pm \prod_{i=1}^N T_i\left(\frac{n\pi}{e_m} \alpha_i \sin \omega_i t\right) \right\}. \quad (5)$$

\sum_R refers to the sum of all possible combinations of

$$\prod_{i=1}^N T_i$$

formed using either sin or cos for T , which satisfy the following rule: If the product

$$\prod_{i=1}^N T_i$$

were written from $\cos(n\pi e_{in}/e_m)$, there must be an even or odd number of cos functions,

* Received by the IRE, August 3, 1961; revised manuscript received, August 21, 1961.

² L. B. Felsen and W. K. Kahn, "Transfer characteristics of $2N$ -port networks," *Proc. Symp. on Millimeter Waves*, New York, N. Y., March 31, April 1-2, 1959, Polytechnic Press, Brooklyn, N. Y., pp. 477-512; 1959.

depending upon whether N were even or odd. The opposite would be true if $\sin(n\pi e_{in}/e_m)$ were being expanded.

The rule for the sign of the product is rather complicated, and since only the magnitude of the output is required, this rule is omitted. When $a_n \sin(n\pi e_{in}/e_m) + b_n \cos(n\pi e_{in}/e_m)$ is expanded in this way, all possible combinations of

$$\prod_{i=1}^N T_i$$

appear. Half of the terms come from $\sin(n\pi e_{in}/e_m)$ and half come from $\cos(n\pi e_{in}/e_m)$. The distribution of these terms comes from the above rule.

Then the well-known Bessel function series may be substituted for T :

$$\begin{aligned} \cos\left(\frac{n\pi\alpha_i}{e_m} \sin \omega_i t\right) &= J_0\left(\frac{n\pi\alpha_i}{e_m}\right) + 2 \sum_{k=1}^{\infty} J_{2k}\left(\frac{n\pi\alpha_i}{e_m}\right) \cos 2k\omega_i t \\ \sin\left(\frac{n\pi\alpha_i}{e_m} \sin \omega_i t\right) &= 2 \sum_{k=1}^{\infty} J_{2k-1}\left(\frac{n\pi\alpha_i}{e_m}\right) \sin((2k-1)\omega_i t). \end{aligned}$$

Then these substitutions may be made and the products evaluated and simplified by repeated application of the trigonometric identities:

$$\begin{aligned} \cos a \cos b &= \frac{1}{2}[\cos(a+b) + \cos(a-b)], \\ \sin a \cos b &= \frac{1}{2}[\sin(a+b) + \sin(a-b)], \end{aligned}$$

whichever is applicable. If this is done, there results an expression

$$\begin{aligned} &\left\{ \begin{array}{l} \cos\left(\frac{n\pi e_{in}}{e_m}\right) \\ \sin\left(\frac{n\pi e_{in}}{e_m}\right) \end{array} \right\} \\ &= 2^r \sum_{k_1=1}^{\infty} \sum_{k_2=1}^{\infty} \cdots \sum_{k_N=1}^{\infty} \left[\prod_{i=1}^N J_{l_i}\left(\frac{n\pi\alpha_i}{e_m}\right) \right] \\ &\quad \cdot T[(l, \omega, \pm l_1\omega_1 \pm \cdots \pm l_N\omega_N)t] \quad (6) \end{aligned}$$

$r =$ the number of components for which $l_i \neq 0$
 $l_i = 2k_i, \quad 2k_i - 1, 0,$

where, if $l_i = 0$, the sum over k_i is not performed, and where α_i is the i th component of input, $T = \sin$ if argument of T contains an odd number of odd harmonics, and $T = \cos$ if argument of T contains an even number of odd harmonics. It is necessary to retain the distinction between even and odd harmonics of the components of the input to determine whether T is \sin or \cos .

Thus, it has been shown that a nonlinear device produces all possible harmonics of each input component plus all possible sums and differences of these harmonics. The magnitude of any component of the output may be determined by returning to the original expansion of $f(e_{in})$ and summing over n . Thus, if e_{in} is a component of the output whose frequency is

$$\omega_e = \sum_{i=1}^N l_i \omega_i,$$

then

$$e_{in} = m_e \sin(\omega_e t + \phi) \quad \phi = 0, \pm \frac{\pi}{2}$$

where

$$m_e = \frac{2^{r+1}}{\pi} \sum_{n=1}^{\infty} \left[\prod_{i=1}^N J_{l_i}\left(\frac{n\pi\alpha_i}{e_m}\right) \right] \cdot \int_{-\pi}^{\pi} f(e_{in}) T\left(\frac{n\pi e_{in}}{e_m}\right) d e_{in}. \quad (7)$$

The l_i in the expression for m_e must be the same as l_i in the expansion for ω_e . $T = \cos$ if an even number of odd harmonics appear in ω_e , and $T = \sin$ if an odd number of odd harmonics appear in ω_e .

The form of the solution will always be the same. The product of Bessel functions is independent of shape in that the number of factors is equal to the number of components of the input. There will be one Bessel function factor for each input component. The argument of the Bessel functions is only dependent on the relative magnitude of the input components and the location of e_m . The effect of the shape of $f(e_i)$ is contained entirely in the integral.

This technique is quite general and may be applied to any nonlinear device which satisfies the conditions listed at the beginning of this letter. A computer could be used to evaluate the components of the output if more than a few components are in the region of interest. If $f(e_i)$ may be approximated by only a few terms of a power series, it may be described more easily by evaluating the resulting polynomial products. However, a piecewise continuous $f(e_i)$ may be expanded in a Fourier series quite efficiently, and so devices which may be described by this type of curve are best analyzed by the technique of this letter.

WILLIAM B. RIBBENS
 Dept. of Elec. Engrg.
 University of Michigan
 Ann Arbor, Mich.

On a Mathematical Description of Noisy Measurement System Performance*

There are many practical measurement systems for which internal noise is the factor which limits the quality of system performance. Such systems, which might be termed noisy measurement systems, have many features in common with the type of random experiments which have been the subject of much discussion in the literature of mathematical statistics.¹ In spite of the available mathematical work, quantitative expressions for the performance of noisy measurement systems do not seem to be commonly used in the engineering literature.

The purposes of this note are: 1) to call attention to the precise definitions of two statistical parameters which can be used as

measures of the performance of certain noisy measurement systems; and 2) to formulate quantitative expressions for measurement-system performance in terms of these quantities.

Consider a noisy measurement system with an input $r_S(t)$, an output $R(x, t)$, and internal noise $n(x, t)$. All of the parameters of $r_S(t)$ but one, denoted by $S(t)$, are assumed to be known. This parameter is the quantity to be measured. The nature of the internal noise is such that it can be best represented mathematically as a stochastic process. The presence of $n(x, t)$ in the system thus makes the output $R(x, t)$ also a stochastic process.

Stochastic processes have been discussed extensively in both mathematical and engineering literature, and the use of such processes as mathematical models for physical noise is well known.² In the notation chosen here, the double argument (x, t) has been adopted to emphasize the fact that the stochastic variables n and R depend not only on the time variable t , but also on the chance state of the internal noise generators represented by the variable x . If x is fixed to correspond to a particular measurement with the measurement system, the functions $n(x, t)$ and $R(x, t)$ thus restrained are commonly called sample functions from the corresponding noise processes. On the other hand, a large number of measurements could be made in such a way that the system output is recorded at a fixed time after exciting the measurement system with the quantity to be measured. If these measurements are performed under identical conditions, except for the chance state of the noise generators, then the collection of values $\{n(x, t)\}$ or $\{R(x, t)\}$, where x varies and t is fixed, would be termed an ensemble of values from the appropriate processes. Moments of the random variables may be defined either as averages over the variable t or as averages over the ensemble. Frequently the averages defined in these two ways are equal, but this is not true in general for measurement systems. Here the ensemble average, denoted $En(x, t)$ or $ER(x, t)$, will be used.

The purpose of a measurement system is to produce in a given measurement (*i.e.*, with x fixed) a function $R(x, t)$ which is an estimate of the unknown parameter $S(t)$ that is being measured. The question naturally arises as to the quality of the estimate produced by a measurement system. If the results of a particular measurement are in hand, and if the true values of the parameter to be measured are known, then the quality of the estimate can be precisely determined. This is seldom the case, however, and a much more interesting question concerns the potential quality of an estimate to be formed by a particular measurement system with the calculation being made prior to the measurement. Thus, *a priori*, $R(x, t)$ can be regarded as a random variable. In fact the ensemble of values of $R(x, t)$ is

* The book by J. L. Doob, "Stochastic Processes," John Wiley and Sons, Inc., New York, N. Y., 1952, is representative of the mathematical literature on the subject of stochastic processes, while the paper by W. R. Bennett, "Methods of solving noise problems," Proc. IRE, vol. 44, pp. 609-638, May, 1956, is typical of the engineering literature on stochastic processes and applications to physical systems.

* Received by the IRE, August 14, 1961.
¹ See, for example, H. Cramér, "Mathematical Methods of Statistics," Princeton University Press, Princeton, N. J., 1945; or H. B. Mann, "Analysis and Design of Experiments," Dover Publications, Inc., New York, N. Y., 1949.

just the collection of all possible measurement system outputs which result from all possible values of the input $S(t)$ and internal noise $n(x, t)$. If the statistical properties of $n(x, t)$ are known, it is then possible to compute the statistical properties of $R(x, t)$ in terms of $S(t)$. Certain of these statistical properties of $R(x, t)$ can then be used to formulate a probabilistic expression for the quality of the estimate of $S(t)$ formed by the measurement system.

In order to be more specific, the discussion will be restricted to those measurement systems having the following properties: 1) $E_n(x, t)$ equals zero; 2) $S(t)$ is a constant, S ; and 3) the elements of the system are linear. Such systems are commonly designed to satisfy the specific condition

$$ER(x, \infty) = kS, \quad (1)$$

where k is a constant scale factor, and the symbol ∞ in the argument of R indicates that t is very large so that the measurement system is in the steady state. This condition is usually met by designing the system so that

$$ER(x, t) = w(t)S,$$

where $w(t)$ accounts for the transient behavior of the system, and

$$\lim_{t \rightarrow \infty} w(t) = k.$$

For systems thus restricted there are two distinct types of error, namely: 1) statistical fluctuation errors caused by internal noise, and 2) errors caused by the fact that $ER(x, t)$ is not proportional to S . Quantitatively these two types of error can be defined as follows:³

$$\text{Bias error} = \epsilon_b(t) = ER(x, t) - kS; \quad (2)$$

Mean-square error

$$= \epsilon_{ms}(t) = E[R(x, t) - kS]^2. \quad (3)$$

Bias error, taken from the statistical use of the term "bias," thus measures the amount by which the ensemble average of the measurement-system output differs from the true value of the quantity being measured. Similarly mean-square error measures the statistical fluctuation about the true value to be expected in the results of a large number of measurements taken with the same instrument.

Now consider the use of these error terms in describing measurement-system performance. Eq. (2) expresses clearly the quantitative effect of bias error. A relation which elucidates the effect of mean-square error can be derived as follows. Eq. (3) for mean-square error can be written as

$$\begin{aligned} \epsilon_{ms}(t) &= \int_{-\infty}^{\infty} [R(x, t) - kS]^2 dF(x) \\ &= \int_{-\infty}^{\infty} \gamma^2 dF(x), \end{aligned}$$

where F is the probability distribution func-

³ In arriving at these definitions, it has been assumed that the scale factor k is known so that in effect kS is the true value of the quantity being measured. If for some reason k is not known, alternative definitions of $\epsilon_b(t)$ and $\epsilon_{ms}(t)$ could be made. For example, these quantities could be defined by replacing kS in (3) and (4) by simply S .

tion of $R(x, t)$, and $\gamma^2 = [R(x, t) - kS]^2$. The chain of inequalities,

$$\epsilon_{ms}(t) \geq \int_A \gamma^2 dF(x) \geq c^2 \epsilon_{ms}(t) \int_A dF(x), \quad (4)$$

where A denotes the set of values of x such that $|\gamma| \geq c\sqrt{\epsilon_{ms}(t)}$, can be easily verified. Eq. (4) leads immediately to an upper bound on the probability of the event $[|R(x, t) - kS| \geq c\sqrt{\epsilon_{ms}(t)}]$, or what is more useful here, the relation⁴

$$P[|R(x, t) - kS| < c\sqrt{\epsilon_{ms}(t)}] > 1 - 1/c^2. \quad (5)$$

Eq. (5) is equivalent to the following statement: "With probability greater than $1 - 1/c^2$, a single reading of a measurement-system output differs in magnitude from the true value of the quantity being measured by no more than c times the root of its mean-square error."

It may be noted that the above discussion again takes cognizance of the well-known fact that at least two different types of error arise from the use of noisy measurement systems. The terms "accuracy" and "reliability"⁵ or "accuracy" and "precision"⁶ seem to be used more frequently than others in identifying these two types of error. Thus (2) calls attention to a mathematical measure of "accuracy" for the class of systems to which it applies, and similarly, (3) calls attention to a measure of "reliability" (or "precision") for the same class of systems. Eq. (5) gives a quantitative relation between a single reading of the output of a measurement system and the true value of the quantity which the system is designed to estimate.

J. L. HAMMOND, JR.
School of Elec. Engrg.
Georgia Inst. of Tech.
Atlanta, Ga.

⁴ This relation is similar to the Bienaymé-Tchebycheff inequality.

⁵ L. Brillouin, "Science and Information Theory," Academic Press, Inc., New York, N. Y., 1956.

⁶ Y. Beers, "Introduction to the Theory of Error," Addison-Wesley Publishing Co., Reading, Mass., 1953.

The Delta Function and the Fourier Integral*

A rather interesting result can be obtained from the use of the delta "function" (to use the word loosely) in the Fourier integral. The delta function is often said to be 1) an even function, and 2) zero everywhere except at the origin, where it is so large that

$$\int_{-\infty}^{\infty} \delta(x) dx = \int_{-c}^c \delta(x) dx = 1, \quad \epsilon > 0. \quad (1)$$

In its use in communications engineering the Fourier integral is written as

$$F(w) = \int_{-\infty}^{\infty} f(t) e^{-iwt} dt, \quad (2)$$

"the direct transform," and

$$f(t) = \frac{1}{2\pi} \int_{-\infty}^{\infty} F(w) e^{iwt} dw, \quad (3)$$

"the inverse transform," where always

$$w = 2\pi f \quad (4)$$

and

$$i = \sqrt{-1}. \quad (5)$$

Consider now a delta function of frequency, from which will be obtained the corresponding time function through the use of (3).

$$f(t) = \frac{1}{2\pi} \int_{-\infty}^{\infty} \delta(w) e^{iwt} dw, \quad (6)$$

which, from the stated property of the delta function in (1), can be reduced immediately to yield

$$\begin{aligned} f(t) &= \frac{1}{2\pi} \int_{-\infty}^{\infty} \delta(w) e^{iwt} dw \\ &= \frac{1}{2\pi} \int_{-\infty}^{\infty} \delta(0) e^{i(0)t} d\omega \\ &= \frac{1}{2\pi} \int_{-\infty}^{\infty} \delta(0) d\omega \\ &= \frac{1}{2\pi}. \end{aligned} \quad (7)$$

Now consider exactly the same equation (6) with the introduction of the apparently trivial change of variable shown in (4).

$$\begin{aligned} f(t) &= \frac{1}{2\pi} \int_{-\infty}^{\infty} \delta(w) e^{iwt} dw \\ &= \frac{1}{2\pi} \int_{-\infty}^{\infty} \delta(2\pi f) e^{i2\pi f t} (2\pi) df \\ &= \int_{-\infty}^{\infty} \delta(2\pi f) e^{i2\pi f t} df. \end{aligned} \quad (8)$$

Evaluation of the final result shown in (8) by the same method used in evaluation of (7) leads to

$$\begin{aligned} f(t) &= \frac{1}{2\pi} \int_{-\infty}^{\infty} \delta(w) e^{iwt} dw \\ &= \frac{1}{2\pi} \int_{-\infty}^{\infty} \delta(2\pi f) e^{i2\pi f t} (2\pi) df \\ &= \int_{-\infty}^{\infty} \delta(2\pi f) e^{i2\pi f t} df \\ &= \int_{-\infty}^{\infty} \delta(2\pi(0)) e^{i2\pi(0)t} df \\ &= \int_{-\infty}^{\infty} \delta(0) df \\ &= 1. \end{aligned} \quad (9)$$

From (7) and (9) come the two different numbers $1/2\pi$ and 1, respectively, as the values of the same definite integral. Perhaps either $1/2\pi$ or 1 is the value of the definite integral, but who can say that $1/2\pi$ and 1 are equal?

The answer, or answers, or neither, obtained above are perhaps no better or no worse than another expression commonly as-

* Received by the IRE, June 9, 1961.

sociated with a delta function of time:

$$\begin{aligned}
 F(w) &= \int_{-\infty}^{\infty} \delta(t) e^{-iwt} dt \\
 &= \int_{-\infty}^{\infty} \delta(0) e^{-i w(0)} dt \\
 &= \int_{-\infty}^{\infty} \delta(0) dt \\
 &= 1.
 \end{aligned}
 \tag{10}$$

There is no "2π-trick" in (10); that is,

$$\begin{aligned}
 F'(w) &= \int_{-\infty}^{\infty} \delta(t) e^{-iwt} dt, \text{ or} \\
 F'(2\pi f) &= \int_{-\infty}^{\infty} \delta(t) e^{-i2\pi f t} dt \\
 &= \int_{-\infty}^{\infty} \delta(0) e^{-i2\pi f(0)} dt \\
 &= \int_{-\infty}^{\infty} \delta(0) dt \\
 &= 1.
 \end{aligned}
 \tag{11}$$

Now to apply the inverse transform of (3) to the common result of (10) and (11):

$$\begin{aligned}
 f(t) &= \frac{1}{2\pi} \int_{-\infty}^{\infty} F'(w) e^{iwt} dw \\
 &= \frac{1}{2\pi} \int_{-\infty}^{\infty} 1 e^{iwt} dw \\
 &= \frac{1}{2\pi} \int_{-\infty}^{\infty} \cos wdw + i \frac{1}{2\pi} \int_{-\infty}^{\infty} \sin wdwt \\
 &= \frac{1}{2\pi} \int_{-\infty}^{\infty} \cos wdwt,
 \end{aligned}
 \tag{12}$$

since $\sin wt$ is an odd function.

Alternatively,

$$\begin{aligned}
 f(t) &= \frac{1}{2\pi} \int_{-\infty}^{\infty} F'(w) e^{iwt} dw \\
 &= \int_{-\infty}^{\infty} F'(2\pi f) e^{i2\pi f t} df \\
 &= \int_{-\infty}^{\infty} 1 e^{i2\pi f t} df \\
 &= \int_{-\infty}^{\infty} \cos 2\pi f t df + i \int_{-\infty}^{\infty} \sin 2\pi f t df \\
 &= \int_{-\infty}^{\infty} \cos 2\pi f t df,
 \end{aligned}
 \tag{13}$$

which agrees with the result of (12), again with no "2π-trick." However, the $f(t)$ of (12) and (13) is the delta function, so that the common result obtained above is

$$\delta(t) = \frac{1}{2\pi} \int_{-\infty}^{\infty} \cos wtdw = \int_{-\infty}^{\infty} \cos 2\pi f t df. \tag{14}$$

This is a rather interesting result, because the integral of (14) does not converge for any value of t . Let $t=0$ in (14). Then,

$$\begin{aligned}
 \delta(0) &= \int_{-\infty}^{\infty} \cos 2\pi f(0) df \\
 &= \int_{-\infty}^{\infty} 1 df.
 \end{aligned}
 \tag{15}$$

Both sides of (15) seem to agree since $\delta(0)$ is commonly said to be "infinite" and the

integral of (15) also appears to be infinite. Next let $t=1$ in (14). Then

$$\begin{aligned}
 \delta(1) &= \int_{-\infty}^{\infty} \cos 2\pi f df \\
 &= \frac{1}{2\pi} [\sin 2\pi f]_{-\infty}^{\infty}
 \end{aligned}
 \tag{16}$$

formally at least.

Now $\delta(1)$ is supposed to be zero. However, the right side of (16) does not converge to any number, and, in approaching the limits $-\infty$ and ∞ , it varies between the lower bound $-1/2\pi$ and the upper bound $+1/2\pi$; similar results are obtained from other values of $t \neq 0$ in (14).

Is (14) the delta "function?"

A. W. McMURTREY
Conduction Corp.
Ann Arbor, Mich.

An Electronically Tunable Up-Converter*

The device to be described in this letter is a lower-sideband up-converter with a single varactor diode. Two-resonator broadbanding filters are used at the signal-input and pump-input ports, and a single-resonator narrow-band filter is used at the lower-sideband output port. Defining f as the input frequency, f^p as the pump frequency, and f_o' as the fixed frequency passed by the narrow-band output filter, for a signal to be amplified, the relation

$$f = f^p - f_o' \tag{1}$$

must be satisfied. Thus, using a voltage-tunable pump oscillator to vary f^p , fast electronic tuning is possible. The design of devices of this type was discussed in a recent paper.¹

To test the previously developed theory, a strip transmission line up-converter of the general form shown in Fig. 1 was constructed. A Hughes 1N896 diode that has a computer-type package with 0.020-inch-diameter wire leads was used. The diode plus its leads makes a resonant circuit which exhibits series resonance at both the center of the signal input band and at the center of the pump input band. The two-resonator signal input broadbanding filter consists of the series resonator formed by the diode and its leads, along with the shunt resonator formed by the shunt capacitor block and the shunt inductor stub. The two-resonator pump input broadbanding filter consists of the diode circuit at its second series resonance, along with the quarter-wavelength-type second pump resonator shown in Fig. 1. The lower-

sideband output filter consists of a half-wavelength resonator capacitively coupled to the diode circuit and to the output line. The band-stop resonators were introduced to prevent leakage of the output signal. In the device constructed, the pump input reflection loss is 3 ± 0.2 db across the pump band, which can be shown to be very nearly optimum for a two-resonator matching filter in this particular device.¹ With this amount of reflection loss, 67 mw of incident pump power were required for optimum operation.

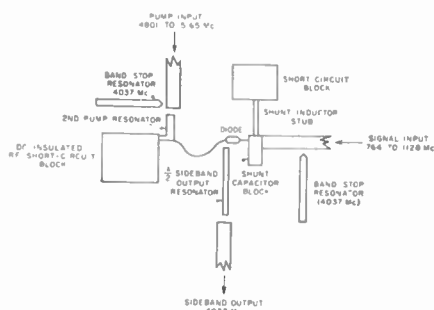


Fig. 1—Simplified drawing of the strip-transmission-line electronically tunable up-converter.

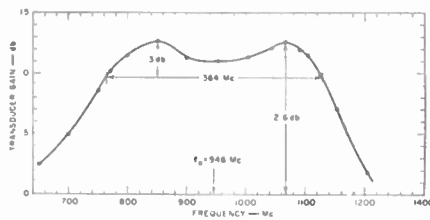


Fig. 2—Measured tuning characteristics of the up-converter. (The output frequency was held fixed at 1037 Mc, while the pump frequency was varied for each input frequency; incident pump power was a constant 67 mw.)

Fig. 2 shows the measured tuning characteristic of the device. The 3-db-down fractional tuning bandwidth is 38.5 per cent, which compares favorably with the design value of 40 per cent. Since the gain has both negative-resistance and up-conversion components, it was possible to make the negative-resistance component relatively small, which makes the device relatively insensitive to small deviations from the design terminating impedances. The theoretical midband noise figure was 2.1 db, and the measured values ranged close to this value over much of the input frequency band, while reaching a peak of 3 db at the upper edge of the band. Of course, even lower noise figures are possible when using higher- Q diodes and larger f_o'/f ratios.

Theory shows that if the diode were lossless, the tuning range possible with devices of this type would be unlimited; with existing diodes, tuning ranges of the order of an octave should be practical.¹ Such up-converters should find application not only as low-noise preamplifiers with electronic tuning, but also as low-noise preamplifiers with manual tuning achieved by a single

* Received by the IRE, September 18, 1961. This research was supported by the U. S. Army Signal Res. and Dev. Lab., Fort Monmouth, N. J., under Contract DA-36-039 SC-87398.

1 G. L. Matthaei, "Design theory of up-converters for use as electronically tunable filters," IRE TRANS. ON MICROWAVE THEORY AND TECHNIQUES, vol. MTT-9, pp. 425-435; September, 1961.

knob on the pump oscillator. If desired, similar results can be obtained with absolutely stable upper-sideband up-converters,^{1,2} but with less gain for a given f_0'/f ratio.

GEORGE L. MATTHAEI
Stanford Research Institute
Menlo Park, Calif.

² G. P. Shepherd and D. G. Kiely report gain of 7 db or greater over a range from 150 to 1800 Mc using an up-converter with a fixed upper-sideband output of 8600 Mc. [See PROC. IRE (Correspondence), vol. 49, p. 966; May, 1961.] They, however, appear to have varied their pump power as their pump frequency was varied. Adjusting the pump power for maximum gain at each frequency not only will overcome variations in pump circuit reflection, but also will vary the average capacitance of the diode so as to retune the diode circuit. The approach here assumes constant incident pump power.

The Linearized Transfer Function of a Phase-Locked Loop Containing an IF Amplifier*

Very commonly, phase-locked loops are constructed with an IF amplifier in the loop, as shown in the typical example of Fig. 1(a). This note will derive a method for finding the exact linear transfer function for such a loop. The effect of the IF transfer function is included. If the IF is narrow compared to the loop bandwidth, the IF transfer function cannot be neglected.

Consider the block diagrams of Fig. 2, and assume that $G(s)$ is a high- Q band-pass transfer function. If $F(s)$ is the Laplace transfer function of some input to $G(s)$ the output is, of course, $F(s)G(s)$. The expressions $F(s)$ and $G(s)$ may be rewritten as $F(s) = F_1(s)F_1^*(s)$ and $G(s) = G_1(s)G_1^*(s)$. This simply allows the upper s -plane singularities to be treated separately from their lower-plane conjugates. This output is multiplied by a cosine wave

$$\frac{E_{02}}{2\pi} \cos \omega_2 t$$

The Fourier transform of this cosine is

$$\mathcal{F} \left\{ \frac{E_{02}}{2\pi} \cos (\omega_2 t - \theta_2) \right\} = \frac{E_{02}}{2} [\delta(\omega - \omega_2) + \delta(\omega + \omega_2)],$$

where $\delta(\omega)$ is the well-known impulse or delta function. Since the Fourier transform of a time product is the convolution of the individual transforms, the transformed output of $h(t)$ of Fig. 2(a) is

$$\begin{aligned} & \frac{K_n}{2} \int_{-\infty}^{\infty} F_1(\omega - \omega_0) F_1^*(\omega - \omega_0) G_1(\omega - \omega_0) \\ & \cdot G_1^*(\omega - \omega_0) [\delta(\omega - \omega_2) + \delta(\omega + \omega_2)] d\omega_0 \\ & = \frac{K_n}{2} [F_1(\omega - \omega_2) F_1^*(\omega - \omega_2) G_1(\omega - \omega_2) G_1^*(\omega - \omega_2) \\ & + F_1(\omega + \omega_2) F_1^*(\omega + \omega_2) G_1(\omega + \omega_2) G_1^*(\omega + \omega_2)], \end{aligned}$$

* Received by the IRE, August 7, 1961.

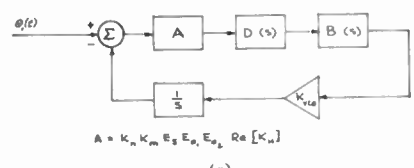
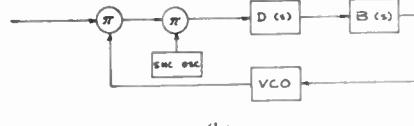
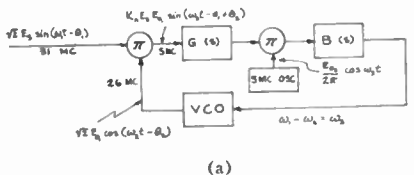


Fig. 1—(a) A typical phase-locked loop. (b) A loop with an equivalent transfer function. (c) The linearized equivalent.

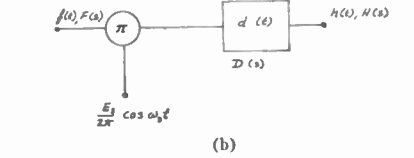
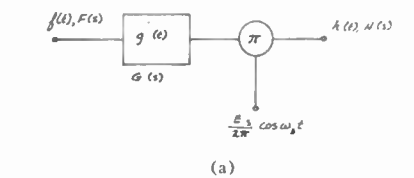


Fig. 2—(a) Filter before the multiplier. (b) Filter after the multiplier.

where K_n is the constant associated with the multiplier. The higher harmonic frequency terms (outside the range of interest) are next evaluated and assumed to be constant in the low-pass range. Then

$$H(\omega) = \frac{K_n}{2} [K_H F_1(\omega - \omega_2) G_1(\omega - \omega_2) + K_H^* F_1^*(\omega + \omega_2) G_1^*(\omega + \omega_2)].$$

This is, in effect, the lower half s plane moved up by ω_2 and the upper half s plane moved down by ω_2 with the high frequency components treated as complex constants. If one may assume that $F_1(\omega)$ and $G_1(\omega)$ are symmetrical about ω_2 ,

$$H(\omega) = K_n \text{Re} [K_H] F_1(\omega - \omega_2) G_1(\omega - \omega_2),$$

or, in Laplace notation,

$$H(s) \propto F_1(s - j\omega_2) G_1(s - j\omega_2).$$

Referring to Fig. 2(b) it is now seen that after the multiplier, where $F(s)$ is shifted by $j\omega_2$, the filter must have the frequency translated dynamics of $G(s)$:

$$D(s) = G_1(s - j\omega_2).$$

The substitution in Fig. 1(b) may now be made. This low-frequency equivalent of $G(s)$ is shown in Fig. 3(b).

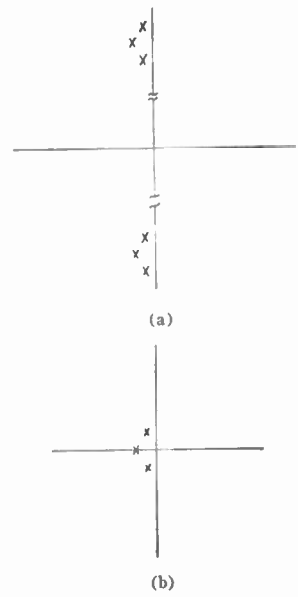


Fig. 3—(a) An example of $G(s)$. (b) $D(s)$, the low-frequency equivalent of $G(s)$.

The output of the multiplier of Fig. 1(b) is then

$$K_n K_m K_s E_1 E_0 E_2 \text{Re} [K_H] \sin (\theta_1 - \theta_2).$$

K_m is the mixer constant. The linearization of the loop can now continue in the conventional manner.¹

The completely linearized loop is shown in Fig. 1(c). The equivalent noise voltage will be the same as given in Weaver.¹ It is seen, for example, that if the low-frequency equivalent in Fig. 3(b) is not wide band compared to $B(s)$, $D(s)$ will definitely affect the compensation needed.

R. LAWHORN
C. S. WEAVER
Western Development Labs.
Philco Corp.
Palo Alto, Calif.

¹ C. S. Weaver, "A new approach to the linear design and analysis of phase-locked loops," IRE TRANS. ON SPACE ELECTRONICS AND TELEMETRY, vol. SET-5, pp. 166-178; December, 1959.

Infrared Fluorescence and Stimulated Emission of Nd^{+3} in CaWO_4 *

Recently, several investigations have confirmed the predictions of Schawlow and Townes¹ concerning the character of stimulated emission in the optical region from an assembly of atoms in a suitable cavity prepared in a state of inverted population in excess of a certain critical number. This letter reports the observation of infrared fluores-

* Received by the IRE, September 20, 1961.
¹ A. L. Schawlow and C. H. Townes, "Infrared and optical masers," Phys. Rev., vol. 112, pp. 1940-1949; December 15, 1958.

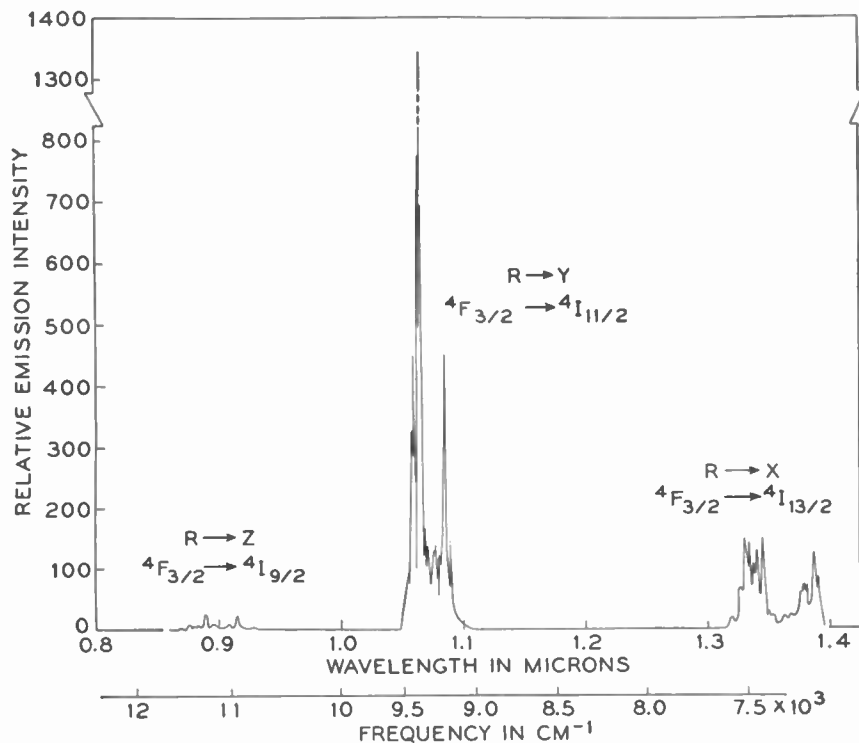


Fig. 1—Near infrared fluorescence spectrum of Nd^{3+} in CaWO_4 at 77°K , with transitions designated.

cence and stimulated emission at room temperature and 77°K in $\text{CaWO}_4:\text{Nd}^{3+}$. Trivalent neodymium is the active medium, and stimulated emission is produced in the infrared fluorescence line at 1.0646 microns (1.063 microns at 77°K).

Ultraviolet and visible absorption and emission spectra of trivalent neodymium ions in LaCl_3 have been analyzed in great detail by Carlson and Dieke.^{2,3} While variations arising from a different crystal field are found in the corresponding energy level diagram for the CaWO_4 host lattice, the gross features are preserved. Indeed, the strongest infrared fluorescence line was found to occur at the same wavelength for both materials.

The infrared fluorescence spectrum at 77°K of a sample cut from a crystal of $\text{CaWO}_4:\text{Nd}$ 0.14 per cent (ratio of neodymium to calcium atoms) is shown in Fig. 1. Emission was excited by an Osram HBO 200 mercury lamp and recorded by a PbS detector in conjunction with a Perkin-Elmer Model-12G grating spectrometer. Excitation is achieved most efficiently by pumping into Nd^{3+} levels lying below $25,000\text{ cm}^{-1}$. The predominant emission arises from de-excitation processes to a resonance level corresponding to the ${}^4\text{F}_{3/2}$ state of the free ion. This is followed by radiative transitions to groups corresponding to ${}^4\text{I}_{13/2}$, ${}^4\text{I}_{11/2}$, and ${}^4\text{I}_{9/2}$ states of the free ion (see Carlson³). The strongest line in the ${}^4\text{F}_{3/2} \rightarrow {}^4\text{I}_{11/2}$ group at 1.063 microns has a normal fluorescence line width of about 7 cm^{-1} at 77°K and exhibits stimu-

lated emission. The terminal state ${}^4\text{I}_{11/2}$ lies some 2000 cm^{-1} above the ground state ${}^4\text{I}_{9/2}$.

The remainder of the crystal was then cut into a cylindrical rod, and both ends were polished to spherical surfaces according to a confocal cavity geometry.⁴ Silver was evaporated on both ends, one end being left with a transmission ≈ 5 per cent. The rod was mounted on one end of a Cu-Ni tube, a window cemented to the other end, and the assembly was placed inside a Pyrex Dewar. The Dewar was centered in a helical GE FT524 xenon flash tube. Measurements at both room temperature and 77°K were made with this configuration. The lamp was flashed by discharging a 100- μf condenser charged typically to 1 kv. Optics were arranged so as to examine the light emerging through the lightly silvered end of the rod up through the tube. An RCA 7102 photomultiplier was employed for oscilloscope display and the emission was detected in conjunction with filters, quartz prism, or grating, or a desired combination.

Shown in Fig. 2 are traces taken at room temperature at progressively higher levels of flash lamp intensity. For the series shown in Fig. 2(a)–(d), only filters were used between sample and detector so as to display simultaneously both the stimulated emission and the combination of normal fluorescence and stray light from the lamp. The upper trace, Fig. 2(a), illustrates behavior at threshold, a single burst of stimulated emission superimposed on a background which closely resembles the intensity variation of the flash lamp with time. The critical

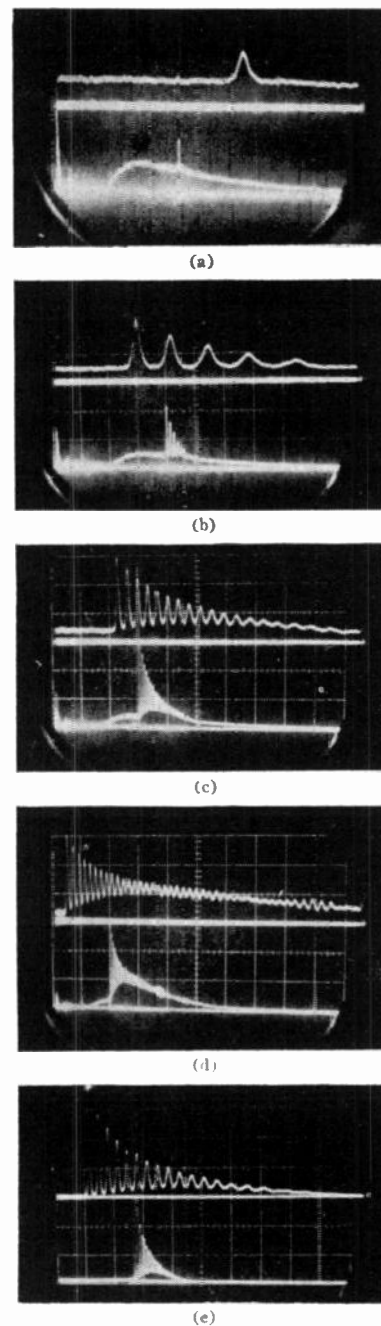


Fig. 2—Oscilloscope traces of stimulated emission at room temperature at progressively higher levels of pumping intensity above threshold. For traces (a) through (d), only wide-band filters were employed between sample and detector so as to display both stimulated emission and the combination of normal fluorescence and stray light from the flash lamp. The bottom trace of (a) illustrates behavior at threshold on a time scale of $100\text{ }\mu\text{sec/division}$. The time scale for the top trace of (a) is expanded to $20\text{ }\mu\text{sec/division}$. [Similarly for (b)–(d)]. (b) 1 per cent above threshold. (c) 17 per cent above threshold. (d) 80 per cent above threshold. (e) Stimulated emission at 1.06 microns at room temperature. The 1.06-micron line has been isolated from normal fluorescence and stray light by means of a grating. One stimulated emission is displayed. Lower trace: $100\text{ }\mu\text{sec/division}$. Upper trace: $20\text{ }\mu\text{sec/division}$, 15 per cent above threshold.

inverted population density is achieved after 250- μsec integration of the lamp intensity. The threshold for stimulated emission for this particular rod is estimated to be ~ 5 joules at room temperature and ~ 3 joules at 77°K . As the exciting intensity is

² E. H. Carlson and G. H. Dieke, "Fluorescence spectrum and low levels of NdCl_3 ," *J. Chem. Phys.*, vol. 29, pp. 229–230; July, 1958.

³ E. H. Carlson, "Absorption and Fluorescence Spectra of NdCl_3 and States of the Neodymium Ion," Johns Hopkins University Spectroscopic Rept. No. 16; March, 1960.

⁴ G. D. Boyd and J. P. Gordon, "Confocal multimode resonator for millimeter through optical wavelength masers," *Bell Sys. Tech. J.*, vol. 40, pp. 489–503; March, 1961.

increased very slightly above threshold, the stimulated emission manifests itself as a series of damped oscillations, the number of such oscillations increasing rapidly with energy above threshold [Fig. 2(b), (c)], while the oscillation amplitude decay time remains roughly constant at about 35 μ sec. At intensities well above threshold, the oscillations take on a "ringing" character [Fig. 2(d)], and occasionally bursts of oscillations follow the main train. At room temperature, the period between oscillations increases with time at all excitation levels employed, but at 77°K the period first increases at low levels above threshold, then decreases at higher intensities.

A more detailed presentation of the stimulated emission pattern as a function of time is obtained when the 1.06-micron line is isolated from the background of stray light and normal fluorescence by utilizing a grating. A typical example of such a pattern, shown in Fig. 2(e), is seen to consist of the relaxation oscillations superimposed on a continuum of stimulated emission which rises slowly as the oscillations decay. It is to be emphasized that the level of spontaneous emission (normal fluorescence) is too weak to be observed, and that the entire pattern consists solely of stimulated emission.

The authors would like to thank C. G. B. Garrett for several valuable discussions, and W. S. Boyle, whose early interest in the Nd^{+3} ion is gratefully acknowledged. They also wish to thank P. M. Ness for preparing the spherical ends, and R. A. Thomas and A. M. Broyer for valuable technical assistance.

L. F. JOHNSON

K. NASSAU

Bell Telephone Laboratories, Inc.
Murray Hill, N. J.

Maser Oscillation Observed from HCN Maser at 88.6 kMc*

In a previous publication,¹ the author reported observed stimulated emission from an HCN maser. At that time, no maser oscillation had been obtained.

Since the time of these earlier experiments, our HCN maser has been rebuilt. In its present form, the maser consists of a Fabry-Perot-type cavity with a plane and a spherically curved reflector ($Q=30,000$). The spacing between the two reflectors is arranged so that it results in a half confocal cavity.² This cavity is surrounded by two circular gas sources that shoot beams radially from many points of the periphery into the center of the circle, at which point the cavity is located. Each of these two planar

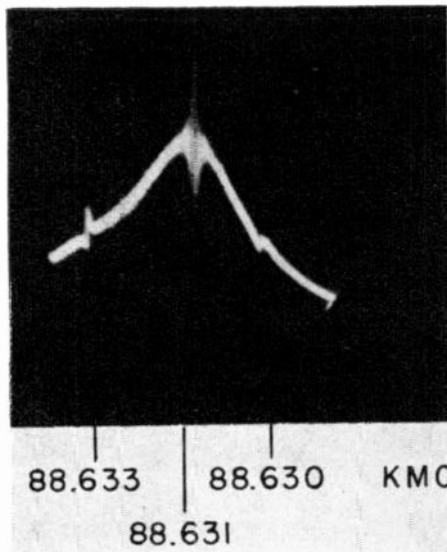


Fig. 1—The line on top of the cavity response curve sustains oscillation as indicated by the beat phenomenon between maser and probing signal.

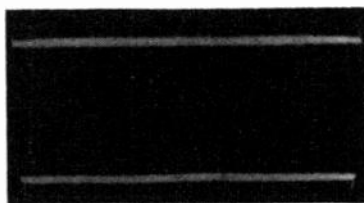


Fig. 2—The upper trace indicates the rectified component of the maser signal at the output of the 70-Mc amplifier. The lower trace is the reference level with the maser turned off. The difference between these two levels is 16 db.

beams passes through a state selector, which consists of two planes which are closely spaced and allow the gas beam to pass between them. Each plane is made of radially arranged rods which are charged alternately to positive and negative potentials of $\pm 10,000$ volts. The whole maser structure is contained in a copper cylinder which can be cooled by liquid nitrogen. Fastened on to this cylinder are copper fins that extend between the state selectors and freeze out that part of the gas beam that is rejected by them. The whole apparatus described above is mounted in a vacuum system.

As in the previous maser,¹ a probing signal can be sent through the transmission-type cavity. Two waveguides are coupled to the cavity by small holes in the flat reflector plate.

Fig. 1 shows the emission spectrum with the strongest line at 88.631 kMc tuned to the peak of the cavity response curve. This line actually sustains oscillation. The picture shows the beat note of the maser oscillation with the probing signal superimposed on the picture of the emission line. This phenomenon needs some further explanation. The cavity allows several different modes to be resonant simultaneously. The maser apparently does not oscillate in the mode that is excited by the probing signal. This explains why the maser breaks into oscillation before any appreciable gain can be observed. The electronic gain reaches only

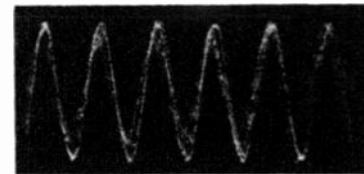


Fig. 3—Display of the 70-Mc signal resulting from heterodyning the maser output with a klystron.

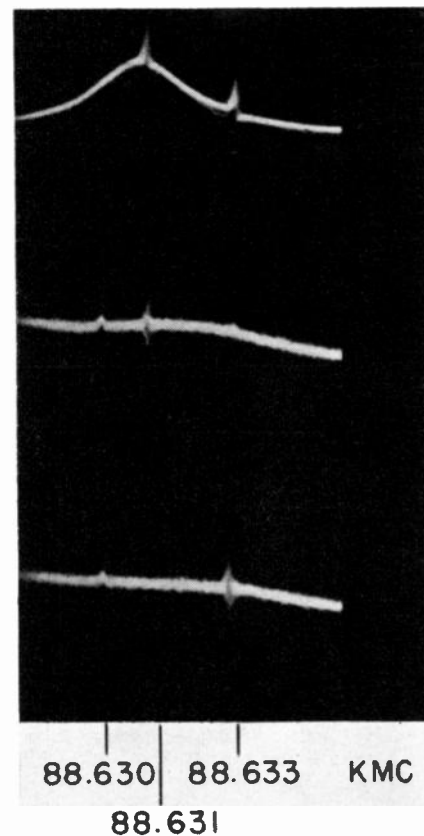


Fig. 4—Upper trace shows relative position of the two major emission lines. The two lower traces show the beat phenomenon between the maser output and the probing signal as one or the other line oscillates.

about 5 db at the point where the maser breaks into oscillation, while the insertion loss of the empty cavity is about 10 db.

The result of the maser output being heterodyned with a klystron is shown in Fig. 2. The resulting 70-Mc signal is amplified, rectified and displayed on the scope. No probing signal was passed through the cavity. The lower trace was obtained with the gas beam turned off and represents the rectified noise level. The upper trace shows the increase in level as a result of the maser output. The difference between the two levels is 16 db. The IF amplifier has a width of 20 Mc between 3-db points.

Fig. 3 shows a stroboscopic oscilloscope picture of the 70-Mc signal that is obtained by mixing the maser output with the signal from the klystron. Due to phase instability of the klystron, the scope did not achieve perfect synchronization, which explains the double trace.

Fig. 4, finally, demonstrates that both of the stronger emission lines at 88.631 kMc

* Received by the IRE, September 19, 1961.

¹ D. Marcuse, "Stimulated emission from HCN gas maser observed at 88.6 kmc," *J. Appl. Phys.*, vol. 32, p. 743, April, 1961.

² G. D. Boyd and J. P. Gordon, "Confocal multimode resonator for millimeter through optical wavelength masers," *Bell Sys. Tech. J.*, vol. 40, pp. 489-508; March, 1961.

and 88.633 kMc sustain maser oscillation. The upper trace shows both lines in their relative position on the cavity response curve. Subsequently, the cavity was tuned to each of the two lines in turn, and the beat note of the maser output with the probing signal (the latter at a much reduced level) is displayed in the two lower traces. As can be seen, both lines give rise to oscillation. The different traces in this picture were obtained by shifting the camera contrary to Fig. 2, where the camera stayed fixed.

DIETRICH MARCUSE

Bell Telephone Laboratories, Inc.
Holmdel, N. J.

giving high performance comparable to special varactor diodes.

High-speed silicon computer diodes accordingly can be considered as an economic and efficient substitute for special-purpose silicon diodes for RF switching applications.

R. E. AITCHISON

School of Elec. Engrg.
University of Sydney
Sydney, N.S.W., Australia

Use of a Coherent Memory Filter in Spectral Measurements of Atmospheric Whistlers*

It is often of interest to know the spectrum of a signal. This measurement has been performed by devices which could be divided, with few exceptions, into two groups: the heterodyne type and the bank-of-filters type. The heterodyne type of spectrum analyzer utilizes a fixed narrow-band intermediate-frequency filter and a tunable local oscillator. This device does not analyze the spectrum in real time, *i.e.*, the read-out time of the device is very long compared to the duration of the signal. It is not possible to measure the entire spectrum without recording the signal and playing it back many times.

The second type of spectrum analyzer employs a bank of filters. The measurement of the spectrum with this device can take place in real time, so that this type of analyzer has an advantage over the previous one in this respect. However, it is cumbersome to implement a bank of filters, and, in addition, it yields only a gross approximation of the signal spectrum.

A different approach to the spectrum analysis measurement problem has been implemented. This approach utilizes a recirculating delay-line-heterodyner feedback loop to obtain an excellent approximation of the signal spectrum in real time, as pointed out previously.¹ This device is known as the coherent memory filter, and it has the advantages with respect to the bank of filters of being capable of observing rapid changes in the input spectrum that occur from one processing period to the next, and of providing continuous spectral coverage. In addition, the processing period, or integration time, of the coherent memory filter is easily adjustable so that variable-resolution analysis of nonstationary spectra is possible. This is the equivalent of continually changing the number of filters, and their bandwidths, in a filter bank consisting of hundreds of filters.

One class of signals whose spectra yield much valuable information is that of atmospheric whistlers. The coherent memory

* Received by the IRE, August 10, 1961. This paper was presented at the URSTI Convention, Washington, D. C., May, 1961.

¹ J. Capon, "High-speed Fourier analysis with recirculating delay-line-heterodyner feedback loops," IRE TRANS. ON INSTRUMENTATION, vol. I-10, pp. 32-37; June, 1961.

High-Speed Silicon Computer Diodes as RF Switches*

The specifications of silicon computer diodes, of the type with switching speeds of less than 10 nsec, indicate the possibility of the use of these diodes as RF switches.

The use of germanium computer diodes as switches has previously been reported by Bloom;¹ at that time, the silicon computer diodes available were not suitable for this application. The low-capacitance, low-slope resistance of the forward characteristic, and high rectification efficiencies at 100 Mc, of present high-speed silicon computer diodes imply high Q and reasonable cutoff frequencies.

The Q of a number of diodes (types 1N914, 1N916, FD100, and FD200) were measured by a cavity perturbation method at 408 Mc, the measured values corresponding to cutoff frequencies of from 20 to 40 kMc at zero bias. The capacitance and capacitance-voltage characteristic were measured at $10/\pi$ Mc at an applied RF level of less than 10 mv. The capacitances at zero bias were considerably smaller than the manufacturer's specified nominal value; for example, the average value for twelve FD200 was 1.63 pf at zero bias (nominal value 5.5 pf), and for twelve 1N916 0.97 pf (nominal value 1.6 pf). The C-V characteristic was also much less nonlinear than expected.

A number of diodes were tested in a SPDT radiometer switch at a frequency of 408 Mc. The insertion loss of typical diodes was 0.3 db, and the isolation greater than 26 db, using appropriate external series and shunt reactances for tuning out the diode internal reactances in the ON and OFF directions.

The RF performance and Q were found to be correlated with the junction capacitance, in that high-capacitance samples gave inferior performance. Measurements of 50 diodes indicate that this type of diode can quite generally be used as an RF switch element at frequencies up to approximately 1.5 kMc, with over 80 per cent of diodes

* Received by the IRE, August, 11, 1961.

¹ M. Bloom, "Microwave switching with computer diodes," *Electronics*, vol. 33, pp. 85-87; January 15, 1960.

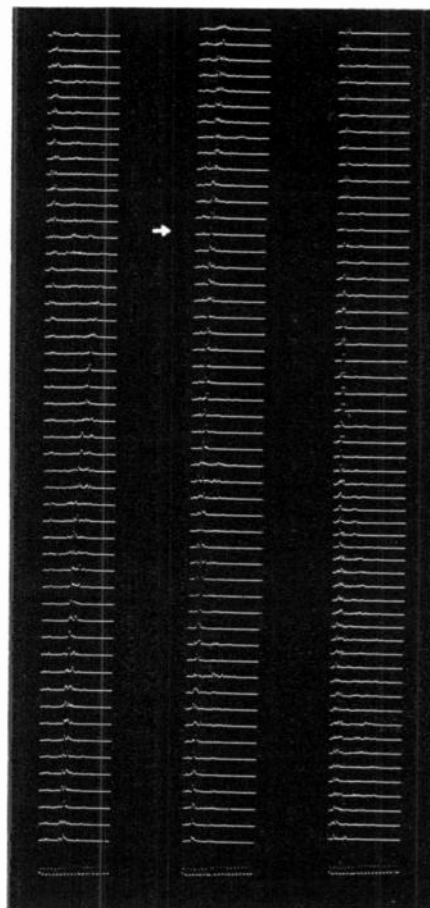


Fig. 1—Spectral analysis illustrating the evolution of an atmospheric whistler.

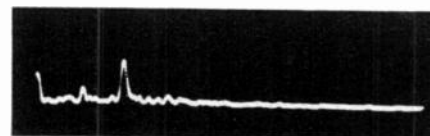


Fig. 2.

filter was used to analyze the spectra of these signals, and the experimental results are shown in Figs. 1 and 2. It was found experimentally that a processing time of about 20 msec is desirable for the measurement of the spectra of these signals. The frequency coverage of the spectral analysis was 0 to 8 kc since it was found that there was very little energy outside this band. The input signal was time-weighted with a symmetrical triangular function, so that an effective resolution of about 73 cps was obtained. Thus, roughly speaking, the equivalent of a filter bank with approximately 110 filters, each with an effective bandwidth of 73 cps, was synthesized.

ACKNOWLEDGMENT

The atmospheric whistler signals were supplied on a tape recording through the kindness of Prof. R. A. Helliwell of Stanford University.

J. CAPON
M. R. WEISS
Federal Scientific Corp.
New York, N. Y.

Injection Efficiency in Double Diffused Transistors*

Emitters in double diffused transistors have a rapidly varying impurity distribution which causes a built-in electric field that opposes the flow of minority carriers injected into the emitter. As a result, the injected minority carrier concentration falls rapidly as a function of distance from the emitter-base junction toward the emitter contact, and it is already low within one diffusion length from the junction. Earlier calculations of injection efficiency neglecting either electric field or carrier lifetime are not adequate for this situation. An approximate formula including both is given in this note.

Consider an n - p - n transistor and define a common-emitter injection efficiency gain parameter by

$$\beta_\gamma = \left| \frac{J_{n1}}{J_{p1}} \right|$$

where J_{n1} is electron density in the base at the edge of the emitter-depletion region and J_{p1} is hole density in the emitter at the edge of the depletion region. In the base it is satisfactory to assume infinite lifetime and to calculate J_{n1} by the method of Moll and Ross.¹

$$J_{n1} = q \frac{D_n N_{A1} n_1}{w \bar{N}_A}$$

where N_{A1} is acceptor concentration in the base at the edge of the depletion region, n_1 is electron concentration, \bar{N}_A is average acceptor concentration in the base, w is base width, q is electron charge, and D_n is electron diffusion constant.

In the emitter, we have in the usual notation

$$p = Z^{(1-a)/2} \frac{A(-iZ)^{(1+a)/2}}{2^{(1+a)/2} \Gamma\left(\frac{3+a}{2}\right)} \left(1 - \frac{1}{1! \left(\frac{3+a}{2}\right)} \left(\frac{-iZ}{2}\right)^2 + \dots\right) + \frac{B(-iZ)^{-(1+a)/2}}{2^{-(1+a)/2} \Gamma\left(\frac{1+a}{2}\right)} \left(1 - \frac{1}{1! \frac{(1-a)}{2}} \left(\frac{-iZ}{2}\right)^2 + \frac{1}{2! \left(\frac{1-a}{2}\right) \left(\frac{3-a}{2}\right)} \left(\frac{-iZ}{2}\right)^4 \dots\right).$$

$$\frac{1}{q} \frac{dJ_p}{dx} + \frac{p}{\tau p} = 0$$

$$J_p = q\mu_p \cdot pE - qD_p \frac{dp}{dx}.$$

Let

$$L_p = \sqrt{D_p \tau_p} \quad Z = \frac{x}{L_p} \quad \eta = \frac{qEL_p}{2kT}.$$

Combining the differential equations and using the Einstein relation, we have

$$\frac{d^2 p}{dZ^2} - 2 \frac{dp}{dZ} - p \left(2 \frac{d\eta}{dZ} + 1 \right) = 0.$$

The field parameter is obtained from the impurity profile by

$$\eta = - \frac{1}{2N_D} \frac{dN_D}{dZ}.$$

Now we represent the impurity profile by an approximate expression which is tractable in the differential equation. We choose

$$N_D = cx^a.$$

Then

$$\eta = - \frac{a}{2Z}.$$

Typical profiles can be represented satisfactorily with a suitable choice of a . For a practical silicon transistor design example, a value of a of about 2.8, with the origin for Z displaced slightly from the emitter junction, gave reasonable agreement with impurity densities and electric-field values calculated from the exact relations.²

The differential equation becomes

$$\frac{d^2 p}{dZ^2} + \frac{a}{Z} \frac{dp}{dZ} - p \left(1 + \frac{a}{Z^2} \right) = 0,$$

which is a form of Bessel's equation. For cases where $(1+a)/2$ is not an integer, the solution is

$p = Z^{(1-a)/2} \cdot 1 [J_{(1+a)/2}(-iZ) + BJ_{-(1+a)/2}(-iZ)]$ where the J 's are Bessel functions and $i = \sqrt{-1}$.

We must calculate the hole current in the emitter at the edge of the depletion region. With the junction forward biased, the depletion region extends about 10^{-6} cm from the junction. If the hole-diffusion constant is as small as $2 \text{ cm}^2/\text{sec}$ and the lifetime as small as 10 nsec , the diffusion length is 1.4×10^{-4} cm. Z is then 10^{-1} or smaller, and we may expand the Bessel functions as follows:³

edge of the depletion region,

$$Z = Z_1, \quad p = p_1 \text{ so } B \approx p_1 Z_1^a$$

and

$$p \approx p_1 Z_1^a \left[Z^{-a} + \frac{Z^{2-a}}{2(1-a)} \right].$$

The first term in the bracket gives the equilibrium hole density at the edge of the depletion region; only the second term contributes to the current. Current density is found from

$$\frac{L_p J_p}{q D_p} = 2\eta p - \frac{dp}{dZ} = \frac{-ap}{Z} - \frac{dp}{dZ}.$$

Evaluating J_p at Z_1 and returning to the original variables we find

$$J_{p1} = \frac{-q D_p p_1}{\frac{q}{kT} E_1 L_p^2} \frac{1}{\left(1 - \frac{1}{a}\right)}.$$

Then

$$\beta_\gamma = \frac{D_n}{D_p} \frac{\frac{q}{kT} E_1 L_p^2 N_{A1} n_1}{w \bar{N}_A p_1} \left(1 - \frac{1}{a}\right)$$

$$\beta_\gamma = \frac{D_n N_{D1}}{w \bar{N}_A} \frac{\frac{q}{kT} E_1 \tau_p}{\left(1 - \frac{1}{a}\right)}.$$

This result differs from previous calculations by the proportionality to lifetime rather than to diffusion length in the emitter, and by the specification of field and donor concentration at the edge of the depletion region in the emitter. A very similar result is obtained for constant field in the emitter.⁴

MELVIN KLEIN

Components Div.

International Business Machines Corp.

Poughkeepsie, N. Y.

⁴ W. E. Harding, private communication.

Antenna Size for a Space Vehicle*

Directional antennas on space vehicles have grown to the size where they have become a significant portion of the space vehicle. With their small beamwidth, they require a considerable amount of associated equipment and structure to control and power them. This letter shows that the weight of an area-limited directional-transmitting antenna, together with all of the associated gear and structure used to operate it, should weigh $\frac{2}{3}$ the weight of the transmitter and its associated gear and structure. Included in the definition of associated gear is everything which is directly needed to operate the device, such as solar panels, storage batteries, structural members for holding the solar panels and batteries, drive motors, control equipment, and heat sinks. It does not include such weights as are associated with data processing, scientific experiments, and receiving equipment.

Redefining the arbitrary constants and retaining only the leading terms,

$$p \approx AZ + B \left[Z^{-a} + \frac{Z^{2-a}}{2(1-a)} \right]$$

We shall now assume that the boundary condition at the emitter contact is such that A is not large compared with B . (The solution to the differential equation can be written in closed form when the parameter a is an even integer. This has been done for $a=2$ and $a=4$ and the ratio $|A/B|$ has been evaluated for the case of an emitter contact with infinite recombination velocity. Provided that the emitter is several diffusion lengths wide, the magnitude of the ratio was found to be less than, or equal to, 1.) We may then drop the first term in p . At the

* Received by the IRE, August 15, 1961.

¹ J. L. Moll and I. M. Ross, "The dependence of transistor parameters on the distribution of base layer resistivity," Proc. IRE, vol. 44, pp. 72-78; January, 1956.

² D. P. Kennedy provided machine calculations based on work that he is publishing.

³ P. M. Morse and H. Feshbach, "Methods of Theoretical Physics, Part I," McGraw-Hill Book Co., Inc., New York, N. Y., p. 619; 1953.

* Received by the IRE, August 18, 1961.

The power P_t of the transmitter is assumed to be directly proportional to its size in terms of its weight W_t :

$$P_t = k_1 W_t$$

It is assumed that a transmitter tube which is capable of putting out twice the power of another tube would require twice the weight in solar panels, structures, heat sinks, etc. The gain of the directional antenna G_a is assumed to be directly proportional to the area of the antenna. The area of the antenna is related to the volume, such that the gain G_a is a direct function of the weight to the $\frac{2}{3}$ power:

$$G_a = k_2 W_a^{2/3}$$

That is, the weight is proportional to the dimension cubed, while the gain is proportional to the dimension squared. The weight of associated equipment to operate the antenna must be added to the actual weight of the antenna. It is assumed to be directly proportional to the weight of the antenna.

For a given weight W of the transmitter and antenna, it is desirable to have the maximum effective power radiated P . This is the product of the transmitter power and the antenna gain.

$$P = P_t G_a = k W_t W_a^{2/3}$$

$$W = W_t + W_a$$

Maximization of P subject to the weight constraint produces the following result:

$$W_a = \frac{2}{3} W_t$$

i.e., the weight of the antenna should be $\frac{2}{3}$ the weight of the transmitter.

C. S. LORENS
Space General Corp.
Glendale, Calif.

Input-Output Relationships for Multisampled Loop Systems*

In his recent note¹ Dr. Tou made a statement to which I wish to take exception. In referring to a paper that I co-authored,² he said, "... the methods proposed in the literature appear either quite involved or lack of generality." The method introduced in my two papers^{2,3} is, I feel, simpler to use than Dr. Tou's, and, furthermore, is just as general an approach for determining the output of these systems in terms of their input(s) and system parameters.

So that the readers may judge for themselves, I will state the method here and illustrate it by solving the same example as Dr. Tou did in his note. Further, I will pre-

sent a more complicated example and ask the reader to try both methods and then judge for himself which is simpler.

Generally speaking, the approach is to represent the given system block diagram by an appropriate signal-flow graph (I call it a sampled-signal-flow graph, he calls it a pulsed-signal-flow graph) to which Mason's theorem can be applied. Note, that in words, both of our techniques sound the same; however, the differences lie in the choice of the type of flow graph used and the procedure employed in going from the block diagram to this flow graph.

I propose a six step procedure for going directly from the block diagram to the sampled-signal-flow graph—no mathematics in between! After this sampled-signal-flow graph is completed, step seven is to apply Mason's theorem and to write the output by inspection. The following is the proposed procedure:

- 1) Eliminate all redundant samplers in the original block diagram. This step is not necessary for correct results, but it simplifies the resulting flow graph.
- 2) Number all samplers (in any fashion desired).
- 3) On a separate sheet of paper draw a node for each sampler indicated in step 2) and label these S_1^* , S_2^* , ..., S_n^* .
- 4) Open all samplers in the block diagram.
- 5) Start from sampler 1 and traverse all possible continuous paths from the output of sampler 1 to the input of all samplers. Where these exist, draw in a branch on the signal-flow graph from node S_1^* to the respective node S_k^* with the direction and the appropriate sampled transfer function indicated. Then start at sampler 2 and repeat procedure until all samplers are covered.
- 6) Now add two other nodes: one labeled with a 1 (the input), and one labeled with a C (the output). From the input node draw a branch to each of the nodes which has a corresponding continuous path in the block diagram, and label with the appropriate gain ($R G_{i0}'$ to the output, and $R G_{i0k}^*$ to the other nodes). Then draw a branch from each of the nodes S_k^* which has a corresponding continuous path in the block diagram to the output node C and label appropriately (G'_{k0}).
- 7) Then to obtain the output of the system, apply Mason's or Coates' method to the nodes marked C and 1 of this sampled-signal-flow graph.

If the sampled form of the output is desired, one may use the standard technique of starting the expression for C obtained in 7).

Let us now work out the example presented by Dr. Tou. After applying step 1) of

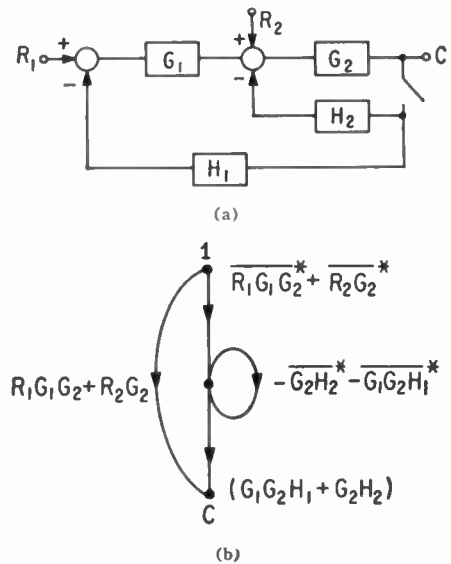


Fig. 1—(a) Block diagram for the illustrative example 1. (b) Sampled-signal-flow graph for this system.

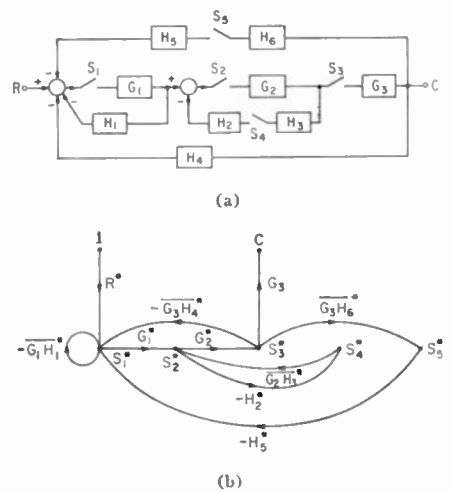


Fig. 2—(a) Block diagram for the illustrative example 2. (b) Sampled-signal-flow graph for this system.

be drawn directly. Then, by applying Mason's theorem to this flow graph, we can write the expression for the output

$$C(s) = \frac{R_1 G_1 G_2(s) + R_2 G_2(s)}{1 + \frac{(R_1 G_1 G_2^* + R_2 G_2^*)(G_1 G_2 H_1 + G_2 H_2)}{G_2 H_2^* + G_1 G_2 H_1^*}} \quad (1)$$

This completes the example.

Let us now consider the system whose block diagram is shown in Fig. 2(a). There are no redundant samplers in this system, so step 1) may be skipped. By applying rules 2-6 to this block diagram, its corresponding sampled-signal-flow graph [Fig. 2(b)] can be drawn directly. Again, by applying Mason's theorem, the expression for the output may be written:

$$C(s) = \frac{R^* G_1^* G_2^* G_3}{1 + \overline{G_1 H_1^*} + \overline{H_2^* G_2 H_3^*} + \overline{G_1^* G_2^* G_3 H_4^* H_5^*} + \overline{G_1^* G_2^* G_3 H_4^*} + \overline{G_1 H_1^* H_2^* G_2 H_3^*}} \quad (2)$$

our procedure, his block diagram reduces to that shown in Fig. 1(a). By applying rules 2-6 to this block diagram, the corresponding sampled-signal-flow graph [Fig. 1(b)] can

GEORGE G. LENDARIS
Dept. of Elec. Engrg.
University of California
Berkeley, Calif.

* Received by the IRE, April, 14, 1961.
¹ J. T. Tou, "A simplified technique for the determination of output transforms of multiloop, multi-sampler, variable-rate discrete-data systems," *Proc. IRE*, vol. 49, pp. 646-647; March, 1961.
² G. G. Lendaris and E. I. Jury, "Input-output relationships for multisampled loop systems," *Trans. AIEE*, vol. 78 (*Applications and Industry*, no. 78), pp. 375-485; January, 1960.
³ G. G. Lendaris, "Discussion on 'A general flow graph technique for the solution of multiloop sampled systems' R. Ash, W. H. Kim, and G. M. Kranc," *Trans. ASME, J. of Basic Engrg.*, vol. 82, pp. 360-370; June, 1960.

Contributors

Willard S. Boyle was born in Nova Scotia, Canada, on August 19, 1924. He received the B.Sc., M.Sc., and Ph.D. degrees from McGill University, Montreal, Canada, in 1947, 1948, and 1950, respectively.

After joining the Technical Staff of Bell Telephone Laboratories, Murray Hill, N. J., he was concerned with electrical discharge phenomena in low-voltage contacts. He later studied optical properties of metals in the far infrared and at very low temperatures. For the past three years, he has headed a group studying optical properties of solids and microwave characteristics of semi-metals. He has also been engaged in research in the infrared spectroscopy of solids.

Dr. Boyle is a member of the American Physical Society and Sigma Xi.



W. S. BOYLE



Robert H. Doherty (SM'59) was born in Albert Lea, Minn., on May 9, 1927. He received the B.S. degree from the University of Colorado, Boulder, in 1950.



R. H. DOHERTY

In 1951 he joined the National Bureau of Standards, Boulder, Colo. In 1954 joined the Navigation Systems Section of the Radio Systems Division, where he is now an Electronic Engineer, and Project Leader of the Navigation Systems Analysis project, and the Loran-C Clock and Distribution System project. His work involves over-all concepts of navigation and timing systems.

Mr. Doherty is an associate member of Commission III of URSI, a member of Sigma Pi Sigma, and of Study Groups VI and XIII of CCIR.



Eduard A. Gerber (A'50-SM'56-F'58) was born in Fuerth, Bavaria, Germany, on April 3, 1907. He received his education at the Institute of Technology in Munich and Berlin, Germany. From the former, he received the M.S. degree in 1930 and the Ph.D. degree in 1934, both in physics.

In 1935 he joined the Scientific Staff of the Carl Zeiss Works, Jena, Germany, and was in charge of research and development in piezoelectric crystals. From 1947 to 1954

he was a Consultant to the Signal Corps Engineering Laboratories, Fort Monmouth, N. J., on all matters pertaining to frequency control, and from 1954 to 1961 he served as Director of the Frequency Control Division, USASRDL. Since February, 1961, he has been Director of the newly organized Solid State and Frequency Control Division.



E. A. GERBER

Dr. Gerber is a member of the IRE Standards Committee and the IRE Committee on Piezoelectric and Ferroelectric Crystals. He was Chairman of the latter Committee from 1958-1960. He is also a member of Commission I of the International Scientific Radio Union and a Technical Advisor, Committee on Piezoelectric Crystals and Associated Devices, U. S. National Committee of the International Electrotechnical Commission.



Gifford Hedley was born in Norman, Okla., on September 12, 1915. He received the B.A. degree from the University of Oklahoma, Norman, in 1938.



G. HEDLEY

He joined the National Bureau of Standards, Washington, D. C., in 1949, and transferred to the NBS Boulder Laboratories in 1951, where he is now Chief of the Navigation Systems Section of the Radio Systems Division. Prior to joining NBS, he was a radio engineer with the U. S. Signal Corps, a Loran Project Engineer with the Air Force at Wright Field, and a Development Engineer with Petty Laboratories. One of his major interests is in time-position relationships; he has supervised the development of the Loran-C clock, done research work on ground conductivity, and has also worked on propagation problems on VLF navigation systems.

Mr. Hedley is a member of RESA, and Study Group VII of CCIR.



G. Clement Ireland (M'60) was born in Vancouver, British Columbia, Canada, on April 18, 1924. After serving in World War

II with the Royal Canadian Artillery, he attended the University of Saskatchewan, Saskatoon, where he received the B.S. degree in electrical engineering in 1950.



G. C. IRELAND

From 1950 to 1957, he was employed by the Department of National Defence, Ottawa, Canada, as a civilian electrical engineer, first with the Naval Services and then with Canadian Military Electronics Standards Agency.

In 1957, he transferred to the Radio Regulations Division of the Canadian Department of Transport, in Ottawa, where he is presently employed in allocation studies for AM, FM, and TV broadcasting stations.

Mr. Ireland is a member of the Association of Professional Engineers of Ontario and of the Engineering Institute of Canada.



Paul P. Kisliuk was born in Philadelphia, Pa., on February 22, 1922. He received the B.S. degree in 1943 from Queens College, N. Y., and the M.A. and Ph.D. degrees from Columbia University, New York, N. Y., in 1947 and 1952, respectively.



P. P. KISLUK

He has been a member of the Technical Staff of Bell Telephone Laboratories, Murray Hill, N. J., since 1952, where he has been engaged in research in contact and surface physics. His studies have included problems at relay contacts and adsorption of gases on metals. Recently his work has been concerned with optical masers.

Dr. Kisliuk is a member of the American Physical Society and Sigma Xi.



Robert F. Linfield (SM'59) was born in Bozeman, Mont., on November 20, 1925. He received the B.S. degree in engineering physics from the University of Colorado, Boulder, in 1956.



R. F. LINFIELD

He joined the National Bureau of Standards, Washington, D. C., in 1948, where he did missile development work; from 1951 to 1954 he was employed at the NBS Missile Division, Corona, Calif.; and from 1954 to 1961 he worked at the NBS Navigation Systems Section in Boulder, Colo. He was a

Project Leader in the NBS Radio Navigation Section and did intensive research on the Loran-C system. Prior to NBS, he was a U. S. Navy Radar Technician, and currently he is employed by DECO Electronics Inc., Boulder, Colo.

Mr. Linfield is an associate member of Commission III of URSL.



Ivars Melngailis (M'59) was born in Riga, Latvia, on November 13, 1933. He received the B.S., M.S., and Ph.D. degrees in electrical engineering from Carnegie Institute of Technology, Pittsburgh, Pa., in 1956, 1957, and 1961, respectively. During the academic year 1957-1958, he studied physics at the University of Munich, Germany, under a Fulbright Fellowship.



I. MELNGAILIS

In 1958-1959 he was an Instructor in electrical engineering at the Carnegie Institute of Technology, and in 1960, a Project Engineer studying low-temperature electrical properties of germanium. At present he is a member of the Applied Solid-State Physics staff at the M.I.T. Lincoln Laboratory, Lexington, Mass., engaged in research on electrical and magnetic phenomena in semiconductors and semiconductor devices.

Dr. Melngailis is a member of Tau Beta Pi, Eta Kappa Nu, and Sigma Xi.



Norman H. Meyers (SM'59) was born in Buffalo, N. Y., on February 11, 1931. He received the B.E.E. degree from Rensselaer Polytechnic Institute, Troy, N. Y., in 1952, and the S.M. and Sc.D. degrees in electrical engineering from the Massachusetts Institute of Technology, Cambridge, in 1954 and 1957, respectively.



N. H. MEYERS

He remained at M.I.T. as an Assistant Professor of Electrical Engineering from 1957 to 1958, and did research in the classical electrodynamics of moving media. In 1958 he joined the staff of the research laboratory of IBM Corporation, Yorktown Heights, N. Y., where he has been engaged in

the research and development of high-speed thin-film superconducting circuitry.

Dr. Meyers is a member of Tau Beta Pi, Eta Kappa Nu, Sigma Xi, and the Scientific Research Society of America.



M. H. Miles was born in Blount County, Ala., on December 26, 1935. He received the B.S. degree in electrical engineering from the



M. H. MILES

University of Tennessee, Knoxville, in 1959. While in school he worked with Southern Bell Telephone and Telegraph Company, Memphis, Tenn. After working briefly with Southern Bell in Nashville, Tenn., he served in the Army from 1959 to 1961 at the U. S. Army Signal Research and Development Laboratory, Fort Monmouth, N. J. In 1961 he returned to his former position as Assistant Engineer with Southern Bell in Nashville.

He has been a member of Eta Kappa Nu and a student member of AIEE.



Arthur G. Milnes (SM'58) was born in England on July 30, 1922. He received the B.S. degree in electrical engineering in 1943, and the M.S. degree in 1947 from the University of Bristol, England. From 1947 to 1950 he carried out research work at the University on magnetic amplifiers. In 1956 for a book on this subject and for other research papers he was awarded the D.Sc. degree.



A. G. MILNES

From 1943 to 1957 he held Scientific Officer posts at the Royal Aircraft Establishment, Farnborough, Great Britain, apart from the academic year 1954-1955, which was spent on a Royal Society-National Academy of Science Fellowship at Carnegie Institute of Technology, Pittsburgh, Pa. In 1957 he returned to C.I.T. where he is now Professor of Electrical Engineering, with major research interests in the semiconductor device and solid-state fields.

Dr. Milnes is a member of the AIEE and the IEE (London).

Robert H. Norton was born in New York, N. Y., on February 5, 1935. He received the B.S. and M.S. degrees in astrophysics from the California Institute of Technology, Pasadena, in 1957 and 1958 respectively. He has been working on a doctoral program in astrophysics at C.I.T. and expects to complete his dissertation in 1962.



R. H. NORTON

From 1958 to 1961 he has been employed part time at the Jet Propulsion Laboratories of the California Institute of Technology and has worked on such projects as the Deep Space Instrumentation Facility in the Telecommunications Division, and the gas bearing research conducted in the Guidance and Control Division. In 1961 he joined JPL full time as Research Engineer in the Guidance and Control Research section.

Mr. Norton is a member of the American Astronomical Society.



Chih-Tang Sah (S'50-M'57), for a photograph and biography, please see page 651 of the March, 1961, issue of these PROCEEDINGS.



Robert L. Wildey was born in Los Angeles, Calif. on August 22, 1934. He received the B.S. and M.S. degrees in astronomy from the California Institute of Technology, Pasadena, in 1957 and 1958, respectively. He is presently completing his doctorate at the Mount Wilson and Palomar Observatories, Pasadena.



R. L. WILDEY

During the summers of 1958 and 1959, he worked in the Guidance Research Section at the Jet Propulsion Laboratory, C.I.T. His research has been in the fields of galactic structure and stellar evolution, photoelectric and photographic stellar photometry, line-blanketing effects in stellar atmospheres, solar corpuscular radiation and the interplanetary dust cloud, and the measurement of planetary diameters.

Mr. Wildey is a member of the American Astronomical Society and Sigma Xi.

Books

Adaptive Control Processes: A Guided Tour, by Richard Bellman

Published (1961) by Princeton University Press, Princeton, N. J. 247 pages+5 index pages+xvi pages+bibliography by chapter. Illus. 6½×9½. \$6.50.

This reviewer should like to state at the outset that if he were asked to name an individual whose work is likely to have by far the greatest impact on the course of development of control theory in the years ahead, he would answer without a moment's hesitation: Richard Bellman.

Until the publication of the present volume, much of Bellman's work was inaccessible to a large body of scientific workers and engineers whose lack of mathematical sophistication prevented them from penetrating the barriers presented by such mathematical elements in Bellman's theory as functional equations, invariant imbedding, policy space, etc. Indeed, it is largely because of the presence of such barriers that there are still many control engineers who have not fully grasped the significance of Bellman's contributions and are only dimly aware of the potency of dynamic programming and related techniques.

On the surface, the book under review gives the appearance of a popularized and somewhat sketchy exposition of a wide gamut of ideas and techniques contributed by Bellman, together with a discussion of their relation to more classical approaches. In fact, it is much more than that. Upon careful perusal, one finds a wealth of incisive comments and enlightening observations which give the reader much insight into some of the most fundamental aspects of modern control theory. Throughout, the major aim is to lay clear the basic ideas and the motivation rather than to fill in the technical details. In this, the author succeeds admirably.

The range of topics covered by the text is extremely wide. Some are treated fairly completely, some are merely touched upon. Understandably enough, the subject that receives most attention is dynamic programming, its applications, and its relation to the calculus of variations.

To be more specific, Chapters 1 and 2 introduce the reader to the concept of state, the fundamentals of dynamical systems, and some variational problems. Chapter 3 is given over to an introductory discussion of multistage decision processes. Here the author states his "principle of optimality" and points out its connection with a basic property of the maximum, namely, $\text{Max}(x_1, x_2, \dots, x_n) = \text{Max}(x_1, \text{Max}(x_2, \dots, x_n))$. Chapters 4 and 6 present a very illuminating analysis of the relation between dynamic programming and the calculus of variations—especially the Lagrange multiplier method. The computational aspects of dynamic programming are discussed in Chapters 5 and 6, with the latter chapter treating the two-point boundary value problems. The application of dynamic programming to some problems in finite-state systems is discussed very briefly in Chapter 8. In the opinion of this reviewer, it is such

systems, both of deterministic and stochastic types, that offer dynamic programming one of its most fruitful areas of application.

The remaining chapters are concerned in the main with stochastic systems and Markovian decision processes. Of particular interest here is a theory of adaptation—based on dynamic programming—which was developed by Bellman and his talented collaborator, R. Kalaba. In contrast with other theories of adaptation, the Bellman-Kalaba theory leads to systems which are optimally adaptive in a well-defined and very reasonable sense. Unfortunately, "the curse of dimensionality" makes the practical implementation of the Bellman-Kalaba theory rather difficult and frequently uneconomical.

The book closes with a chapter devoted to the subject of successive approximations. Such techniques, as well as iterative procedures based on the contraction principle, are particularly well suited for use with machine computers and, thus, are likely to gain increasing importance with advances in computer technology. Another important advantage of such techniques, particularly when they lead to monotone convergence, is that the iteration may be stopped as soon as the solution is judged to be "good enough" rather than truly optimal. In this way, one obtains, in effect, a "suboptimal" policy which is acceptably close to the optimal policy.

The book is written in a style which is Bellman's trademark—fresh, non-conformist, incisive and impatient with detail. It is replete with numerous comments, observations, quotations, anecdotes, references and, most important, carefully chosen examples. It is addressed to the neophyte and yet contains much that is new to the expert. In short, it is the work of a leading thinker of our time and a master of both oral and written exposition.

L. A. ZADEH
Dept. Elec. Engrg.
University of California
Berkeley, Calif.

The Physical Theory of Transistors, by Leopoldo B. Valdes

Published (1961) by McGraw-Hill Book Co., Inc., 330 W. 42 St., New York 36, N. Y. 358 pages+12 index pages+xiv pages. Illus. 6½×9½. \$10.50.

This is a textbook which covers precisely the field stated in its title. It is unusually well organized to teach a well-defined subject. While providing the necessary background, diversions are carefully avoided. For the teacher, student, or practicing engineer entering the field, this book deserves first consideration. Although not intended as a reference work, the book will also be useful to the specialist who occasionally needs to

refresh his memory on a textbook point.

Dr. Valdes has divided his book into three parts. Part I, Introductory Concepts, provides an easy entrance, a welcome mat, to the student. The student will encounter no difficulty here other than that imposed by new concepts. This sixty page, elementary but thorough, introduction will be very helpful. Problems are provided with each chapter.

Part II, Electronic Properties of Semiconductor Materials, occupies slightly more than one-half of the 360 pages of the book and is the "main course." Although the basic physics may be familiar to physics students, the detailed application to the electronic behavior of semiconductors will be new. The student lacking in physics background will find the text sympathetic but nature unmerciful. This book provides a clearer introduction to semiconductor physics than will be found among most books of comparable depth, but the electrical engineering student is well advised to cultivate in advance at least a liking for physics.

Electron energy levels in atoms and in crystals are discussed without actually giving Schrodinger's equation. Hence the mathematical tools and physics of quantum mechanics are not required although the pertinent results are given. The Fermi statistics is similarly treated. Following the universal practice, the approach to statistical equilibrium is treated as a topic unrelated to the statistical state of equilibrium. A better appreciation of the physical processes might be given by keeping these topics together. Also, the replacement of physical models by mathematical models in quantum theory does not justify the loss of mechanical visualization throughout physics. Specifically, the generation and recombination of carriers can better be taught in terms of probability theory, using models resembling the dog-flea problem, for special cases, rather than by a generalized, mathematical treatment. With an appropriate Fermi distribution of anti-social fleas, the dog-flea analogs for holes, electrons, and traps will provide unlimited material for visualization. The teacher will find no single source of good tutorial material on this topic.

Part II concludes with a lucid discussion of thermoelectric, optical, magnetic, and surface effects. The treatment of the first three of these phenomena is appropriately brief since they are peripheral topics in transistor physics.

Part III, Properties of Semiconductor Devices, applies the ideal $p-n$ junction theory developed in detail in Part II to real diodes and transistors. Fabrication methods and limitations are mentioned. Some equivalent circuits are included to describe devices, but circuit analysis, as such, is not within the province of this text.

The teacher and student will find the book exceptionally well planned and rich in clear explanations of new concepts.

M. A. CLARK
Pacific Semiconductors, Inc.
Culver City, Calif.

An Introduction to the Principles of Communication Theory, by John C. Hancock

Published (1961) by McGraw-Hill Book Co., Inc., 330 W. 42 St., New York 36, N. Y. 248 pages+5 index pages+x pages. Illus. 6 $\frac{1}{2}$ ×9 $\frac{1}{2}$. \$9.50.

Those of us who have been out of touch with undergraduate engineering education for 20 years or more may have something of a shock in store if we have occasion to investigate what has happened in the meantime. For this reviewer, the first indication of the drastic change that has taken place came when his son reported having finished calculus in the first two terms of his freshman year and devoting the third term to differential equations. A further indication was the fact that the son's sophomore year included subjects the father studied in graduate school. Despite these forewarnings, it still comes as a shock to learn (on reviewing the current book) that undergraduates now learn at least the rudiments of Wiener filter theory as a minor sub-topic of a one semester, senior level, required course. Those who can recall the awe with which Wiener's original "Yellow Peril" was regarded can appreciate the significance of this development.

Of course, the treatment of Wiener filters is by no means complete and neither is it rigorous. The essence is nevertheless there including the concept of spectrum factorization. Though the development does not exactly prove the result, it does have an element of plausibility that may satisfy the less critical student. The one real serious omission is the lack of any mention of Wiener's name. It is true that the undergraduate is likely to derive little benefit from a reference to the original work, but it does seem that the author of so important a contribution deserves some mention. Similar comments can be made about several other sections of the book, there being no mention of important contributors such as Nyquist, North, VanVleck and Middleton, etc., although their results are presented.

As indicated, Wiener filters are only a minor sub-topic in this book. The book is primarily an introduction to the use of probabilistic and statistical methods for handling noise and other nondeterministic problems. According to the author's preface, prerequisites include two semesters of electronics and a networks course which treats Fourier and Laplace transforms. A course in probability is regarded as helpful but not required. The book starts with a review of frequency and time domain relations and includes chapters on modulations, random signal theory, noise, and communication systems. The chapter titles are not too descriptive. The chapter on network analysis is actually concerned with operations on random signals and it is here that Wiener filters are treated as a sub-topic of the topic "Optimum Systems." Similarly, the chapter on communication systems includes a treatment of radar detection problems.

In such a book, one cannot, of course,

expect great depth of treatment. Shannon's basic coding theorem, for example, is stated but not proved. The section on radar detection makes no mention of fluctuating targets. On the other hand, the student who completes this course will have had at least nodding acquaintance with a wide variety of topics including autocorrelation and spectral density; Gaussian and Rayleigh probability distributions; delta functions; Bessel and hypergeometric functions; the sampling theorem; entropy, redundancy, and equivocation; etc. The reviewer cannot help but approve of including this type of material in the undergraduate curriculum.

The author appears to have done a good job of matching the material to the capabilities of the students. He has also included a liberal supply of problems to be solved. These problems appear well designed to impress the basic points on the minds of the students. Perhaps the greatest danger of such a course is that the student will emerge unaware of his own ignorance or of how much there is yet to be learned. Reasonable precautions on the part of the instructor, however, will minimize this danger.

WARREN D. WHITE
Airborne Instruments Lab. Div.
Cutler-Hammer, Inc.
Melville, N. Y.

Proceedings of URSI Thirteenth General Assembly, John P. Hagen, Ed.

Publication 880 (1961), National Academy of Sciences, Printing and Publishing Office, Washington 25, D. C. 595 pages+ii pages. Illus. 9×11. Paper Binding. \$5.00.

For the first time, the Proceedings of a General Assembly of URSI are being made available to the general public in book form. The International Scientific Radio Union (abbreviated as URSI from the French title, Union Radio Scientifique Internationale), with several hundred delegates from some 20 different countries, holds its General Assembly every three years. Recent assemblies have been held in Zurich, Switzerland, Sydney, Australia, The Hague, Netherlands, Boulder, Colo.; and this one (the thirteenth) in London, England. The functions of a General Assembly are to review, on a world-wide basis, the progress of the past 3 years in radio science, and to plan for the future. This book, constituting the report of the USA National Committee of URSI, records the progress of radio science from 1957 to 1960, perhaps the most exciting three-year period in its history.

The fields of URSI are delineated by its seven commissions which are: I, Radio Standards and Methods of Measurement; II, Tropospheric Radio Propagation; III, Ionospheric Radio Propagation; IV, Radio Noise of Terrestrial Origin; V, Radio Astronomy; VI, Radio Waves and Circuits; VII, Radio Electronics. The book presents a wealth of up-to-the-minute research results in each of these areas. Of great value to the nonspecialist in a particular area will be the survey papers which introduce most of the sessions. Each survey paper, presented by an international authority in his field,

undertakes to summarize the present state of recently acquired knowledge in the field, and to lay the groundwork and provide the understanding for the detailed papers which follow. Most of the survey papers are reproduced in full, but many of the specialized papers are reported in summary form only, to keep the size of the book within bounds.

The unifying theme that ties together these diverse fields is the absorbing story of nearly 3 years of concentrated research which was carried out during the International Geophysical Year and the succeeding International Geophysical Cooperation of 1959. This is the period that saw the successful launching of artificial earth satellites, and the consequent development of new techniques for the scientific exploration of our earth, its atmosphere and the space beyond. In this book, the major role played by radio science in space research is described by the men who directed much of the research. From the results of this research there now emerges a surprisingly coherent and comprehensive picture of the natural processes that encompass the earth and interplanetary space.

E. C. JORDAN
Dept. Elec. Engrg.
University of Illinois
Urbana, Ill.

The Antenna, by H. Thourel

Published (1961) by John Wiley and Sons, Inc., 440 Fourth Ave., New York 16, N. Y. 378 pages+5 index pages+23 appendix pages. Illus. 6 $\frac{1}{2}$ ×9 $\frac{1}{2}$. \$12.50.

"The Antenna" was originally published in French in 1956, and the translation into English was performed by H. de Laistre Banting. American readers will find the text clearly written, with familiar terminology used throughout. There is heavy dependence upon American papers and books as sources of information, but, in addition, much worthwhile material has been obtained from the European literature.

This book is less theoretical and more practical in its approach than other textbooks commonly used for first-year graduate courses (for example, "Antennas," by J. D. Kraus). Its level would be more suitable for a one-semester senior-year course. However, the instructor should bear in mind that the book was intended for familiarizing the reader with important antenna types and design techniques, rather than for imparting fundamental knowledge.

Antennas for all frequency ranges are considered, from mammoth sheets of wires at 15 kc to reflectors and lenses used at microwave frequencies. The broadcast and short-wave bands, for example, receive more attention than has been customary in recent books on antennas.

The practical orientation of this book will make it a useful reference for the design engineer. The wide coverage of antenna types will assist him in making the correct choice for a given application, while the formulas, curves, and referenced literature will help him perform his design task.

SEYMOUR B. COHN
Rantec Corp.
Calabasas, Calif.

¹ Norbert Wiener, "The Extrapolation, Interpolation, and Smoothing of Stationary Time Series with Engineering Applications," John Wiley and Sons, Inc., New York, N. Y.; 1949. Originally published as a classified report to Section D, National Defense Research Committee.

Antenna Engineering Handbook, Henry Jasik, Ed.

Published (1961) by the McGraw-Hill Book Co., Inc., 330 W. 42 St., New York 36, N. Y. 1010 pages +30 index pages +xx pages. Illus. 6 $\frac{1}{2}$ ×9 $\frac{1}{2}$. \$22.00.

Antenna engineering is a field which has grown very rapidly in the last two or three decades, having received a great impetus from military applications in communications, radar, radio aids to navigation, etc. In the past, engineers who have been faced with antenna problems have had to search the extensive technical literature for design information, so there has existed a real need for a handbook. The editor and authors are to be commended for tackling the difficult task of collecting and organizing the material for this handbook.

As stated in the preface, "The Antenna Engineering Handbook" is intended to serve as a compendium of antenna design data and principles. Although it is expected that it will prove most useful to the engineer who is actively engaged in designing antennas, it will also be of considerable use to the electronic systems engineer who desires to understand the capabilities and limitations of the antenna as a component. The treatment is at the engineering level and is directed toward an understanding of antenna problems . . . in addition to presenting an extensive collection of design data." Hence, being an engineer's handbook, it does not contain much in the way of detailed mechanical design data such as belongs more properly in a radio amateur's handbook.

The book is organized into four sections, comprising Introduction and Fundamentals, Antenna Types and Methods, Applications, and Topics Associated with Antennas. The first section, which is brief, contains basic definitions and fundamental formulas. The second section contains engineering design information and performance data on the basic types of antennas. The system of classification is somewhat arbitrary but appears to be quite comprehensive. The third section treats antennas for specific types of applications, and again the classification has been a bit arbitrary. The fourth section contains information on a variety of topics of interest to the antenna engineer such as transmission lines and waveguides, impedance matching, radomes, measurements, as well as a chapter on propagation and one on mechanical considerations in antenna design.

It is inevitable that, in a book written by thirty-nine authors, there should be some variation in the thoroughness with which the different topics are treated. The chapter on loop antennas is rather sketchy and does not contain even as much information on loops as may be found in textbooks such as Kraus's "Antennas." The chapter on Surface- and Leaky-Wave Antennas is quite comprehensive and represents an excellent summary of the state of the art in this field. The chapter on Frequency-Independent Antennas will be welcomed by many engineers. The chapter on Antenna Measurements is not as extensive as might be expected (and it was disappointing to find no reference to IRE Standards on Antennas: Method of Test).

The chapter on Methods of Obtaining Circular Polarization uses the term "ellipticity" to describe the polarization, whereas

the chapter on Helical Antennas uses the more-commonly accepted term "axial ratio." The use of the term "ellipticity" is to be deprecated since it does not conform to the mathematical definition of the term (see IRE Standards on Antennas and Waveguides: Definitions of Terms, 1953). The chapter on Corner Reflector Antennas might have mentioned Cottony's empirical design data for corner reflector antennas. The handbook contains very little on the subject of noise, a topic what might well have constituted a separate chapter.

The main shortcoming of the handbook is its index. The index appears to be little more than an expansion of the Table of Contents, so it is necessary for the reader to be familiar with the particular organization of material used in the handbook in order to locate a specific item of information. For the antenna specialist this will not be important, but for the nonspecialist it could be frustrating. A few examples will illustrate the problem. One might reasonably expect the definition of "antenna temperature" to occur in the section on Fundamentals and be listed in the Index under "A" or "T." It actually is listed under Radio Telescope Antennas. Similarly, the topic "noise" is listed only under Radio Propagation. Dielectric rod antennas are not listed under "D" or "A," but under Surface Wave Antennas, Specific Structures. Friis' Transmission Formula occurs in at least three places in the book but does not rate a listing in the Index.

In the opinion of this reviewer, the "Antenna Engineering Handbook" represents an important contribution to the literature and will be welcomed by all antenna engineers. It should find a place on the bookshelf not only of antenna engineers but all engineers concerned with systems employing antennas. The editor and the authors are to be congratulated for producing such an excellent and complete summary of the present state of the art.

GEORGE SINCLAIR
University of Toronto
Toronto, Ont., Canada

Electronic Circuits, Signals, and Systems, by Samuel J. Mason and Henry J. Zimmerman

Published (1960) by John Wiley and Sons, Inc., 440 Fourth Ave., New York 16, N. Y. 611 pages +4 index pages +1 appendix page +xviii pages. Illus. 6 $\frac{1}{2}$ ×9 $\frac{1}{2}$. \$12.50.

A more revealing title for the contents of this remarkable book might be, "Introductory System Theory with Applications to Electronic Circuits." The book is noteworthy for the inventiveness and originality of its approach and for the conceptual richness of its presentation. Although it is intended for use by undergraduates, it will provide rewarding, stimulating (and perhaps even difficult) reading for the older, experienced engineer and teacher who wishes to strengthen his comprehension of

several major aspects of modern system theory.

System theory is primarily concerned not with the *things* which comprise the system but rather with the *relations* between the signals (*i.e.*, observables) that characterize these things. The recognition of system theory as a distinct engineering discipline has been slow in coming. A major obstacle has been that much of the traditional symbolization of engineering has denoted the things comprising the system rather than the signal relationships which are of importance for theoretical purposes. Thus, the description of the "things" has been made to seem concrete and real whereas the signal relationships, described in traditional mathematical notation, have seemed more abstract and difficult to comprehend.

With the publication nearly a decade ago of his paper on signal flow graphs,¹ Mason provided an explicit symbolism for representing these signal relationships. For linear and constant-parameter systems, Mason showed that the flow graph can be solved directly so as to permit one to write, by simple inspection, the solution of the system equations. For nonlinear and time-varying systems, where analytical solution usually becomes very difficult, the flow graph leads directly to the programming of analog or digital computers.

The merit of any notational innovation, such as this, can only be evaluated by examining its usefulness in practice. Flow graphs are used throughout this book to portray the signal relationships which are peculiar to the particular system property being illustrated. The reader is thus given an opportunity to evaluate the importance of signal flow graphs by seeing in detail how they have been used by their inventor. In my opinion, the signal flow graph is an important innovation—a kind of mathematical "esperanto"—which is particularly well suited to the modeling, simulation, and analysis of systems in many diverse fields. Although a discussion of flow graphs is now included in most recent books on linear systems analysis, none thus far has illustrated their usefulness as thoroughly as does the present book.

The emphasis on flow graphs is but one of many unusual features of this book. Prior to the flow graph development of Chapters 4 and 5, the authors give concise treatments of matrix and topological methods for the analysis of electric circuits. These early chapters are very tightly written and presume that the reader is already familiar with elementary notions of electric circuits.

Chapters 6 and 7 constitute the main bulk of the book. In Chapter 6 on Signal Analysis, an astonishing array of important concepts and results are set forth in 110 pages of beautifully written and clearly illustrated text. Pulsed, periodic, almost periodic, and random signals are introduced, in that order, to motivate a brief discussion of random processes. Next comes a discussion of the geometrical representation of

¹ S. J. Mason, "Feedback theory: some properties of signal flow graphs," *PROC. IRE*, vol. 41, pp. 1144-1156; September, 1953. Also, "Feedback theory: further properties of signal flow graphs," *PROC. IRE*, vol. 44, pp. 920-926; July, 1956.

signals by vectors in some appropriate signal space and the geometrical interpretations of approximation and correlation. This leads easily to auto- and cross-correlation functions for stationary random signals. Only at this point is the trigonometric Fourier series introduced and extended to yield the Fourier integral. To estimate bounds on the Fourier spectrum of a signal, the "content," "variation," and "wiggleness" measures are defined. The chapter closes with specific examples of the application of Fourier theory to the analysis of a wide variety of signals.

Chapter 7 deals with the transmission of signals through linear systems. It contains more content in 163 pages than is usually found in entire books on this subject. An interesting feature is that the authors define the familiar system function $H(s)$ as the transmittance of a linear stationary operator H for the characteristic signal, $\exp(st)$, thus focusing attention upon the meaning of $H(s)$ rather than upon the mathematical formalism of the Laplace transformation.

The last two chapters deal respectively

with nonlinear and time-varying linear systems and the negative-feedback concept.

The clear, precise, but rather terse style of writing demands and deserves a careful reading—each word counts. The discussion of each topic is complete but without the customary redundancy and occasional verbosity ordinarily found in books at this level. A large assortment of thought-provoking problems (342 in all) are given to illustrate and extend the material of each chapter. I found the book most rewarding—a rich source of new ideas, accurate and authoritative in its development of many of the major concepts needed in systems work. Perhaps it is because I learned so much from reading this book that it is difficult to believe that all of this material is accessible to juniors and seniors today. However, even if it should be a few years ahead of its time, the book will certainly have a major constructive influence on the future development of systems education.

W. H. HUGGINS
The Johns Hopkins University
Baltimore, Md.

RECENT BOOKS

Blanco, V. M. and McCluskey, S. W. *Basic Physics of the Solar System*. Addison-Wesley Publishing Co., Inc., Reading, Mass. \$7.50. For the reader at the intermediate level not a specialist in astronomy who is interested in space technology. Examples of computations and practice problems are presented.

Bundy, F. P., Hibbard, W. R., Jr., and Strong, H. M., Eds. *Progress in Very High Pressure Research*. John Wiley and Sons, Inc., 440 Park Ave. S., New York 16, N. Y. \$12.00. The book consists of papers and discussions presented at an International Conference held in June, 1960, under sponsorship of Materials Central, Wright Air Development Div., U. S. Air Force and the Research Lab. of the General Electric Co. It includes a review of high pressure work in the U.S.S.R.

Hocking, John G., and Young, Gail S. *Topology*. Addison-Wesley Publishing Co., Inc., Reading, Mass. \$8.75. A book on abstract mathematical topology.

Scanning the Transactions

The Case of the Missing Bass has been causing a bit of a stir in audio circles lately. Several home loudspeaker systems have been marketed recently which sound very good, and yet, when subjected to careful measurements, apparently have shown a deficient bass response. Several theories have been advanced to account for this discrepancy. One explanation for the "apparent bass" effect is based on a psychoacoustic phenomenon in which a person listening to a complex tone thinks he hears the fundamental frequency even though it is absent. Experiments have been conducted in which a series of pulses, set to a periodic repetition rate lying within the audible band, is passed through a high-pass filter with a cutoff frequency higher than that of the pulse rate. Subjects listening to the pulse train have reported being able to hear a frequency corresponding to the pulse repetition frequency. Biophysicists, noting that this effect is present only at loud levels, have suggested that it might be attributed to neural and middle-ear distortion. It has also been noted that in small inexpensive loudspeakers, a large excursion of the voice coil will move it out of the gap of uniform flux density of the magnet, causing a nonlinear clipping action on the sound wave. This latter effect has now been explored further by means of listening tests. Twenty subjects were asked to listen to various kinds of high-quality tape-recorded music over a special circuit that simulated and introduced the clipping distortion of a small loudspeaker, and to compare what they heard with the undistorted rendition of the same music, especially with respect to the bass content. The results confirm that the "apparent bass" effect does indeed exist, and that it is due to some degree to loudspeaker distortion. The degree to which neural and middle-ear distortion also contribute is as yet unknown but will no doubt be investigated further. (J. D. Griffiths, "Apparent bass' and nonlinear distortion," IRE TRANS. ON AUDIO, July-August, 1961.)

The slowness of light may prove to be a basic limitation

on the speed of ultra-high-speed digital computers. For example, a computer with a one nanosecond access time must have an average radius of less than one foot simply because, at the speed of light, it takes at least one nanosecond for a piece of information to be transmitted over a distance of one foot. This restriction, which is inherent in all present-day serial computers where all information is passed through a central processing unit, might be somewhat overcome by "parallel" machines. Thus a digital computer of the future might contain a great many local processing units distributed uniformly throughout the memory storage area and under the control of a central processing unit, in order to reduce the distance over which information is required to flow. Whatever evolves, it is apparent that the phrase "with the speed of light" is rapidly losing its awesome reputation. (W. W. Bledsoe, "A basic limitation on the speed of digital computers," IRE TRANS. ON ELECTRONIC COMPUTERS, September, 1961.)

A radio-fed radio antenna may sound like too much of a good thing, even to radio engineers. Nevertheless, a new method of exciting dipole antennas by coupling them electromagnetically to a two-wire transmission line is showing considerable promise for high-power VHF-UHF communications. The array consists of several dipoles situated in a plane parallel to that of the two-wire line, with the dipole centers situated opposite positions of voltage maximum along the line. When the dipole axes are oriented in a direction other than parallel to the direction of the line, the antennas are excited by the charges on and currents in the line. The advantage of this arrangement is that only a single transmission line is required to feed the several dipoles, thus avoiding the problem of balancing a large number of interacting feed lines and minimizing the difficulty of obtaining the desired field pattern. (K. M. Chen and R. W. P. King, "Dipole antennas coupled electromagnetically to a two-wire transmission line,"

IRE TRANS. ON ANTENNAS AND PROPAGATION, September, 1961.)

The use of capacitors as memory elements is being explored for a new semipermanent storage system, *i.e.*, a storage system in which the stored information will not be changed by the machine that is able to consult it. Present systems of this type are limited in speed, where rotating magnetic drums are used, or rely on expensive and complicated error detection and correction circuitry where use is made of destructively read magnetic stores. To overcome these shortcomings two systems were recently developed: the flying spot store, which makes use of cathode-ray access to information stored on photographic emulsion, and the permanent magnetic twistor, in which information is stored by magnetically biasing the twistor. A third system has now been developed in which the memory consists of a matrix of printed capacitors. Since there is a great need for reliable, economical, high-speed permanent stores for electronic telephone switching systems, as well as for modern digital computers, it is likely that this system will have a promising future. (D. H. Macpherson and R. K. York, "Semipermanent storage by capacitive coupling," IRE TRANS. ON ELECTRONIC COMPUTERS, September, 1961.)

Trouble-shooting the trouble shooters reveals some interesting statistics on the behavior of maintenance technicians in locating faults in equipment. In a recent study, detailed records were kept of each successive move which was made in trouble-shooting simple radio and radar circuits. When 422 of the records were analyzed later, it was found that in 87 per cent of the cases the technicians had accumulated enough

information to identify the faulty stage, but only 3 per cent of them utilized this information immediately. The remainder went on making redundant or irrelevant checks before they finally identified the faulty stage. Similar results were found in finding the faulty component within the stage. Only 14 per cent of those who had accumulated sufficient information to identify the faulty component immediately recognized this fact. The study points up the fact that searching for symptoms and the correct interpretation of them occur on two different behavioral levels which are not necessarily closely coordinated. (J. W. Rigney, *et al.*, "Analysis of fault-location behavior in electronic equipment," IRE TRANS. ON HUMAN FACTORS IN ELECTRONICS, September, 1961.)

The simulation of cognitive processes has received a great deal of attention recently. Considerable effort is being devoted to developing machine with capabilities for self-organizing and cognitive behaviors previously thought to be exclusively the domain of organisms. At the same time, behavioral and life scientists are very much interested in the analysis and synthesis of organic behaviors in terms of machines which can simulate them. The result has been a marked increase in the volume of papers on this subject. It seems safe to say that over two-thirds of the literature on the simulation of cognitive processes has been written just in the past four years. The appearance of an annotated bibliography covering 498 papers in this burgeoning field, therefore, comes at a most propitious time. (P. L. Simmons and R. F. Simmons, "The simulation of cognitive processes: An annotated bibliography," IRE TRANS. ON ELECTRONIC COMPUTERS, September, 1961.)

Abstracts of IRE Transactions

The following issues of TRANSACTIONS have recently been published, and are now available from The Institute of Radio Engineers, Inc., 1 East 79 Street, New York 21, N. Y., at the following prices. The contents of each issue and, where available, abstracts of technical papers are given below.

Sponsoring Group	Publication	IRE Members	Libraries and Colleges	Non-Members
Antennas and Propagation	AP-9, No. 5	\$2.25	\$3.25	\$4.50
Audio	AU-9, No. 4	2.25	3.25	4.50
Automatic Control	AC-6, No. 3	2.25	3.25	4.50
Broadcasting	BC-7, No. 3	2.25	3.25	4.50
Broadcast and Television				
Receivers	BTR-7, No. 2	2.25	3.25	4.50
Component Parts	CP-8, No. 3	2.25	3.25	4.50
Electronic Computers	EC-10, No. 3	2.25	3.25	4.50
Human Factors in Electronics	HFE-2, No. 2	2.25	3.25	4.50
Industrial Electronics	IE-8, No. 2	2.25	3.25	4.50
Radio Frequency Interference	RFI-3, No. 1	2.25	3.25	4.50
Reliability and Quality Control	RQC-10, No. 2	2.25	3.25	4.50
Space Electronics and Telemetry	SET-7, No. 3	2.25	3.25	4.50
Vehicular Communications	VC-10, No. 2	2.25	3.25	4.50

Antennas and Propagation

VOL. AP-9, No. 5, September, 1961

Philip S. Carter 1897-1961 (p. 424)

Dipole Antennas Coupled Electromagnetically by a Two-Wire Transmission Line—K. M. Chen and R. W. P. King (p. 425)

The circuit properties of a dipole antenna coupled electromagnetically to a two-wire transmission line are studied theoretically and experimentally. Some arrays constructed of a number of dipole antennas coupled electromagnetically to a two-wire line are considered and the radiation patterns are found.

Mutual-Coupling Effects in Scanning Dipole Arrays—L. A. Kurtz, R. S. Elliott, S. Wehn, and W. Flock (p. 433)

The perturbations in mutual coupling due to finiteness of a dipole array and its ground plane have been studied. Experimental procedures were evolved to measure these perturbations and their influence on antenna performance as a function of beam position. Data for one- and two-dimensional dipole arrays are presented and interpreted, particularly with reference to edge effects.

Optimum Feeds for All Three Modes of a Monopulse Antenna I: Theory—P. W. Hannan (p. 444)

In a monopulse antenna for use in a tracking radar, the requirements for the sum and difference modes are not the same. For the amplitude-comparison type of monopulse having an antenna whose main aperture is illuminated by

a feed, these independent requirements can be met by a feed designed to fulfill two conditions. One is that excitation of the feed aperture in the difference modes be effectively about twice as wide as in the sum mode. The other is that the shapes of all the feed excitations be free of any avoidable irregularities.

The amount of improvement available when these conditions are met depends on the optimization point desired for each mode, as well as the design of the reference antenna. In a typical case, the gains and slopes in the difference modes should increase by several db. Furthermore, the near sidelobes and the spillover radiation in the difference modes should decrease by an order of magnitude. A small increase of gain in the sum mode is also available, and finally, the criticalness of positioning the feed may be appreciably reduced.

Optimum Feeds for All Three Modes of a Monopulse Antenna II: Practice—P. W. Hannan (p. 454)

In an amplitude-monopulse antenna whose main aperture is illuminated by a feed, it is desired to control the feed excitation independently in the sum, azimuth difference, and elevation difference modes. It is possible to describe a feed system, comprising an infinite array of radiators and hybrid junctions, which demonstrates the principle of complete independent control of the three modes.

There are several practical feeds which approach a hypothetical ideal one in varying degrees. One representative type is the "twelve-horn feed," although it has some disadvantages, it is versatile and quite useful. However the most attractive type for many applications appears to be one having a combination of multiple-horn excitation in one plane and multimode-waveguide excitation in the other. With a simple form of the "multihorn-multimode" feed, the ideal is substantially realized, and a major improvement in monopulse performance can be obtained.

A New Way of Solving Maxwell's Equations—V. H. Rumsey (p. 461)

A general solution of Maxwell's equations for a single frequency can be expressed as the combination of two types of solution, each of which is characterized by an electric vector which is equal to the magnetic vector times the intrinsic impedance of free space but a quarter cycle out of phase. These two types are mathematically orthogonal, and each can be conveniently expressed by means of a single scalar. The method leads to circularly polarized surface waves propagating along anisotropic sheets which are perfectly conducting in one tangential direction and perfectly transparent in the orthogonal tangential direction.

Correlation of Wind Shear with Tropospheric Scatter Signals—L. H. Bauer (p. 466)

Examination of the hourly values of the 10-90 per cent fading range of selected 915 Mc tropospheric scatter records of a 400-mile path have shown unusual behavior which correlates well with wind shear through the scatter volume. Although the meteorological data were of a gross nature and were collected at a point at least 70 miles from the common volume, correlation coefficients of 0.76 to 0.8 were obtained. The data indicate that the fading range (10-90 per cent in this case) increases by 1.4 db per meter/sec/km increase in average wind shear through the scatter volume.

Coherent and Incoherent Scattering of Microwaves from the Ocean—C. I. Beard (p. 470)

This report, the third in a series, summarizes experimental studies of microwave over-ocean propagation on line-of-sight paths. Measurements at 5.3, 3.2, and 0.86 cm wavelength in 1955, in the Gulf of Mexico, between two oil drilling platforms one mile apart are compared with the results of the phenomenological model developed earlier. The total field was measured at maxima and minima of the

interference patterns using a sequence of receiver beam widths. The scattered field alone was measured by means of a narrow beam. The 1955, Gulf of Mexico, data are consistent with the previous 1953, Golden Gate data in regions of overlap of certain parameters, and provide extended coverage for other values under different conditions.

Specifically, some of the new findings are: a) The experimental values of the coherent reflected field are larger than $\exp[-2(2\pi h\psi/1000\lambda)^2]$ for values of "apparent ocean roughness" ($h\psi/\lambda$) greater than 110 milliradians. h = standard deviation of water surface, ψ = grazing angle in milliradians, and λ = electromagnetic wavelength. b) After rising from zero, the incoherent scattered power exhibits a downtrend for $h\psi/\lambda$ greater than 110. The incoherent power divided by the square of the smooth sea reflection coefficient shows no polarization dependence. c) The distribution along the surface as measured by the narrow-beam antenna shows that the coherent and incoherent power are markedly peaked in the specular direction. d) The ratios of coherent-to-incoherent power (m^2) obtained from the shapes of the probability distributions agree with the power ratios obtained by measurements of the magnitudes of the signals. e) Total signal spectra broaden with increasing $h\psi/\lambda$ as found at the Golden Gate; the relative shapes of spectra agree with those from the Golden Gate. Horizontally- and vertically-polarized total signal spectra are the same.

Electromagnetic Propagation in an Exponential Ionization Density—L. S. Taylor (p. 483)

The propagation of a plane electromagnetic (TE) wave into a plane stratified medium in which the ionization density varies as $\exp(z/z_0)$ is investigated. The solution of the wave equation appears as a combination of Bessel functions of imaginary order and complex argument, but the magnitude of the reflection coefficient (taken at $z = -\infty$) is given by the simple expression $\exp\{-4\pi z_0 \cos \theta_e/\lambda \tan^{-1}(\nu_e/\omega)\}$, where θ_e is the angle of incidence, λ is the free-space wavelength and (ν_e/ω) is the ratio of electron collision frequency to the frequency of the field. In general, the field components must be obtained from a complex series, but at depths beyond the critical density asymptotic forms are given which display the rapid decay of the evanescent field in terms of elementary functions.

Some Propagation Characteristics of High UHF Signals in the Immediate Vicinity of Trees—A. H. LaGrone and C. W. Chapman (p. 487)

Results are reported of measurements made at very low angles of 2880-Mc vertically-polarized signals over wooded areas, with the elevation angle to the transmitter the principal variable. The effects of one tree and of many trees on the apparent location of a signal source, as determined with a narrow-beam antenna, are reported. A hypothetical direction-finding system is assumed and its pointing characteristics determined.

Tropospheric Scatter Propagation and Meteorological Conditions in the Caribbean—R. E. Gray (p. 492)

Results are given of radio propagation measurements which have recently been made in the Caribbean. The transmission loss on beyond-the-horizon paths in this region was found to be considerably less than that measured over paths of similar length in temperate climates.

The fact that the path loss is, in general, relatively low in the Caribbean is believed to be chiefly due to the large gradient of the refractive index of the atmosphere which normally prevails in the first few hundred feet above the earth's surface in that area.

Communications (p. 497)

Contributors (p. 503)
Papers to be Published in Future Issues
(Inside Back Cover)

Audio

VOL. AU-9, No. 4, JULY-AUGUST, 1961

Message from the New Chairman—C. M. Harric (p. 97)

The Editor's Corner—M. Camras (p. 98)
National Officers of the PGA, 1961-1962 (p. 99)

PGA Awards for 1960 (p. 102)

Chapter News—W. M. Ihde (p. 102)

More on Nonlinear Distortion Correction—J. R. MacDonald (p. 103)

Further consideration is given to basic amplitude limitations which may apply to the complementary distortion method of nonlinear distortion correction. It is found, in disagreement with others, that points at which the differential gain is zero or infinite do not limit the amplitude over which complete correction is possible but that relative maxima, minima, gain zeros, and infinite-gain points in the characteristic do set limitations when the usual simply connected tandem configuration is employed. When the characteristic to be corrected is multiple valued or passes through points of zero or infinite gain within a given amplitude range, a multiply connected correction circuit must be used for perfect correction of distortion over the amplitude range in question.

A Simplified Noise Theory and Its Application to the Design of Low-Noise Amplifiers—A. E. Sanderson and R. G. Fulks (p. 106)

Any noisy amplifier can be represented by an equivalent noiseless amplifier plus two noise generators either at the input or the output of the amplifier. The choice of two particular noise generators (the equivalent short-circuit noise voltage and the open-circuit noise current) to characterize a noisy amplifier has a number of advantages over the concept of noise figure. The noise generators can easily be measured separately from the source noise, and the optimum source impedance and the noise figure at any source impedance can then be calculated. Since the amplifier noise is measured separately from the source noise, low noise figures can be easily measured. The optimum source impedance equals the quotient of the two noise generators, and the noise figure depends upon their product. Neither feedback nor input impedance is a consideration in determining noise figure and optimum source impedance.

Several transistor noise diagrams show how the two noise generators are affected by emitter current, collector voltage, and frequency. Noise diagrams can be used to select the most suitable amplifying devices and optimum operating conditions for various applications.

Average vs RMS Meters for Measuring Noise—J. J. Davidson (p. 108)

It appears that the controversy is still alive over whether average reading or root-mean-square reading meters should be specified as standard for the measurement of noise. This being the case, it is worthwhile to consider the entire subject from the standpoint of basic fundamentals, to determine what are the significant quantities involved, and then proceed to investigate which type of meter yields the most significant results.

The following is the result of such an investigation. The entire discussion rests on 1) an axiom, that energy transfer is the fundamental interaction within the universe, and 2) a premise, that for the type of measurements under discussion (audio), all significant processes are linear. Given these two starting points, the conclusion is reached that the meaningful quanti-

ties are found by rms measurements.

It is shown further, by concrete example, that measurements made with average reading meters can depart widely from those made with an rms meter. This being the case, it is necessary that *measurement standards* specify the use of rms meters. Those who elect to use average meters, then, bear the responsibility of determining the accuracy of their results in terms of the fundamentally important quantities.

An Adjustable Shelf-Type Equalizer with Separate Control of Frequency and Limiting Attenuation or Amplification—R. H. Rose (p. 112)

This device provides for control of the high-frequency content of an audio program, allowing the operator to choose independently:

- 1) the frequency above which equalization is to occur, and
- 2) the maximum correction in signal strength which results in the range of frequencies under correction.

Three operating controls are used. One control determines whether the high-frequency signals shall be increased, left unchanged, or decreased in strength relative to the low-frequency signals. A second control is calibrated in terms of the frequency above which correction shall occur. The third control adjusts the asymptote which represents the maximum correction which shall occur for frequencies considerably higher than that chosen by the frequency control described above.

The circuit can be described briefly as follows: for high-frequency attenuation, the operation employs a negative feedback amplifier whose output may have high-frequency loss inserted by an RC network following the amplifier; for high-frequency boost, the RC network is inserted in the amplifier feedback path so that the amplifier output (which now becomes the system output) has a rising high-frequency response which corresponds to the attenuation of the RC network. All three controls are continuously adjustable within their ranges of operation.

"Apparent Bass" and Nonlinear Distortion—J. D. Griffiths (p. 117)

A discrepancy between the "apparent bass" response heard by the average music listener and anechoic-chamber measurements has been noted for some small loudspeaker systems. This may be caused by the psychoacoustic response to the generation of harmonic distortion by the nonlinear suspension and the inhomogeneous flux gap density in a small speaker. An electrical analog, with controllable distortion, of such a speaker has been subjected to listener tests and evaluation to determine if this is the cause of the apparent bass effect. An analysis of the listener reactions to various music stimuli through the system indicates that this is the case.

The Concept of Linear Interpolation in Spectral Compensation—C. E. Maki and J. M. Chirnitich (p. 122)

Spectral compensation is usually achieved with equalizers cascaded so as to generate a desired response. In the concept of linear interpolation, a series of points are located along the desired response and linear interpolation provided between adjacent points. This is accomplished with contiguous band-pass filters arranged so as to minimize the effect of filter crossover. The performance limitations depend upon the filter characteristics, crossover ripple, and the type of response to be equalized. This approach to compensation has two advantages. First, automatic control of the spectrum can be achieved when the input signal is a random noise voltage. Second, discreet points on the frequency axis permit control using digital techniques. Data is presented for some cases of peak-notch resonances encountered in acoustic and vibration systems.

Contributors (p. 131)

Automatic Control

VOL. AC-6, NO. 3, SEPTEMBER, 1961

Rising Costs, Editorial (p. 249)

The Issue in Brief (p. 250)

The Sensitivity Problem in Sampled-Data Feedback Systems—I. M. Horowitz (p. 251)

This paper is devoted to a discussion of the effect of parameter variations on the system response in sampled-data feedback systems. It is shown that in any single degree of freedom feedback configuration, the system response and especially its overshoot are inherently very sensitive to parameter variation. By means of a suitable transformation, the properties of the sensitivity function can be studied in terms of the usual continuous system frequency concepts, e.g., bandwidth and loop transmission shaping on the Bode plane. There is a basic limitation on the loop transmission bandwidth that can be obtained in any sampled-data feedback configuration. This limitation makes it impossible to secure the unlimited sensitivity reduction which is theoretically available in minimum phase continuous systems. It is shown how one must achieve a compromise between the values of the sampling period, the system response, and the sensitivity function. The design procedure is illustrated in detail with a numerical design problem in which there is substantial parameter variation.

Self-Optimization of a Control System by Means of a Logic Circuit—T. Isoe (p. 260)

The self-optimization of a control system has been tried by means of a logic circuit. The device makes successive trials by giving values of a parameter to the system and, on the basis of the resulting successive observations of the mean-square error, finally finds the value of the parameter giving the minimum error. The device is also able to follow the change of the system conditions to keep the system optimum. The optimum value of damping ratio of a second-order system with LF Gaussian noise input is also discussed on the basis of the data obtained with the device.

Stability Conditions of Pulse-Width-Modulated Systems Through the Second Method of Lyapunov—T. T. Kadota and H. C. Bourne, Jr. (p. 266)

PWM systems contain inherent nonlinearities which arise from their modulation scheme. Thus, for a legitimate study of stability, such systems must be treated as nonlinear sampled-data systems without initially resorting to linear approximations. For a nonlinear system whose dynamic behavior is described by a set of first-order difference equations, one of the theorems in the second method of Lyapunov gives, as a sufficient condition for asymptotic stability in the large, the existence in the whole space of a positive-definite Lyapunov's function V , whose difference ΔV is negative definite. Hence, by choosing a positive-definite quadratic form as V , the sufficient condition is reduced to the negative-definiteness in the whole space of ΔV . Upon this basis, a systematic procedure of obtaining analytically a sufficient condition for asymptotic stability in the large is developed for various types of PWM systems; the condition is stated as the negativeness of all the eigenvalues of three matrices associated with the PWM system.

Stability and Graphical Analysis of First-Order Pulse-Width-Modulated Sampled-Data Regulator Systems—E. Polak (p. 276)

Pulse-width-modulated sampled-data systems are described by nonlinear difference equations which do not lend themselves to an exact analytic treatment.

This paper presents a graphical technique for the analysis of PWM sampled-data systems with first-order plants. This technique provides a sufficient condition for asymptotic sta-

bility in the large, a method for examining the damping properties of the system, a method for computing the step response from any initial condition and, finally, a method for observing and interpreting the effect of varying the system parameters on the step response of the system.

Analysis of Pulse-Width-Modulated Control Systems—F. R. Delfeld and G. J. Murphy (p. 283)

Previous work on the analysis and design of pulse-width-modulated control systems is reviewed, and the limitations of some of the earlier contributions are discussed. A mathematical development of an orderly and relatively simple method for the exact determination of the response of closed-loop pulse-width-modulated control systems to arbitrary input is then presented. Through the use of difference equations and the separation of linear and nonlinear terms, the output at the sampling instants is expressed as a function of the sampled error, and z -transform theory is then employed to obtain an exact solution for the error at the sampling instants.

A technique for studying the stability and other performance characteristics of pulse-width-modulated feedback systems is next presented. The exact method of analysis developed earlier and a modified describing-function technique are utilized together to investigate stability without overlooking pulse-width saturation.

Three illustrative examples are also presented to demonstrate the relative simplicity of the methods described in the paper as well as the accuracy of the results obtained by the use of these methods.

Effects of Quantization on Feedback Systems with Stochastic Inputs—R. Kramer (p. 292)

An approximate analysis of the effects of quantization in a feedback system is made. The system input is a Gaussian random signal. The error autocorrelation as a function of the quantizer box size is the goal of the analysis. The approximation lies in the assumption that certain error joint distributions are Gaussian. In the limit as the quantizer box size approaches zero, these distributions do become Gaussian.

On the basis of the approximation, a nonlinear integral equation relating the error autocorrelation to the system parameters is developed. An iteration procedure for successive approximations to the solution is outlined, and several examples are presented. Finally, experimental results obtained on a digital computer are shown.

Minimizing Effects of Disturbing Signals Through a Minimum Square-Error Criterion—M. Sobral, Jr. (p. 306)

One of the reasons for using feedback is the improvement in the rejection of disturbing signals. This improvement can be obtained through an analytical design utilizing as a performance index the integral square-error criterion. In the usual technique the sum of the command signal plus the disturbing signal transferred to the input of the system is used as the input signal. When this is done, one of the two compensating transfer functions (for the particular case of a system with two degrees of freedom) has to be fixed arbitrarily. Then the optimum over-all transfer function, which minimizes the integral of the square of the error between the desired output and the actual one, is calculated and thus the remaining compensator can be obtained. As the technique does not provide a method for determining one of the compensators, and the transferred disturbing signal is a function of this compensator, a required rejection of the disturbing signal may not be satisfied. The purpose of the present paper is to suggest an analytical technique for determining both of the two compensators which have the

minimum bandwidth necessary to satisfy a desired over-all transfer function and a required rejection of a disturbing signal. In addition, the technique provides physically realizable compensating transmissions.

Discussion of Paper Above—O. J. M. Smith (p. 310)

Integral Transforms for a Class of Time-Varying Linear Systems—K. S. Narendra (p. 311)

This paper presents an extension of the transform method to systems having parameters which vary with time. By using the general λ domain approach suggested by Zadeh for the analysis and synthesis of linear time-varying systems, a system function $H(\lambda)$ independent of time may be defined for the linear system. Such a system function has many of the advantages of that obtained for stationary systems using the Laplace transformation. By making $H(\lambda)$ a ratio of polynomials in the complex variable λ the pole-zero synthesis technique used for fixed systems may be applied to the time-varying case as well. Recently, a "building block" for the synthesis of a class of time-varying systems was suggested by Kilmer and Johnson. A similar building block for systems with exponentially varying coefficients is suggested in this paper.

Signal Stabilization of Self-Oscillating Systems—R. Oldenburger and T. Nakada (p. 319)

The hunt (self-oscillations) of a physical system may often be removed by the introduction of an appropriate stabilizing signal which changes the open loop gain in a nonlinear manner. More generally, the performance of nonlinear systems in many cases may be improved by the introduction of extra signals. The theory of signal stabilization developed here extends the earlier work by Oldenburger and Liu involving an equivalent gain concept. It is shown that with the aid of the Fourier series the designer can determine the periodic signal to be inserted at one point in a loop to yield a desired stabilizing input to a nonlinear element in the loop. The use of sinusoidal and triangular inputs to a limiter are compared. An example where a limiter is the only nonlinearity is employed to illustrate the theory. The approach developed here explains experimental results previously reported by Oldenburger.

An Analytical Approach to Root Loci—K. Steiglitz (p. 326)

The general algebraic equations of root loci for real K are found in polar and Cartesian coordinates. A synthesis method is then suggested which leads to linear equations in the coefficients of the open-loop transfer function when closed-loop poles and their corresponding gains are specified. Equations are also found for the gain corresponding to a given point on the root locus.

A superposition theorem is presented which shows how the root loci for two open-loop functions place constraints on the locus for their product. With a knowledge of the simple lower-order loci, this theorem can be used in sketching and constructing root loci.

s-Plane Design of Compensators for Feedback Systems—C. D. Pollak and G. J. Thaler (p. 333)

The poles and zeros of a compensator affect the s -plane gain and phase of the open-loop system at every point in the s -plane. These effects are studied for open-loop poles and zeros on the negative real axis, and a family of curves summarizes the results. A design technique is developed which permits compensation design to satisfy simultaneous specifications of root location and system gain. The method clearly defines the minimum number of compensator sections required and leads to a logical interpretation of relative needs for phase-lead and phase-lag compensators.

Correspondence (p. 341)

Recent PGAC Chapter Meetings (p. 363)
Contributors (p. 364)
Announcements (p. 367)

Broadcasting

VOL. BC-7, No. 3, AUGUST, 1961

N.A.B. Engineering Achievement Award (p. 1)

Scan Converter for Broadcast Use—A. W. Malang (p. 2)

Minimizing the Effects of Vidicon Lag with a Long Video Delay Line—W. L. Hughes (p. 8)

A common complaint among people who utilize vidicon cameras is the "stickiness" or "lag" effect which is encountered when these tubes are used at low light levels. This paper discusses a method of minimizing this effect using a wide band video delay line with a time length equal to 262 television lines. This technique is an outgrowth of an extensive color television systems research program carried on at Iowa State University for the last several years.

Improved Video Recording System—F. Gillette (p. 11)

Uniform terminology and a method of graphical representation are established. Factors affecting exposure uniformity are described by reviewing fundamental relations between the film exposure cycle and the television scan. Practical arrangements for recording television pictures on motion-picture film are described and analyzed. Effects of phosphor persistence are considered, and a detailed analysis of persistence effects in single-field recording is offered.

Recent Advances in Vidicons—M. Rome (p. 12)

The last few years have seen the introduction of many new vidicon types. Sensitivity, lag, response, resolution, and miniaturization of the new tubes are reviewed. In addition a brief discussion on the variation of gamma with dark current and light level of broadcast vidicons is included.

An Improved Loudness Indicator—J. L. Hathaway (p. 19)

The standard type VU meter has for many years been employed almost exclusively by broadcasters in the United States as a program level indicator. A new unit which should give better indication of peak loudness has now been developed and is being evaluated. This unit operates within the range of time constants specified by the FCC for transmitter aural modulation meters. A field test is now in progress, with a number of the new indicators in various studios throughout the country.

The International Broadcasting System of the Voice of America—G. Jacobs and E. T. Martin (p. 25)

The Voice of America, the international broadcasting service of the U. S. Information Agency, speaks for America in thirty-five different languages to a worldwide audience. The technical facilities that make this possible literally encircle the globe. Thirty shortwave transmitters at seven locations in the continental United States range in power from 25 to 200 kilowatts. Overseas, the VOA has nine relay stations with forty-seven transmitters ranging in power from 35 to 1000 kilowatts. This presentation discusses the development of this technical system from its war-time inception. Highlighted in the discussion are the problems encountered in the development of the system, the techniques designed to counteract these obstacles, and future plans for strengthening the signal of the Voice of America.

FCC Laboratory Observations of Precision Frequency Control of TV Stations—E. W. Chapin (p. 36)

Observations on the use of both high- and low-frequency precision offset for interference reduction have not indicated any severe problems due to propagation, at least for Channel 4. Arrangements are being made for further observations on high VHF channels.

The CBS NetALERT—A System for Network Signaling—A. A. Goldberg, A. Kaiser, G. D. Pollack, and D. Vorhes (p. 43)

Broadcasting and Television Receivers

VOL. BTR-7, No. 2, JULY, 1961

IRE Professional Group on Broadcast and Television Receivers (p. 1)

Program for PGBTR Radio Fall Meeting (p. 2)

1961 Chicago Spring Conference Highlights (p. 3)

PGBTR Administrative Committee (p. 4)
Some Considerations in the Application of Mechanical and Piezoelectric Filters—H. J. Benzly (p. 5)

The operation of and design approaches to mechanical and piezoelectric electric wave filters are discussed. The literature is reviewed and typical values for resonator and filter characteristics are presented.

Comments on impedance levels, insertion loss, spurious responses and stability are included.

Component tests are discussed and the application of ceramic elements to the IF circuit of a transistorized broadcast receiver is described.

A Second Progress Report on TV-Receiver Reliability—E. H. Boden (p. 11)

The Midwest Program on Airborne Television Instruction—An Experiment in Progress—J. S. Miles (p. 14)

This paper is intended to describe an experiment now in progress. Considerable work has been and is being done. A great deal has been learned, but tentative conclusions currently arrived at are based almost wholly on subjective evidence.

Satellite Broadcasting?—S. G. Lutz (p. 17)

Now that the first demonstrations of satellite-relayed transoceanic television may occur within two years, what is the probable future of satellite broadcasting? This study examines problems of broadcasting via satellites directly to home television receivers, compared with those of relaying to earth-terminals and re-broadcasting locally. The former eventually may be possible, but would require high-power, highly engineered satellites and would involve other problems, which are discussed here. Direct FM audio broadcasting may be less difficult but also less spectacular and rewarding.

A Complete Specification of the Gain Control Characteristics of RF and IF Transistors—L. A. Weldon (p. 23)

This paper describes a unique method for specifying the gain control characteristics of high-frequency transistors over their entire AGC range. The forward gain control characteristics of transistors can be measured by means of a curve tracer to permit the specification, within published limits, of the high frequency power gain versus collector to emitter voltage curve. While this report describes the specification of forward gain control characteristics the system can also be used for reverse gain control specifications.

Operation of the curve tracer system is discussed and a description of the AGC specification is given as well as a method for its use in accurately predicting the gain and the AGC range spread for equipment in production.

Equations are given for calculating the base control voltage characteristics and the value of

collector bias resistor required for optimum operation.

A New Compact TV Tuner—T. F. Gossard, W. G. Delp, and J. F. Stolte (p. 29)

A brief review of the performance requirements and other factors influencing the design of VHF television tuners is presented, including some of the unforeseen problems encountered during development of a new design. The basic electrical similarity between tuners of different manufacturers is pointed out, which suggests that significant design improvement might best be obtained by concentrating attention on mechanical rather than electrical factors. Development of a new compact tuner was begun with maximum use of molded plastic parts, reduction of the number of mechanical parts, and suitability for automatic production techniques as the main design objectives. A final design was completed and the tuner is now in production. A description of the novel features of this tuner indicates how the design objectives were reached and greater product uniformity and lower costs realized.

An Efficient Noise Immune Sync and AGC Circuit for Television Receivers—R. N. Rhodes and W. F. Dietz (p. 35)

A Precision-Tuned Receiver Employing Solid-State Tuning Elements—E. M. Aupperle and T. W. Butler, Jr. (p. 39)

The capability of rapid frequency selection coupled with crystal controlled tuning accuracy are the salient features of this solid-state receiver. The heart of the system is a discrete local oscillator. It consists of an electronically tuned oscillator which is phase-locked to a selected harmonic of a master crystal. Since there are no mechanical adjustments necessary, the receiver can be built in a small, light-weight package.

An experimental AM-FM receiver covering the range 80–102 Mc in 100-ke steps was built. This paper presents a discussion of the design principles, the applications of such a receiver, and the techniques required in constructing the receiver.

Dynamic Polar Display of Transfer Characteristics of Television Receivers—P. H. Van Anrooy (p. 47)

A polar plot displays amplitude, as well as phase response versus frequency, in one single figure. This is interesting for evaluation of the influence of pole zero (circuit parameter) adjustments of transfer networks immediately, without time consuming transforms (from electrolytic—P. Z. "domain"—or other "analogs").

A Solid State Oscilloscope Display—S. Talesnick and S. Yando (p. 54)

A new solid-state display device utilizing certain unique properties of piezoelectric and electroluminescent materials is described and the principles of operation are reviewed. The device requires only four properly timed electrical inputs to produce a spot of light at any selected point on the display panel. The timing relationships are derived and a system capable of producing the required drive signals is described. Oscilloscope patterns are generated on the panel by a point-by-point plot of suitably processed X- and Y-input signals.

Factors Affecting Overall Performance of FM Stereophonic Receivers—A. Csicsatka and R. M. Linz (p. 59)

A flat phase linear IF pass band should be designed into a high fidelity stereo tuner.

A vector analysis of a tuner exhibiting an equivalent 5- μ sec deemphasis in its output voltage vs frequency characteristics shows that the major cause of poor stereo performance is related to the level differences of the L+R and L-R channels. A simple adjustment of the L+R level control in the synchronous oscillator stereophonic adapter circuit described can correct this difference.

Curves relating channel gain and phase difference indicate that 30-db separation can be maintained if the channel gain difference is less than $\pm \frac{1}{2}$ db and the channel phase difference is 3° or less. By observing the discriminator output of a receiver it is possible to judge separation capability of a transmission system using a specially developed visual analysis.

The synchronized oscillator circuit discussed in this paper uses the 19 kc/s pilot as a synchronizing signal for the 38 kc/s regenerated subcarrier and a simple matrix to recover the L and R channels. It is found that the phase of the reinserted subcarrier can shift up to $\pm 35^\circ$ from correct insertion before stereo separation is reduced to 20 db.

Design of Stereophonic Receiver for a Stereo System in the FM Band Using an AM Subcarrier—A. J. DeVries (p. 67)

From the FM discriminator in the receiver we derive the composite signal containing a low frequency audio signal, a modulated subcarrier and a pilot signal related to the subcarrier. The stereophonic signal demodulator can operate on the composite signal in such fashion as to produce directly a left and right stereophonic signal.

Analytically it is shown that this can be accomplished by multiplying the composite signal by the appropriate function. Carrier regeneration can be accomplished in several ways.

It is also possible to construct a multiplex receiver by operating independently on the low frequencies and the modulated subcarrier information.

Stereophonic FM Broadcasting—C. G. Eilers (p. 73)

In arriving at a suitable choice of transmission parameters for stereophonic FM broadcasting, consideration must be given to several factors, as follows:

1. The modulation choice should provide an aurally-balanced program for the monophonic listener.
2. A reasonable compromise should be made between the stereophonic signal-to-noise ratio and the monophonic signal-to-noise ratio as compared to monophonic broadcasting.
3. Receivers designed for the system should be capable of reliable operation yet should be reasonably inexpensive.
4. If possible, the system should provide an additional channel for other services without degrading the desired service.

The transmission parameters should be selected with the present state of the electronic art in mind; however, it should be recognized that advances in the art will always take place. Thus, one must also keep the future in mind when selecting these parameters.

An Ultra-Low-Distortion Transistorized Power Amplifier—H. M. Kleinman and C. F. Wheatley (p. 81)

The development of a new type of power transistor has made possible the construction of ultra-high-performance audio-frequency amplifiers which can equal the performance of the finest vacuum-tube amplifiers available. The design, construction, and performance characteristics of such an amplifier, using RCA drift-field power transistors, is discussed. The amplifier is capable of providing a power output of 50 watts at less than one-half per cent distortion from 20 cycles to 20,000 cycles. Also discussed are a five-watt class A amplifier and a 15-watt-per-channel stereo amplifier which combine high performance with economy.

The Nuvistor Triode in Video IF-Amplifier Circuits—K. W. Angel and J. Gote (p. 88)

This paper discusses the use of the Nuvistor triode in two- and three-stage IF amplifiers and places particular emphasis on neutralization. Theoretical stable-gain limits are also discussed

and the results of practical designs are presented.

Component Parts

VOL. CP-8, No. 3, SEPTEMBER, 1961

Information for Authors (p. 97)

Who's Who in PGCP: Kathryn M. Schwartz (p. 98)

Realization of a Filter with Helical Components—A. I. Zverev and H. J. Blinchikoff (p. 99)

In the VHF range, high-quality narrow-band filters with reasonable physical dimensions are extremely difficult to realize. Excessive passband insertion loss accompanies filters employing lumped constant elements, and unreasonable size is a natural consequence of coaxial-resonator filters. Harmonic crystal filters are inadequate because of the unpredictable amount of spurious modes above the harmonic frequency; and hence they can only be used for very low percentage bandwidths. A solution to the above problems is provided by the use of helical resonators for high-quality filters.

This paper describes the helical resonator, measurement of its Q, and coupling to the resonator. A procedure for the design and construction of a filter using helical circuits is then presented. Finally an example is given illustrating the design method, and several photographs of helical-resonator filters are shown.

The Split-Feedback Push-Pull Magnetic Amplifier—I. M. Horowitz (p. 110)

This paper describes a high-gain phase-sensitive magnetic amplifier which simultaneously possesses the high-gain property of the self-saturating (100 per cent positive feedback) amplifiers and the limited circulating current property of the low-gain zero feedback amplifiers. These features are obtained by using feedback windings to obtain the self-saturating large-gain property. However, the feedback windings are arranged so that the feedback is positive only when load current flows and is zero when circulating currents flow. The circuit is analyzed and its various modes of operation are described. The theory is verified with numerous experimental results.

Radio-Frequency Autotransformers with Coaxial-Transmission-Line Windings—J. F. Cline (p. 119)

Impedance transformations are derived for radiofrequency autotransformers wound with sections of coaxial-transmission line. The outer conductors of the transmission-line sections all are connected in parallel to form a single-turn secondary winding, while the primary winding consists of this single turn plus all of the inner conductors connected in series. The circuit also can be used in single-port applications as a loop antenna, coupling link, or magnetic probe, the impedance being increased because of the transformer effect. A general method of analysis is described for an N-turn primary winding and explicit expressions are given for N=2 and N=3. From the standpoint of frequency response, the principal difference between this circuit and an ordinary autotransformer is that the ordinary leakage-inductance effect is replaced by a transmission-line effect that leads to alternate bands of usefulness and nonusefulness as the frequency is increased above the normal cutoff range.

Transient Effects of Pulsed Nuclear Radiation on Electronic Parts and Materials—H. J. Degenhart and W. Schlosser (p. 123)

Nuclear radiation induced transient changes in the electrical characteristics of electronic parts and materials obtained in recent experiments at the GODIVA II pulse reactor are described and discussed. The electronic parts investigated and monitored during exposure in-

clude: coaxial cables; resistors of various types and manufacture, ranging in value from 100 ohms to 1 megohm; sensistors; capacitors, ceramic and tantalum; rectifiers, silicon and selenium; and magnetic cores, ferrite. Most of the parts during exposure show transient parameter changes which exceed the tolerance values and then recover generally to the nominal value within two to five msec. This behavior is of serious concern in data and information processing equipment and in high-frequency and high-accuracy instrumentation which are exposed to such a nuclear environment, yet which must maintain their operational tolerance even for short periods of time.

Contributors (p. 129)

Electronic Computers

VOL. EC-10, No. 3,
SEPTEMBER, 1961

Logic and Switching Theory

Editorial—N. R. Scott (p. 345)
An Algorithm for Path Connections and Its Applications—C. Y. Lee (p. 346)

The algorithm described in this paper is the outcome of an endeavor to answer the following question: Is it possible to find procedures which would enable a computer to solve efficiently path-connection problems inherent in logical drawing, wiring diagramming, and optimal route finding? The results are highly encouraging. Within our framework, we are able to solve the following types of problems:

- 1) To find a path between two points so that it crosses the least number of existing paths.
- 2) To find a path between two points so that it avoids as much as possible preset obstacles such as edges.
- 3) To find a path between two points so that the path is optimal with respect to several properties; for example, a path which is not only one of those which cross the fewest number of existing paths, but, among these, is also one of the shortest.

The minimal-distance solution has been programmed on an IBM 704 computer, and a number of illustrations are presented. The class of problems solvable by our algorithm is given in a theorem in Section III. A byproduct of this algorithm is a somewhat remote, but unexpected, relation to physical optics. This is discussed in Section VI.

Cascaded Finite-State Machines—A. Gill (p. 366)

In this paper, networks of finite-state machines, rather than individual machines, are discussed. The investigation centers around cascade networks, where the output of one machine serves as an input to another. It is shown how, by means of connection matrices, the characteristics of such a network can be obtained from those of the component machines, and how a specified machine can be decomposed into a number of cascaded components. The advantages of such a decomposition, as well as some of the problems that remain to be solved in this area, are discussed.

The Realization of Symmetric Switching Functions with Linear-Input Logical Elements—W. H. Kautz (p. 371)

The problem of synthesizing switching networks out of linear-input (threshold) elements is studied for the class of symmetric switching functions. Tight bounds are derived for the number of elements required in a minimal realization, and a method of synthesis is presented which yields economical networks. Minimal networks result for all symmetric functions of no more than about twelve variables, and for several other cases. In particular, it is shown how the parity function of any number

n of variables can be realized with about $\log_2(n)$ elements.

Orthogonal Functions for the Logical Design of Switching Circuits—R. P. Coleman (p. 379)

A new approach to the mathematical representation of switching functions is presented. It was developed in connection with a theoretical study of magnetic-core logic, but the results are considered to be more basic and general than the core-logic problem. The ampere-turns (MMF) expression for core switching is shown to be part of a special type of Fourier series expansion of a switching function, in which the turns are directly related to the spectrum of the function. Fourier's transform methods, used for analysis of X-ray diffraction, have been adapted to the representation of switching functions. The method leads not to Boolean algebra, but to ordinary algebra in terms of the orthogonal functions

$$(-1)^{k_1x_1+k_2x_2+\dots+k_nx_n}$$

where

$$x_1, x_2, \dots, x_n = 0, 1,$$

and

$$k_1, k_2, \dots, k_n = 0, 1.$$

Methods of application are described for magnetic-core logic and for character recognition.

Autocorrelations for Boolean Functions of Noiselike Periodic Sequences—B. M. Eisenstadt and B. Gold (p. 383)

One method of generating a waveform whose correlation function resembles that of noise is by means of combinations of periodic binary sequences. In this paper the properties of the correlation function for arbitrary functions of n periodic binary sequences are investigated. An especially simple formulation is obtained when each binary variable in all the sequences has equal probability of being 0 or 1. For this case, it is shown that there are only two functions which result in a correlation function like true purely random noise. One of these two functions corresponds to addition modulo 2. Also the correlation for the case of a random function of n sequences is derived. Finally, expressions are obtained for the number of degenerate Boolean functions.

Computer Systems and Circuits

Signed-Digit Number Representations for Fast Parallel Arithmetic—A. Avizienis (p. 389)

This paper describes a class of number representations which are called signed-digit representations. Signed-digit representations limit carry-propagation to one position to the left during the operations of addition and subtraction in digital computers. Carry-propagation chains are eliminated by the use of redundant representations for the operands. Redundancy in the number representation allows a method of fast addition and subtraction in which each sum (or difference) digit is the function only of the digits in two adjacent digital positions of the operands. The addition time for signed-digit numbers of any length is equal to the addition time for two digits. The paper discusses the properties of signed-digit representations and arithmetic operations with signed-digit numbers: addition, subtraction, multiplication, division and roundoff. A brief discussion of logical design problems for a signed-digit adder concludes the presentation.

Computing Machine Aids to a Development Project—C. W. Rosenthal (p. 400)

A system of integrated computer programs which provide useful machine assistance to the development of a digital system will be described. The individual programs are capable of such separate engineering tasks as verifying design data, optimally locating electronic logic packages on a chassis, routing interconnecting wires and preparing documents like wiring diagrams and wire running lists.

The engineer using the system need not be

a computer programmer because the machine aids programs are called into operation with a simple mnemonic language keyed to the engineer's traditional tasks. This aspect of the work as well as the accomplishment of the individual engineering tasks are emphasized in this paper.

Improvement of Electronic-Computer Reliability through the Use of Redundancy—W. G. Brown, J. Tierney and R. Wasserman (p. 407)

Physical elements used for switching logic have finite probability of failure. The application of redundancy to logic circuits is presented for improving computer reliability. This paper shows various redundant configurations considered and the conclusion drawn.

From all of the considerations, the majority gate provides a practical method for increasing the reliability. It shows that for operating periods which are short compared to the mean time to failure of the elements, a substantial increase in system reliability is obtained with majority-gate redundancy.

Some Thoughts on Digital Components and Circuit Techniques—A. W. Lo (p. 416)

Signal standardization and control directivity are emphasized as the basic physical requirements in considering components and circuit techniques for the handling of digital information. The significance and the ways and means of meeting these requirements are most revealing when illustrated by the operations of the parametric phase-locked oscillator and the tunnel diode. A categorical listing of digital-gain elements, accompanied by illustrative comments, is presented to offer a unified viewpoint on digital components and circuit techniques in connection with present-day practice and prospective future development.

UNIVAC-LARC High-Speed Circuitry: Case History in Circuit Optimization—N. S. Prywes, H. Lukoff, and J. Schwartz (p. 426)

In recent years, the design of computer circuits has become a thorough and complex job. Factors such as logical design, behavior of components, manufacturing techniques, and life tests are playing an even more important role in the design of an efficient circuit.

This paper will discuss how circuit optimization techniques and use of the UNIVAC® I computing system aided in reducing cost and avoiding many of the pitfalls in the design and production of efficient high-speed circuitry for UNIVAC-LARC.

Digital Storage

Coincident-Current Superconductive Memory—L. L. Burns, Jr., G. A. Alphonse, and G. W. Leek (p. 438)

In a continuous superconductive film memory, elements are obtained through discrete regions of circulation of persistent currents near the intersection of x - y conductors deposited on the film. Analysis and confirming experiments show that these regions are stable. The elimination of edges of discrete film dots removes the main cause of variation of critical currents. Reproducibilities better than one quarter per cent were obtained. Simplicity of construction permits high bit densities. Memory planes of one-hundred cells were made. Advisable speed of operation depends mainly on addressing and sensing circuits. Write-in in 3 nsec was obtained in single elements with only 60 milliamperes drive.

Semipermanent Storage by Capacitive Coupling—D. H. MacPherson and R. K. York (p. 446)

The need arises for reliable, economical high-speed, semipermanent stores for electronic-telephone switching systems, as well as for modern digital computers. A semipermanent or fixed store is one in which the stored information may not be changed by the machine that is able to consult it. These stores provide data security for such information as operational programs and test routines.

A random-access store system where the memory elements consist of a matrix of printed capacitors has been developed. The store has a cycle time of 3 μ sec and contains 1024 words each 34 bits long.

The access circuits developed enable one to utilize a matrix arrangement of components where a need exists for stores of thousands of words. These circuits consist of diodes and biased square-loop ferrite cores in the input, and magnetic gates, utilizing three transformers in a novel arrangement, in the output.

A Card-Changeable Permanent-Magnet-Twistor Memory of Large Capacity—W. A. Barrett, F. B. Humphrey, J. A. Ruff, and H. L. Stadler (p. 451)

The card-changeable permanent-magnet-twistor memory is a large capacity (ca 10^5 bits) storage media for information that is infrequently changed. The information is stored in the form of small bar magnets bonded to a removable plastic card. The magnets, when magnetized, inhibit the switching of a section of twistor wire at a twistor-wire-solenoid crosspoint. For maximum information density the magnet shape and strength must be optimized with respect to the magnet's action on the inhibited crosspoint and the fringing action on neighboring crosspoints. The objective is a magnet with a small dipole moment, but with adequate inhibition of the twistor switching over a reasonable range of misposition. Suitable magnet shapes and a general discussion of the stray fields in a large array of magnets are given. For maximum capacity, the transmission characteristics of the twistor wire and the character of the access switch must be considered. Two novel structures of this memory permit increased information density and capacity. The feasibility of a random-access high-density memory submodule containing 360,000 bits in 0.7 foot with a cycle time of 5 μ sec has been demonstrated.

Correction to "Reducing Computing Time for Synchronous Binary Division"—R. G. Saltman (p. 461)

Symbol Manipulation, Artificial Intelligence The Simulation of Cognitive Processes: An Annotated Bibliography—P. L. Simmons and R. F. Simmons (p. 462)

A Note on the System Requirements of a Digital Computer for the Manipulation of List Structures—H. Gelernter (p. 484)

The technique of programming within the framework of the so-called Newell-Shaw-Simon (NSS) associative list memory is currently the subject of much interest among workers in the area of advanced programming research. Unfortunately, committing a given program to list memory generally entails accepting a significant loss of speed and efficiency in information processing, so that the advantages accruing from the use of list memory must be carefully balanced against its weaknesses. This paper is concerned with the system requirements of a digital computer for which the use of list techniques is to be competitive with standard programming, so that the particular memory organization for a given problem may be chosen on the basis of suitability and ease of programming alone. A description of a list-processing 7090-type computer is appended in order to make our discussion concrete, although engineering and economic feasibility is not implied.

Simulation of Three Machines Reading Arabic Numbers—L. A. Kamentsky (p. 489)

Three machines have been simulated using an optical scanner and the IBM 704 computer. Each of these simulated machines has read documents containing rows of handwritten Arabic numbers. Sample numbers were produced by at least 20 people for each simulation study. The three machines simulated differ in the control required of the writer during document preparation and in the complexity of the

machines. Writing controls were required for the preparation of the first two types of documents. A section of this paper concerns experiments with and a mathematical model of controlled writing. The third simulated machine was applied both to numbers written within preprinted boxes and to numbers written without any guide marks. About one per cent of 2180 of these numbers were misread as the wrong character. This error rate is based on a sequential experiment in which the recognition logic is constructed from all characters not recognized and thus rejected prior to each input character. Numbers, when rejected, cause the program to identify them from a table. Their structure is then entered into the recognition logic. The rejection rate decreased throughout the experiment. The last rejection rate was about 10 per cent.

An Analog Method for Character Recognition—W. H. Highleyman (p. 502)

A method for character recognition which is capable of an analog implementation has been studied by simulation on a digital computer. In essence, this method involves maximizing the cross-correlation value between the unknown character and a set of average characters, there being one average character for each allowed character class. An average character is represented by a two-dimensional function. The value of this function at a point is the probability of occurrence of a mark at that point for the character class represented by the average character. Negative weights are given to areas of low probability in each average character to improve discriminability.

The simulation results indicate that this method is applicable to the recognition of machine printing, and perhaps to the recognition of constrained hand printing. The method can be implemented in an economical manner using electro-optical techniques.

Analog Computers

The Hall-Effect Analog Multiplier—G. Kovatch and W. E. Meserve (p. 512)

The application of the Hall effect to a general-purpose four-quadrant multiplier is discussed. Circuit diagrams for the transistor amplifiers are given. An evaluation of the experimental results is given for a breadboard model of the multiplier. Static accuracies on the order of 1 per cent to 3 per cent are obtained for the Hall channel and the magnetic channel, respectively. Bandwidths of 25 kc and 1.3 kc are achieved for the Hall channel and the magnetic channel, respectively.

Copper-Mandrel Potentiometer Dynamic Error and Compensation—C. H. Single and J. A. Brussolo (p. 516)

A simple potentiometer equivalent circuit is presented that is valid for single or multiturn, copper-mandrel, wire-wound precision potentiometers. Developed to obtain a practical approximation of potentiometer ac characteristics, it is particularly useful in error analyses where small phase errors are critical.

Capacitive compensation techniques are also given that can achieve considerable reduction in potentiometer dynamic error. Even for heavy capacitive loading it is possible virtually to eliminate potentiometer phase error (important in most analog computer circuits). Correspondingly, high-frequency square waves can be attenuated reasonably by such capacitively-compensated potentiometers.

Design of the ESIAIC Algebraic Computer—M. L. Morgan and J. C. Looney (p. 524)

The concept of a pair of potential-plane "factor analogs," in which voltage measurements at the zeros and poles of a function are used for the calculation, is employed in the design of a general-purpose computer for algebraic functions of a complex variable. The logarithmic complex plane is used in order to represent a wide range of zeros and poles with uniform

accuracy. Plotting facilities provide direct graphical output for applications such as frequency response plots and root-locus plots.

Correspondence (p. 530)

Reviews of Books and Papers in the Computer Field (p. 541)

Abstracts of Current Computer Literature (p. 555)

PGEC News (p. 575)

Notices (p. 579)

Human Factors in Electronics

VOL. HFE-2, No. 2,

SEPTEMBER, 1961

The Diagnostic Process in Men and Automata—E. M. Bennett and J. W. Degan (p. 68)

Diagnostic skill involves recognizing symptoms of unusual or atypical functioning or structure, understanding the meaning of these symptoms, and evolving the ways in which such knowledge can be applied in the discovery of other existing symptoms and in the isolation of existing defects. The talents involved in diagnosis and the characteristics of the search for symptoms and defects are outlined.

An Overview of Human Factors in Electronic Maintenance—B. H. Manheimer and J. R. Kelley (p. 73)

Electronic equipment is becoming increasingly complex, and proper performance and high availability are becoming more crucial. A recent emphasis on improving maintenance planning and implementation is one method being used to assure meeting availability requirements. Human-factors contributions are essential to electronic-maintenance planning and implementation in all phases of equipment design and support. Much effort has been devoted to preparing guides for designing more maintainable equipment, but results have been little used. In the areas of equipment support, maintenance methods and procedures (both in general and for specific equipments) are being improved, but they still reflect too little knowledge of the maintenance man in the maintenance environment. Human-factors skills are being applied, with varying degrees of effectiveness, to the formulation of maintenance-manpower data, planning of support environment, installation, publications, and training. Trends, particularly those noted in manned space-travel programs, indicate that human-factors efforts in the area of electronic maintenance will improve and form a very valuable contribution to the over-all efforts to improve maintenance.

The Influence of Teaching Machine Technology on Electronic Systems Maintenance Training—L. C. Silvern (p. 78)

The evolution of electronic systems maintenance philosophy is explored in terms of performance requirements, studies of behavioral patterns, technical training requirements, engineering design, and management competences. The probable degree of success in utilizing the teaching machine for employee and customer technical training involving the maintenance of complex electronic systems is considered.

Analysis of Fault-Location Behavior in Electronic Equipment—J. W. Rigney, D. H. Schuster, T. L. Runyan, and I. J. Budnoff (p. 84)

Two analyses of maintenance technicians' intermediate behavior in trouble-shooting electronic equipment are reported. In the first, 422 records of this behavior were analyzed to describe the characteristics of the process. It was found that technicians frequently accumulated sufficient symptom information from test points to isolate a malfunctioning stage or to identify a faulty component, before they recognized this fact. Typically, either they continued to make redundant or irrelevant checks before

entering the correct stage or replacing the correct part, or they never did use the information and thus failed to solve the problem. Also, 71 per cent of the first replacements of components were incorrect. Evidently, searching for symptom information and interpretation of that information occur on two different behavioral levels, which are not necessarily closely coordinated.

The second analysis revealed the differential effects of practice in applying a trouble-shooting strategy for two subsamples of technicians, one experienced and the other inexperienced in the circuitry involved. Subsequent to the practice, the experienced group made a higher proportion of most efficient moves, whereas the inexperienced group made a lower proportion, per problem, of completely irrelevant moves. It was concluded that the former improved primarily in terms of their trouble-shooting techniques and that the latter gained chiefly in their understanding of gross circuit relationships.

Why Design for Maintainability?—J. G. Wohl (p. 87)

The relationships among down time (a system-maintainability measure), time between failures (a system-reliability measure), equipment availability, number of equipments, number of on-call technicians, and system-readiness reliability are developed under the assumption of constant failure and repair rates. Design trade-off between reliability and maintainability is shown to be feasible with resulting reduction in both design and operating costs. A technique for specifying combined reliability, maintainability, and availability constraints to manufacturers is reported which allows the latter a great deal of design flexibility in meeting operational requirements at least cost. Finally, the need for research to establish the quantitative effects of maintainability-design practice upon down time is explored.

Designing Maintainable Circuits—J. M. McKendry, J. F. Corso, and G. Grant (p. 93)

A study was conducted to answer certain questions basic to the design of more maintainable circuits. The subjects were 210 engineers, all of whom had considerable experience in electronics. Questionnaires, designed to elicit information on the primary factors affecting fault-location time, were devised for 13 representative circuits varying over a wide frequency range. A statistical analysis of the subjects' responses was conducted to determine whether any general conclusions could be drawn from the replies taken as a group. Results indicated that certain parameters yield more trouble-shooting information on all circuits and that these parameters remain approximately the same for the whole frequency range studied. In addition, it was found that oscilloscopes were considered to be the most efficient test device available. This result points out a problem, since a number of studies have shown that technicians have difficulty in using oscilloscopes and, as a result, prefer meters. Suggestions are made for circumventing this problem. A number of other analyses pointed out areas in which no generalities could be drawn, e.g., regarding the most efficient test-point locations. An attempt was made to reconcile these problems temporarily until more data are available.

Quantification of Expert Judgment in Maintenance Design Decisions—M. R. Munger, M. P. Willis, and J. W. Altman (p. 97)

Generalized findings, based on work carried out in the development of the Index of Electronic Maintainability for the U. S. Army Signal Corps, are reported on the quantification of expert judgment in the area of maintenance and maintainability. Results of this study indicated that judgments of maintenance consequences can be reliably obtained from field-maintenance personnel if proper precautions are observed in the development and utilization of the rating

instruments. Further, these results revealed considerable consistency of ratings across various types of equipment, thus implying that this generality may be extended to new equipments. This generality also eases the problem of obtaining adequate numbers of raters, since the type of experience that the rater bases his judgments on does not appear to be highly specific. No evidence was presented concerning the amount or degree of experience required for competent raters. Finally, three suggested applications of the techniques described are presented, and some of the benefits to be derived from these applications are briefly discussed.

Evaluation of Trouble-Shooting Overlay Designs—W. L. Wasserman (p. 102)

An experiment was conducted to compare two parameters of trouble-shooting overlay design: type of point-to-point connection and type of coding. Eighteen subjects were used in the experiment. They were asked to trace four tests on each of four different designs encompassing the two parameters. The results indicated that the optimum design is straight-line point-to-point connection with color coding.

Human-Initiated Failures and Malfunction Reporting—J. Cooper (p. 104)

Two studies were conducted to determine the extent and nature of human-initiated failures in missile systems. The first study compared malfunction data obtained from written reports with data gathered from interviews with line and supervisory personnel. The study revealed large discrepancies in emphasis and extent of data between the reporting methods. Written reports generally were concerned only with failed equipment; interview data with operational, near, or possible malfunctions. The results indicated that personnel tend to report human-initiated malfunctions as equipment malfunctions, thus avoiding incrimination of themselves or their fellow workers. The second study attempted to establish the extent of unreported human-initiated malfunctions. Examination indicated that in individual missile systems, human-initiated malfunctions comprised from 20 to 53 per cent of all system malfunctions. It was also revealed that in two missile systems, human-initiated holds accounted for 16 and 23 per cent of total holds, respectively. Human-initiated malfunction data were further classified into the kinds of operations in which these malfunctions occurred. The percentages in these classifications are indicated in this report. Malfunction-reporting practices were reviewed to establish their effectiveness in revealing these data and to indicate the way in which the reporting schemes serve, or fail to serve, the problem of indicating human-initiated malfunction in order that corrective action may be taken.

Communications (p. 110)

Contributors (p. 114)

Reviews of Current Literature (p. 118)

Industrial Electronics

VOL. IE-8, No. 2, AUGUST, 1961

Transistorizing the Industrial Image Orthicon Camera—R. W. Cook (p. 1)

This paper describes the design of a fully transistorized image orthicon camera. Through the use of detailed circuit descriptions in areas such as the preamplifier, shading circuits and focus current regulator, the advantages transistors offer are pointed out. These advantages show themselves in the form of substantial reduction in weight, size, cost and operating power. Charts and photographs are used to describe in detail the sensitivity, capabilities and applications of such a camera. Schematics are used in describing pertinent circuit advantages.

Computers for Industrial Control—R. W. Sonnenfeldt (p. 10)

General Purpose Digital Computers are now making their appearance in industrial plants. For the most part, they do not merely mechanize tasks previously handled by humans but make possible an entirely new era in control of complicated processes. Industrial Control Computers are now being designed for such applications. This paper discusses in basic terms the characteristics and performance features of industrial Computers, and how they can increase process profitability.

Computer Speed, Memory Capacity, Kind of Memory, Mechanical Design, Programming Features, Reliability and other specifications are related to requirements of Industrial Control. A typical application analysis is explained through use of a high-speed tin plate line as an illustrative example. Several suggestions are offered as an aid in the writing of better purchase specifications.

Currently about three years are needed to go from first conception to an operating Industrial Computer installation. A discussion is given of the many tasks to be completed by user and supplier in this process.

The Infrared Radiometric Method and its Application to Remote Temperature Measurement—H. L. Berman (p. 18)

The principles of infrared thermometry are reviewed. Basic properties of infrared optical materials and detectors are presented with reference to design and performance of the radiation thermometer. Application of the radiometric method to a broad class of common industrial materials forms the substance of this paper. Recent extensions of the method to temperature measurement of flames, glass and plastics are described. Applications of special interest to the Radio Engineer are included.

A Phase-Shift Data-Transmission System for Analog to Digital or Digital to Analog Conversion—H. Kilroy (p. 31)

A block diagram of the basic building blocks of phase-shift data-transmission systems is outlined in Figure 1. These basic blocks establish a reference time base in one or more synchro receivers to which phase signals may be compared.

A pulse source generates a train of pulses which provide this time base for the system. This chain of pulses is divided down in the reference counter and provides two 400-cycle (chosen for convenience) square-wave signals which are 90° out of phase. These signals are filtered and amplified in the synchro exciter and appear as outputs of the exciter in the form of two sinusoidal, 400-cycle signals 90° out of phase. The two sinusoids are used to excite the two stator windings of one or more synchro resolvers. The voltage induced in the rotor of each synchro resolver is a constant-amplitude, 400-cycle sinusoid whose phase angle with respect to the reference is equal to the mechanical angle of the rotor.

Radio Frequency Interference

VOL. RFI-3, No. 1, MAY, 1961

Scanning the Issue—A. R. Kall (p. 1)
Response of Ideal Radio Noise to Continuous Sine Wave, Recurrent Impulses, and Random Noise—D. B. Geselowitz (p. 2)

The responses of an ideal radio noise meter to continuous sine wave, recurrent impulses, and random noise are evaluated and tabulated. The ideal meter consists of a narrow-band linear low noise superheterodyne network followed by a detector which responds to the envelope of the intermediate frequency and a dc voltmeter which indicates the detector output. Four detector circuits—peak, quasi-peak, average, and rms—are considered. Their "ideal" characteristics are defined in the text.

Signal Acceptability Criteria—R. F. Schwartz (p. 11)

The detailed study of interference of unwanted radio signals having arbitrary modulation, with a specified co-channel signal carrying the desired intelligence, forms the basis for this paper. Detailed information about the modulation characteristics, as well as the transfer function of the receiver from antenna to output channel, are needed in order to predict acceptance ratios, or what this author has called TSI ratios. In some cases, masking of one intelligence by another needs to be taken into account, in others, beat note interference is the prime culprit, while in still others, the mechanism is far more complex. Representative TSI ratios are deduced and presented for a large number of systems, but the set of figures is by no means complete.

Interference Computations for a Complex Signal Environment—L. Katz (p. 18)

A digital computer has been programmed to evaluate the interference existing at each receiver in a large-scale army deployment involving about 20,000 receivers and transmitters. In order to reduce data handling problems, spurious responses are considered to be due to separate receivers and transmitters. Propagation path losses are statistically tailored to the terrain. The model is suitable for a parametric analysis of path loss, selectivity, spurious emissions, sensitivity, etc.

Radio Interference Reduction and Spectrum Utilization of VHF FM Net Equipment in a Mobile Environment—F. E. Rock (p. 27)

Spectrum conservation and interference reduction are not mutually complementary in a field area complex. Spectrum economy implies minimum utilization of RF channels, whereas interference-free operation requires an extensive number of channels. A certain minimum level of interference is tolerable in practice. Therefore, it follows that a system designer achieves realistic spectrum economies by designing the frequency assignment plan for a "calculated risk" level of interference.

Frequency assigners have, in fact, been doing just this sort of thing on a "rule of thumb" basis. An evaluation is made of what the use of such a practical rule means in terms of the probability of interference. The analyses is based on a statistical propagation model called "Universal Terrain." A procedure is established for conserving spectrum when unlike combinations of equipment are employed. Curves of propagation loss and interference statistics are presented.

Measurement and Suppression of VHF Radio Interference Caused by Motorcycles and Motor Cars—C. Egidi and M. Nano (p. 30)

The problem of ignition interference and its reduction has been emphasized in Europe, due to the simultaneous growth in both the number of motor vehicles, and in the number of FM and TV receivers. The paper reports the results of a large number of interference measurements made on automobiles and motorcycles. The data include the effects of various suppression schemes. As a result of these measurements, and taking into account existing European standards, a draft of an international standard was prepared for submittal to CISPR. This proposed standard covers both methods of measurement and limits.

Correspondence (p. 39)

Abstracts of Books on Topics of Interest (p. 46)

Reliability and Quality Control

VOL. RQC-10, No. 2, AUGUST, 1961

Reliability in Missile and Space Operation—Maj. Gen. L. I. Davis (p. 1)

Reliability—Whose Responsibility?—H. L. Hoffman (p. 4)

Do Present Government Procurement Practices Promote Delivery of UNRELIABLE Equipment?—Panel Discussion (p. 9)

This round table discussion was established in the belief that much of the problem of unreliability stems from inadequate communication of concepts and understanding between the top people in military and industry. Open discussion of the common problems should be beneficial to the common cause.

This compilation is a follow-up action to record for further study and discussion the major points brought out at the meeting. Comments from the reader and suggestions on how to make progress in the problem areas described will be appreciated.

Reliability Planning for Space Systems—N. E. Golovin (p. 20)

The Space Environment and Its Effects on Materials and Component Parts—S. N. Lehr and V. J. Tronolone (p. 24)

The best available preliminary information has been gathered on what materials can be used successfully and how these materials react in various space environments. Such information is necessary as a guide to space vehicle design engineers.

In addition to the factors presented here, such items must be considered as: the exact nature of the missile of a space vehicle, the type of orbit, the length of time the vehicle is expected to function, the reliability objective, and similar goals, although regardless of the mission certain general effects of the space environment present problems which must be met in the design itself. Data have been gathered on these general effects, which include high vacuum, magnetic fields, gravitational fields, micrometeorites, cosmic rays, neutrons, trapped charged particles, and electromagnetic radiation, including ultraviolet light, X rays, and gamma rays. This information is summarized in Table I.

Small Subcontractors in Reliability Programs—D. C. Berman (p. 38)

Today's military systems contracts invariably have numerical and organizational reliability requirements. With systems of any size, it is advantageous for the prime contractor to subcontract out many equipments and units. Small firms often provide superior specialized technical competence, more favorable prices, faster delivery, and a more conscientious effort; however, the small firm's lack of continuing and repetitive contractual requirements for reliability usually results in organizational weakness in this area. These firms are unable to support the cost of permanent reliability, standards, and quality control functions of the type required by these contracts.

A standard comprehensive quality or reliability survey would eliminate these organizations from competition, and a superficial survey leading to their acceptance would result in the acquisition of an ineffective subcontractor. As a substitute, a specially designed analytical survey is performed which investigates the quality, reliability, standards, and design functions of the prospective subcontractor, and indicates not only the deficiencies, but also the remedial action required.

If, on the basis of price, delivery and technical competence, a firm in this category is awarded a subcontract, procedures are instituted which invariably result in a reliability achievement at least equal to that of some large organizations which, at times, have inflexible and incompatible procedures.

This paper describes, in brief, the survey techniques and the remedial procedures instituted.

The Economics and Reliability of Multi-function Devices—J. A. Davies and C. D. McCool (p. 42)

The widely prevalent assumption that device failure rates are multiplied when two or more functions are incorporated in a single enclosure is examined with respect to actual experience on single-element vs multiple-element electron tubes. The feasibility and economics of multi-element structures are considered in the light of the recent trend toward greater and greater complexity of device combinations. The natural limits to this trend are predicted by extrapolating known factors related to spread of characteristics, random catastrophic failures, and life. Some of the most recent examples of this philosophy are described and discussed in comparison to earlier versions providing similar functional performance.

Military System Reliability: Some Department of the Air Force Contributions—J. Spiegel and E. M. Bennett (p. 53)

This report discusses the evolution, since the formation of the Department of the Air Force in 1947, of the Air Force's administrative policy concerning the reliability of complex military electronic equipment and systems. It describes developments in defining and regulating the contractor reliability effort and the monitoring and advisory activity of the Air Force procuring agencies. By reference to numerous policy statements made by the Air Force, the report demonstrates that, within only a few years after its first stated concern regarding reliability, the Air Force has succeeded in developing a reliability program which is sufficiently detailed and integrated to provide substantial assurance of reliable equipment.

Letters to the Editor (p. 64)

Biographies (p. 67)

Space Electronics and Telemetry

VOL. SET-7, No. 3,

SEPTEMBER, 1961

Availability of Moon for Global Communications—P. M. Hahn and N. C. Randall (p. 57)

This paper describes a method for quickly and quite accurately estimating the time that the moon is in common view of two stations on earth during the lunar day. A mathematical derivation and a detailed description of the method are given, together with a nomogram which simplifies the calculation. A sample problem is solved and a short table of time availability for several links of interest is included.

Thresholds and Tracking Ranges in Phase-Locked Loops—C. S. Weaver (p. 60)

This paper presents a general discussion of phase-locked-loop thresholds and tracking ranges. A typical phase-locked loop and its linear equivalent are introduced, and there is a brief discussion of application of the root locus method and the Bode amplitude plot to this circuit. Calculation of the maximum allowable deviation is considered for both phase and frequency modulation (sinusoidal).

The SNR threshold is a function of tracking and modulation, and may vary considerably. Threshold behavior—with and without limiting—is discussed, and methods are presented for estimating the threshold in each case. Calculating the tracking range and variation of the tracking range with threshold variation are also discussed. Since an increase in tracking range and a decrease in threshold are obvious design objectives, procedures are given for achieving these goals.

After a description of the effects of interference on tracking and the threshold, there is a brief report of a phase-locked-loop intelligibility study conducted by Philco Western Development Laboratories.

Appendixes I-IV consider: 1) a phase-locked loop containing an IF amplifier, 2) designing a loop to track Doppler shift only, and 3) improving the SNR by increasing deviation.

The Effect of Antenna Characteristics on Antenna Noise Temperature and System SNR—M. L. Livingston (p. 71)

With the development of low-noise amplifiers, the noise contribution of the antenna has become a limiting factor on system performance in many applications. This paper discusses the calculation of the equivalent noise temperature contribution of parabolic reflector antennas using their radiation characteristics and environment. As an example, the equivalent noise temperature of an 85-foot reflector at 2 kMc is estimated as a function of orientation for two different primary illuminations. The relative contributions of the mainlobe, sidelobes and backlobes to the total antenna noise temperature is determined in each case to show the effect of antenna radiation characteristics on noise temperature. A functional relationship between the primary illumination of a parabolic reflector antenna and the system SNR is then derived from which the edge illumination producing the maximum SNR can be specified for a given family of primary illuminations.

Fundamental Accuracy Limitations in a Two-Way Coherent Doppler Measurement System—J. A. Develet, Jr. (p. 80)

This paper derives relationships which express the contributions of ground-receiver noise and round-trip transit time to the errors in two-way radio Doppler measurements.

Only one method of Doppler measurement is considered. This is the method of counting the number of cycles in a given time interval. From this measurement the signal frequency may then be determined. In usual tracking systems this frequency measurement is further utilized to determine the range-rate of the vehicle with respect to the tracking station.

The power-spectral densities of additive-receiver noise and oscillator-frequency noise are assumed white. This situation prevails when the random disturbances are thermal in origin. This is a tractable assumption when one seeks *fundamental* accuracy limitations for Doppler measurement.

The results of this paper should be useful to those concerned with radio tracking and, in particular, tracking of space probes.

Contributors (p. 86)

Vehicular Communications

VOL. VC-10, No. 2, AUGUST, 1961

World Wide Communications Using Satellite Repeaters—R. D. Campbell (p. 2)

Mobotry: The New Art of Remote Handling—J. W. Clark (p. 12)

Equipment to perform a great variety of tasks within hostile environments has been designed and built utilizing well-proven electronic techniques. Such systems perform most of the operations which would be performed

manually were it possible for a man to enter the hazardous area. Examples of hostile environments include space, the ocean, nuclear laboratories, and numerous others.

A simple trinary coding command system has proved quite practical and is capable of commanding mobile remote systems having 50 or more degrees of freedom. Conventional closed-circuit television systems may be used for driving and steering remotely-controlled vehicles and for accomplishing manipulative tasks. Two or more such cameras are highly desirable for obtaining good spatial perception.

Examples of remotely-controlled systems for hostile environments include the Hughes Mark II Mobot system for nuclear hot laboratories, the RUM (Remote Underwater Manipulator) built by Scripps Institute of Oceanography for scientific and military operation in the depths of the ocean, and a variety of outdoor remotely-controlled vehicles designed and operated by Engineer Research and Development Laboratory at Fort Belvoir, Virginia, and by Air Force Special Weapons Center in Albuquerque, New Mexico.

Air Lines Radio Communications—G. Kidd (p. 25)

Thin Route Tropo—A New Approach to Long Range Communications—H. H. Davids (p. 28)

This new system of communications makes use of tropospheric scatter for the transmission of digital information over long distances more reliably than high frequency radio; more economically than wire; less vulnerably than microwave or VHF and cheaper than conventional tropospheric scatter systems. Using only a narrow-band width, it can be used for transmission of data (teletype, telemetry, canned messages, facsimile, etc.) over distances of upwards to 500 miles, using relatively low power transmitters and simple antenna systems. It will provide a useful link in the radio communication systems for many government agencies, both military and non-defense. While limited to these under the present regulations, it has potential for use for commercial applications in the future.

A New Helical Ground Plane Antenna—L. H. Hansen (p. 36)

A unity gain ground plane antenna of greatly reduced size is presented. The ground plane consists of four evenly spaced sloping helices. The feed element is constructed of double helical windings. All the helices are enclosed in Fiberglass tubes.

Wide-Band Channels for Emergency Communication—H. Magnuski (p. 40)

A single wideband channel could be assigned to all short range emergency communication systems, resulting in better service and better spectrum utilization. Many independent VHF or UHF mobile users or military nets could use this one channel at random without any form of centralized control or synchronization, and each could transmit different simultaneous emergency messages without significant mutual interference.

In reviewing wideband modulation and addressing (coding) techniques, it is shown that Delta modulation and discrete frequency coding is best suitable for this application.

Tone Signaling Increases Mobile Radio Efficiency—T. G. Humphreys, Jr. (p. 45)

A New Approach to Transistorization of Mobile Radio Telephone Equipment—I. Teese (p. 49)

An equipment design is described in which transistors are employed in both receiver and transmitter to reduce power drain and increase reliability. The following design objectives are believed successfully met:

Low power drain in receive condition.

Tuning adjustments minimized by use of lumped ferrite filters for both first and second I.F. selectivity of receiver.

All components easily and quickly accessible for maintenance.

Up to eleven r.f. channels available within a one Mc/s band for both receiver and transmitter. Thus particularly adaptable to Maritime VHF.

Manufacturing cost of same order as vacuum tube designs of similar r.f. power output.

A detailed description is given of a compact unit suitable for either underdash or trunk mounting in vehicular installation.

A 150-Mc Personal Radio Signaling System—D. Mitchell and K. G. Van Wynen (p. 57)

An experimental 150-Mc personal signaling system has been set up in New York City to evaluate over-all technical performance and explore subscriber reactions to the system. The system includes pocket receivers equipped with tuned reeds and central office arrangements adapted for direct customer dialing. The paper describes the system in over-all terms, and tells how it was engineered. It also compares this system with present 35 Mc-systems and discusses traffic and radio transmission problems.

Splitting the 450-Mc Channels—C. J. Schultz (p. 71)

A recently released FCC Notice of Proposed Rule Making, Docket No. 13847, contains a proposal to subdivide the existing 50-kc channels in the 450-470-Mc private land mobile band into twice as many 25-kc channels.

Field and laboratory tests conducted to date indicate that the proposed technical standards can be successfully implemented in *closely controlled* test systems. Some significant problems may arise in actual "user" systems, however, if transmitters and receivers are not properly netted and held to a close RF channel tolerance. Considerable attention must be given to the various factors which determine the amount of receiver performance degradation experienced, if successful implementation of "same area" adjacent channel operation is to be achieved.

Existing 450-Mc equipment of recent manufacture should provide adequate performance in most systems until the 25-kc split channels are assigned to new users in the same area.

Abstracts and References

Compiled by the Radio Research Organization of the Department of Scientific and Industrial Research, London, England, and Published by Arrangement with that Department and *Electronic Technology*, Dorset House, Stamford St., London, S.E. 1, England

NOTE: The Institute of Radio Engineers does not have available copies of the publications mentioned in these pages, nor does it have reprints of the articles abstracted. Correspondence regarding these articles and requests for their procurement should be addressed to the individual publications, not to the IRE.

Acoustics and Audio Frequencies	1726
Antennas and Transmission Lines	1727
Automatic Computers	1728
Circuits and Circuit Elements	1728
General Physics	1730
Geophysical and Extraterrestrial Phenomena	1731
Location and Aids to Navigation	1734
Materials and Subsidiary Techniques	1734
Mathematics	1736
Measurements and Test Gear	1736
Other Applications of Radio and Electronics	1737
Propagation of Waves	1737
Reception	1738
Stations and Communication Systems	1738
Subsidiary Apparatus	1738
Television and Phototelegraphy	1738
Tubes and Electronics	1739
Miscellaneous	1740

The number in heavy type at the upper left of each Abstract is its Universal Decimal Classification number. The number in heavy type at the top right is the serial number of the Abstract. DC numbers marked with a dagger (†) must be regarded as provisional.

UDC NUMBERS

Certain changes and extensions in UDC numbers, as published in PE Notes up to and including PE 666, will be introduced in this and subsequent issues. The main changes are:

Artificial satellites:	551.507.362.2	(PE 657)
Semiconductor devices:	621.382	(PE 657)
Velocity-control tubes, klystrons, etc.:	621.385.6	(PE 634)
Quality of received signals, propagation conditions, etc.:	621.391.8	(PE 651)
Color television:	621.397.132	(PE 650)

The "Extensions and Corrections to the UDC," Ser. 3, No. 6, August, 1959, contains details of PE Notes 598-658. This and other UDC publications, including individual PE Notes, are obtainable from The International Federation for Documentation, Willem Witsenplein 6, The Hague, Netherlands, or from The British Standards Institution, 2 Park Street, London, W.1., England.

ACOUSTICS AND AUDIO FREQUENCIES

- 534.121.1-8 3213
Experimental Confirmation of Lamb Waves at Megacycle Frequencies—D. C. Worlton. (*J. Appl. Phys.*, vol. 32, pp. 967-971; June, 1961.) Confirmation of a theory formulated in 1916 by

A list of organizations which have available English translations of Russian journals in the electronics and allied fields appears each June and December at the end of the Abstracts and References section.

The Index to the Abstracts and References published in the PROC. IRE from February, 1960, through January, 1961, is published by the PROC. IRE, May, 1961, Part II. It is also published by *Electronic Technology* and appears in the March, 1961, issue of that journal. Included with the Index is a selected list of journals scanned for abstracting with publishers' addresses.

Horace Lamb predicting that plates may vibrate in an infinite number of modes.

534.2+538.566 3214
Wave Propagation in an Inhomogeneous Waveguide—Brekhovskikh and Eliseevnin. (See 3339.)

534.2 3215
Nonlinear Effects in some Acoustic Problems—M. A. Isakovich. (*Akust. Z.*, vol. 6, no. 3, pp. 321-325; 1960.) In contrast to the case of propagation in an unbounded space, the secular terms are missing in the solution for waveguide propagation, with the exception of degenerate cases. The absence of secular terms is dependent on dispersion.

534.2-8 3216
Finite-Amplitude Ultrasonic Wave Propagation in Relaxing Media—A. L. Polyakova. (*Akust. Z.*, vol. 6, no. 3, pp. 356-359; 1960.) If the sound amplitude is less than the value characterizing the dispersion and relaxation absorption, the second-harmonic content is determined basically by the absorption.

534.232 3217
Maximum-Power Criterion for the Vibrating Free-Edge Disk—R. N. House, Jr. (*J. Acoust. Soc. Am.*, vol. 33, pp. 561-565; May, 1961.) A method of determining safe power levels for piezoelectrically driven flexural-mode transducers has been developed.

534.232 3218
On Correlating the Loss Factors of Cylindrical and Spherical Resonators—P. D. Edmonds. (*J. Acoust. Soc. Am.*, vol. 33, pp. 615-622; May, 1961.)

534.232:538.652 3219
Magnetostrictive Ferrites as Materials for Electroacoustic Transducers—I. P. Golyamina. (*Akust. Z.*, vol. 6, no. 3, pp. 311-320; 1960.) Investigation of Ni, Ni-Zn and Ni-Co ferrites shows that their magnetostrictive properties are comparable in magnitude with the corresponding parameters of more generally used metals.

534.232-8 3220
Coupling of Ultrasonic Resonators to Self-Excited Single-Stage High-Frequency Generators—W. Steglich. (*NachrTech.*, vol. 10, pp. 446-449; October, 1960.) The coupling of piezoelectric and magnetostrictive resonators to an oscillator circuit is discussed, with examples.

534.26-14 3221
Experimental Study of the Scattering of Acoustic Energy from Solid Metal Spheres in Water—L. D. Hampton and C. M. McKinney. (*J. Acoust. Soc. Am.*, vol. 33, pp. 664-673; May, 1961.) The spheres cannot be counted as rigid bodies as appreciable energy penetrates the surface, which causes a complicated echo pattern to be returned. The acoustic energy distribution for spheres of diameter 5 in and 7 in is illustrated.

534.417 3222
Factors that Determine the Equivalent Noise Pressure, Free-Field Voltage Response, and Efficiency of a Transducer at Low Frequencies—P. M. Kendig. (*J. Acoust. Soc. Am.*, vol. 33, pp. 674-676; May, 1961.) A well-designed hydrophone should have an equivalent noise pressure well below zero sea-state ambient. The equivalent noise pressure or efficiency of a transducer gives an essential indication of ability to measure low-level signals but the free-field voltage response does not.

534.75:534.32 3223
What do we Sense as Uniform Noise?—L. Schreiber. (*Frequenz.*, vol. 14, pp. 399-403; December, 1960.) Theoretical consideration of Dirac-type noise and the minimum pulse frequency at which a succession of pulses is heard as uniform noise. The results of subjective tests are given and discussed, in which the effect of varying the parameters of an inserted low-pass filter is also investigated.

534.78 3224
Liveness Effects on the Intelligibility of Noise-Masked Speech—P. O. Thompson, J. C. Webster, and R. S. Gales. (*J. Acoust. Soc. Am.*, vol. 33, pp. 604-605; May, 1961.) Speech is more intelligible against a noise background when the reverberant components associated with "liveness" are not present.

534.78:621.391 3225
Bandwidth Compression of Speech—J. Das. (*Electronic Tech.*, vol. 38, pp. 298-300; August, 1961.) A method of reducing the bandwidth of time-varying signals by sampling in the frequency domain alone is discussed. Intelligible signals can be obtained even with large bandwidth compression.

534.793 3226
The Development of a Level-Distribution Meter for the Assessment of Audibility in Rooms—H. Niese. (*NachrTech.*, vol. 10, pp. 487-494; November, 1960.) The equipment de-

scribed uses a source of periodic pulses and a stereophonic microphone; the sound level distribution in a lecture hall has been measured and results are illustrated.

534.8-8:539.32.08 3227

Notes and References for the Measurement of Elastic Moduli by Means of Ultrasonic Waves—H. J. McSkimin. (*J. Acoust. Soc. Am.*, vol. 33, pp. 606-615; May, 1961.) Aspects of wave propagation applicable to the measurement of elastic moduli of solids are reviewed. Experimental techniques and factors affecting accuracy are discussed. 111 references.

534.83 3228

The Effect of Open Acoustic Screens in Interior Rooms—H. Börner. (*Hochfrequenz und Elektroak.*, vol. 69, pp. 221-225; December, 1960.) The effectiveness of noise-reducing screens is calculated; experimental results are also given.

534.846 3229

Recent Applications of Acoustical Engineering Principles in Studios and Review Rooms—W. B. Snow. (*J. Soc. Mot. Pic. Telev. Engrs.*, vol. 70, pp. 33-38; January, 1961.)

534.861 3230

Statistical Properties of a Radio Broadcast Signal—A. V. Rimskil-Korsakov. (*Akust. Z.*, vol. 6, no. 3, pp. 360-369; 1960.) Analysis of experimental results obtained by various authors relating to the distribution of instantaneous values and of the dynamic levels of broadcast music and speech.

534.88 3231

Measuring the Transverse Correlation Coefficient of a Continuous Acoustic Signal in the Sea—S. G. Gershman and Yu. I. Tuzhilkin. (*Akust. Z.*, vol. 6, no. 3, pp. 292-298; 1960.) Investigation showed that at a frequency of 7.5 ± 0.2 kc, for distances between the wave front and the source of up to 12 km, and for a spacing of receivers along the wave front of up to 3 km, the correlation coefficient had a value close to unity.

534.88 3232

Effect of an Internal Wave on Sound in the Ocean—O. S. Lee. (*J. Acoust. Soc. Am.*, vol. 33, pp. 677-681; May, 1961.) A comparison of computed sound fields with and without an oscillation of the thermoclines for an ideal ocean medium with three distinct layers. Intensity changes of as much as 22 db may occur over one internal wavelength.

621.395.61 3233

The Insensitivity to Noise of Gradient Microphones of First and Higher Order—K. Feik and G. Kaszynski. (*Hochfrequenz und Elektroak.*, vol. 69, pp. 201-211; December, 1960.) Theoretical and experimental investigation is made of first- and second-order gradient microphones.

621.395.61:681.84 3234

Guidance on the Microphone Distance in Sound Recordings—E. Briner-Aimo. (*Tech. Mitt. PTT*, vol. 39, pp. 5-20; January, 1961.) Aspects of sound field distribution and reverberation effects which are important to the sound recording engineer are summarized.

621.395.623.7 3235

Electrodynamic Loudspeaker has Totally Active Surface—S. R. Rich. (*Electronics*, vol. 34, pp. 49-51; June 16, 1961.) A system giving excellent response over the whole AF range is described. It consists of a nonresonant, pneumatically loaded bass unit and a current-carrying sheet within a magnetic field as a treble unit. High-frequency performance is improved

by a thin corrugated Al diaphragm as a secondary radiator, mounted near the driver coil of the treble unit.

621.395.625.3:538.221 3236
Magnetic Recording—Sebestyen and Takacs. (See 3493.)

ANTENNAS AND TRANSMISSION LINES

621.315.212 3237

A Liquid-Helium-Cooled Coaxial Termination—C. T. Stelzried. (*Proc. IRE*, vol. 49, p. 1224; July, 1961.) This unit is useful for low-noise calibrations.

621.372.823 3238

The Effect of Guide Irregularities on the Transmission of TE_{11} Waves—M. Jouguet. (*Câbles & Trans. (Paris)*, vol. 15, pp. 3-26; January, 1961.) An examination of the parasitic waves generated in waveguides including estimates of their amplitude and power. Numerical results are given for a circular waveguide of diameter 50 mm operated at 35 Gc. See also 2080 of August.

621.372.824 3239

The Suppression of Parasitic Gap Resonances on Noncontacting Short-Circuiting Plungers for Coaxial Resonant Circuits—W. Spindler. (*Arch. elekt. Übertragung*, vol. 14, pp. 554-560; December, 1960.) An exact equivalent circuit is derived for the plunger gap with slots [see 644 of 1948 (Huggins)]. New types of pattern are described which provide greater mechanical stability and a wider useful band for the coaxial resonator.

621.372.824:621.316.8 3240

A Precision Coaxial Termination Resistor—C. Stäger. (*Tech. Mitt. PTT*, vol. 39, pp. 25-28; January, 1961.) The design of a 50- Ω reflectionless termination for use in the frequency range 1-9 Gc is described.

621.372.829 3241

TM Modes in Parallelogrammic Waveguides—R. J. Doviak, D. J. Lewis, and P. P. Lombardini. (*Proc. IRE*, vol. 49, p. 1222; July, 1961.) TM modes can exist in parallelogrammic waveguides and an approximate formula for f_c is given.

621.372.832.4 3242

A Variable Microwave Power Divider—D. Milanovic. (*Onde élect.*, vol. 41, pp. 180-183; February, 1961.) A practical form of power divider is described using directional coupling between two waveguides and the Faraday effect in a ferrite rod.

621.372.832.43 3243

The Use of Asymmetric Coupling for Waveguide Directional Couplers with Frequency-Independent Coupling Factor—W. Nowak. (*Hochfrequenz und Elektroak.*, vol. 69, pp. 179-188; October, 1960.) The asymmetric H_z-H_z multiaperture coupler described has a flat frequency response and is suitable for coupling factors of the order of 3-20 db.

621.372.832.43 3244

The Oblique-Slot Coupler, a New Waveguide Directional Coupler for Frequency-Independent Loose Couplings—W. Nowak. (*Hochfrequenz und Elektroak.*, vol. 69, pp. 193-201; December, 1960.) The coupler described is suitable for coupling factors of about 10-60 db. An arrangement for closer coupling is described in 3243 above.

621.372.837:621.382.23 3245

Semiconductor-Diode Waveguide Switch—T. H. B. Baker. (*Electronic Tech.*, vol. 38, pp. 300-304; August, 1961.) The relation of the

switching ratio, bandwidth and power-handling capabilities to diode and transmission-line parameters is given.

621.372.852.2 3246

Reciprocal and Nonreciprocal Phase Shifters in Rectangular Waveguide—E. Pivitt. (*Frequenz*, vol. 14, pp. 369-378; November, 1960.) Theoretical and experimental investigation of the dielectrically loaded waveguide as reciprocal phase shifter. Experimental results of measurements on ferrite-loaded nonreciprocal phase shifters are discussed, with particular reference to the temperature compensation of phase shift.

621.372.852.323:538.632 3247

Microwave Isolator combines Hall Effect and Tunnel Diodes—C. H. Hubbard, L. A. LoSasso, and E. Rouso. (*Electronics*, vol. 34, pp. 56-57; June 16, 1961.) A simple circuit is described giving useful isolation up to about 30 Mc, and performance parameters are discussed. The InSb Hall-effect plate is provided with a thermoelectric cooler to provide additional circuit adjustment. Tunnel-diode lead inductance limits its performance.

621.396.67 3248

Some Problems regarding Medium-Wave Broadcast Aerials with Cross-Section Gradually Increasing towards the Centre (Fish-Belly Aerials)—N. Stanulov. (*Hochfrequenz und Elektroak.*, vol. 69, pp. 161-170; October, 1960.) Determination of the current distribution along this type of antenna and of its vertical radiation characteristics. Methods of improving the antifading properties are suggested.

621.396.67:621.318.134 3249

A Nondirectional Ferrite Rod Antenna Arrangement Suitable for AM Radios—O. K. Nilssen. (*Proc. IRE*, vol. 49, pp. 1222-1223; July, 1961.) Signals from orthogonal ferrite rod antennas are added in quadrature.

621.396.67:621.396.669 3250

The Suppression of Corona- and Precipitation-Interference in V.H.F. Reception—Page. (See 3531.)

621.396.67.012.12 3251

A Method for the Synthesis of Radiation Patterns at Finite Distances—L. Caprioli, L. Ronchi, A. Scheggi, and G. Toraldo di Francia. (*Alta Frequenza*, vol. 29, pp. 653-666; December, 1960.) A semi-empirical procedure is described for an approximate synthesis using a finite number of spherical waves.

621.396.673 3252

The Behaviour of Linear Short and Thin Aerials with a Variation in Current Distribution—G. D'Auria and F. Todero. (*Alta Frequenza*, vol. 30, pp. 28-42; January, 1961.) The effect of top loading on antenna performance is investigated. Expressions are derived for input impedance and radiation efficiency as a function of current distribution.

621.396.677.85 3253

Dielectric Lenses and Reflectors made from Homogeneous Spherical Layers—P. M. Prache. (*Ann. Télécommun.*, vol. 16, pp. 85-95; March/April, 1961.) A method which is given for calculating the ray paths in manufactured lenses and reflectors is also used to determine the equivalent surface of a reflector as a function of the angle between the incident and reflected rays. Theoretical results are in good agreement with results of measurements on a reflector of diameter 175 mm.

621.396.679 3254

The Achievement of Optimum Vertical Field Strength at the Ground by means of Wire

Grids—K. Baur. (*Elektrotech. Z., Edn. A.*, vol. 82, pp. 13-18; January 2, 1961.) The effect of SW reflection at the foot of receiving antennas is considered, and details are given of the design of wire grids for producing a maximum of the interference field strength at ground level.

AUTOMATIC COMPUTERS

681.142 3255

Design and Application of a Digital Differential Analyser—D. Lamb. (*Proc. IRE (Australia)*, vol. 22, pp. 243-249; April, 1961.) The principles of operation and limitations of a digital incremental computer are given and fields of research in which its accuracy and speed would be useful are suggested.

681.142 3256

Full Binary Adder with One Tunnel Diode—B. Rabinović and C. A. Renton. (*Proc. IRE*, vol. 49, pp. 1213-1214; July, 1961.) Three resistors and one tunnel diode in a Wheatstone bridge network give both "sum" and "carry" outputs.

681.142:512.3 3257

A Program for finding the Zeros of a Polynomial by Analogue Computer—A. Lepšchy. (*Alta Frequenza.*, vol. 30, pp. 21-27; January, 1961.)

681.142:621.318.134 3258

A Magnetic Associative Memory—J. R. Kiseda, H. E. Petersen, W. C. Seelbach, and M. Teig. (*IBM J. Res. Dev.*, vol. 5, pp. 106-121; April, 1961.) A computer storage system is described in which data flow in and out on the basis of content rather than location. A small experimental model of the system using ferrite cores is also described.

681.142:621.319 3259

A Probability Distribution Analyser utilizing Electrostatic Storage—I. K. Harvey. (*Electronic Engrg.*, vol. 33, pp. 432-436; July, 1961.) The instrument has a linearity within ± 0.25 per cent and analyzes input waveforms of frequency of 0-20 kc.

681.142:621.372.54:621.391 3260

A Universal Nonlinear Filter, Predictor and Simulator which Optimizes itself by a Learning Process—D. Gabor, W. P. L. Wilby and R. Woodcock. (*Proc. IEE*, pt. B, vol. 108, pp. 422-435; July, 1961. Discussion, pp. 436-438.) After a discussion of some cybernetic principles a machine is described which, by a process of successive runs on an input function, ultimately produces a target function with least error. The machine incorporates a 20-track tape recorder, and 80-analog multipliers of a novel piezomagnetic type which perform 1000 multiplications per second with errors not exceeding 0.5 per cent.

681.142:621.385.832 3261

A Cathode-Ray-Tube Output for a Digital Computer—R. L. Grimsdale and N. Barraclough. (*J. Brit. IRE*, vol. 21, pp. 497-501; June, 1961.) A variety of displays can be programmed and are photographed by a camera controlled by the computer.

681.142:621.385.832 3262

Radar-Computer Display traces Alpha-numeric Characters—K. E. Perry and E. J. Aho. (*Electronics*, vol. 34, pp. 75-79; June 30, 1961.) The 64 available characters are displayed by the spot deflection method at a rate of 13,500/sec. A full description of the system with block and circuit diagrams is given.

681.142:621.398 3263

Logarithmic Compression of Binary Numbers—D. H. Schaeffer. (*Proc. IRE*, vol. 49,

p. 1219; July, 1961.) This 19-to-8 bit converter uses 4 bits for the most significant figures and 4 bits to indicate the position of the binary point. Accuracy is within ± 3 per cent.

CIRCUITS AND CIRCUIT ELEMENTS

621.3.049.7:539.23 3264

Step-by-Step Design Techniques for Multi-layer Thin-Film Networks—W. N. Carroll and F. F. Jenny. (*Electronics*, vol. 34, pp. 90-93; May 10, 1961.) Performances of various circuits incorporating thin-film passive networks and those with conventional components are compared.

621.318.43:621.396.962.33 3265

Magnetics in Doppler Signal Data Extraction—R. J. Metz and J. G. Fay. (*Commun. and Electronics*, no. 53, pp. 33-43; March, 1961.) Doppler radar data extraction problems such as detection, integration and interrogation using devices with magnetic cores are discussed.

621.318.57 3266

A Magnetic Device for High-Speed Sensing of Small Currents—J. A. Baldwin, Jr. (*Commun. and Electronics*, no. 53, pp. 1-3; March, 1961.) The structure and operation of the "ferrod" device are described. It comprises a bar of low-coercive-force square-loop ferrite with two holes transverse to the long axis. The material around the holes acts as a pair of toroidal cores whose switchable flux may be controlled by a solenoid current.

621.319.4:621.317.72 3267

The Vibrating Capacitor, Theory and Application—Riegler. (See 3510.)

621.372.44 3268

The Energy Properties of Nonlinear Reactance Circuits—J. Neirynek. (*Rev. HF, Brussels*, vol. 5, no. 1, pp. 13-17; 1961.) There will be a conversion of power at one frequency to power at another frequency if one frequency is a rational fraction of the other or if at least one intermodulation frequency exists.

621.372.5 3269

A Network Theorem—J. B. Rudd. (*AWA Tech. Rev.*, vol. 11, pp. 107-128; December, 1960.) The problem of determining the transfer impedance between a generator EMF at one end of a resistance-terminated ladder network and the load current at the other end is simplified by splitting the circuit into two sections.

621.372.5 3270

On Scattering Matrices Normalized to Complex Port Numbers—D. C. Youla. (*Proc. IRE*, vol. 49, p. 1221; July, 1961.) A 2n-terminal network with generators having complex impedances is considered.

621.372.5:517.94 3271

A Review of Methods of Linear Network Analysis in the Steady State: Parts 1 and 2—P. W. Seymour. (*Proc. IRE (Australia)*, vol. 22, pp. 77-96 and 253-270; February and April, 1961. Correction, *ibid.*, p. 249.) The establishment of an independent set of network variables permits various methods of network solution. The four-terminal network and the use of reference parameters are also considered.

621.372.51 3272

Wide-Band Impedance Transformers—J. B. Rudd. (*AWA Tech. Rev.*, vol. 11, pp. 179-194; December, 1960.) An analysis of networks consisting of cascades of lumped-circuit $\lambda/4$ sections of graded impedance level.

621.372.54 3273

A Property of Passive Lossless Quadripoles and its Application in the Design of Ladder

Filters—Y. Peltier. (*Câbles & Trans. (Paris)*, vol. 15, pp. 27-50; January, 1961.) The validity of formulas giving the values of elements of various filter structures is established by expressing the insertion loss as a function of the iterative parameters of a fictitious network.

621.372.54:517.7 3274

Using Jacobians for Frequency-Selective Networks—T. R. Nisbet and W. W. Happ. (*Electronic Ind.*, vol. 20, pp. 86-89; January, 1961.) The advantages of the use of Jacobians for synthesis of networks to give a specific frequency response is demonstrated with a simple network.

621.372.54:534.143 3275

Computation of Mechanical Filters—M. Bärner. (*Elektron. Rundschau*, vol. 15, pp. 11-14; January, 1961.) Filter-design procedure and data are summarized.

621.372.54:621.372.57 3276

Active Low-Pass RC Filters—D. P. Franklin. (*Electronic Tech.*, vol. 38, pp. 278-282; August, 1961.) A method is described of synthesizing the over-all response of active cascaded low-pass filters using simple RC ladders and buffer amplification.

621.372.632:621.382.23 3277

Tunnel-Diode Down-Converters—D. G. Peterson. (*Proc. IRE*, vol. 49, pp. 1225-1226; July, 1961.) Different circuit analyses are compared.

621.373:621.372.44 3278

The Dynamics of a Subharmonic Oscillator with Linear Dissipation—G. J. Lasher. (*IBM J. Res. Dev.*, vol. 5, pp. 157-161; April, 1961.) A mathematical analysis is made of the dynamic behavior of subharmonic oscillators (parametrons) assuming a nonlinear reactance but a linear dissipation or resistance.

621.373+621.375]029.65 3279

Present State of Millimetre-Wave Generation and Amplification—W. Veith. (*Nachricht. Z.*, vol. 13, pp. 592-597; December, 1960.) A review of techniques, particularly those based on the use of conventional microwave valves.

621.373.42.072.7 3280

Pull-In Frequency of the Phase-Controlled Oscillator—A. J. Goldstein and C. J. Byrne. (*Proc. IRE*, vol. 49, p. 1209; July, 1961.) The pull-in frequency derived by Goldstein and confirmed experimentally by Byrne is lower than that recently derived by Rey (81 of February).

621.373.422 3281

Additional Negative-Resistance Oscillation Modes—W. N. Carr and T. C. Matty. (*Proc. IRE*, vol. 49, p. 1225; July, 1961.) Several "class-C" modes are considered.

621.373.43 3282

Voltage-Variable Capacitors make a Relaxation Oscillator—J. Lopez and J. Brown. (*Electronics*, vol. 34, pp. 96-98; May 19, 1961.) The controllable frequency range is 15 cps-1.5 kc.

621.374 3283

Random-Pulse Generator tests Circuits, encodes Messages—B. K. Ericksen and J. D. Schmidt. (*Electronics*, vol. 34, pp. 56-59; June 23, 1961.) The shift-register generator uses high-speed logic circuits in producing complicated pulse sequences up to 4×10^9 bits in length.

621.374:621.3.018.782 3284

Testing the Linear Distortion of Transmis-

- sion Systems by means of Rectangular Pulses and Application of this Method for Explaining the Differential Equalization used in Magnetic-Tape Equipment—H. Kumpfert. (*Frequenz*, vol. 14, pp. 416-421; December, 1960. Correction. *ibid.*, vol. 15, p. 31; January, 1961.)
- 621.374:621.382.23 3285
Generation of Nanosecond Carrier Pulses at X Band with Tunnel Diodes—L. U. Kibler. (Proc. IRE, vol. 49, p. 1204; July, 1961.)
- 621.374.32:621.382.23 3286
100-Mc Tunnel-Diode Ring Counter—F. P. Heiman. (Proc. IRE, vol. 49, p. 1215; July, 1961.)
- 621.374.32:621.398 3287
Multiaperture-Core Counters give Non-destructive Storage Read-Out—W. R. Johnston. (*Electronics*, vol. 34, pp. 62-64; June 16, 1961.) Description of a counter circuit and its use in a missile guidance control system.
- 621.374.33 3288
R.F. Gate with 10³ Carrier Suppression—R. J. Blume. (*Rev. Sci. Instr.*, vol. 32, pp. 554-556; May, 1961.) A 10.7-Mc RF gate is described with a carrier suppression ratio >180 db. The ungated CW signal is continuously available. Circuitry, leakage measurements, and screening techniques are described.
- 621.374.4 3289
Frequency Multiplication by Large Factors by means of the Oscillation-Build-Up Method—G. Becker. (*Frequenz*, vol. 14, pp. 412-416; December, 1960.) Frequency multiplication by factors of several thousands can be achieved with the oscillator described, which is pulse-controlled at the fundamental frequency and produces a harmonic spectrum of few components during the build-up of oscillations.
- 621.374.4:529.786 3290
Methods of Pulse Selection to Produce Accurate Timing Marks from Standard Frequencies—G. Becker. (*Arch. elekt. Übertragung*, vol. 14, pp. 539-542; December, 1960.) Counter circuits are given which are suitable for the production of low-frequency timing pulses independent of phase fluctuations in the frequency dividers of crystal clocks.
- 621.375:512.83 3291
A Matrix Representation of Linear Amplifiers—K. G. Nichols. (*J. Brit. IRE*, vol. 21, pp. 517-533; June, 1961.) Expressions are developed for the transfer matrices of combinations of bilateral and unilateral networks, and of some passive and active networks including feedback amplifiers.
- 621.375.049.7:621.317.7 3292
Designing for Low-Level Inputs—D. B. Schneider. (*Electronic Ind.*, vol. 20, pp. 81-85; January, 1961.) Difficulties arising in low-level input instrumentation, and methods of checking and evaluating the performance of such equipment are given.
- 621.375.121.1 3293
Interstage Design for Stagger-Loaded Amplifiers—L. A. Beattie. (*Electronics*, vol. 34, pp. 60-63; May 26, 1961.) A family of low-pass Butterworth amplifiers, each stage having a different load impedance, is described. The resulting stagger-loaded amplifier has high gain and large bandwidth; an example shows half-power points at 2.7 Mc and 25 Mc and a mid-band gain of 95.
- 621.375.132 3294
The Theory of Negative-Feedback Voltage Amplifiers—C. H. Vincent. (*Electronic Engrg.*, vol. 33, pp. 442-444; July, 1961.) A modification of the standard method of analysis taking account of the fact that the attenuated feedback voltage cannot always be subtracted directly from the input voltage in practice.
- 621.375.2.024 3295
D.C. Amplifier with Particularly High Zero-Level Stability—H. L. König. (*Arch. elekt. Übertragung*, vol. 14, pp. 543-553; December, 1960.) A push-pull circuit for drift compensation in dc amplifiers is described and details are given of its practical application and performance.
- 621.375.221 3296
Contribution on the Dynamic Plate-Load Amplifier—K. Emden. (*Arch. elekt. Übertragung*, vol. 14, pp. 487-490; November, 1960.) A method is described for improving frequency and phase response of the type of amplifier considered in 2163 of 1959 (Brown).
- 621.375.3:621.3.087.6 3297
Single-Ended Self-Balancing Magnetic Amplifiers for Changing the Effective Impedance of Ink Recorders—W. A. Geyger. (*Commun. and Electronics*, no. 53, pp. 8-13; March, 1961.)
- 621.375.4 3298
Common-Emitter Amplifier—R. Loek. (*Electronic Tech.*, vol. 38, pp. 285-297; August, 1961.) The medium-frequency performance of common-emitter amplifiers is examined in terms of the simple equivalent circuit for a transistor. Formulas enabling the best type of transistor to be selected are derived.
- 621.375.4 3299
Transistor Cascode Circuit Improves Automatic Gain Control in Amplifiers—J. F. Perkins, Jr. (*Electronics*, vol. 34, pp. 49-51; June 2, 1961.) An improved method, with circuit details, for applying AGC to transistor IF tuned amplifiers is described. The effects of changes in the transistor parameters, with change of operating point, on the Q-factor and the center frequency of the tuned circuit are minimized.
- 621.375.4:621.391.822 3300
A Theoretical Comparison of Average- and Spot-Noise Figure in Transistor Amplifiers—J. A. Ekiss and J. W. Halligan. (Proc. IRE, vol. 49, pp. 1216-1217; July, 1961.)
- 621.375.9:538.569.4 3301
Investigation of the Performance of Coupled-Cavity Maser-Type Amplifiers: Part 2—G. Broussaud and L. Malnar. (*Onde élect.*, vol. 41, pp. 184-199; February, 1961.) A general formula is developed to determine the equivalent noise temperature and gain stability of several elementary structures. By comparing these results, interesting features of multicavity masers are demonstrated. Part 1: *ibid.*, vol. 40, pp. 555-572; September, 1960.
- 621.375.9:538.569.4 3302
Traveling-Wave Maser with Instantaneous Bandwidths in Excess of 100 Mc—S. Okwit and J. G. Smith. (Proc. IRE, vol. 49, p. 1210; July, 1961.) Broad bandwidths, more than twice the intrinsic linewidth of ruby, were obtained by stagger-tuning the applied external magnetic field.
- 621.375.9:621.372.44 3303
Parametric Circuits with Nonlinear Reactances and Resistances—K. H. Steiner. (*Arch. elekt. Übertragung*, vol. 14, pp. 482-486; November, 1960.) Equivalent circuits of nonlinear reactances and resistances are derived for calculations on parametric amplifiers. Expressions giving the circuit voltages are tabulated for parametric amplifiers, up-converters and down-converters of the dynatron type and the nonlinear-capacitance type.
- 621.375.9:621.372.44 3304
Sensitivity of the Degenerate Parametric Amplifier—J. T. de Jager and B. J. Robinson. (Proc. IRE, vol. 49, pp. 1205-1206; July, 1961.) Although the noise temperature of a degenerate parametric amplifier is half that for a nondegenerate amplifier, the minimum detectable signal is only $\sqrt{2}$ better because the post-detector noise fluctuation increases by a $\sqrt{2}$ factor.
- 621.375.9:621.372.44 3305
Noise Measure of Distributed Negative-Conductance Amplifiers—A. van der Ziel. (Proc. IRE, vol. 49, pp. 1212-1213; July, 1961.) The modification required to the noise measure M for circuits in which the characteristic impedance has a reactive part is given.
- 621.375.9:621.372.44 3306
The Noise Temperature of Cascade-Connected Amplifiers—W. Dahlke and H. Rieck. (*Telefunken-Röhre*, no. 38, pp. 37-60; December, 1960.) A formula is derived for the noise temperature of a cascade-connected amplifier with negative conductances as active elements. This permits a simple graphical representation of noise characteristics; examples are given of parametric-amplifier stages, and the influence of isolators and circulators on noise temperature and bandwidth is discussed.
- 621.375.9:621.372.44 3307
Parametric Amplification with a Low-Frequency Pump—G. F. Montgomery. (Proc. IRE, vol. 49, pp. 1214-1215; July, 1961.) The degenerate form of a three-frequency parametric amplifier is considered.
- 621.375.9:621.372.44 3308
An L-Band Traveling-Wave Parametric Amplifier—S. J. Tetenbaum, F. A. Olson, and A. Savarin. (Proc. IRE, vol. 49, pp. 1230-1231; July, 1961.) A gain of 10 db over a 10 per cent band around 1.35 Gc has been achieved.
- 621.375.9:621.372.44:621.382.23 3309
Reactance Diodes and their Application in Wide-Band Waveguide Amplifiers—Bobisch and Sondhauss. (See 3571.)
- 621.375.9:621.372.44:621.385.63 3310
Noise in Beam-Type Parametric Amplifiers—Gordon. (See 3592.)
- 621.375.9:621.372.44:621.385.63 3311
Parametric Coupling between the Transverse Waves on O- and M-Type Beams—Klüver. (See 3593.)
- 621.375.9:621.372.44:621.385.63 3312
Transduction of Noise Theory of a Generalized Travelling-Wave Coupler—Pease. (See 3594.)
- 621.375.9:621.382.23 3313
Selective High-Frequency Amplification with Tunnel Diodes—K. H. Müller. (*Elektronik*, vol. 10, pp. 39-43; February, 1961.) The design of a VHF FM tuner using tunnel diodes is detailed.
- 621.375.9:621.382.23 3314
Minimum Noise Figure of the Negative-Resistance Amplifier using Esaki Diodes—M. Müller. (*Arch. elekt. Übertragung*, vol. 14, pp. 499-502; November, 1960.) The minimum noise figure is determined for a nonreciprocal single-stage amplifier, and the result is extended to cover multistage amplifiers. A noise figure of about 5 db can be achieved for high-gain single-stage or multistage amplifiers.

621.375.9:621.382.23 3315

Semiconductor Diode Circuit Provides Gain—S. Ritterman. (*Electronics*, vol. 34, pp. 60-62; June 2, 1961.) The forward-reverse characteristics of a diode can be used to provide amplification (see 987 of 1955). The characteristics of a circuit operating with power-supply frequency considerably higher than the signal frequency are noted.

621.375.9:621.382.23 3316

Noise Measure of Lossy Tunnel-Diode Amplifier Stages—A. van der Ziel. (*Proc. IRE*, vol. 49, pp. 1211-1212; July, 1961.) The influence of circuit losses and the diode series resistance on the noise figure of tunnel-diode amplifiers is considered. The calculation is repeated for a stable parallel circuit.

621.376.2:621.318.435 3317

A Saturable-Core Modulation Integrator—R. C. Barker and A. J. Gruodis. (*Commun. and Electronics*, no. 53, pp. 13-17; March, 1961.) A circuit is discussed which illustrates the use of saturable-core reactors for operating directly on a modulation carrier. Use is made of the ability of a saturable reactor to convert a voltage integral to a magnetic flux and store it until required.

621.376.223 3318

Constant-Resistance Modulators—D. G. Tucker. (*J. Brit. IRE*, vol. 21, pp. 491-496; June, 1961.) Zobel's constant-resistance networks are interpreted in terms of constancy with time, when the elements of the network are time-variable, and simultaneously in the same network the original conception of constancy with frequency, when the elements are frequency-variable, may be realized. The application to rectifier modulators is examined.

621.376.23 3319

Requirements regarding Electrical Squaring Circuits and Practical Possibilities for the Realization of Square-Law Characteristics—E. Sonntag. (*Hochfrequenz. und Elektroak.*, vol. 69, pp. 211-216; December, 1960.) The design of square-law detector circuits for use in the measurement of rms values is discussed and the characteristics of various types of circuit using diodes or amplifier valves are examined.

621.376.23 3320

Squaring Circuits with Staggered Diodes—E. Sonntag. (*Hochfrequenz. und Elektroak.*, vol. 69, pp. 217-221; December, 1960.) With the circuit described a square-law characteristic can be synthesized over a range of about 30 db. Ge diodes give better results than those obtained with thermionic valves. See also 3319 above.

621.376.233.029.65 3321

Crystal Biasing Improves Millimeter-Wave Detector—K. Ishii and A. L. Brault. (*Electronics*, vol. 34, p. 65; June 16, 1961.) At 73 Gc a 14-db improvement in noise figure could be obtained by suitable biasing.

GENERAL PHYSICS

537.311.1 3322

Variational Method for Transport Parameters in Electron Conductors—R. Klein. (*Z. Naturforsch.*, vol. 16a, pp. 116-121; January, 1961.) The method described results in a simplification and clarification of calculation procedure.

537.311.1 3323

Derivation of the Boltzmann Transport Equation for Inelastic Collisions—P. N. Argyres. (*J. Phys. Chem. Solids*, vol. 19, pp. 66-72; April, 1961.) A quantum-mechanical

treatment similar to that developed by Kohn and Luttinger for elastic collisions (1105 of 1958). For Fermi-Dirac particles the scattering in the collision term of the transport equation is restricted to unoccupied states only.

537.311.33 3324

Negative Resistance and Hot Electrons—I. Adawi. (*J. Appl. Phys.*, vol. 32, pp. 1101-1111; June, 1961.) I/V characteristics of hot electrons are analyzed for negative-resistance regions. Electrons in a homogeneous semiconductor are assumed to interact only with acoustic phonons and charged centers of heavy mass which could be ionized impurities or heavy holes.

537.52:537.533.8 3325

Electron Bunching in the Multipacting Mechanism of High-Frequency Discharge—A. J. Hatch. (*J. Appl. Phys.*, vol. 32, pp. 1086-1092; June, 1961.) Electron bunching is analyzed by an extension of simple multipacting theory.

537.525 3326

Electronic and Ionic Current at the Cathode of a Hollow-Cathode Discharge—V. K. Rohatgi. (*J. Appl. Phys.*, vol. 32, pp. 1173-1174; June, 1961.) The fractions of electronic and ionic current densities in the discharge are estimated. The possibilities of other electron-emission mechanisms are discussed.

537.56 3327

Instability of a Plasma with an Anisotropic Distribution of Ion and Electron Velocities—A. V. Kitsenko and K. N. Stepanov. (*Zh. Eksp. Teor. Fiz.*, vol. 38, pp. 1840-1846; June, 1960.) Investigation of the propagation of magneto-hydrodynamic waves in an infinite rarefied plasma. A kinetic treatment leads to an increase of the instability region compared to that obtained in the quasi-hydrodynamic approximation.

537.56 3328

Fluctuations in a Multicomponent Plasma—C. Buneman. (*J. Geophys. Res.*, vol. 66, pp. 1978-1979; June, 1961.) A theory of fluctuations in a plasma consisting of electrons and one kind of ion (3391 below) is generalized to apply to several species of ions.

537.56:534.1 3329

Electrostatic Sound Wave Modes in a Plasma—F. W. Crawford. (*Phys. Rev. Lett.*, vol. 6, pp. 663-665; June 15, 1961.) The ratios between the frequencies of the peaks observed in the anode voltage fluctuations in Hg discharge tubes agree with those calculated using a simple theory of radial modes.

537.56:538.56 3330

Coupling Mechanisms between Longitudinal and Transverse Waves in a Plasma—G. Burkhardt, C. Fahl, and R. W. Lenz. (*Z. Phys.*, vol. 161, pp. 380-387; January 27, 1961.) The possible coupling mechanisms are deduced on the basis of fundamental plasma equations. The existence of a nonlinear "internal coupling" effect is proved which can cause electro-motive radiation.

537.56:538.56 3331

Enhanced Diffusion and Oscillations in Weakly Ionized Plasmas—J. F. Bonnal, G. Briffod and C. Manus. (*Phys. Rev. Lett.*, vol. 6, pp. 665-667; June 15, 1961.)

538.3 3332

Average Forces in Electromagnetic Systems—W. E. Smith. (*Aust. J. Phys.*, vol. 14, pp. 152-159; March, 1961.) For a linear and loss-free system, it is shown that the time-aver-

age force can be expressed in directly measurable circuit-theory parameters.

538.56 3333

A Supplement to a Study of Electromagnetic Point Sources—M. Bouix. (*Ann. Télécommun.*, vol. 16, pp. 105-107; March/April, 1961.) A supplement to a previously published paper (*ibid.*, vol. 14, pp. 143-150; May/June, 1959) establishing that there are only two fundamental fields which can effectively be replaced by a point source, corresponding to a distribution concentric about its origin.

538.561:537.122 3334

Cherenkov Radiation for a Dipole Moment in a Medium with Spatial Dispersion—G. A. Begiashvili and É. V. Gedalin. (*Zh. Eksp. Teor. Fiz.*, vol. 38, pp. 1738-1739; June, 1960.) Treatment of electric and magnetic dipoles in an isotropic nongyrotropic medium. Radiation from a ring-current in such a medium is also considered.

538.561:537.56 3335

Radiation by Charged Particles passing through an Electron Plasma in an External Magnetic Field—S. K. Majumdar. (*Proc. Phys. Soc. (London)*, vol. 77, pp. 1109-1120; June 1, 1961.) Coupling between the longitudinal plasma wave and the transverse electromagnetic wave modifies the nature of the radiation. At particle velocities greater than that required for the excitation of plasma waves, a non-Cherenkov type of radiation will occur.

538.561:537.56 3336

Incoherent Microwave Radiation from a Plasma in a Magnetic Field—J. L. Hirshfield and S. C. Brown. (*Phys. Rev.*, vol. 122, pp. 719-725; May 1, 1961.) "The microwave emission from a plasma in a magnetic field is calculated theoretically using Kirchhoff's radiation law for cases when characteristic waves do not couple within the plasma. Experimental observations of radiation temperatures and cyclotron radiation line breadth and shape are cited to illustrate applications of the theory to experiment."

538.561:539.12 3337

Classical Electrodynamics Equations of Motion with Radiative Reaction—G. N. Plass. (*Rev. Mod. Phys.*, vol. 33, pp. 37-62; January, 1961.) The classical theory is reviewed; previous objections to it are shown to be largely invalid.

538.561:539.12 3338

Radiation from Fast Particles Moving through Magnetic Materials—T. B. Day. (*Phys. Rev.*, vol. 122, pp. 1028-1036; May 15, 1961.) Under certain conditions of frequency and angle of observation "ringing" of the spin system occurs. Differences from the normal Cherenkov effect are discussed, also the possibility of using the effect as a neutral-magnetic-moment detector or as a probe of magnetic materials.

538.566+534.2 3339

Wave Propagation in an Inhomogeneous Waveguide—M. M. Brekhovskikh and V. A. Elisavinn. (*Akust. Z.*, vol. 6, pp. 284-291; 1960.) Analysis of the propagation of acoustic waves in a waveguide whose properties vary along its length. The theory developed is applied to the propagation of acoustic and electromagnetic waves in natural waveguides which may extend to distances of 1000 km and more.

538.566 3340

Study of the Electromagnetic Field produced by a Magnetic Doublet in the Presence of Two Media Separated by a Plane Surface—L. Robin. (*Ann. Télécommun.*, vol. 16, pp. 96-

104; March/April, 1961.) A rigorous treatment for the general case of a doublet with its axis at any angle to the surface between the media. The effects of special media are also considered.

538.566:[535.312+535.34] 3341

The Reflection of Electromagnetic Waves at a Plane Metal Surface Covered with an Absorbing Layer—B. Unbehauen and H. J. Hoffman. (*Arch. elekt. Übertragung*, vol. 14, pp. 521–530; December, 1960.) The reflection coefficient is calculated as a function of λ for an electromotive wave incident perpendicularly on a thin absorption layer. Numerical and graphical methods are given for the evaluation of layer parameters which make the reflection coefficient as small as possible over a wide range of λ .

538.566:535.42]+534.26 3342

A Note on the Back-Scattering of a Circular Disk—S. R. Seshadri. (*Proc. Nat. Inst. Sci. India*, pt. A, vol. 26, pp. 609–616; November 26, 1960.) Asymptotic series are obtained for the back-scattering cross sections of an acoustically hard disc, an acoustically soft disc and a perfectly conducting disc.

538.566:535.42 3343

The Diffraction of Electromagnetic Waves at Rectangular Apertures in Plane Metal Screens—H. Severin and K. Körper. (*Z. angew. Phys.*, vol. 13, pp. 41–47; January, 1961.) An approximation method of calculating the diffraction field [see, e.g., 2694 of 1951 (Severin)] is applied to the case of rectangular apertures; results are compared with those obtained experimentally.

538.566:535.42 3344

Diffraction by an Elliptic Cone—L. Kraus and L. M. Levine. (*Commun. Pure Appl. Math.*, vol. 14, pp. 49–68; February, 1961.) Two Green's functions are derived for the reduced wave equation in the exterior or interior of an elliptic cone.

538.566:535.43 3345

A Note on the Back-Scattering by an Infinite Strip—S. R. Seshadri. (*Proc. Nat. Inst. Sci. India*, pt. A, vol. 26, pp. 603–608; November 26, 1960.) The first few terms in the asymptotic series of the back-scattering cross section of an infinite strip lying in a plane perpendicular to the direction of propagation of an electromotive wave are calculated for all angles of incidence.

538.566:535.43 3346

Scattering of a Surface Wave by a Discontinuity in the Surface Reactance on a Right-Angled Wedge—F. C. Karal, Jr., S. N. Karp, T. S. Chu, and R. G. Kouyoumjian. (*Commun. Pure Appl. Math.*, vol. 14, pp. 35–48; February, 1961.) An examination of the electromotive field produced when a surface wave travels along the front face of a right-angled wedge and is scattered by the tip.

538.566:535.43 3347

An Experimental Study of Bistatic Scattering from some Small, Absorber-Coated, Metal Shapes—R. J. Garbacz and D. L. Moffatt. (*Proc. IRE*, vol. 49, pp. 1184–1192; July, 1961.) The absorber coating reduces energy scattering in the back hemisphere but increases the energy scattered in the forward hemisphere.

538.569.4:538.22 3348

Mechanisms of Double Resonance in Solids—J. Lambe, N. Laurance, E. C. McIrvine, and R. W. Terhune. (*Phys. Rev.*, vol. 122, pp. 1161–1170; May 15, 1961.)

538.569.4:538.221 3349

Ferromagnetic Relaxation: Part I—Theory

of the Relaxation of the Uniform Precession and the Degenerate Spectrum in Insulators at Low Temperatures—M. Sparks, R. London, and C. Kittel. (*Phys. Rev.*, vol. 122, pp. 791–803; May 1, 1961.) Scattering by surface polishing imperfections, equalization of degenerate-mode populations, and Raman scattering are considered theoretically and compared with experiment.

538.569.4:538.221 3350

Theory of Magnetostatic Modes in Long, Axially Magnetized Cylinders—R. I. Joseph and E. Schlömann. (*J. Appl. Phys.*, vol. 32, pp. 1001–1005; June, 1961.) The characteristic equation determining the eigen frequencies of the magnetostatic modes is derived from the equations of motion and the boundary conditions.

538.569.4:538.221 3351

Instability of Spin Waves and Magnetostatic Modes in a Microwave Magnetic Field Applied Parallel to the D.C. Field—E. Schlömann and R. I. Joseph. (*J. Appl. Phys.*, vol. 32, pp. 1006–1014; June, 1961.) Two methods of calculating the instability threshold are described, a plane-wave analysis strictly applicable only in an infinite medium and a more rigorous theory in which the boundary conditions at the surface of the sample are taken into account.

538.569.4:538.222 3352

The Role of Phonons in Paramagnetic Relaxation—B. W. Faughnan and M. W. P. Strandberg. (*J. Phys. Chem. Solids*, vol. 19, pp. 155–166; April, 1961.) Theory is given for the coupled spin-lattice-bath system, with nonequilibrium phonons. Experiments fail to indicate the presence of such phonons.

538.569.4:621.375.9:535.61–2 3353

Observation of Forbidden Resonances in Optically Driven Spin Systems—W. E. Bell and A. L. Bloom. (*Phys. Rev. Lett.*, vol. 6, pp. 623–624; June 1, 1961.)

538.569.4:375.9:535.61–2 3354

Thermal Tuning of Ruby Optical Maser—I. D. Abella and H. Z. Cummins. (*J. Appl. Phys.*, vol. 32, pp. 1177–1178; June, 1961.)

GEOPHYSICAL AND EXTRATERRESTRIAL PHENOMENA

523+55]:621.396 3355

Radio Techniques and Space Research—(*Wireless World*, vol. 67, pp. 394–395; August, 1961.) A brief review of the papers on radio topics presented at the British IRE Convention, 1961.

523.15 3356

The Stability of Force-Free Magnetic Fields—B. B. Chakraborty and P. L. Bhatnagar. (*Proc. Nat. Inst. Sci. India*, pt. A, vol. 26, pp. 592–597; November 26, 1960.) The condition is derived for a force-free magnetic field to exercise a stabilizing influence on an equilibrium configuration; several cases are given for which the condition is satisfied. See also 784 of 1959 (Woltjer).

523.164 3357

The Technique of Radio Astronomy—F. Tank. (*Bull. Schweiz. elektrotech. Ver.*, vol. 52, pp. 69–75; February 11, 1961.) Review of applications of radio techniques in modern astronomy, including radio telescopes, interferometers and echo equipment.

523.164 3358

Results of Radio Astronomy—M. Waldmeier. (*Bull. Schweiz. elektrotech. Ver.*, vol. 52, pp. 75–80; February 11, 1961.) Review of the

field of radio-astronomy measurements, particularly with regard to solar observations.

523.164:621.317 3359

Radio Astronomy—P. G. Mezger. (*Nachricht. Z.*, vol. 13, pp. 579–591; December, 1960.) Various measurement techniques in the three main fields of research are described and their limitations discussed.

523.164:621.396.677.833.2 3360

The Radio Telescope Interferometer at the Royal Radar Establishment—J. S. Hey. (*Nature*, vol. 190, pp. 1150–1152; June 24, 1961.) Two mobile and steerable radio telescopes, with parabolic reflectors 25 m in diameter, are used either separately or in conjunction as an interferometer. The system is designed to operate in a wide frequency range down to 10 cm λ .

523.164.3 3361

A New Source of Centimetre Radio-Waves—Yu. N. Pariiskii. (*Dokl. Akad. Nauk SSSR*, vol. 137, pp. 307–309; March 11, 1961.) During observations carried out at Pulkov Observatory on March, 1959, on 9.4 cm. λ , a new RF source, of energy $>3 \cdot 50^{10}$ erg, was detected in the galactic plane, the coordinates being $\alpha_{1950} = 18^h 53^m 38^s$ and $\delta_{1950} = 1^\circ 15'$.

523.164.3:523.3 3362

Lunar Occultation of a Radio Source—C. Hazard. (*Nature*, vol. 191, p. 58; July 1, 1961.) By observation of the times of disappearance and reappearance of a radio star behind the moon, the position of the source can be obtained with great accuracy. Taking into account all sources of error, the estimated position is probably correct to within 5'' of arc.

523.164.32 3363

Solar Radio Astronomy in Italy—G. Righini. (*Ricerca Sci.*, pt. 1, vol. 1, pp. 25–37; January, 1961.) The development of radio astronomy outside and inside Italy is traced, and details are given of installations at the Astrophysical Observatory at Arcetri. Some results of observations made there are illustrated and discussed.

523.164.32 3364

Observations of 26.3-Mc/s Solar Radio Noise during August 1959—W. C. Erickson. (*J. Geophys. Res.*, vol. 66, pp. 1773–1780; June, 1961.) Solar RF noise during the noise storm in August, 1959, showed that the intense amplitude scintillation does not appear to extend down to frequencies as low as 26 Mc, and that the 26-Mc storm both began and ended before the $m\lambda$ storm did so.

523.164.32 3365

Very-Low-Frequency Modulation of Discrete-Frequency Solar Noise Bursts—J. Aarons, S. Basu, W. Kidd and R. Allen. (*Nature*, vol. 191, pp. 56–57; July 1, 1961.) Measurements of Type II and Type IV bursts at 220, 400 and 3000 Mc show envelope fluctuations which were examined over the range 5–550 cps. The observed narrow-band structure is illustrated.

523.164.32:523.75 3366

A Relation between Solar Radio Emission and Low-Energy Solar Cosmic Rays—K. Sakurai and H. Maeda. (*J. Geophys. Res.*, vol. 66, pp. 1966–1969; June, 1961.)

523.164.4 3367

Characteristics of the NGC 4486 Radio Emission—Yu. N. Pariiskii. (*Dokl. Akad. Nauk SSSR*, vol. 137, pp. 49–50; March 1, 1961.) Observations carried out with the Pulkov radiotelescope of Virgo-A showed that the angular extensions of the RF source on 9.4

cm are smaller than those determined by Mills on 3.5 m. Brightness distribution depended essentially on wavelength.

523.165 **3368**
Radiation Measurements to 1500 Kilometers Altitude at Equatorial Latitudes—F. E. Holly, L. Allen, Jr, and R. G. Johnson. (*J. Geophys. Res.*, vol. 66, pp. 1627–1639; June, 1961.) The relative fluxes, energy spectra, and angular distributions of electrons and protons determined during three flights are reported. The electron spectrum appears to be softer than that expected from a neutron beta-decay origin.

523.165 **3369**
Effect of Hydromagnetic Waves on the Lifetime of Van Allan Radiation Protons—A. J. Dragt. (*J. Geophys. Res.*, vol. 66, pp. 1641–1649; June, 1961.) Hydromagnetic waves with frequency less than 5 cps and amplitude 3γ at two or three earth radii are capable of removing all high-energy outer-belt protons (maximum energy ≈ 10 Mev) in about $\frac{1}{2}$ day. If an albedo neutron source is assumed for the inner-belt protons the calculated proton flux, as a function of radial distance from the earth, agrees well with Pioneer III results.

523.165:523.75 **3370**
Cosmic-Ray Phenomena during the November 1960 Solar Disturbances—J. G. Roederer, J. R. Manzano, O. R. Santochi, N. Nerurkar, O. Troncoso, R. A. R. Palmeira, and G. Schwachheim. (*J. Geophys. Res.*, vol. 66, pp. 1603–1610; June, 1961.) Cosmic-ray data for high- and middle-latitude stations are examined to investigate the interaction of a solar-flare increase and Forbush decrease.

523.165:523.75 **3371**
The Spectrum and Propagation of Relativistic Solar Flare Particles during July 17–18, 1959—H. S. Ghielmetti. (*J. Geophys. Res.*, vol. 66, pp. 1611–1625; June, 1961.) An examination of cosmic-ray data reveals two increases of solar protons for which the time variations are quite different. This difference is attributed to a change in the interplanetary field.

523.3+523.4:621.396.96 **3372**
A Theory of Radar Reflection from the Moon and Planets—F. B. Daniels. (*J. Geophys. Res.*, vol. 66, pp. 1781–1788; June, 1961.) Relations between the surface statistics of an irregular radar target and the angular power spectrum and autocorrelation function of the reflected signal are derived. The spatial correlation function is also computed. The theory is used to investigate the small-scale structure of the moon's surface.

523.53 **3373**
Meteorites and Meteors—N. Carrara. (*Ricerca Sci.*, pt. 1, vol. 1, pp. 14–24; January, 1961.) A general outline of the field of meteor studies with a few details of meteor tracking equipment at the Microwave Centre in Florence and results obtained there.

523.53 **3374**
The Distribution of Meteor Masses for Sporadic Meteors and Three Showers—A. A. Weiss. (*Aust. J. Phys.*, vol. 14, pp. 102–119; March, 1961.) Distributions of maximum line densities in meteor trails are derived from echo data for sporadic and shower meteors.

523.53:621.396.96 **3375**
Attachment Processes in Meteor Trails—J. S. Greenhow and J. E. Hall. (*J. Atmos. Terr. Phys.*, vol. 21, pp. 261–271; July, 1961.) The effects of electron attachment to neutral particles on the characteristics of long-duration meteor echoes are considered. Two-body and three-body attachment processes produce

differing effects and these are compared with observations. See also 2339 of 1960 (Davis et al.).

523.53:621.396.96 **3376**
The Characteristics of Persistent Sporadic Meteor Echoes—J. W. Smith. (*Aust. J. Phys.*, vol. 14, pp. 89–101; March, 1961.) For sporadic meteors whose trails have an electron line density greater than 10^{13} electrons/cm, the observed distribution of meteor echo duration cannot be explained by power-law distributions. There is no significant seasonal or diurnal variation in the mass distribution of the meteors examined.

523.53:621.396.96 **3377**
A Possible Explanation of the Long-Duration Radar Echoes of Ionized Trails in the Upper Atmosphere—C. L. Tang. (*J. Geophys. Res.*, vol. 66, pp. 1974–1975; June, 1961.) In ionospheric regions where the plasma frequency is near the frequency of the incident wave, the local wavelength of the latter is very long and the destructive interference of the fields scattered from the dispersed trail is less effective.

523.53:621.396.96 **3378**
Volume Density of Radio Echoes from Meteor Trails in Radar-Type Reception—N. Carrara, P. F. Ceccacci, A. Consortini, and L. Ronchi. (*Alta Frequenza*, vol. 29, pp. 615–638; December, 1960.) The echo density is evaluated taking into account trail orientation, the meteor evaporation process and the characteristics of the transmitter/receiver system used for back-scatter reception.

523.53:621.396.96 **3379**
Volume Density of Reflection Points of Meteor Trails in Radio Links—N. Carrara, P. F. Ceccacci, L. Ronchi, and G. Tassinario. (*Alta Frequenza*, vol. 29, pp. 639–652; December, 1960.) The procedure developed for back-scatter systems (3378 above) is applied to the case of forward-scatter links.

550.385.35:523.75 **3380**
Geomagnetic Crochet of 15 November 1960—M. Yasuhara and H. Maeda. (*J. Atmos. Terr. Phys.*, vol. 21, pp. 289–293; July, 1961.) Discussion of the geomagnetic and ionospheric effects of a large solar flare.

550.385.4 **3381**
A Possible Explanation of sc^* Observed at High Geomagnetic Latitudes—T. Ondoh. (*J. Atmos. Terr. Phys.*, vol. 21, pp. 284–286; July, 1961.) An explanation of sc^* is given in terms of hydromagnetic waves propagating along the geomagnetic field lines.

551.507.362.2 **3382**
The Scientific Uses of Earth Satellites—J. H. Blythe. (*Marconi Rev.*, vol. 24, pp. 84–97; 2nd Quarter, 1961.) A survey is given of the effect of the use of artificial satellites on measurements relating to the gravitational field, the atmosphere, the upper ionosphere, magnetic fields near to the earth and interplanetary space, and the zones of trapped radiation.

551.507.362.2 **3383**
On Simulation Studies of Motion of Bodies in Ionized Atmosphere—K. P. Chopra. (*Z. Phys.*, vol. 161, pp. 445–453; January 27, 1961. In English.) The problems involved in laboratory model studies on satellite motion in an ionized atmosphere are analyzed. Scaling relations obtained satisfy the conditions for aerodynamic, magnetohydrodynamic and electrodynamic similitude. Flight conditions corresponding to the earth's upper atmosphere can be simulated by suitable scaling of the test model.

551.507.362.2 **3384**
On the Long-Period Lunisolar Effect in the Motion of the Artificial Satellite—P. Musen. (*J. Geophys. Res.*, vol. 66, pp. 1659–1665; June, 1961.) Formulas for the determination of long-period effects caused by the sun and the moon on the motion of satellites and the stability of their orbits are developed.

551.507.362.2 **3385**
Rapid Variations of the Rotation Period of the Second Soviet Artificial Earth Satellite with respect to the Transverse Axis—V. M. Grigorevskii. (*Dokl. Akad. Nauk SSSR*, vol. 137, pp. 572–575; March 21, 1961.) A table is given of data on the rotation period during March/April, 1958.

551.507.362.2 **3386**
Determination of the Vertical Distribution of Ozone by Satellite Photometry—S. V. Venkateswaran, J. G. Moore, and A. J. Krueger. (*J. Geophys. Res.*, vol. 66, pp. 1751–1771; June, 1961.)

551.507.362.2 **3387**
Density of the Upper Atmosphere Determined from Satellite Orbits, and its Variation during 1957–61—D. G. King-Hele and D. M. C. Walker. (*Nature*, vol. 191, pp. 114–118; July 8, 1961.) Calculations from the orbits of 29 satellites in the height range 180–700 km show a decrease in density as the sunspot activity declined between 1957 and 1961. The influence of latitude on density and the large day-to-night variation above 400 km are also considered.

551.507.362.2:551.510.535:621.3.087.4 **3388**
Satellite Sounder and Telemeter Chart Ionosphere Electron Density—S. Horowitz and L. Humphrey. (*Electronics*, vol. 34, pp. 50–53; June 23, 1961.) A satellite-borne ionosonde is described which is to be launched (into a 2000 km orbit) by the U.S.A. Measurements will be made on six log-spaced frequencies between 3 and 15 Mc, by transmitting 20 pulses of each frequency in turn: crossed dipole receiving antennas are connected in phase quadrature, and the receiver is arranged to receive 10 echo pulses of one polarization and then 10 pulses of opposite polarization. A transistorized transmitter gives a peak power of 150 w with pulse length 500 μ sec. Data will be recorded by the satellite and transmitted on command to ground stations.

551.510.535/536 **3389**
The Atmospheric Density in the Earth's Ionosphere and Exosphere—H. K. Paetzold. (*Naturwiss.*, vol. 48, pp. 39–40; January, 1961.) The atmospheric density distribution in the exosphere and the F layer, as determined from satellite observations, is plotted, and causes of density fluctuations with height are briefly discussed.

551.510.535 **3390**
Rate of Ion-Atom Interchange—D. R. Bates and M. Nicolet. (*J. Atmos. Terr. Phys.*, vol. 21, pp. 286–287; July, 1961.) Conclusions about the rate of conversion of atomic ions into molecular ions in the ionosphere (*J. Atmos. Terr. Phys.*, vol. 18, pp. 65–70; April, 1960) are reiterated, and an alternative suggestion [1838 of June (Hertzberg)] is discounted.

551.510.535 **3391**
Density Fluctuations in a Plasma in a Magnetic Field, with Applications to the Ionosphere—T. Hagfors. (*J. Geophys. Res.*, vol. 66, pp. 1699–1712; June, 1961.) General expressions are derived for the fluctuation in density of electrons, ions and net charge in a plasma in thermal equilibrium in an external magnetic field. Coulomb interaction and two-body col-

lisions are taken into account. The total scattered power and Doppler spectrum are calculated for incoherent scatter from the ionosphere at 300–2000 km with a radar at 50–3000 Mc. The total power is unaffected by the magnetic field, but resonance peaks at multiples of the ion gyro-frequency appear in the spectrum when the radar beam is within 5° of orthogonality with the field lines.

551.510.535 3392

Extensions of the 'Chapman' Theory of Layer Formation—C. H. Cumback. (*J. Geophys. Res.*, vol. 66, pp. 1685–1697; June, 1961.) "An attempt has been made to establish some of the theorems necessary for the extension of the "Chapman" theory of layer formation to the case where a spectrum of ionizing radiation acts on an atmosphere with any temperature profile. Some invariant properties of the electron production function have been established, and they have proved useful in estimating the temperature and temperature variations in the ionosphere."

551.510.535 3393

Theory of Electrostatic Fields in the Ionosphere at Polar and Middle Geomagnetic Latitudes—J. R. Spreiter and B. R. Briggs. (*J. Geophys. Res.*, vol. 66, pp. 1731–1744; June, 1961.) Analysis of the elongated electrostatic fields which provide the coupling in the dynamo-motor concept of the *E* and *F* regions. The electrostatic field is taken to be of arbitrary horizontal scale, and numerical solutions are determined for the attenuation of the field with height. Fields with a horizontal scale as small as 3 or 4 km can extend from 130 to 400 km height with a reduction of only about 25 per cent, but the coupling efficiency is critically dependent on ionospheric conditions.

551.510.535 3394

Photoionization Heating in the F Region of the Atmosphere—D. C. Hunt and T. E. Van Zandt. (*J. Geophys. Res.*, vol. 66, pp. 1673–1682; June, 1961.) An estimate of the total *F* region heating due to photoionization is made, based on a comparison of theoretical and observed models of several atmospheric parameters. The heat flux due to photoionization is estimated to be approximately 1.0 erg/cm²/sec which would be a major, if not predominant, source of heat in this region.

551.510.535 3395

Observations on the Ionospheric F Layer at Night: Part 1—Height of Maximum Ionization, Critical Frequency and 'Semi-thickness' of F Layer at Night—C.S.G.K. Setty. (*J. Inst. Telecommun. Engrs., India*, vol. 7, pp. 21–26; January 1961.) Measurements taken at Cambridge, England, agree with those for other stations. The scale height determined from the "semi-thickness" of the layer is too small when compared with rocket and satellite observations.

551.510.535 3396

Group and Phase Velocities of a Travelling Disturbance in the F Region of the Ionosphere—L. H. Heisler and J. D. Whitehead. (*Nature*, vol. 191, p. 157; July 8, 1961.) The disturbances cause gross distortions of ionogram records, and have a velocity of about 10 km/min. They are associated with sporadic-E patches having a velocity of about 5 km/min which is the phase velocity of the disturbances.

551.510.535 3397

On Vertical Drift Velocities of the F₂ Layer—H. Unz. (*J. Atmos. Terr. Phys.*, vol. 21, pp. 237–242; July, 1961.) Vertical drift velocities in the *F*₂ layer are deduced by evaluating the equation of continuity of electron density, and

compared with observed movements. Some correlation is found.

551.510.535:523.164 3398

A Statistical Study of Ionospheric Drifts Measured by the Radio Star Scintillation Technique—H. J. A. Chivers. (*J. Atmos. Terr. Phys.*, vol. 21, pp. 221–224; July, 1961.) The method gives the E-W component of the drift velocity throughout the day. This component is commonly found to reverse suddenly near 2300 L.T. but the complementary reversal occurs at a less definite time during the following day.

551.510.535:551.507.362.1 3399

Rocket Measurements of F-Layer Electron Density and their Interpretation—S. A. Bowhill. (*J. Atmos. Terr. Phys.*, vol. 21, pp. 272–283; July, 1961.) Theoretical considerations about the shape of the electron density profile near the *F*₂ peak are compared with data obtained from rockets [882 of April (Nisbet and Bowhill)]. The results are consistent with day and night temperatures of about 1500°K and 1200°K respectively. Numerical values of the loss coefficient and other parameters are given.

551.510.535:551.507.362.1 3400

An Ion-Trap Measurement of the Ion Concentration Profile above the F₂ Peak—W. B. Hanson and D. D. McKibbin. (*J. Geophys. Res.*, vol. 66, pp. 1667–1671; June, 1961.) The results of a winter evening rocket flight give the ion concentration from 240 to 750 km, and indicate a constant scale height (152 km) above 350 km.

551.510.535:551.507.362.2 3401

An Annual Variation of the Density of the Upper Atmosphere of the Earth—H. K. Paetzold. (*Z. Naturforsch.*, vol. 16a, pp. 50–56; January, 1961.) The various causes of the fluctuations of upper air densities (see e.g. 1839 of July) which result in observed changes of satellite orbits are discussed. The possible influence of interplanetary matter and of an interstellar wind is mentioned.

551.510.535:621.3.087.4 3402

Active High-Frequency Spectrometers for Ionospheric Sounding: Part 4—Numerical Recording of Delay Times—E. Harnischmacher and H. Porsche. (*Arch. elekt. Übertragung*, vol. 14, pp. 503–507; November, 1960.) Equipment for the automatic determination and printing of echo heights in numerical form is described. Part 3: 2973 of September (Paul).

551.510.535:621.3.087.4 3403

Active High-Frequency Spectrometers for Ionospheric Sounding: Part 5—Methods of Automatic Determination of True Height—A. K. Paul, H. Porsche, and K. Rawer. (*Arch. elekt. Übertragung*, vol. 14, pp. 561–569; December, 1960.) The direct evaluation of *N(h)* profiles from the echo delays measured at the output of an ionosonde is proposed. Three digital and three analog methods are discussed and block diagrams given. Part 4: 3402 above.

551.510.536 3404

Density in a Planetary Exosphere—J. Herring and L. Kyle. (*J. Geophys. Res.*, vol. 66, pp. 1980–1982; June, 1961.)

551.510.536:621.396.96 3405

Evidence on the Laminar Nature of the Exosphere Obtained by means of Guided High-Frequency Wave Propagation—R. M. Gallet and W. F. Utlaut. (*Phys. Rev. Lett.*, vol. 6, pp. 591–594; June 1, 1961.) Radar pulses at 14 Mc were transmitted in the direction of the earth's magnetic field from Washington, D. C. Delayed echoes were found on many occasions from distances between 20,000 and

30,000 km. Each echo remained at a constant range. A possible explanation is given.

551.594.5 3406

Orientation of Polar Auroras—J. V. Denholm and F. R. Bond. (*Aust. J. Phys.*, vol. 14, pp. 193–195; March, 1961.) Observations of "homogeneous arc" auroras at three antarctic stations are presented and show a diurnal variation of orientation, thus supporting the observations of Weill (*C.R. Acad. Sci. (Paris)*, vol. 246, pp. 2925–2927; May 19, 1958).

551.594.5 3407

The East-West Drift of Auroral Forms determined from All-Sky Camera Films—W. Stoffregen. (*J. Atmos. Terr. Phys.*, vol. 21, pp. 257–260; July, 1961.)

551.594.5 3408

Thickness of an Active Auroral Curtain—S. I. Akasofu. (*J. Atmos. Terr. Phys.*, vol. 21, pp. 287–288; July, 1961.)

551.594.5:621.396.96 3409

Models of Auroral Ionization: Part 1—Auroral Ionization Models and their Radio-Reflection Characteristics—D. R. Moorcroft. (*Canad. J. Phys.*, vol. 39, pp. 677–694; May, 1961.) Several general models of auroral ionization are developed. By considering the ionization as an assembly of scattering centers, it is possible to include a unified treatment of weak scattering and critical reflection.

551.594.5:621.396.96 3410

Models of Auroral Ionization: Part 2—Applications to Radio Observations of Aurora—D. R. Moorcroft. (*Canad. J. Phys.*, vol. 39, pp. 695–715; May, 1961.) The radio reflection characteristics are examined in the light of the theory developed in 3409 above. Critical reflection at 30–50 Mc implies electron densities up to 3×10¹⁰ electrons/cm³. The observations are consistent with the existence of clouds of electrons elongated in the ratio of 5 or 10:1 parallel to the field lines and a few meters in diameter perpendicular to the field.

551.594.6 3411

Atmospheric Noise Levels from 0.6 to 10 Kilocycles per Second—L. H. Ginsberg and D. J. Blattner. (*J. Geophys. Res.*, vol. 66, pp. 1745–1749; June, 1961.) A comprehensive series of observations on atmospheric noise in California and Florida for frequencies below 10 kc is described and analyzed. The diurnal variation for N-S loop orientation is a minimum in the interval 0400–1200 L.T. at both sites, and minimum noise levels are found to occur between 3 and 5 kc. The latter result is in agreement with the theory of Wait (2886 of 1957).

551.594.6 3412

A Study of Whistling Atmospherics: Part 1—Occurrence—J. Crouchley. (*Aust. J. Phys.*, vol. 14, pp. 22–39; March, 1961.) Results of I.G.Y. whistler observations at Brisbane, Adelaide, Hobart and Macquarie Island are presented, and the seasonal, diurnal and latitude variations of incidence of occurrence are discussed.

551.594.6 3413

A Study of Whistling Atmospherics: Part 2—Diffuseness—J. Crouchley and R. J. Finn. (*Aust. J. Phys.*, vol. 14, pp. 40–56; March, 1961.) Diffuseness, defined as the average time duration of whistler energy on a fixed frequency, is found to be twice as large for long as for short whistlers, to be independent of season and time of day, and to be linearly related to geomagnetic latitude and whistler dispersion. Part 1: 3412 above.

551.594.6:550.385.37 3414

Observations of Hydromagnetic Emissions—L. R. Tepley. (*J. Geophys. Res.*, vol. 66, pp. 1651-1658; June, 1961.) A frequency/time analysis of geomagnetic pulsations was made in the range 0.5-5 cps for the period November 18-21, 1960. The oscillations were observed simultaneously in California and Nevada and were probably influenced by solar flares which occurred before and during the dates mentioned.

551.594.6:621.391.812.63 3415

Two-Hop 18.6-kc/s Whistler-Mode Echoes Received at Seattle—Willard. (See 3528.)

LOCATION AND AIDS TO NAVIGATION

621.396.933 3416

Servo Filter and Gain Control Improve Automatic Direction Finder—P. V. Sparks. (*Electronics*, vol. 34, pp. 110-113; June 9, 1961.) The principles and circuit details of a light-weight low-power airborne DF system are given. The goniometer is driven by a servo system to keep it at the point of minimum gain. Ambiguity of the bearing is resolved by switching in a vertical sense antenna.

621.396.933:621.376.56 3417

Pulse-Duration Coding as a Means of Increasing the Number of Channels in the Australian 200-Mc/s D.M.E. System—B. R. Johnson. (*AWA Tech. Rep.*, vol. 11, pp. 129-142; December, 1960.) The number of channels is increased from 12 to 48 by the use of pulse-duration as well as the present pulse-separation coding. Interference from other beacons is reduced.

621.396.962.33:621.318.43 3418

Magnetics in Doppler Signal Data Extraction—Metz and Fay. (See 3265.)

621.396.969.18 3419

Principles of Three-Dimensional Radar Location (3-D Radar)—K. Röhrich. (*Nachricht. Z.*, vol. 13, pp. 571-570; December, 1960.) Review of existing techniques. 32 references.

MATERIALS AND SUBSIDIARY TECHNIQUES

533.5:621.38 3420

The Interplay of Electronics and Vacuum Technology—J. M. Lafferty and T. A. Vander-slice. (*Proc. IRE*, vol. 49, pp. 1136-1154; July, 1961.) A review of modern ultra-high-vacuum systems and the electronic components used in them. 53 references.

535.215:539.23 3421

Light Interference and Internal Photoeffect in Thin Photoconductive Films—D. Kossel and W. Schmidt. (*Naturwiss.*, vol. 48, pp. 67-68; February, 1961.) Investigations were carried out on Sb_2S_3 films at $\lambda=550 \mu\mu$; absorption and photocurrent were measured as a function of film thickness to determine the effect of interference phenomena.

535.215:546.47'221 3422

Infrared Enhancement and Quenching of Photoconduction in Single Crystals of ZnS:Cu—F. G. Ullman and J. J. Dropkin. (*J. Electrochem. Soc.*, vol. 108, pp. 154-159; February, 1961.) Photoelectric currents produced by infrared radiation may either enhance or quench the currents resulting from ultraviolet irradiation of the crystals.

535.215:546.48'221 3423

Low-Field Breakdown, Non-ohmic Conductivity, and Photoconductivity of CdS at Low Temperatures—H. Shenker. (*J. Phys. Chem. Solids*, vol. 19, pp. 1-7; April, 1961.)

535.37:539.12.04 3424

Luminescence Damage of Inorganic Phosphors by Ions—R. Grasser and A. Scharmann. (*Z. Naturforsch.*, vol. 16a, pp. 10-12; January, 1961.) The effect on luminescence of ion bombardment is investigated as a function of ion mass and energy. See also 1440 of 1958 (Martin).

535.37:546.47'221:539.12.04 3425

Effects of a Radiation on Zinc Sulphide Phosphors—N. Riehl, R. Sizmann, and O. J. Stadler. (*Z. Naturforsch.*, vol. 16a, pp. 13-20; January, 1961.) Investigation of changes in glow curves and the luminescence spectrum of ZnS and ZnO phosphors following irradiation by α particles. No new glow curves were found.

537.226:539.23 3426

Anomalous Capacitance of Thin Dielectric Structures—C. A. Mead. (*Phys. Rev. Lett.*, vol. 6, pp. 545-546; May 15, 1961.) Measurements are made of the capacitance across thin Ta oxide films on Ta using Au or Bi upper electrodes. This shows that the inverse of the capacitance varies linearly with film thickness, extrapolating to give an apparently noninfinite capacitance at zero thickness. This anomaly is explained by a density-dependent penetration of the oxide into the metal of the electrodes.

537.227 3427

Ferroelectricity in $Bi_2Ti_2O_{12}$ and its Solid Solutions—E. C. Subbarao. (*Phys. Rev.*, vol. 122, pp. 804-807; May 1, 1961.)

537.227 3428

Effect of Two-Dimensional Mechanical Stress on the Dielectric Properties of Poled Ceramic Barium Titanate and Lead Zirconate Titanate—R. F. Brown. (*Canad. J. Phys.*, vol. 39, pp. 741-753; May, 1961.) The dielectric constant decreases and the dielectric loss increases with increasing stress; part of the change is irreversible and part reversible. The dielectric constant appears not to change instantaneously on application of stress but decreases linearly with the logarithm of time.

537.228.1:548.0].001.4(083.7) 3429

IRE Standards on Piezoelectric Crystals: Measurements of Piezoelectric Ceramics, 1961—(PROC. IRE, vol. 49, pp. 1161-1169; July, 1961.) Standard 61 IRE 14.S1.

537.228.4 3430

Microwave Modulation of the Electro-optic Effect in KH_2PO_4 —I. P. Kaminow. (*Phys. Rev. Lett.*, vol. 6, pp. 528-530; May 15, 1961.) Light of wavelength about 8000 Å is modulated at 9.25 Gc by a cavity-resonance method using the linear electro-optic effect of KDP crystals. The presence of the modulation is confirmed by two methods. Future developments and applications are suggested.

537.311.33 3431

Scattering of Electrons by Phonons and Impurities in Semiconductors—H. Reiss and A. I. Anderman. (*Phys. Rev.*, vol. 122, pp. 1135-1140; May 15, 1961.) A formula is developed for the carrier mobility in the presence of both types of scattering in n -type semiconductors for small relaxation times.

537.311.33 3432

A Group of Ternary Semiconducting Compounds—L. S. Polatnik, Yu F. Komnik, V. M. Koshkin, and E. K. Belova. (*Dokl. Akad. Nauk SSSR*, vol. 137, pp. 68-71; March 1, 1961.) The lattice parameters of six ternary semiconductors such as Cu_2GeS_3 , Cu_2SnS_3 , and Cu_2GeTe_3 are given.

537.311.33:538.63 3433

Some Theoretical Considerations on the

Longitudinal-Magnetic-Field-Induced Oscillations in Semiconductors (the Oscillator) and a Tentative Explanation—A. C. Prior. (*Proc. Phys. Soc.*, vol. 77, pp. 1121-1124; June 1, 1961.) Conditions under which oscillations have been observed are such that a system of circulating currents could arise. These currents could tend to increase the carrier concentration at one surface and oscillations of a relaxation type could result.

537.311.33:538.63 3434

Esaki Tunneling in the Presence of Magnetic Fields—R. R. Haering and E. N. Adams. (*J. Phys. Chem. Solids*, vol. 19, pp. 8-17; April, 1961.) The theory for Esaki tunneling in the presence of a magnetic field is given for both transverse and longitudinal magnetic fields; it is shown that there are important qualitative differences between the two cases.

537.311.33:539.23 3435

Use of Monomolecular Layers in Evaporated-Film Tunneling Devices—J. L. Miles and H. O. McMahon. (*J. Appl. Phys.*, vol. 32, pp. 1176-1177; June, 1961.) Samples have been made to measure tunneling currents between Sn-Pb and Sn-In evaporated-film pairs by using a monolayer of Ba stearate as a barrier.

537.311.33:546.23 3436

Space-Charge-Limited Current Flow and Deep Trapping in Selenium—H. P. D. Lanyon and W. E. Spear. (*Proc. Phys. Soc. (London)*, vol. 77, pp. 1157-1165; June 1, 1961.) I/V characteristics show an ohmic part at low applied voltages and, with increasing hole injection, a V^2 region which precedes the trap-filled limit predicted by theory.

537.311.33:546.24:539.23 3437

Variation of Field-Effect Mobility and Hall-Effect Mobility with the Thickness of the Deposited Films of Tellurium—S. K. Ghosh. (*J. Phys. Chem. Solids*, vol. 19, pp. 61-65; April, 1961.) Experimental measurements of the mobilities and the conductivity of Te films are reported. A tentative explanation is given for the low values found for Hall mobility.

537.311.33:[546.28+546.289] 3438

Field Emission from Silicon and Germanium; Field Desorption and Surface Migration—F. G. Allen. (*J. Phys. Chem. Solids*, vol. 19, pp. 87-99; April, 1961.) Desorption has been used to produce clean Ge patterns on a field-emission microscope.

537.311.33:[546.28+546.289] 3439

Oxygen Adsorption on Silicon and Germanium—H. D. Hagstrum. (*J. Appl. Phys.*, vol. 32, pp. 1020-1022; June, 1961.)

537.311.33:[546.28+546.289]:538.569.4 3440

Cyclotron Resonance in Germanium and Silicon and the Effect of Negative Effective Masses—Yu. Kagan. (*Zh. Eksp. Teor. Fiz.*, vol. 38, pp. 1854-1865; June, 1960.) The frequency (effective-mass) spectra of degenerate semiconductors are determined for the case of a magnetic field parallel to the [001] axis. The existence of negative-frequency branches is demonstrated and the problem of negative absorption is considered.

537.311.33:546.28 3441

Preparation of Uniform-Resistivity n -Type Silicon by Nuclear Transmutation—M. Tanenbaum and A. D. Mills. (*J. Electrochem. Soc.*, vol. 108, pp. 171-176; February, 1961.) The technique has been used to produce n -type Si with resistivity between 0.1 and 20 Ω -cm, uniform to within ± 5 per cent.

537.311.33:546.28 3442

The Manufacture of Silicon Single Crystals

- by the Czochralski Method—G. Greger. (*Z. Angew. Phys.*, vol. 13, pp. 47–51; January, 1961.) Problems involved in obtaining crystals of highest purity and a homogeneous distribution of resistivity are discussed.
- 537.311.33:546.28 3443**
Investigations on the Diffusion of Minority Carriers from a Point on Silicon—C. H. Champness. (*Canad. J. Phys.*, vol. 39, pp. 754–767; May, 1961.) The field-free diffusion of minority carriers injected at a point has been studied and the time from injection to the maximum of the collector signal due to the arriving carriers has been measured for various emitter-collector distances. For different samples, the time to maximum varied as the distance raised to powers 1.2 and 1.6. The decay times following the maximum decreased with distance. The results may be explained by assuming that the effective lifetime is dependent on the excess carrier density and decreases as the emitter point is approached.
- 537.311.33:546.28 3444**
Theory of Microplasma Instability in Silicon—R. J. McIntyre. (*J. Appl. Phys.*, vol. 32, pp. 983–995; June, 1961.) A statistical theory is presented to explain microplasma instability at the onset of avalanche in reverse-biased Si. The agreement between theory and experiment for the turn-off probability is sufficiently good to suggest that the turn-off mechanism is the correct one. This implies that microplasmas turn off because the number of carrier pairs happens to fluctuate to zero.
- 537.311.33:546.28 3445**
Study of Li-O Interaction in Si by Ion Drift—E. M. Pell. (*J. Appl. Phys.*, vol. 32, pp. 1048–1051; June, 1961.) Ion drift in a reverse-biased *p-n* junction has been used to measure the effective drift mobilities of Li⁺ between 20° and 125°C in Si samples with oxygen concentration up to 1.3×10^{18} atoms/cm³.
- 537.311.33:546.28 3446**
Recombination Kinetics for Thermally Dissociated Li-B Ion Pairs in Si—E. M. Pell and F. S. Ham. (*J. Appl. Phys.*, vol. 32, pp. 1052–1063; June, 1961.)
- 537.311.33:546.28 3447**
Surface Potential of Silicon—C. T. Raymo, C. W. Brands, and B. Schwartz. (*J. Appl. Phys.*, vol. 32, pp. 1165–1166; June, 1961.) A simple experimental method using the dc field effect is described.
- 537.311.33:546.28 3448**
Valence Spin-Orbit Splitting and Conduction g Tensor in Si—L. Liu. (*Phys. Rev. Lett.*, vol. 6, pp. 683–685; June 15, 1961.) An orthogonalized-plane-wave method is used for calculating the g factor of electrons in Si. The two-band approximation used by Roth (4288 of 1960) is shown to be inadequate.
- 537.311.33:546.28:621.317.3 3449**
Radio-Frequency Carrier and Capacitive Coupling Procedures for Resistivity and Lifetime Measurements on Silicon—I. R. Weingarten and M. Rothberg. (*J. Electrochem. Soc.*, vol. 108, pp. 167–171; February, 1961.) By using an RF bridge capacitive-coupling technique, ohmic contacts are avoided when measuring lifetime by photoconductivity decay.
- 537.311.33:546.281'26 3450**
Measurement of Minority-Carrier Lifetime in SiC by a Novel Electroluminescent Method—G. G. Harman and R. L. Raybold. (*J. Appl. Phys.*, vol. 32, pp. 1168–1169; June, 1961.) The method is applicable to large-energy-gap semiconductors.
- 537.311.33:546.289 3451**
Acoustic-Mode Scattering of Holes—M. Tiersten. (*IBM J. Res. Dev.*, vol. 5, pp. 122–131; April, 1961.) Matrix elements are calculated for acoustic-mode scattering of holes in the valence-band structure typified by Ge and a general expression for the electron-phonon interaction matrix element is obtained.
- 537.311.33:546.289 3452**
Optical Constants of Germanium in the Region 0–27 eV—O. P. Rustgi, J. S. Nodvik, and G. L. Weisler. (*Phys. Rev.*, vol. 122, pp. 1131–1134; May 15, 1961.)
- 537.311.33:546.289 3453**
Low-Temperature Thermal Resistance of *n*-Type Germanium—R. W. Keyes. (*Phys. Rev.*, vol. 122, pp. 1171–1176; May 15, 1961.)
- 537.311.33:546.289 3454**
Imaginary Part of X-Ray Scattering Factor for Germanium. Comparison of Theory and Experiment—B. W. Batterman. (*J. Appl. Phys.*, vol. 32, pp. 998–1001; June, 1961.)
- 537.311.33:546.289 3455**
Kinetics of Donor Reactions in Oxygen-Doped Germanium—C. S. Fuller. (*J. Phys. Chem. Solids*, vol. 19, pp. 18–28; April, 1961.)
- 537.311.33:546.289:539.12.04 3456**
Effect of Fission-Spectrum Neutrons on *n*-Type Germanium—D. Binder. (*Phys. Rev.*, vol. 122, pp. 1147–1148; May 15, 1961.) The electron removal rate per neutron is roughly constant.
- 537.311.33:546.289:539.12.04 3457**
Effects of Monolayer Adsorption and Bombardment Damage on Auger Electron Ejection from Germanium—H. D. Hagstrum. (*J. Appl. Phys.*, vol. 32, pp. 1015–1019; June, 1961.) See also 233 of January.
- 537.311.33:546.289:539.23 3458**
Hall Effect and Conductivity of Vapour-Deposited Germanium Films—F. Eckart and G. Jungk. (*Ann. Phys. (Lps.)*, vol. 7, pp. 210–215; January 30, 1961.) The films investigated exhibited *p*-type conductivity irrespective of the type of material used. The Hall coefficient was found to increase with magnetic field strength.
- 537.311.33:546.289:539.23 3459**
Germanium Films on Germanium Obtained by Thermal Evaporation in Vacuum—O. Weinreich, G. Dermitt, and C. Tufts. (*J. Appl. Phys.*, vol. 32, pp. 1170–1171; June, 1961.) The method of preparation and results of measurements are described.
- 537.311.33:546.681'19 3460**
Determination of the Effective Ionic Charge of Gallium Arsenide from Direct Measurements of the Dielectric Constant—K. G. Hambleton, G. Hilsun, and B. R. Holeman. (*Proc. Phys. Soc. (London)*, vol. 77, pp. 1147–1148; June 1, 1961.)
- 537.311.33:546.681'86 3461**
Diffusion of Tin in Gallium Arsenide—B. Goldstein and H. Keller. (*J. Appl. Phys.*, vol. 32, pp. 1180–1181; June, 1961.)
- 537.311.33:546.682'19'241 3462**
Electrical and Optical Properties of InAs-In₂Te₃ Alloys—J. C. Woolley, B. R. Pamplin, and J. A. Evans. (*J. Phys. Chem. Solids*, vol. 19, pp. 147–154; April, 1961.)
- 537.311.33:546.682'241 3463**
Solid Solutions of In₂Te₃ in Sb₂Te₃ and Bi₂Te₃—A. J. Rosenberg and A. J. Strauss. (*J. Phys. Chem. Solids*, vol. 19, pp. 105–116; April, 1961.)
- 537.311.33:546.682'86 3464**
Thermal Conductivity, Electrical Conductivity, Hall Effect and Thermo-E.M.F. of InSb—G. Busch and E. Steigmeier. (*Helv. Phys. Acta*, vol. 34, pp. 1–28; February 15, 1961. In German.) Measurements were made on single-crystal material in the temperature range 195°–715° K. 49 references.
- 537.311.33:546.682'86 3465**
Antimony Edge Dislocations in InSb—H. C. Gatos, M. C. Finn and M. C. Lavine. (*J. Appl. Phys.*, vol. 32, pp. 1174–1175; June, 1961.)
- 537.311.33:546.817'241:538.63 3466**
Observations of de Haas-van Alphen Oscillations in *p*-Type PbTe—P. J. Stiles, E. Burstein, and D. N. Langenberg. (*Phys. Rev. Lett.*, vol. 6, pp. 667–669; June 15, 1961.) Magnetic susceptibility oscillations, examined by pulsed-magnetic-field techniques, are reported.
- 537.311.33:546.824-31 3467**
Electric Strength of Rutile Single Crystals—D. A. Powers and I. J. T. Johansen. (*J. Appl. Phys.*, vol. 32, pp. 1083–1085; June, 1961.)
- 537.311.33:546.863'873'241'231 3468**
Relations between the Electronic Properties and the Chemical Bonding of Sb₂Bi_{2-x}Te_{3-y}Se_y System—I. Teramoto and S. Takayanagi. (*J. Phys. Chem. Solids*, vol. 19, pp. 124–129; April, 1961.)
- 537.311.33:546.873'241 3469**
***n*- and *p*-Type Single-Crystal Bismuth Telluride**—A. C. Yang and F. D. Shepherd. (*J. Electrochem. Soc.*, vol. 108, pp. 197–198; February, 1961.) Both crystal types have been grown using the Czochralski method for pulling rates between 0.2 cm/h and 20 cm/h.
- 537.312.62 3470**
Some New Superconducting Compounds—B. T. Matthias, V. B. Compton, and E. Corenzwit. (*J. Phys. Chem. Solids*, vol. 19, pp. 130–133; April, 1961.) Superconductivity and crystal structure data are tabulated. The new compounds: ThRu₂, ThOs₃, and ThIr₃ have transition temperatures of 3.56, 1.51 and 1.52°K respectively.
- 537.312.62 3471**
Study of Superconductors by Electron Tunneling—I. Giaever and K. Megerle. (*Phys. Rev.*, vol. 122, pp. 1101–1111; May 15, 1961.) The energy-gap width variation with temperature agrees with the Bardeen-Cooper-Schrieffer theory of superconductivity. The energy gap in thin films decreases with increasing applied magnetic field.
- 537.312.62 3472**
Superconductivity at High Magnetic Fields and Current Densities in some Nb-Zr Alloys—T. G. Berlincourt, R. R. Hake, and D. H. Leslie. (*Phys. Rev. Lett.*, vol. 6, pp. 671–674; June 15, 1961.)
- 537.312.62 3473**
Variation of the Elastic Moduli at the Superconducting Transition—G. A. Alers and D. L. Waldorf. (*Phys. Rev. Lett.*, vol. 6, pp. 677–679; June 15, 1961.)
- 537.312.62 3474**
First- and Second-Order Stress Effects on Superconducting Transitions in Ta and Sn—D. P. Seraphim and P. M. Marcus. (*Phys. Rev. Lett.*, vol. 6, pp. 680–682; June 15, 1961.)

- 537.312.62 3475
Superconductivity in the Neighbourhood of Metallic Contacts—L. N. Cooper. (*Phys. Rev. Lett.*, vol. 6, pp. 689-690; June 15, 1961.) Theoretical discussion of the effect described by Smith *et al.* (3476 below).
- 537.312.62:539.23 3476
Superconducting Characteristics of Superimposed Metal Films—P. H. Smith, S. Shapiro, J. L. Miles and J. Nicol. (*Phys. Rev. Lett.*, vol. 6, pp. 686-688; June 15, 1961.) A report of experiments showing that a normal conductor film in contact with a superconducting film acts as a superconductor.
- 537.533 3477
Temperature Dependence of the Work Function of Metals (Mo, Ni)—G. Comsa, A. Gelberg, and B. Iosifescu. (*Phys. Rev.*, vol. 122, pp. 1092-1100; May 15, 1961.) Detailed report of measurements made using the electron-beam method.
- 537.583 3478
On the Thermionic Properties of ZrC, UC, and a ZrC:UC Mixture—W. E. Danforth and A. J. Williams, III. (*J. Appl. Phys.*, vol. 32, pp. 1181-1182; June, 1961.)
- 538.221 3479
Ferromagnetism in Dilute Solutions of Cobalt in Palladium—R. M. Bozorth, P. A. Wolff, D. D. Davies, V. B. Compton, and J. H. Wernick. (*Phys. Rev.*, vol. 122, pp. 1157-1160; May 15, 1961.)
- 538.221:534.283-8 3480
The Influence of Bloch-Wall Displacements on the Attenuation of Ultrasonic Waves in Ferromagnetic Metals—G. Simon. (*Ann. Phys. (Lpz.)*, vol. 7, pp. 140-148; January 30, 1961.) The investigation of the dynamic behavior of the Bloch walls is based on Kersten's model (1825 of 1957).
- 538.221:538.632 3481
Wall Effect and Resistance in the Iron-Cobalt Series—W. Jellinghaus and M. P. de Andrés. (*Ann. Phys. (Lpz.)*, vol. 7, pp. 149-158; January 30, 1961.) For results of measurements on Fe-Ni alloys see *ibid.*, vol. 5, pp. 187-199; January 15, 1960.
- 538.221:538.632 3482
Influence of Neighbour Elements of Iron on the Hall Effect of Mixed Crystals with High Iron Content—W. Jellinghaus and M. P. de Andrés. (*Ann. Phys. (Lpz.)*, vol. 7, pp. 189-200; January 30, 1961.)
- 538.221:539.23 3483
Polarity of the Domain Boundaries in Thin Ferromagnetic Films—L. V. Kirenskiĭ and V. A. Buravikhin. (*Dokl. Akad. Nauk SSSR*, vol. 136, pp. 575-576; January 21, 1961.) Results of experimental investigations show that in thin films Bloch walls are of alternating polarity and that the polarity in Néel boundaries is not sharply defined. With the application of a magnetic field perpendicular to the surface of the film this polarity becomes more distinct.
- 538.221:621.318.134 3484
A Neutron Diffraction Study of the Temperature Variation of the Spontaneous Sublattice Magnetization of Ferrites and the Néel Theory of Ferrimagnetism—T. Riste and L. Tenzer. (*J. Phys. Chem. Solids*, vol. 19, pp. 117-123; April, 1961.)
- 538.221:621.318.134 3485
The Ideal Magnetization Curve of Ferrites with Differing Hysteresis Loops—M. Kornetzki and E. Röss. (*Z. angew. Phys.*, vol. 13, pp. 28-31; January, 1961.) The ideal magnetization curve is derived from Preisach diagrams obtained experimentally for various ferrites. A finite gradient at zero field strength, the ideal initial permeability, was found in all cases.
- 538.221:621.318.134 3486
Measurements of Long-Term Magnetic After-Effects of Remanence in Ferrites—F. Pliquet. (*Ann. Phys. (Lpz.)*, vol. 7, pp. 216-219; January 30, 1961.) Magnetometer equipment is described and test results obtained with Ni-Zn ferrites are given.
- 538.221:621.318.134 3487
Square-Loop Ferrites with Temperature-Independent Properties and Improved Disturb Ratio—R. S. Weisz. (*J. Appl. Phys.*, vol. 32, pp. 1152-1153; June, 1961.) Magnetic annealing of Mn-ferrous ferrites and Ni-ferrous ferrites has produced storage-type cores with improved properties. Preparation of the cores, their switching properties and an explanation of their behavior are given.
- 538.221:621.318.134 3488
Manganese-Zinc Ferrites with Different Types of Hysteresis Loop—M. Kornetzki, E. Moser, and E. Röss. (*Z. angew. Phys.*, vol. 13, pp. 31-36; January, 1961.) Normal, square, isoperm and permivar types of hysteresis loop can be obtained by varying the FeO₃ content of the ferrites investigated.
- 583.221:621.318.134 3489
Elastic Constants of Single-Crystal YIG—A. E. Clark and R. E. Strakna. (*J. Appl. Phys.*, vol. 32, pp. 1172-1173; June, 1961.)
- 538.221:621.318.134:534.13-8 3490
Extremely Low-Loss Acoustic Resonance in Single-Crystal Garnet Spheres—R. C. Le-Craw, E. G. Spencer, and E. I. Gordon. (*Phys. Rev. Lett.*, vol. 6, pp. 620-622; June 1, 1961.) An acoustic resonance has been observed at 9.2 Mc in spheres of Y-Fe garnet at room temperature with losses an order of magnitude less than for other materials in similar conditions.
- 538.221:621.318.134:538.569.4 3491
Magnetic Resonance in Canted Ferrimagnets—P. A. Mies. (*Phys. Rev.*, vol. 122, pp. 1143-1146; May 15, 1961.) It should be possible to detect and analyze the structure of canted ferrimagnets as their magnetic resonance spectra differ characteristically from ferrimagnets with collinear sublattices.
- 538.221:621.318.134:548.5 3492
Growth Orientation in Ferrite Single Crystals—G. Elbinger and U. Rösler. (*Ann. Phys. (Lpz.)*, vol. 7, pp. 111-112; January 12, 1961.) Note on results obtained using a very low pulling speed. See also 2725 of September (Rösler and Elbinger).
- 538.221:621.395.625.3 3493
Magnetic Recording—L. G. Sebestyen and J. Takacs. (*Electronic Tech.*, vol. 38, pp. 274-278; August, 1961.) A new theory of the magnetization of tape and the role played by ac bias is described. The theory accounts for several previously unexplained phenomena.
- 538.222:534.283-8:621.375.9 3494
Amplification of 9.3-kMc/s Ultrasonic Pulses by Maser Action in Ruby—E. B. Tucker. (*Phys. Rev. Lett.*, vol. 6, pp. 547-548; May 15, 1961.) Experimental evidence is produced for amplification of 9.3-Gc ultrasonic pulse by spin-phonon interaction in a pumped Linde pink crystal. The system was similar to that used previously to observe attenuation of these pulses (1952 of July) but with the spin population inverted. Experimental details are given and the conditions for realizing a phonon maser are briefly considered.
- 538.222:537.228.5 3495
Splitting of the Emission Lines of Ruby by an External Electric Field—W. Kaiser, S. Sugano, and D. L. Wood. (*Phys. Rev. Lett.*, vol. 6, pp. 605-607; June 1, 1961.) An additional splitting of the doublet comprising each emission line is shown to take place in an external electric field. This effect should allow frequency modulation of the output of a ruby optical maser.
- 538.222:538.569.4 3496
Paramagnetic Resonance of Gd³⁺ in Al₂O₃—S. Geschwind and J. P. Remeika. (*Phys. Rev.*, vol. 122, pp. 757-761; May 1, 1961.) The substitution of Gd³⁺ impurities for Al³⁺ has been examined using the paramagnetic resonance spectrum at 24 Gc.
- 538.222:538.569.4 3497
Paramagnetic Resonance of Cr³⁺ in Yttrium Oxide—J. W. Carson, D. P. Devor, and R. H. Hoskins. (*Phys. Rev.*, vol. 122, pp. 1141-1143; May 15, 1961.)
- 538.652 3498
Investigations on Magnetostrictive Circular Rings and Rods for the Determination of the Dynamic Magnetostrictive Coefficient as a Function of External Field Strength—J. Narrog. (*Hochfrequenz- und Elektroak.*, vol. 69, pp. 225-229; December, 1960.)

MATHEMATICS

- 517.918 3499
Concerning the Partition Theory and Associated Transform Methods—E. V. Bohm. (*Proc. IRE*, vol. 49, pp. 1215-1216; July, 1961.) Critical comment on earlier papers [*e.g.* 2854 of 1960 (Ku and Wolf)].

- 517.94:621.372.5 3500
A Review of Methods of Linear Network Analysis in the Steady State: Parts 1 and 2—Seymour. (See 3271.)

MEASUREMENTS AND TEST GEAR

- 621.317.3:621.391.822 3501
A Voltage Comparator for Low-Frequency Noise Measurements—F. A. Spelman. (*Elect. Engrg.*, vol. 80, pp. 200-201; March, 1961.) A circuit is given which was designed to measure low-frequency noise in transistors but is suitable for the study of any noise in the range of 50-5000 cps.

- 621.317.3.029.6:621.391.822 3502
Techniques of Microwave Noise Measurement—B. G. Bosch and W. A. Gambling. (*J. Brit. IRE*, vol. 21, pp. 503-515; June, 1961.) Some aspects of microwave oscillator noise are discussed and measurement techniques applicable to oscillators and to modulation noise in amplifiers are described. These techniques include AM and FM direct-detection methods, the superheterodyne method, and systems for the measurement of correlation.

- 621.317.3.029.63:621.391.822 3503
New Microwave Noise Generator for the 200-Mc/s Band—G. Almásy and I. Frigyes. (*Period. Polyt., Bp., Elect. Engrg.*, vol. 4, no. 4, pp. 293-303; 1960.) Description of a small and easily operated microwave noise generator comprising a gas-discharge tube built into the inner conductor of a coaxial line. The output power depends exclusively on the noise temperature of the plasma.

- 621.317.337.029.6 3504
Measurement of Resonance Coefficients of the Order of a Million in the Microwave Field

—F. Parisi. (*Alta Frequenza*, vol. 30, pp. 14–20; January, 1961.) Equipment is described which is designed for Q -factor measurement in mm- λ H_{01} -mode circular waveguide systems; experimental results are given as examples.

621.317.35 3505

A Direct Digital Method of Power Spectrum Estimation—P. D. Welch. (*IBM J. Res. Dev.*, vol. 5, pp. 141–156; April, 1961.) A method is discussed for the estimation of a digital power spectrum which involves the direct combination of the sample time function with sines and cosines; practical design details are given.

621.317.36:621.376.3 3506

Measurement of Frequency Deviation in F.M.—J. Marique. (*Rev. HF, Brussels*, vol. 5, no. 1, pp. 1–12; 1961.) Two methods are described: one suitable only for symmetrically modulated waves, using a spectrum analyzer, the other based on reconstructing the modulator signal and measuring its peak-to-peak value.

621.317.44 3507

Field Measurements by the Method of Harmonics: Angle Probes—J. Greiner. (*Nachricht.*, vol. 10, pp. 495–498; November, 1960.) Description of various types of probe for magnetometer measurements using the method of perpendicularly superposed magnetic fields. See also 1608 of June and back references.

621.317.44 3508

Induction Probe with Microscope for the Measurement of Field-Strength Distribution in Magnetic Fields—F. Graul. (*Nachricht.*, vol. 10, pp. 499–501; November, 1960.) The principle of operation is electrodynamic, indication being provided by the deflection of a current-carrying wire in the unknown magnetic field.

621.317.7:621.382.3.001.4 3509

Pulse-Sampling Voltmeter and its Application to Transistor Testing—L. J. Herbst and J. R. W. Smith. (*J. Sci. Instr.*, vol. 38, pp. 242–245; June, 1961.) A 100-cps signal is applied to the transistor under test and also to the voltmeter which generates a 20- μ sec sampling pulse at the same frequency. The transistor output waveform can be examined at any phase in the cycle for voltages between 100 mv and 75 v. The sampled voltage is rectified and measured to an accuracy within 1 per cent.

621.317.72:621.319.4 3510

The Vibrating Capacitor, Theory and Application—H. Riegler. (*Nachricht.*, vol. 10, pp. 501–505; November, 1960.) The design of vibrating capacitors for use in electrometer amplifiers is discussed.

621.317.755:621.3.012.11 3511

A Circle-Diagram Recorder for Frequencies between 10 kc/s and 200 Mc/s—P. Thilo. (*Frequenz*, vol. 14, pp. 403–412; December, 1960.) Description of equipment for the display of locus curves and diagrams of the Smith-chart type on a CR tube screen.

621.317.755:621.372.2.001.4 3512

Testing Microwave Transmission Lines using the Sampling Oscilloscope—H. Halverson. (*Electronics*, vol. 34, pp. 86–88; June 30, 1961.) By using pulse reflection techniques and a CRO with a fast rise time direct readings of characteristic impedance can be made. Discontinuities along the line can also be identified.

621.317.789.029.65 3513

100–200-kMc/s Water Calorimeter—J. B. Thaxter and J. McGowan, III. (*Rev. Sci. Instr.*, vol. 32, pp. 605–606; May, 1961.) The mini-

mum detectable signal is 5×10^{-5} w with response time of 20 sec, and sensitivity about 10 μ v/mw. An important feature of the calorimeter is that heat losses from the water are nearly the same for the microwave and dc calibrating power sources.

621.317.79:538.569.4:535.33 3514

Sensitive Triple Modulation Method for Measuring Widths of Microwave Spectral Lines—E. A. Rinchart and C. C. Lin. (*Rev. Sci. Instr.*, vol. 32, pp. 563–563; May, 1961.) The method eliminates from the CRO display the power fluctuations due to the klystron. The technique may be useful for resolving closely spaced lines.

621.317.79.020.64:551.510.62 3515

The Construction and Performance of an Airborne Microwave Refractometer—J. A. Lane, D. S. Froome and G. J. McConnell. (*Proc. IEE*, pt. B, vol. 108, pp. 398–402; July, 1961.) "The paper describes the construction of a Birnbaum-type microwave refractometer and its application in studies of refractive-index variations at heights up to 20,000 ft. Practical problems encountered in airborne measurements are discussed in detail. Some typical results are given which illustrate the performance obtained in measurements of refractive-index profiles and discontinuities."

OTHER APPLICATIONS OF RADIO AND ELECTRONICS

621.362+621.56 3516

New Concepts in Thermoelectric Device Design—W. H. Clingman. (*Proc. IRE*, vol. 49, pp. 1155–1160; July, 1961.) Examples are given in which an analysis based on irreversible thermodynamics can be useful.

621.384.611.2 3517

The CERN 600-MeV Synchrocyclotron at Geneva—(*Philips Tech. Rev.*, vol. 22, pp. 141–180; March 6, 1961.)

Part 1—Object and Design. W. Gentner (pp. 142–149).

Part 2—The Radio-Frequency System. K. H. Schmitter and S. Kortleven (pp. 149–161).

Part 3—The Tuning-Fork Modulator. B. Bollé and F. Krienen (pp. 162–180).

621.56:537.322.1 3518

Peltier-Effect Cooling Blocks—M. Fournet. (*Onde élect.*, vol. 41, pp. 140–141; February, 1961.) A note on the construction and characteristics of semiconductor thermoelements.

681.61 3519

Neon Diode/Resistor Matrix controls Electronic Typewriter—M. Ruderfer. (*Electronics*, vol. 34, pp. 108–109; June 9, 1961.) An improved printing mechanism is described using a printing type which is controlled by the matrix. This system allows faster operation, easy change of printing wheels and type faces and is of small and light construction.

PROPAGATION OF WAVES

621.371 3520

An Iteration-Variation Method for Wave Propagation Problems—W. J. Byatt and G. P. DeVault. (*J. Geophys. Res.*, vol. 66, pp. 1793–1797; June, 1961.) An inhomogeneous wave equation in which refractive index is a function of one space coordinate and time is reduced to an ordinary differential equation by transform methods. An equivalent integral equation is formed with a symmetric kernel so that an iterative expansion has radius of convergence given by the numerical value of the smallest eigenvalue. A variational solution similar to the Rayleigh-Ritz method is given.

621.391.812.6.029.64/.65 3521

Microwave Absorption in the Earth's Atmosphere—S. N. Ghosh and V. Malaviya. (*J. Atmos. Terr. Phys.*, vol. 21, pp. 243–256; July, 1961.) The absorption for different atmospheric layers, and for the whole atmosphere, is calculated for frequencies between 10 and 100 Gc. The profiles and half-widths for principal absorption lines are given.

621.391.812.62 3522

Results and Evaluation of Measurements of Tropospheric Transhorizon Propagation over several Paths of Different Type in Central and South-East Europe—H. Carl. (*Nachricht. Z.*, vol. 13, pp. 566–570; December, 1960.) Results are given of measurements of transhorizon loss made on radio links of length 230–400 km, some purely over land and others over sea, during periods of 4–6 weeks between February and May. The dependence of loss on elevation angle and dew point was in accordance with theory and some correlation with other meteorological conditions was found.

621.391.812.62.029.63 3523

Space-Diversity Measurements on a Radio-Link Path within Optical Range—U. Kühn. (*Nachricht.*, vol. 10, pp. 430–435; October, 1960.) Measurements were made over a period of 21 months for transmissions at 1.3 Gc over an 82-km path with antennas vertically spaced by 250 λ . Long-term as well as short-term fluctuations are frequently reduced by the system. See also 1753 of 1960.

621.391.812.624:621.396.677 3524

Tropospheric Scatter Observations at 3480 Mc/s with Aerials of Variable Spacing—R. W. Meadows. (*Proc. IEE*, pt. B, vol. 108, pp. 349–360; July, 1961.) Measurements are described of signal amplitude, fading characteristics, correlation distances, and height gain at ranges of 130, 258 and 398 km in southern England, the 130-km path being largely over sea. Cross-correlation measurements showed definite evidence of the steady drifting of scattering centers.

621.391.812.63 3525

Scattering of Radio Waves by an Ionized Gas in Thermal Equilibrium in the Presence of a Uniform Magnetic Field—J. A. Fejer. (*Canad. J. Phys.*, vol. 39, pp. 716–740; May, 1961.) The earlier theory (1290 of May) was restricted to cases where the "characteristic scale" was much greater or less than the Debye length, and where only one type of singly charged ion was present. Ion and electron temperatures were assumed equal and the external magnetic field was ignored. These restrictions have now been removed. The total power is independent of the magnetic field and an expression for the frequency spectrum of the power in the presence of the field is given. The field may be ignored in interpreting the results of Bowles (*Phys. Rev. Lett.*, vol. 1, pp. 454–455, December 15, 1958) and Pineo *et al.* (188 of January) but it could be important at great heights.

621.391.812.63 3526

Long-Distance One-Hop F_1 Propagation through the Auroral Zone—L. H. Tveten. (*J. Geophys. Res.*, vol. 66, pp. 1683–1684; June, 1961.) "The existence of one-hop F_1 propagation through the auroral zone over a 4495-km path is described, and an example of a sweep-frequency record illustrating this F_1 mode is shown."

621.391.812.63:551.507.362.2:621.396.43 3527

The Propagation of Wide-Band Signals through the Ionosphere—Staras. (See 3537).

621.391.812.63:551.594.6 3528
Two-Hop 18.6-kc/s Whistler-Mode Echoes Received at Seattle—H. R. Willard. (*J. Geophys. Res.*, vol. 66, pp. 1976-1977; June, 1961.) The observation of delay times ranging from 0.7 to 1.7 sec suggests the existence of whistler propagation paths at quite different latitudes.

621.391.812.63.029.51 3529
A Diffraction Theory for L.F. Sky-Wave Propagation—J. R. Wait. (*J. Geophys. Res.*, vol. 66, pp. 1713-1724; June, 1961.) The propagation of radio waves via discrete ionospheric reflections is treated theoretically with the earth and the ionosphere represented by two concentric spherical surfaces of known reflection characteristics. The *m*th-hop sky wave may generally be represented by a complex integral, and geometrical-optics formulas are developed for special cases and their limitations discussed. Techniques for evaluating the complex integral for sky waves near and beyond the caustics are discussed. For an additional note reporting some numerical results see *ibid.*, pp. 1725-1729 (Wait and Conda).

RECEPTION

621.391.814.2.029.53 3530
Temporal Variation of Medium-Frequency Ground-Wave Field Strength—J. M. Dixon. (*Proc. IRE, Aust.*, vol. 22, pp. 250-252; April, 1961.) The results of field-strength measurements are analyzed to show the variation to be expected under Australian conditions, with particular reference to path conductivity.

621.396.669:621.396.67 3531
The Suppression of Corona- and Precipitation-Interference in V.H.F. Reception—H. Page. (*Proc. IEE*, pt. B, vol. 108, pp. 469-470; July, 1961.) A note describing the results of preliminary tests on systems designed to screen television receiving antennas from such effects.

STATIONS AND COMMUNICATION SYSTEMS

621.376.5 3532
The Elimination of Intersymbol Interference by Input Signal Shaping—I. Gerst and J. Diamond. (*Proc. IRE*, vol. 49, pp. 1195-1203; July, 1961.) The problem is treated mathematically by considering the effect of the input wave shape on the output tail.

621.391 3533
Signal Detection and Establishment of the Mean Value in Periodic Signal Sequences with Superimposed Fluctuations—C. Moeller. (*Hochfrequenz- und Elektroak.*, vol. 69, pp. 189-192; October, 1960.)

621.391:534.78 3534
Bandwidth Compression of Speech—M. Das. (See 3225.)

621.396:523+55 3535
Radio Techniques and Space Research—(See 3355.)

621.396.43:551.507.362.2 3536
Economic Potential of Communication Satellites—W. Meckling. (*Science*, vol. 133, pp. 1885-1892; June 16, 1961.) Communication satellites may reduce costs if high rates of utilization can be achieved.

621.396.43:551.507.362.2:621.391.812.63 3537
The Propagation of Wide-Band Signals through the Ionosphere—H. Staras. (*Proc. IRE*, vol. 49, p. 1211; July, 1961.) Differential group delay across the frequency band can cause distortion of television signals relayed by satellites. This distortion is strongly dependent

on frequency and it may be necessary to use carriers in excess of 1 Gc.

621.396.65:621.396.43 3538
Results and Experience Gained from a Transhorizon Link in the Long-Distance Communications Network of the German Federal Post Office—E. Dietrich. (*Nachtech. Z.*, vol. 13, pp. 563-565; December, 1960.) Report dealing with the Berlin-West Germany radio link operating at 2 Gc. See also 1635 of June (Hoffmann).

621.396.933 3539
Automatic Techniques in Civil Air Line Communication Systems—W. E. Brunt. (*J. Brit. IRE*, vol. 21, pp. 549-553; June, 1961. Discussion, pp. 554-555.) Methods of modulation and coding are considered.

621.396.97:534.76 3540
The H.M.D. System—a Method for the Transmission of Stereophonic Broadcasts—E. Frank and J. Ratsch. (*Elektron. Rundschau*, vol. 14, pp. 463-466; November, 1960.) Description of a single-carrier time-multiplex system using half-wave modulation with signal-difference control.

621.396.97:621.391.812.63 3541
An Investigation of the Usefulness of Back-Scatter Sounding in the Operation of H.F. Broadcast Services—E. D. R. Shearman. (*Proc. IRE*, pt. B, vol. 108, pp. 361-372; July, 1961. Discussion, pp. 372-374.) Echo patterns measured at 15 and 21 Mc agreed well with those calculated from parabolic ionospheric-layer theory. Further tests, including listeners' reports, at night showed that propagation modes to 5000 km were correctly evaluated when predictions, corrected by local vertical-incidence soundings, gave erroneous results.

SUBSIDIARY APPARATUS

621-52 3542
Complex-Plane Charts for Obtaining Closed-Loop Frequency Responses in Linear Control Systems—F. Csáki. (*Period. Polyt., Bp., Elec. Engrg.*, vol. 4, no. 4, pp. 361-378; 1960.) Summary of graphical methods for plotting complex-plane charts.

621.3.087.4:621.395.625.3 3543
Outside-Coil Magnetic Head Improves High-Frequency Recording—N. Camras and R. Sears. (*Electronics*, vol. 34, pp. 89-91; June 30, 1961.) High resolution is obtained as a result of smaller air gaps and on improved field configuration.

621.314.58 3544
Replacing Sine-Wave Sources with Solid-State Inverters—D. Levy. (*Electronics*, vol. 34, pp. 80-83; June 30, 1961.) A series magnetic amplifier or a saturable reactor is used following a solid state inverter to give a modified square-wave output such that the heater and direct voltages available are the same as would be obtained from a sinusoidal ac supply.

621.314.58:621.382.23 3545
Converter Efficiency and Power Output of a Tunnel-Diode Relaxation Oscillator—S. Wang. (*Proc. IRE*, vol. 49, pp. 1219-1220; July, 1961.) A simple dc/ac converter is discussed.

621.314.58:621.382.3 3546
Control of Frequency and Phase Displacement in Transistor Converter Circuits by means of RC Networks—F. V. Kadri. (*Commun. and Electronics*, no. 53, pp. 43-48; March, 1961.) A new type of adjustable-frequency transistor converter is described in which the operating frequency is controlled by an RC network and is independent of the direct voltages. Power

regulation by means of RC phase control of a pair of transistor converters is discussed.

621.314.63:621.374 3547
Controlled Rectifier Produces Quarter-Megawatt Pulse Power—H. G. Heard. (*Electronics*, pp. 54-55; June 23, 1961.) Circuit details are given of pulse generator equipment using solid-state devices as active elements. A *p-n-p-n* Si controlled rectifier acts as the switch, and two-layer and four-layer diodes are used in the trigger generator.

621.314.634 3548
Recent Developments in Selenium Rectifiers—C. Loeffler. (*Onde Elect.*, vol. 41, pp. 123-131; February, 1961.) An account of phenomena occurring during the construction and operation of different types of Se rectifier.

621.316.72:621.382.3 3549
A Note on Transistorized Ripple Filters—B. W. Moore and J. P. O'Neil. (*AWA Tech. Rep.*, vol. 11, pp. 169-177; December, 1960.) A smoothing circuit providing optimum efficiency over a wide range of load currents is described.

TELEVISION AND PHOTOTELEGRAPHY

621.397.12:621.396.4:523.5 3550
Transmitting Facsimile Messages over Meteor-Burst Paths—B. F. Gedaminski and W. F. Griffin, Jr. (*Electronics*, vol. 34, pp. 85-89; May 19, 1961.) Average information rate for $\frac{1}{2}$ -hr periods was 2 300 bits/sec, in a 220 kc bandwidth.

621.397.13 3551
B.B.C. Television 1939-60—E. L. E. Pawley. (*Proc. IEE*, pt. B, vol. 108, pp. 375-397; July, 1961.) A comprehensive technical review of progress in planning and equipment.

621.397.13(083.7) 3552
IRE Standards on Video Techniques: Definition of Terms relating to Television, 1961—(*Proc. IRE*, vol. 49, pp. 1193-1195; July, 1961.) Standard 61 IRE 23. S1.

621.397.132 3553
Land's System of Two-Colour Projection—M. H. Wilson and R. W. Brocklebank. (*J. Brit. IRE*, vol. 21, pp. 535-536; June, 1961. Discussion, pp. 546-548.) A brief discussion of the physical principles involved.

621.397.132 3554
The Range of Colours Excited by a Two-Colour Reproduction System—W. N. Sproson. (*J. Brit. IRE*, vol. 21, pp. 537-544; June, 1961. Discussion, pp. 546-548.) An assessment of the accuracy with which colors can be reproduced relative to those of a three-color system. The two-color process is considered to be insufficient for a good approximation to true color.

621.397.331.222 3555
Modifying Vidicon Camera Chain for Slow-Scan Television Systems—F. F. Martin and C. T. Shelton. (*Electronics*, vol. 34, pp. 101-103; June 9, 1961.) In order to reduce bandwidth and transmitter power the use of low scan rates is discussed; further advantages are increased resolution, and more time available to interpret the scene. Disadvantages are microphonic signals due to vibration and critical beam setting.

621.397.6.001.4 3556
A Television Imagery Simulator—J. P. Smith and J. F. Baumunk. (*J. Soc. Mot. Pic. Telev. Engrs.*, vol. 70, pp. 27-32; January, 1961.) A high-quality television chain suitable for testing television systems and providing means for comparing them.

- 621.397.61/.62].029.63** 3557
U.H.F. Television Techniques—C. Reuber. (*Elektrotech. Z., Edn B*, vol. 13, pp. 135-141; March 20, 1961.) Review of problems concerning transmitter-network planning, transmitter design, receiving antennas and antenna cables, and the design of UHF tuners.
- 621.397.621** 3558
Reflected Images on Curved and Plane Television-Tube Front Plates—R. Suhrmann. (*Elektron. Rundschau*, vol. 14, pp. 467-468; November, 1960.) The use of a flat, instead of a curved, safety-glass plate in front of television tubes minimizes interference by reflections particularly if the plate is inclined slightly downwards.
- 621.397.621** 3559
Electronic Brightness Contouring—R. L. Hallows. (*J. Soc. Mot. Pic. Telev. Engrs.*, vol. 70, pp. 23-27; January, 1961.) A circuit technique is described for producing an "equal-brightness contour" which may be superimposed on a television picture and set to any level of brightness.
- TUBES AND ELECTRONICS**
- 621.382.004.6** 3560
Life Characteristics of some Typical Semiconductor Devices—R. Brewer and D. J. E. Richards. (*J. Brit. IRE*, vol. 21, pp. 485-489; June, 1961.) Changes in characteristics after many thousands of hours in service, and the incidence of inoperative failures are discussed. Results from field reports and laboratory measurements are compared.
- 621.382.22** 3561
Influence of Surface Currents on the Characteristics of Formed Point-Contact Rectifiers—R. Ebbhardt, E. Hofmeister, and E. Groschwitz. (*Z. angew. Phys.*, vol. 13, pp. 16-28; January, 1961.) Results of measurements on point-contact semiconductor diodes are given and analyzed with reference to previous theoretical work [3180 of October (Groschwitz *et al.*) and back references].
- 621.382.22:621.372.44** 3562
High-Frequency Silicon Varactor Diodes—C. A. Burrus. (*J. Appl. Phys.*, vol. 32, pp. 1166-1167; June, 1961.) By adopting point-contact diode geometry, Si varactor diodes with zero-bias junction capacitances at least an order of magnitude below the minimum value associated with the Si mesa diode have been made.
- 621.382.22:621.372.622** 3563
Excess Noise in Microwave Mixer Crystals—B. G. Bosch, W. A. Gambling, and T. H. Wilmshurst. (*Proc. IRE*, vol. 49, pp. 1226-1227; July, 1961.) Noise-temperature measurements have been made over a frequency range 25 cps-80 Mc.
- 621.382.23** 3564
Tunnel-Effect Diodes—R. Deschamps. (*Onde élect.*, vol. 41, pp. 132-139; February, 1961.) A description of the mechanism and characteristics of the tunnel diode. Optimum operating conditions are considered and possible applications are noted.
- 621.382.23** 3565
The Technology of Tunnel Diodes—J. Hartmann and M. Michelitsch. (*Elektrotech. Z., Edn A*, vol. 82, pp. 114-116; February 13, 1961.) Types of construction and manufacturing techniques are discussed.
- 621.382.23** 3566
Stability Criteria for Tunnel Diodes—L. I. Smilen and D. C. Youla. (*Proc. IRE*, vol. 49, pp. 1206-1207; July, 1961.) Various conditions for stability are stated and discussed.
- 621.382.23** 3567
Electrical Characteristics of Diffused InAs p-n Junctions—G. Lucovsky. (*Brit. J. Appl. Phys.*, vol. 12, pp. 311-312; June, 1961.) Rectification properties are examined at 300°K, 196°K and 77°K. At 196°K, the I/V characteristic was in good agreement with conventional diode theory [e.g. 2906 of 1958 (Moll)]. Deviations noted at the other temperatures are accounted for.
- 621.382.23** 3568
Gallium Arsenide Esaki Diodes for High-Frequency Applications—A. C. Burrus. (*J. Appl. Phys.*, vol. 32, pp. 1031-1036; June, 1961.) "Esaki diodes which show promise of usefulness into the millimeter-wave region have been made from both p- and n-type GaAs. Both diodes were alloyed junctions having point-contact geometry and dimensions. The fabrication of these diodes is briefly described, and their initial performance as oscillators in mechanically simple circuits is discussed. Fundamental oscillations to 103 kMc have been obtained." See also 3184 of October.
- 621.382.23:621.372.44** 3569
Circuit Control of Tunnel-Diode Negative-Resistance Characteristics—W. N. Carr and A. G. Milnes. (*Proc. IRE*, vol. 49, pp. 1204-1205; July, 1961.) Typical control circuits and characteristics are given.
- 621.382.23:621.374** 3570
Application of Tunnel Diodes in Pulse Techniques—U. L. Rohde and H. J. Thaler. (*Elektronik*, vol. 10, pp. 33-37; February, 1961.) Design procedures for multivibrator circuits are described.
- 621.382.23:621.375.9:621.372.44** 3571
Reactance Diodes and their Application in Wide-Band Waveguide Amplifiers—P. Bobisch and C. Sondhauss. (*Telefunken-Röhre*, no. 38, pp. 115-124; December, 1960.) Semiconductor reactance diodes with disc electrodes housed in a cartridge of greatly reduced size are used in the construction of a two-stage traveling-wave parametric amplifier for the frequency range 2.7-2.9 Gc. The construction and performance of a frequency multiplier for use up to 6 Gc are also described.
- 621.382.233** 3572
The p-n-p-n Diode—M. Chappex. (*Onde élect.*, vol. 41, pp. 99-113; February, 1961.) The characteristics of the diode applicable to heavy-current uses, calculating machines or switching circuitry are discussed. An elementary theory of its operation and details of its production by double diffusion, simple diffusion, or alloying are given.
- 621.382.233:621.373.44** 3573
Silicon Four-Layer Devices as High-Power Pulse Generators—R. P. F. Lauder. (*Electronic Engrg.*, vol. 33, pp. 426-431; July, 1961.) "Several circuits are presented showing that p-n-p-n devices in the two- or three-terminal configuration may be used as pulse generators delivering accurately rectangular power pulses for a variety of purposes including transmitters in the 20-kw peak input power region."
- 621.382.3** 3574
Thermal Problems in Transistors—H. J. Thuy. (*Elektron. Rundschau*, vol. 15, pp. 15-18 and 61-65; January and February, 1961.) The problems reviewed include the dependence of transistor life on junction temperature, the calculation and measurement of internal thermal resistances, the measurement of heat inter-
- change of cooling surfaces and the runaway effect and related stability criteria. 38 references.
- 621.382.3.001.4:621.317.7** 3575
Pulse-Sampling Voltmeter and its Application to Transistor Testing—Herbst and Smith. (See 3509.)
- 621.382.333.33** 3576
The Calculation of Cut-Off Frequencies of Minority-Carrier Transport Factors in Drift Transistors when the Mobilities are not Constant—T. Sugano and F. Koshiga. (*Proc. IRE*, vol. 49, p. 1218; July, 1961.)
- 621.382.333.4** 3577
The Field-Effect Tetrode—H. A. Stone, Jr., and R. M. Warner, Jr. (*Proc. IRE*, vol. 49, pp. 1170-1183; July, 1961.) The field-effect tetrode is described and its applications are discussed. The equations for its behavior as a gyrator, an isolator, a negative resistance and an electronically variable resistor are developed.
- 621.382.333.4** 3578
Examination of a New Tetrode Field-Effect Device: the Alcatron—J. Grosvalet. (*Onde élect.*, vol. 41, pp. 114-122; February, 1961.) A transistor field-effect device of annular construction is described. It contains a small control grid and a second larger grid which removes the dissipation power and modifies the equivalent circuit at high frequencies. It gives values beyond the limits suggested by Dacey and Ross (1240 of 1956). See also 1670 of June (Martin).
- 621.383.032.217.2** 3579
Bismuth-Silver-Oxygen-Cesium Photocathode—A. H. Sommer and W. E. Spicer. (*J. Appl. Phys.*, vol. 32, pp. 1036-1042; February, 1961.) Chemical and physical studies on the Bi-Ag-O-Cs photocathode to gain an understanding of the chemical nature and the energy band model of the material are reported.
- 621.383.032.217.2** 3580
Measurement of the Partial Pressure of Cesium over Cesium Antimonides—K. Miyake. (*J. Appl. Phys.*, vol. 32, pp. 1132-1136; June, 1961.)
- 621.385.032.269.1** 3581
Electron Gun for the Generation of a Hollow Beam—R. John and W. Henne. (*Telefunken-Röhre*, no. 38, pp. 99-114; December, 1960.) Design calculations for the electrodes of the gun are based on the assumption that the hollow beam can be regarded as a strip-beam system. Results obtained with an experimental gun confirm the validity of the assumption when the ratio of beam thickness to beam diameter is small.
- 621.385.3/.4].029.63** 3582
New Ceramic Power Triodes and Tetrodes Operating at Very High Frequencies—P. Gerlach. (*Onde élect.*, vol. 41, pp. 167-171; February, 1961.) Negative-grid valves are described which, when giving 10 kw CW power at 1 Gc, have an envelope temperature of several hundred °C.
- 621.385.4:621.397.61** 3583
Electron-Transit-Time Effects in Transmitter Tetrodes for Television Bands IV/V—W. Seiffarth. (*Arch. elektr. Übertragung*, vol. 14, pp. 491-498; November, 1960.) The method used by Hülster (3449 of 1955) for triodes is applied to high-power transmitter tetrodes for operation at 800 Mc. Problems of valve design are considered with reference to these calculations.

- 621.385.6 3584
An Approximation Method for the Determination of the Quadrupole Characteristics of Electron Beams with the Aid of Elementary Functions—K. B. Niclas. (*Telefunken-Röhre*, no. 38, pp. 61–70; December, 1960.) The solution obtained for the quadrupole parameters are given in graphical form. The method is applied to the study of the transformation region in a low-noise traveling-wave tube.
- 621.385.6:621.396.65 3585
Microwave Valves for Radio-Link Systems—W. Klein. (*Telefunken-Röhre*, no. 38, pp. 5–36; December, 1960.) The operation of the principal types of microwave tube is described and their performance in the local oscillator, microwave modulator and power amplifier stages is discussed.
- 621.385.62 3586
On the Possibility of Drift-Tunnel Oscillations in High-Power Klystrons—K. Tomiyasu. (*Proc. IRE*, vol. 49, pp. 1207–1208; July, 1961.) Spurious oscillations observed in high-power klystrons are discussed. The evidence which suggests they may be drift-tunnel oscillations is examined.
- 621.385.623.5 3587
Theory of Reflex Klystron with Inhomogeneous Retarding Field—K. H. Kupferschmidt. (*Arch. elekt. Übertragung*, vol. 14, pp. 477–481; November, 1960.) The influence of the inhomogeneity on the build-up of oscillations and on the efficiency of the klystron is investigated. Measurements on a reflex klystron provide confirmation of the theoretical considerations.
- 621.385.623.5 3588
The Influence of Mechanical Vibrations on Reflex Klystrons—P. Hain, H. Lind, and W. Henne. (*Telefunken-Röhre*, no. 38, pp. 135–150; December, 1960.) Methods are described for measuring the influence of sound and mechanical shock on the frequency stability of reflex klystrons. Results obtained on various klystrons are given and discussed.
- 621.385.623.5 3589
Electrically Tuned Klystron—R. Musson-Genon and J. Faralier. (*Onde élect.*, vol. 41, pp. 155–158; February, 1961.) An X-band reflex klystron has been developed which is tuned electronically over a range of 300 Mc the range being covered in approximately 200 μ sec.
- 621.385.63 3590
Tubes with Crossed Electric and Magnetic Fields—P. Guénard and O. Doehler. (*Onde élect.*, vol. 41, pp. 142–154; February, 1961.) Various types of crossed-field tubes are classified according to beam geometry and interaction mechanism. A description is given of results obtained with backward-wave oscillators and forward-wave amplifiers.
- 621.385.63:621.375.9:621.372.44 3591
Energy Interchange between Cyclotron and Synchronous Waves in Quadrupolar Pump Fields—E. I. Gordon and A. Ashkin. (*J. Appl. Phys.*, vol. 32, pp. 1137–1144; June, 1961.) "The various coupling interactions which occur in quadrupolar pump fields have been described using a coupled-mode formalism and from knowledge of the beam orbits. Experiments have been described which verify the basic interactions. Further experimental work is required in order to assess the usefulness of these interactions in low-noise microwave amplification."
- 621.385.63:621.375.9:621.372.44 3592
Noise in Beam-Type Parametric Amplifiers—E. I. Gordon. (*Proc. IRE*, vol. 49, p. 1208; July, 1961.) Some additional noise which arises from the finite electron temperature and the size of the beam is discussed.
- 621.385.63:621.375.9:621.372.44 3593
Parametric Coupling between the Transverse Waves on O- and M-Type Beams—J. W. Klüber. (*J. Appl. Phys.*, vol. 32, pp. 1111–1114; June, 1961.) To couple only two waves the pump field should be two-dimensional. For HF pumping only waves of the same polarization can couple while for LF pumping only two waves of opposite polarization can couple. Except for cyclotron-cyclotron wave coupling the pump wave will always be in synchronism with a beam wave and thus interact actively or passively with the beam.
- 621.385.63:621.375.9:621.372.44 3594
Transduction of Noise Theory of a Generalized Travelling-Wave Coupler—M. C. Pease. (*J. Appl. Phys.*, vol. 32, pp. 1145–1151; June, 1961.) A study is made of the response to noise of systems described as "generalized lossless networks" which may include, for example, electron beams and parametrically pumped components. The theory is applied to a generalized coupler.
- 621.385.632.1 3595
The Uniformity of Active Lines for Microwaves—W. Klein. (*Telefunken-Röhre*, no. 38, pp. 71–84; December, 1960.) Various influences affecting the uniformity of helix or delay-line structures in traveling-wave tubes are investigated.
- 621.385.633 3596
The Resonant-Type Backward-Wave Oscillator: a Generator of Microwaves—H. Heynisch. (*Arch. elekt. Übertragung*, vol. 14, pp. 531–538; December, 1960.) The oscillator described differs from the normal type of backward-wave tube in that it uses the resonance effect produced by short-circuiting the delay line at both ends. The expressions giving the parameters of the normal backward-wave oscillator are modified by the introduction of the Q factor of the short-circuited delay line to become applicable to the resonant type of oscillator. Experimental results are given for a resonant backward-wave tube operating in the range 3.5–4.7 Gc.
- 621.385.633.14 3597
O-Type Carcinotron Tubes and their Applications in V.H.F. Measurements—R. Olivier and D. Reverdin. (*Flektrotech. Z., Edn. A.*, vol. 82, pp. 41–46; January 16, 1961.) Applications described include an UHF wobulator and a wide-band spectrum analyzer.
- 621.385.65 3598
Design Aspects regarding Travelling-Wave Tubes with Tubular-Magnet Focusing for Radio-Link Applications—W. Klein, J. Bretting, and E. Mayerhofer. (*Telefunken-Röhre*, no. 38, pp. 85–98; December, 1960.) The use of a straight-field focusing by means of barrel-shaped permanent magnets [see e.g., 3697 of 1957 (Glass)] is shown to be advantageous in respect to stray magnetic fields and of power-supply equipment.
- 621.387 3599
Relaxation Oscillations in a Plasma Diode—J. M. Rocard and G. W. Paxton. (*J. Appl. Phys.*, vol. 32, pp. 1171–1172; June, 1961.) The dependence of the oscillation frequency on the various diode parameters is investigated.
- 621.387.132.223:621.376.5 3600
Measurement of Energy Losses in a Hydrogen-Filled Thyatron in Modulator Duty—H. de B. Knight and J. Lord. (*Proc. IEE*, pt. B, vol. 108, pp. 455–464; July, 1961.) Values of dissipation at the leading and trailing edges of a current pulse and during the steady state are separated by a pulse-chopping process.

MISCELLANEOUS

- 621.4:621.38.002.3 3601
Radio Components Show—(*Wireless World*, vol. 67, pp. 361–367; July, 1961.) Review of new equipment and developments exhibited at the Radio and Electronic Components Show, London, May 30–June 2, 1961.
- 621.4:621.39 3602
Soviet Exhibition in London—(*Wireless World*, vol. 67, pp. 398–399; August, 1961.) Specifications are given of some of the industrial and domestic equipment which was displayed at Earls Court, London.